Characterisation of Mineral Matter in South African Coals Using Micro-Raman Spectroscopy and Other Techniques

Nthabiseng Beauty Maledi

Thesis submitted to the Faculty of Engineering and the Built Environment, University of the Witwatersrand, in fulfilment of the requirements for the degree of Doctor of Philosophy

Johannesburg, 2017

DECLARATION

I declare that this thesis is my own unaided work. It is being submitted for the degree of Doctor of Philosophy to the University of the Witwatersrand, Johannesburg. It has not been submitted before for any degree or examination to any other University.

_____

Nthabiseng Beauty Maledi

Date: 13 September 2017

ABSTRACT

Three medium rank C coals and a discard coal from different coalfields within the Karoo Basin were investigated. In this study, physico-chemical properties, ash fusion tests, quantitative single particle -electron probe X-ray microanalysis (SPA-EPXMA), petrography, X-ray diffraction (XRD), Fourier Transform Infrared (FTIR), and micro-Raman spectroscopy (mRs) were used as analytical techniques of choice to investigate the heterogeneous nature of coals, including mineralogical structure, mode of occurrence, and association of mineral matter in coals. The aim of the work was to highlight the significance of understanding the heterogeneous nature of coals, and to develop comprehensive and reliable approaches of characterising coals, coal ashes, and predict the behaviour of coals in coal conversion processes. The FTIR technique identified a well ordered kaolinite of authigenetic origin, characterised by inner hydroxyl group with H_2O vibration at 3618 cm^{-1} absorption bands as the major mineral. Smectite and muscovite were identified at peaks 797 cm^{-1} and 799 cm^{-1} respectively, with quartz confirmed by the υ (Si-O-Si) and δ (Si-O) bands. The SPA-EPXMA data, modelled using principal component analysis (PCA) and chemical boundary classification (CBC), identified a diverse range of minerals such as alunite, chlorite, fayalite, almandine, anatase, ilmenite, brushite, goyazite, gypsum, dolomite, calcite, sodalite, rhodochrocite, and halite in raw coal samples. The mRs technique showed that in addition to bassinite, other oxidation products that formed at low temperature included lepidocrite and coquimbite. The technique proved to be ideal for the characterisation of high temperature ashes. High spatial resolution of mRs confirmed the presence of mixtures of anatase, brookite, and rutile, hematite, nephaline, apatite, crednerite and apatite in high temperature ashes. The SPA-EPMXA and mRs technique probed minerals on a micro-scale and their application could be extended to prediction of slagging and fouling behaviour in coals. The multiple technique approach revealed the importance of using a combination of techniques to characterise coals, and provided useful information that can help understand and relate the mineralogical and elemental composition of coals.

This knowledge could be useful in designing conversion processes, and necessary downstream manipulations.

Keywords: Characterisation, mineral matter, single particle analyses-electron probe micro X-ray, micro-Raman spectroscopy, Fourier Transform Infrared spectroscopy (FTIR), X-ray diffraction (XRD), coal ashes.

Contributions to Science

The following work was presented at several international conferences listed below:

Conferences

Potgieter-Vermaak, S, Maledi, N., Wagner, N., Godoi, R.H., Potgieter, J.H. (2013), Multiple technique approach to characterise the inorganic matter in coal and its ashes

http://www.minersoc.org/minerals-for-life.html

Maledi, N, Potgieter, J.H., Wagner, N, Potgieter-Vermaak, S., (2013) Using multiple techniques approach to determine mineral matter in low temperature and high temperature ashes
http://www.iccst.info/live/index.php?c=

Publications

Potgieter-Vermaak, S., Maledi, N., Wagner, N., van Heerden, J.H.P., van Grieken, R., and Potgieter, J.H, (2011), Raman spectroscopy for the analysis of coal: a review, Journal of Raman Spectroscopy, Vol. 42, Issue 2, pp 123-129.

Maledi, N.B., Potgieter-Vermaak, S.S. Wagner, N.J., Potgieter, J.H.P., Ward, C.R., A novel approach to characterise South African coals, under preparation.

Maledi, N.B., Potgieter-Vermaak, S.S. Wagner, N.J., Potgieter, J.H.P., Ward, C.R., Understanding the behaviour of SA coals using SPA-EPXMA and thermodynamic modelling, under preparation.

Dedications

I dedicate this work to my living GOD, my precious daughter Keamogetswe Maledi, my parents, brothers and sisters.

Proverbs 3:5-6

Trust in the Lord with all your heart; do not depend on your own understanding.

Seek his will in all you do, and he will show you which path to take.

Acknowledgements

I would like to extend my sincere gratitude to my supervisors, Prof. S. S. Potgieter-Vermaak, Prof. N.J Wagner, and Prof. J.H. Potgieter for their guidance, advice, patience, understanding, love, and support they showed throughout the research work. This work would not have been possible without their immense contributions.

I would like to acknowledge Dr. Henry Matjie, Prof. Colin Ward, Dr. Majanovic, Liberty Chipise, and Mr Tshepo Ntsoane for their contribution, and the assistance in analysing the coal samples, and Ms. Itumeleng Thobadi for her immense help with FACTSAGE modelling.

I will also like to thank my colleagues for their continued support, the Clean Coal Technology (CCT) group – (University of the Witwatersrand), friends, and loved ones for the support and motivation. I thank you dearly.

The financial support from National Research Fund (NRF), and the University of the Witwatersrand to complete the work is highly appreciated.

Lastly, I would like to extend a warm and heartfelt gratitude to my family, and most especially my daughter, for the undying and amazing love that got me through my lowest times. I appreciate and love you all.

Table of content

DECLARATION i

ABSTRACT ii

Contributions to Science iv

Dedications v

Acknowledgements vi

Table of content vii

List of Figures xiv

List of Tables xix

List of Acronyms, Abbreviations and Symbols xxii

CHAPTER 1: INTRODUCTORY CHAPTER 1

1.1 Introduction 1

1.2 Background 1

1.3 Coal overview and challenges presented by mineral matter in coal conversion processes 7

1.3.1 Acid mine drainage (AMD) 9

1.3.2 Emissions from coal utilisation processes 14

1.3.3 Clean coal technologies (CCT) 18

1.4 Motivation for research 21

1.5 Research questions 21

1.6 Hypothesis 24

1.7 Aim and objectives of the research 24

1.8 Approach 25

1.9 Layout of thesis 26

CHAPTER 2: LITERATURE REVIEW 27
2.1 Introduction 27
2.2 Geological setting of coal deposits in South Africa 27
2.2.1 Lithostratigraphies of South African coalfields 31
2.3 Coal chemistry and petrographic composition 38
2.4 Maceral groups 38
2.4.1 Vitrinite maceral group 39
2.4.2 Liptinite maceral group 40
2.4.3 Inertinite maceral group 40
2.5 Mineral matter in coal 43
2.5.1 Dissolved salts 44
2.5.2 Inorganic elements associated with organic matrix 44
2.5.3 Discrete inorganic particles 45
2.6 Formation of mineral matter in coals 45
2.7 Mode of occurrence of mineral matter in coals 47
2.8 Mineral groups in coals 50
2.8.1. Silicate minerals 52
2.8.1.1 Kaolinite 54
2.8.1.2 Illite 54
2.8.1.3 Chlorites 55
2.8.2 Silica minerals 55
2.8.3 Carbonates 55
2.8.4 Sulphides 57
2.8.5 Sulphates 59

2.8.6 Phosphates 60
2.8.7 Oxides and other minerals 60
2.9 Chapter summary.....61
CHAPTER 3: THE EFFECT OF MINERAL MATTER IN COAL UTILISATION PROCESSES.....62
3.1 Introduction 62
3.2 Coal conversion processes.....62
3.2.1 Transformation of carbonate minerals.....68
3.2.2 Transformation of carbonate minerals.....68
3.2.3 Transformation of iron-containing minerals 69
3.2.4 Transformation of organically-bound mineral matter 70
3.3 Slagging and fouling deposition mechanisms 70
3.3.1 Ash particle transport mechanisms and ash deposits 72
3.3.2 Prediction of ash deposition in coal conversion processes.....74
3.3.2.1 Ash deposition indices.....75
3.3.2.2 Ash fusibility and ash flow temperature (AFT) 78
3.3.2.3 Correlation between ash chemistry and AFT 79
3.4 Chapter summary.....80
CHAPTER 4: REVIEW OF CHARACTERISATION TECHNIQUES USED TO DETERMINE MINERAL MATTER IN COALS 81
4.1 Introduction 81
4.2 Coal petrography 85
4.3 Characterisation of inorganic and mineral matter in coals using XRD technique.....87
4.4 Elemental analyses of coal 89

4.4.1 X-ray Fluorescence (XRF) spectroscopy 89
4.4.2 Electron microprobe analyses (EPMA).....91
4.5 Fourier Transform Infra-Red (FTIR) spectroscopy.....93
4.6 Micro Raman Spectroscopy (mRs) 95
4.6.1 Application of Raman spectroscopy within the coal industry.....97
4.7 Scanning Electron Microscope (SEM) and Computer Controlled Scanning Electron Microscope (CCSEM) 101
4.8 Chapter summary.....103
CHAPTER 5: EXPERIMENTAL PROCEDURE 104
5.1 Introduction 104
5.2 Geographical overview of the coals studied.....105
5.3 Sample preparation.....106
5.4 Proximate analyses 106
5.5 Ultimate analysis 107
5.6 Forms of sulphur.....108
5.7 Ash fusion temperature (AFT) 108
5.8 X-ray fluorescence (XRF) analyses of coal ash samples 109
5.8.1 Preparation of pellets.....109
5.9 FactSage modelling 110
5.10 Electron Probe X-ray Microanalysis (EPXMA).....110
5.11 Petrographic analyses 113
5.12 Powder X-ray Diffraction (PXRD) analyses.....113
5.13 Fourier Transform Infrared (FTIR) analyses.....114
5.14 Micro-Raman Spectroscopy (mRs) analyses.....115

5.15. Low temperature ashing (LTA) 116
5.16 High temperature ashing (HTA) 117
CHAPTER 6: RESULTS AND DISCUSSION 118
6.1 Introduction 118
6.2 Physico-chemical analyses of raw coals 118
6.2.1 Proximate and ultimate analyses of coals 118
6.2.2 Forms of sulphur 121
6.2.3 Relationship between ash chemistry and mineralogy of coals 122
6.3 Ash classification 127
6.4 Geochemical indicators used to predict slagging and fouling propensities 129
6.4.1 Silicon (Si) ratio 130
6.4.2 Base-acid (B/A) ratio 131
6.4.3 Detrital-authigenic index (DAI) 132
6.4.4 Silica-Alumina ratio 135
6.5 Relationship between ash fusion temperatures (AFT) and coal chemistry 136
6.6 Thermodynamic equilibrium modelling-FACTSAGE 140
6.7 Coal petrographic analyses of raw coals 144
6.7.1 Maceral group analyses 145
6.7.1.1. Inertinite maceral group 146
6.7.1.2 Vitrinite maceral group 148
6.7.1.3 Liptinite maceral group 148
6.7.2 Mineral matter found in South African coals and their mode of occurrence 149
6.7.2.1 Clay minerals 151
6.7.2.2 Quartz 152

6.7.2.3 Carbonates 153
6.7.2.4 Sulphides 154
6.8 Relationship between mineral matter determined by petrographic methods and ash content 158
6.9 Structural analyses of mineral matter in coals 159
6.9.1 X-ray diffraction (XRD) analyses of raw coals 160
6.9.2 X-ray diffraction (XRD) analyses of low temperature ashes 165
6.9.3 X-ray diffraction (XRD) analyses of high temperature ashes 170
6.9.4 Fourier Transform Infra-Red (FTIR) analyses of raw coals 174
6.9.5 Fourier Transform Infra-Red (FTIR) analyses of low and high temperature ashes 178
6.9.6 Micro-Raman spectroscopy (mRs) analyses of raw coals 181
6.9.6.1 Raman spectra of sulphides 182
6.9.6.2 Raman spectra of oxides 185
(ii) Raman spectra of anatase and rutile (TiO_2) 186
6.9.7 Micro-Raman Spectroscopy (mRs) analyses of low temperature ashes 189
6.9.8 Micro-Raman Spectroscopy (mRs) analyses of high temperature ashes 191
6.9.8.1 Raman spectra of TiO_2 polymorphs 191
6.9.8.2 Raman spectra of chromite 192
6.9.8.3 Raman spectra of hematite (Fe_2O_3) 194
6.9.8.4 Raman spectra of phosphates 196
6.9.8.5 Raman spectra of anhydrite 198
6.9.8.6 Raman spectra of unknown white particle 200
6.9.8.7 Raman spectra of mixture of minerals 201
6.10 Single particle analyses (SPA) clustering 203

6.11 Discussion.....214
6.12 Chapter summary.....230
CHAPTER 7: CONCLUSIONS AND RECOMMENDATIONS 235
7.2 Recommendations 240
8. References 242
Appendix A: Ultimate analyses, ash chemistry and forms of sulphur 274
Appendix B: Slagging and fouling indices calculations.....275
Appendix C: Ash fusion temperature 275
Appendix D: Thermodynamic equilibrium modelling-FactSage 7.0 276
Appendix E: Petrographic composition of selected South African coal samples 277
Appendix F: XRD analyses of low temperature and high temperature ashes 278
Appendix G: FTIR analyses of raw coals, low temperature and high temperature ashes 289
Appendix H: micro-Raman analyses of raw coals, low temperature and high temperature ashes 293
Appendix I: SPA-EPXMA analyses of raw coals 296
Publication.....299

List of Figures

Figure 1-1. Acidic, iron-rich water filling a collapsed coal mine [McCarthy and Pretorius, 2009] 12
Figure 1-2: Association of trace elements in coal [Vejahati *et al.*, 2010] 17
Figure 2-1: Map of coal deposition in South Africa [Jeffrey, 2005].....30
Figure 2-2: Coalfield ranking by ROM production [Xmp consulting, 2009] 31
Figure 2-3. Diagrammatic representation of the coal seam stratigraphy and lithology in the main Karoo basin [McCarthy and Pretorius, 2009].....34
Figure 2-4: Stratigraphy of Waterberg coalfield [Wagner and Tlotleng, 2012].....35
Figure 2-5: Forms of main mineral groups in coals: a) silicates, b) pyrite, c) carbonates [Falcon and Snymann, 1986].....46
Figure 2-6: Layered structure of kaolinite showing inter and inner layer hydroxyl groups [Sperinck *et al.*, 2011] 53
Figure 3-1: Ash formation mechanisms during coal combustion [Tomeczek and Palugniok, 2002].....64
Figure 3-2: Fouling deposit on tubes in convective pass [Ma *et al.*, 2007] 71
Figure 3-3: Loose, bound, sintered and melted slag deposits that are typically found in boiler tubes [Hatt, 1990].....74
Figure 3-4: Ash fusion standard method for the determination of fusion behaviour of ashes (following the ISO 540 standard) [Akar and İpekoğlu, 2007].....78
Figure 4-1: Raman spectra of condensed aromatic hydrocarbons [Nakazimo *et al.*, 1974].....99
Figure 4-2: Vibrational modes for single crystal graphite [Wang *et al.*, 1990] 99
Figure 5-1: Experimental work overview.....105
Figure 6-1: Correlation between carbon and ash content. 120
Figure 6-2: Oxides composition and the respective association with mineral matter [Huggins, 2002].....124
Figure 6-3: Ash classification system of investigated samples 128
Figure 6-4: The relationship between ash content and DAI of the four investigated coals 133

Figure 6-5: Relationship between detrital authigenic index and ash content of coal samples. 134
Figure 6-6: Predicted high temperature phases in Coal A using FactSage thermodynamic modelling package.....141
Figure 6-7: Predicted high temperature phases in Coal B using FactSage thermodynamic modelling package.....142
Figure 6-8: Predicted high temperature phases in Coal C using FactSage thermodynamic modelling package.....143
Figure 6-9: Predicted high temperature phases in Coal D using FactSage thermodynamic modelling package.....144
Figure 6-10: Examples of maceral composition in the bituminous South African coal samples; (a) Inertinite-rich with some vitrinite bands; (b) banded semifusinite at bottom, (c) carbonate minerals associated with organic matter (d) Centre: Flocculated clays contained in vitrinite (x500 magnification, oil immersion lens). 145
Figure 6-11: Comparison of inert semifusinite and inertodetrinite concentration in the coal samples.....147
Figure 6-12: Mineral matter in coals as determined by optical microscopy [including organic matter].....151
Figure 6-13: a) Disseminated syngenetic clay minerals b) Epigenetic kaolinite mineral deposited in organic matter (Magnification, X500, oil immersion lens, reflectance microscope).....152
Figure 6-14: a) Authigenetic quartz with internal reflection, b) Rounded quartz and epigenetic pyrite infilling vitrinite structure. (Magnification, X500, oil immersion lens, reflected light).....153
Figure 6-15: a) Carbonate-siderite mineral in inertodetrinite. b) Carbonates in organic matter (Magnification X500, oil immersion lens, reflectance microscope.) 154
Figure 6-16: The different morphologies of pyrite in coals. a) Nodular syngenetic pyrite in vitrinite. b) Epigenetic cleat in-filling; c) Cell in-filling; and d) Pyrite lens in clay-rich particle. (Magnification X500, oil immersion lens, reflected light.).....155

Figure 6-17: Relation between petrographically determined mineral matter and ash content 158
Figure 6-18: XRD diffractograph pattern of raw coal samples collected at room temperature 161
Figure 6-19: Correlation between kaolinite and quartz in raw coal and LTAs determined by XRD.....167
Figure 6-20: Correlation between ash compositions determined by XRD and proximate analyses 170
Figure 6-21: HTA XRD of the different high temperature minerals formed at 815°C. 171
Figure 6-22: Correlation between degree of crystallinity and ash content.....173
Figure 6-23: FTIR spectrum of kaolinite in raw coals within the 500-4000cm^{-1} spectral region. 174
Figure 6-24: FTIR spectrum of high temperature ash of sample B (HTA-B).....179
Figure 6-25: FTIR spectrum of high temperature ash of sample D 180
Figure 6-26: Raman spectra of sulphide minerals found in coal sample B in the wavenumber range 50-1500 cm^{-1} (Micro Raman, excitation 532 nm) 183
Figure 6-27: Raman spectra of quartz as observed using the 532 nm wavelength in the range 500-1500 cm^{-1} (micro-Raman, excitation 532 nm). 186
Figure 6-28: (a)Raman spectra of anatase (top) and (b) rutile (bottom) in the wavenumber range 50-1500 cm^{-1} (Micro Raman, excitation 532 nm), (c) White anatase particles dissiminated in coal A.....187
Figure 6-29: Raman spectra of LTA sample showing the presence of iron sulphate, iron hydroxide and calcium sulphate.....189
Figure 6-30: Raman spectra of a mixture of brookite, anatase, and rutile in HTA- D 191
Figure 6-31: Raman spectra of chromite found in HTA-D 193
Figure 6-32: Raman spectra of hematite in high temperature ash.....195
Figure 6-33: Raman spectrum of apatite as observed in high temperature coal ashes 197

Figure 6-34: The Raman spectra of anhydrite mineral (i) and (ii) a mixture of anhydrite, hematite and gypsum in coal 198
Figure 6-35: Raman spectra of an unknown white mineral particle identified in coal B 201
Figure 6-36: Discard coal, anatase associated with quartz in high ash coals (sample C). 201
Figure 6-37: Raman spectra of a mixture of anhydrite and aragonite 202
Figure 6-38: Raman spectra of HTA sample showing a mixture of anatase, quartz, nephaline, apatite, and crednerite 203
Figure 6-39: Elemental composition of raw coal samples 205
Figure 6-40: Rotated component matrix clustering of mineral matter in coal A 208
Figure 6-41: Rotated component matrix clustering of mineral matter in coal B.....209
Figure 6-42: SPA clustering of mineral matter in coal using chemical boundary classification method 211
Figure F-1: As measured diffraction pattern of HTA-A. 281
Figure F-2: Background subtracted diffraction pattern of HTA-A overlaid with stick pattern of the proposed phases 281
Figure F-3: As measured diffraction pattern of HTA-B.....282
Figure F-4: Background subtracted diffraction pattern of HTA-B overlaid with stick pattern of the proposed phases 283
Figure F-5: As measured diffraction pattern of HTA-C.....285
Figure F-6: Background subtracted diffraction pattern of HTA-C overlaid with stick pattern of the proposed phases 284
Figure F-7: As measured diffraction pattern of HTA-D 285
Figure F-8: Background subtracted diffraction pattern of HTA-D overlaid with stick pattern of the proposed phases 288
Figure G-1: FTIR spectra of LTA-A 289
Figure G-2: FTIR spectra of LTA-B 289
Figure G-3: FTIR spectra of LTA-C 290
Figure G-4: FTIR spectra of LTA-D 290

Figure G-5: FTIR spectra of HTA-A.....291
Figure G-6: FTIR spectra of HTA-B.....291
Figure G-7: FTIR spectra of HTA-C.....292
Figure G-8: FTIR spectra of HTA-D.....292
Figure H-1: Raman spectra of jarosite observed in coal B, in the 50-1500 cm^{-1} range (Micro Raman, excitation 532 nm). 293
Figure H-2: Raman spectra of a mixture of anatase, quartz, nepheline, apatite, and crednerite in HTA in the 50-1500 cm^{-1} range (Micro Raman, excitation 532 nm)..293
Figure H-3: Raman spectra of a mixture of anatase, rutile and brookite in HTA-D in the 50-1500 cm^{-1} range (Micro Raman, excitation 532 nm). 294
Figure H-4: Raman spectra of a mixture of anatase, rutile, anhydrite in HTA-B in the 50-1500 cm^{-1} range (Micro Raman, excitation 532 nm). 294
Figure H-5: Raman spectra of a mixture of anatase and rutile in HTA-D in the 50-1500 cm^{-1} range (Micro Raman, excitation 532 nm). 295

List of Tables

Table 2-1: Lithostratigraphy of the Karoo sequence in the main basin and inferred climate conditions [Snyman and Botha, 1993].....29
Table 2-2:Typical analyses of raw coal for coalfields on the Karoo basin [Cairncross, 2001].....37
Table 2-3: Macerals and group macerals recognised in hard coals [McCabe, 1984].41
Table 2-4: Probable mode of occurrence of selected elements [Finkelman, 1982] ...49
Table 2-5: Major minerals identified by various authors in bituminous coals as summarised by Ward (1989). 51
Table 3-1: Differential thermal analysis (DTA) data for minerals occurring in coals-determined under a nitrogen atmosphere [O'Gorman and Walker, 1973].....66
Table 3-2: Summary of key empirical correlations for slagging and fouling [Raask, 1985].....76
Table 4-1: Mineral groups identified in Raman spectroscopy 100
Table 5-1: Characterisation methods conducted on raw and ash samples. 104
Table 6-1: Proximate, ultimate analyses and forms of sulphur (wt.%) of selected South African coals (air dry basis) 104
Table 6-2: Nominal ash oxide analyses of major and minor elements as determined by XRF 123
Table 6-3: Ash deposition, slagging and fouling predictive indices of the investigated coals.....130
Table 6-4: Ash fusion temperatures of the investigated coal samples 136
Table 6-5: Petrographic composition of macerals in South African coals (vol. %) mmf basis.....146
Table 6-6: Mineral matter composition in volume percent (organic matter free basis) of coal samples determined by petrographic point counting method.....150
Table 6-7: Detailed analyses of mineral matter of the investigated samples (Vol. %) showing the mode of occurrence in coals.....156

Table 6-8: Quantitative crystalline mineral matter composition for the coal samples after normative calculations based on XRD identification. Concentrations are expressed in weight %. 162
Table 6-9: Mineralogy and ash composition of LTA samples based on XRD Siroquant analyses (wt. %) 166
Table 6-10: Clay mineralogy of fractions less than 2 µm from oriented aggregate XRD analysis of low temperature ash samples 166
Table 6-11: Inferred ash chemistry based on Siroquant data 169
Table 6-12: X-ray diffraction (XRD) phases of high temperature ashes 170
Table 6-13: A summary of FTIR band position (cm^{-1}) identified in raw coals and theoretical kaolinite and muscovite [Saikai and Parthasarathy, 2010]. 175
Table 6-14: Peak position (cm^{-1}) of vibrational modes of pure anatase and mineral matter in coal ashes [Mahdjoub *et al.,* 2010; Yin *et al.,* 2017]. 188
Table 6-15: Assignment of rutile spectra obtained from coal samples 188
Table 6-16: Raman peaks of brookite in HTA-D 192
Table 6-17: Raman peaks (cm^{-1}) and assignment for $FeCr_2O_4$ spinel structure 194
Table 6-18: Raman shift and assignment of hematite found in high temperature coal ashes [de Farai *et al.,* 1997; Jubb and Allen, 2010]. 196
Table 6-19: Phosphate and hydroxyl vibration modes in apatitic [Penel *et al.,* 1997] and HTA-A sample 198
Table 6-20: Anhydrite Raman band position (cm^{-1}) in HTA-B 199
Table 6-21: Raman peak position of a mixture of hematite and anhydrite [Yin *et al.,* 2017] 200
Table 6-22: Elemental abundance in raw coal samples 205
Table 6-23: Varimax rotated component matrix of SPA data 207
Table 6-24: Clustering of different mineral matter using chemical composition and phase boundaries (Kandler *et al.,* 2007) 210
Table 6-25: Minor groups of silicate minerals in raw coal samples 212
Table 6-26: Mineral matter identified in raw South African coals 223
Table 6-27: Mineral matter identified in low temperature ashes 224

Table 6-28: Mineral matter identified in high temperature ashes 226
Table 6-29: Summary of the different techniques.....234
Table A-1 shows the ultimate, ash analysis, forms of sulphur of four coals samples submitted at the ALS laboratories in Witbank. 274
Table C-1: Ash fusion temperature of SA coals.....275
Table D-1: Thermodynamic modelling data coal A.....276
Table D-2: Thermodynamic modelling data coal B.....276
Table D-3: Thermodynamic modelling data coal C.....276
Table D-4: Thermodynamic modelling data coal D.....276
Table E-1: Maceral group and mineral matter analyses (presented as a percentage of total sample point counts) of four South African coals calculated on a mineral matter free (mmf.) and including mineral matter. 277
Table F-1: X-ray diffraction (XRD) analyses of LTA-A (48.7 wt. %) 279
Table F-2: X-ray diffraction (XRD) analyses of LTA-B (31.6 wt. %) 279
Table F-3: X-ray diffraction (XRD) analyses of LTA-C (77.9 wt. %) 279
Table F-4: X-ray diffraction (XRD) analyses of LTA-D (24.1 wt. %) 279
Table F-5: Mineralogy of < 2 μm fraction (wt.%) in low temperature ash samples by oriented-aggregate XRD analysis.....279
Table I-1: Single particle analysis (SPA)-elemental abundance in raw coals (mol.%) 296
Table I-2: Component matrix extraction loading.....297
Table I-3: Chemical boundary classification (CBC) mineral composition in raw coals (mol.%).....298

List of Acronyms, Abbreviations and Symbols

Air pollution control devices	APCD
American Society for Testing and Materials	ASTM
Atomic absorption spectroscopy	AAS
Atomic emission spectroscopy	AES
Acid mine drainage	AMD
Accentuated total reflectance	ATR
Ash fusion temperature	AFT
Automated Image Analyzer	AIA
Backscattered electrons	BSE
Charge couple device	CCD
Chemical boundary conditions	CBC
Clean coal technology	CCT
Coal to liquid	CTL
Commonwealth Scientific and Industrial Research Organization	CSIRO
Computer Controlled Scanning Electron Microscope	CCSEM
Clean Air Act Amendments	CAAA
Circulating fluidised bed combustion	CFBC
Computational fluid dynamics	CFD
Council of Geosciences	CGS
Detrital authigenic index	DAI
Differential thermal analysis	DTA
Diffuse Reflectance Infrared Fourier Transform	DRIFT
Energy dispersive X-ray	EDX
Electric Power Research Institute	EPRI
Electron probe X-ray micro-analyser	EPXMA
Electrostatic precipitators	ESP
Energy dispersive X-ray fluorescence spectrometer	EDXRF
European Union	EU
Fabric filters	FF
Factor analysis	FA
Flue gas scrubbers	FGS

Fourier Transform Infrared Spectroscopy	FTIR
Greenhouse gas	GHG
Hazardous air pollutants	HAPs
Hemispherical temperature	HT
Hierarchical cluster analysis	HCA
High temperature ashing	HTA
High temperature fouling	HTF
International Committee for Coal and Organic Petrology	ICCP
Inductively coupled plasma	ICP
Inductively coupled plasma-atomic emission spectroscopy	ICP-AES
Inductively coupled plasma-mass spectroscopy	ICP-MS
Inductively coupled plasma optical emission spectroscopy	ICP-OES
Initial deformation temperature	IDT
Intergrated gasification combined cycle	IGCC
Instrumental neutron activation analysis	INAA
Infrared	IR
International Organization of Standardization	ISO
King-Marie-Crossley	KMC
Low temperature ashing	LTA
Low temperature fouling	LTF
Mass spectroscopy	MS
Micro-Raman spectroscopy	mRs
Mid Infrared	MIR
Mineral matter free	mmf
Net neutralizing potential	NNP
Neutron activation	NA
Non-hierarchical clustering analysis	NHCA
Organic sulphur	S_{org}
Oxy-fuel circulating fluidised bed combustion	OFCFBC
Oxy-fuel coal combustion	OFCC
Particulate matter	PM
Parts per billion	ppb

Parts per million	ppm
Principal component analysis	PCA
Pressurised fluidised bed combustion	PFBC
Pyritic sulphur	S_{pyr}
Quantitative mineral analysis	QMA
Quantitative evaluation of minerals by scanning electron microscope	QEMSCAN
Run of mine	ROM
Scanning Electron Microscope	SEM
Single particle analysis	SPA
Softening temperature	ST
South Africa	SA
South African Bureau of Standards	SABS
Supercritical pulverised coal combustion	SCPCC
Trace elements	TEs
Transmission electron microscope	TEM
Ultra Clean Coals	UCCs
United Nations Framework Convention on Climate Change	UFCCC
Volatile organic compounds	VOCs
Wavelength dispersive spectrometry	WDS
Wavelength dispersive X-ray fluorescence	WDXRF
X-ray absorption fine structure	XAFS
X-ray diffraction	XRD
X-ray fluorescence	XRF
Yancey, Geer, and Price	YGP
Absorbance	A
Amplitude	E_o
Degrees celsius	$^{\circ}C$
Depth of penetration	d_p
Frequency of light	v_o
Gram	g
Kilometer	km
Wavelength of radiation	λ

Mega Watt	MW
Metre	m
Micrometer	μm
Millimetre	mm
Nanometer	nm
Pi	π
Refractive index	n_1
Regression	R
Second	s
Theta	θ
Transmittance	T
Volume percentage	Vol.%
Wavenumber	cm^{-1}
Weight percentage	Wt.%
Beta	β
Gamma	γ

CHAPTER 1: INTRODUCTORY CHAPTER

1.1 Introduction

The introductory chapter gives insight on the background of the study, highlighting key areas that influenced the conceptualisation of this research investigation. This chapter also gives a brief overview of the research study; it introduces the hypothesis, research questions, aims, and objectives of the investigation. The last section of the chapter gives the breakdown, layout and scope of the research work.

1.2 Background

Energy generation using fossil fuels is in a global crisis, with the local coal industry facing challenges to meet soaring energy demands that are fuelled by economic growth, and industrialisation of the developing nations [Rubiera *et al.,* 2002]. In South Africa (SA), the steadily increasing energy demand is projected to increase at a rate of 1000 MW per annum [Engelbrecht *et al.,* 2008]. However, with the aging power generation fleet, and the low power plant efficiencies that are below 40%, it is becoming almost impossible to meet the required energy demands.

In an attempt to curb electricity shortages, Eskom embarked on expanding the capacity of its existing power generation fleet by building new power stations (Medupi and Kusile), with a nominal capacity of 4800 MW. The newly built power plants are designed to operate at supercritical conditions to improve plant efficiencies, and reduce CO_2 emissions by nearly 22%.

Another probable solution aimed at increasing power plant efficiencies, and reducing CO_2 emissions, is based on using renewable resources (biomass) derived from various sources such as sewage sludge, bio-solids, woody plants, municipal green waste, forestry, agricultural, and organic waste by-products [Tchapda and Pisupati, 2014]. It is anticipated that the renewable energy sources will become increasingly important [Buhre *et al.,* 2005] and supplement the declining fossil fuel resource. The inclination towards using renewable resources has led to a steady increase in funds estimated at $4.8 billion, to conduct feasibility studies of introducing renewable energy in SA [Baker, 2015].

Strydom *et al.* (2015) investigated the influence of biomass such as hardwood, softwood, and pinewood chips (supplied by Sappi forest division, SA), and sugarcane bagasse (supplied by TSB sugar company, SA) on the co-pyrolysis of medium rank C South African coal. The results of the investigation indicated that co-pyrolysis of the different coals blended with biomass showed a slight improvement on the pyrolysis rate of medium rank bituminous coals.

Moreover, the realisation of the practical application of using biomass can be noted with the recent increases in the number of European countries that are adopting co-firing processes. The biomass-coal ratio is expected to increase from the current 20 wt. % to 30 wt. % in utility boilers [Izquierdo *et al.,* 2008], particularly in countries (Belgium, The Netherlands, UK, Spain, Italy, Poland) where co-firing of biomass in coal-fired power plants is subsidised by governments. It has also been estimated that the use of biomass will contribute 17% towards total energy generation by 2020 [Scarlat *et al.,* 2015].

Despite the attractive benefits of co-firing with biomass, which include among other benefits, the reduction of greenhouse gas (GHG) emissions, there are technological problems related with biomass-firing technologies.

The alkali and alkali earth inorganic compounds (K_2O, Na_2O, CaO, and Cl) found in biomass are known to cause operational problems such as slagging, fouling, and corrosion on super heater tubes, reactors, furnaces, turbines, and emission control devices [Demirbas, 2005; Nutalapi *et al.*, 2007].

Slagging and fouling reduces heat transfer of combustor surfaces, whilst corrosion and erosion reduce the lifespan of equipment [Demirbas, 2005]. However, this challenge can be controlled by using water leaching pre-treatment to removes water soluble ions such as Na, K, Ca, Mg, and Cl, subsequently improving ash fusion temperatures, and slagging, fouling and corrosion conditions [Arvelakis *et al.*, 2001, Liu and Bi 2011].

Although there are few viable energy source alternatives (biomass, nuclear, and solar) other than fossil fuels, it is predicted that these energy sources will not completely replace fossil fuels. Therefore, coal will remain the primary source of energy for a foreseeable future [Buhre *et al.*, 2005], primarily because coal is abundant and relatively cheap compared to other energy source alternatives.

While coal usage is still relevant and important, the challenges related to coal quality remain valid and therefore need to be addressed. Detailed coal quality and holistic coal characterisation is critical in predicting coal behaviour, particularly its influence on technological performance, health impact, and the environment [Reyes *et al.*, 2003; Oliviera *et al.*, 2011]. Therefore, a comprehensive investigation of mineral matter should encompass and identify minerals of economic value and minerals that may have a negative effect during coal exploration, processing, and subsequent saleability and applicability of coals.

Unfortunately, the coal resources are becoming depleted, and the grade is becoming low and poorer on a global scale. In SA, high grade coal from Witbank-Highveld coalfields are decreasing, and the extraction of the remaining coal is becoming challenging to access due to difficult mining conditions [Jeffrey, 2005]. The decline in coal reserves was also reported in the recent evaluations conducted by the Council of Geosciences (CGS) [Hartnardy, 2010].

As the low grade coals dominate the markets, coal users are compelled to pursue benign innovative solutions by using advanced characterisation techniques, and burning coal efficiently using clean coal technology (CCT) processes such as: integrated gasification combined cycle (IGCC), pressurised fluidised bed combustion (PFBC) or alternatively, retrofit the current pulverised fuel combustion processes with low NO_x burners and flue gas desulphurisation technologies, and also underground coal gasification(UCG) processes.

The new technologies are designed to minimise greenhouse gas emissions, and allow for capture and sequestration of CO_2 gas [Buhre *et al.*, 2005]. However, it is to be acknowledged that not all CCTs will be applicable and suitable to the South African context, mainly because of the difference in the quality and mineralogical structure of the local coal, to that of the northern hemisphere coals.

The challenge presented by low grade coals is often related to the abundance and composition of mineral matter, which negatively influences the potential end use of coal. Over $1.2 billion are lost annually in coal utilisation processes [Harding and Connor, 2007; Nayak, 2013] due to slagging, fouling, erosion and plant shutdowns [Oliviera *et al.*, 2011].

Several well documented studies [Gupta *et al.,* 1999; Pinetown *et al.,* 2007; Swaine, 2000; Wells *et al.,* 2004; Wells *et al.,* 2005; Hai-tao *et al.,* 2015] have shown that problems related to mineral matter are pronounced at various processing stages that includes mining activities, beneficiation, conversion (i.e. combustion, pyrolysis, gasification, and liquefaction), and emissions of gases (NOx, SOx, CO_2), trace elements (TEs), and particulate matter (PM) into the environment [Özbayoğlu and Özbayoğlu, 2006].

With coal quality at the centre stage of improving coal conversion processes, it is understood that detailed and comprehensive information derived from mineral matter, but not exclusively, such as the nature, amount, and the mode of occurrence of mineral matter in coals is becoming increasingly necessary in various coal conversion processes that use coal as the heterogeneous feedstock [Babat *et al.,* 2011; Matjie *et al.,* 2011; Oliviera *et al.,* 2011; Soundarrajan *et al.,* 2012].

With the developments in various studies conducted on coal mineral matter, it has been acknowledged that detailed knowledge about mineral matter and its association in coals is fundamental and crucial in addressing the underlying challenges presented by mineral matter mining, transportation, pyrolysis, gasification, liquefaction, combustion and pollution [Liu *et al.,* 2005; Saikia and Ninomiya, 2011; Matjie *et al.,* 2011; Matjie *et al.,* 2016; Vassilev and Tascón, 2003].

The success of addressing complex issues presented by the heterogeneous nature of coal depends mainly on the correct choice of advanced characterisation methods, for both qualitative and quantitative analyses of mineral matter. For these reasons, adequate understanding of coal geochemistry, chemical composition, association, and abundance of mineral matter using multidisciplinary techniques provides insight, with less ambiguity on the suitability of a specific type of coal, in various coal conversion processes.

As such, consideration is to be given to the selection and suitability of characterisation methods employed, so that useful information can be derived to influence decision making regarding unit designs, and the optimisation of production rate.

Studies in literature have shown that interest in understanding mineral matter has been on the rise since the early 1960's, when some of the first publications were made available. Early work of mineral matter in coals involved studies on the occurrence and distribution of mineral matter in Australian coals [Kemezys and Taylor, 1964]. Similar studies were conducted by Garcia-Vallès *et al.* (1993), Kimura (1998); Ward *et al.* (1999), and Ward (2002).

Spears (1987) studied the origin, composition and mode of occurrence of mineral matter in coals from East Pennine and Midlands coalfields, whilst other studies focused on the behaviour and impact of various mineral matter on coal conversion processes [Shirazi *et al.,* 1995; Gupta *et al.,* 2006; Matjie *et al.,* 2011; Soundarrajan *et al.,* 2012].

The work described in this thesis involves a detailed investigation of a combination of characterisation techniques that will be used to determine the character and nature of mineral matter in coals, to add on the understanding and knowledge of mineral matter in SA coals, and to possibly help predict coal behaviour and their impact on combustion performance.

This research work will focus on using traditional physico-chemical analyses, single particle analyses with electron probe micro X-ray analyses (SPA-EPXMA), coal petrography, X-ray diffraction (XRD), and spectroscopic techniques such as Fourier Transform Infrared (FTIR) and micro-Raman spectroscopy (mRs), to characterise mineral matter in coals.

A more robust approach to determine elemental composition of major and minor elements can be obtained by employing SPA-EPXMA methods. The SPA-EPXMA method allows for very small particles (< 1 μm) to be analysed individually. The analysis of single particles is well established within environmental studies, which involve characterisation of PM [Jambers *et al.*, 1997; Stefaniak *et al.*, 2009; Jung *et al.*, 2014]. The use of SPA-EPXMA is adopted in this study to determine composition and the mode of occurrence of mineral matter in coal samples. The FTIR and mRS are complementary techniques, and they will be used to analyse raw coals and coal ashes. The use of these techniques is to address among other reasons, the shortcomings presented by XRD and related traditional methods.

1.3 Coal overview and challenges presented by mineral matter in coal conversion processes

Coal remains the primary, most abundant, inexpensive energy source (compared to gas, oil, and alternatives such as nuclear power, wind, biomass and solar energy) used for power generation worldwide. The available coal resources are supplying an estimated 42% of the total global energy sector [Speight, 2013], with an estimated 245 million tonnes of coal produced annually from South African coalfields. SA is ranked the 7th largest producer of coal in the world [Hancox and Götz, 2014], with economical reserves of approximately 55 billion tonnes. The available economical reserves are expected to last a foreseeable 40-50 years at the current consumption rate.

Coals produced in SA are utilised by various industries, with the electricity generating sector being the major consumer. An estimated 46% of the annual coal produced in SA, is utilised by Eskom for the production of electricity in coal-fired thermal power plants designed specifically to handle South African low grade coals.

The Eskom power plants have a total nominal capacity of 42011 MW, and a net maximum capacity of 36208 MW, making Eskom the third largest company in the world producing electricity from coal [Steyn and Minnit, 2010].

About 26% of coal produced in SA is exported to various countries including Europe, South America, China and India; 18% of the coal is consumed by the coal to liquid (CTL) synthetic fuels conversion process via gasification process (SASOL); and only 9% of the total coal produced is utilised by the metallurgical industry, for making coking coal. The coking coal is used as a reducing agent in the production of metals such as titanium, ferrochrome, ferromanganese, and steel. Only a small percentage of coal is used for domestic purposes [Hancox and Götz, 2014].

Every sector that consumes coal has different specifications in terms of coal quality, thermal characteristics, particle size, compositional make up, and physical properties. The coal fed into South African boilers and gasifiers is typically a low grade high volatile bituminous coal. The typical specifications are high ash content of approximately 20-33 wt. %, and a calorific value between 20-23 MJ/kg [Snyman and Botha, 1993; Steyn and Minnitt, 2010; Matjie *et al.*, 2011]. However, the use of low grade coal, the nature of mineral matter; its composition, mode of occurrence, association, particle size, and operating conditions may present serious technological and environmental challenges in coal conversion processes if not correctly understood [Wee *et al.*, 2005; Steyn and Minnitt, 2010; Matjie *et al.*, 2011; Matjie *et al.*, 2016].

Numerous studies have shown that challenges related to mineral matter are pronounced at various stages of coal processing, from mining activities, which involves beneficiation problems such as grindability characteristics and washability, heat transfer and efficiencies in conversion processes, and lastly emission of toxic gases (SO_x, NO_x, CO_2) and particulate matter (PM) into the environment [Gupta *et al.,* 1999; Özbayoğlu and Özbayoğlu, 2006]. For example, the presence of pyrite mineral in coal leads to the acid mine drainage (AMD) phenomenon. Hard minerals such as pyrite and quartz, with high Mohr's index cause abrasion and wear on milling equipment. High ash content leads to operational problems such as slagging, fouling, corrosion, and erosion [Raask, 1985]. It is therefore apparent that the effect and impact of mineral matter in coal conversion processes remain quite significant.

Some of the challenges highlighted will be briefly discussed in subsequent sections. The major areas that are addressed but are not within the scope of this research work include challenges and negative impact of coal activities that leads to the formation of AMD. A more detailed discussion on the subject of the effect of mineral matter on coal combustion (i.e. slagging and fouling) is addressed in Chapter 3.

1.3.1 Acid mine drainage (AMD)

It is generally considered that a prominent environmental problem associated with mineral matter and coal mining activities is the generation and production of the controversial AMD phenomenon. Therefore, the AMD phenomenon is a crucial subject around the world and particularly in a water stressed country such as SA.

The AMD is a waterborne contaminant that is formed as a result of the removal of the overburden rock, leaving behind sulphide minerals such as pyrite exposed to oxidation [McCarthy, 2011]. The AMD problem has raised concerns over the long term effect the coal mining industry will have, most especially over the future prospects and coal mining activities around the Waterberg coalfield, which is being explored for future supply of coal to the new Eskom power stations.

Hill and Bates [1979] investigated the effect of increasing coal usage, and its impact on AMD. From the study it was found that different morphological structure of pyrite minerals oxidised differently. According to the results, it was found that crystalline pyrite was less susceptible to weathering and oxidation, compared to amorphous pyrite. Therefore, the amount and rate at which the acid is formed depend on the type of pyrite found in the overburden rock. Other factors that influence the amount and rate of acid formation include [Silva *et al.*, 2012]:

(i) the rate of oxidation,

(ii) the amount of available water,

(iii) oxygen concentration, and

(iv) the microbial population, (oxidising ferrooxidans).

The formation of AMD is an intensively investigated process that follows a complex series of reactions as illustrated by Equations 1-1 to 1-4 [Ríos *et al.*, 2008, McCarthy, 2011; Silva *et al.*, 2013].

$$FeS_2 + 3.5O_2 + H_2O \rightarrow Fe^{2+} + 2SO_4^{2-} + 2H^+ \quad Equation\ 1-1$$

$$4Fe^{2+} + O_2 + 4H^+ \rightarrow 4Fe^{3+} + 2H_2O \quad Equation\ 1-2$$

$$4Fe^{3+} + 12H_2O \rightarrow 4Fe(OH_3)(s) + 12H^+ \quad Equation\ 1-3$$

$$FeS_2 + 14Fe^{3+} + 8H_2O \rightarrow 15Fe^{2+} + 2SO_4^{2-} + 16H^+ \quad Equation\ 1-4$$

The reactions described in Equations 1-1 to 1-4 show that pyrite undergoes oxidation following a two-stage process. The first stage produces sulphuric acid and ferrous sulphate. The second stage produces ferric hydroxide from oxidation of Fe^{2+} ions, and more sulphuric acid, as described by Equation 1-2 [McCarthy, 2011]. In the third reaction described in Equation 1-3, Fe^{3+} (ferric hydroxide) is hydrolyzed by water at pH above 3.5, forming ferric hydroxide precipitates such as ferrihydrite, goethite, jarosite, lepidocrocite, and more acid. The last Equation 1-4, shows a further oxidation process of FeS_2 by Fe^{3+}. A successful oxidation process of FeS_2 is dependent on the presence of bacterial species, particularly the *acidithiobacillus ferroxidans*, whose growth rate is pH dependent. Although the formation of AMD follows the sequence of reactions described in Equations 1-1 to 1-4, it is important to note that there are other factors such as the geology of the environment, which significantly contribute to the amount of acid formation. However these vary substantially from one region to the next.

In an acidic environment of pH below 3, the AMD phenomenon leads to an increase in the mobility and solubilisation of toxic heavy metals such as Fe^{3+}, Al^{3+}, Cr^{2+}, Cu^{2+}, Zn^{2+}, Cd^{2+}, Pb^{2+}, and Mn^{2+} found in the surrounding rocks, and metal ions associated with pyrite [Willscher *et al.,* 2007]. The accumulation of non-biodegradable heavy metals in the environment has a detrimental effect on humans and the ecological systems [Chen *et al.,* 2014]. The overall effect of the AMD phenomenon results in the depletion of oxygen in water solutions, and heavy metals contamination of domestic, aquatic, and industrial water.

The major source of AMD in SA is from drainage of underground mine shafts, runoff mines, discharge from open pit mines, waste dumps, tailings, and ore stockpiles [Potgieter, 2010]. AMD is a major concern, particularly within the Witwatersrand area, and around several coalfields that are either still operational or abandoned around the Witbank coal mines [Geldenhuis, and Bell, 1998; McCarthy, 2011; Moyo *et al.,* 2011]. Water contamination around the Loskop dam and Olifants River, is also linked to the AMD phenomenon [McCarthy, 2011; Moyo *et al.,* 2011].

A case study by Geldenhuis and Bell (1998) found that AMD at the Loubert mine (Mpumalanga province) was emanating from an old backfilled open cast mine, and Figure 1-1 shows acidic water that formed due to high concentrations of iron that was emanating from a collapsed mine [McCarthy and Pretorius, 2009].

Figure 1-1. Acidic, iron-rich water filling a collapsed coal mine [McCarthy and Pretorius, 2009]

Dams around the Middelburg and Witbank area in SA are experiencing ever increasing concentrations of heavy metals such as iron, manganese, and aluminium. The oxidation of these heavy metal leads to a reduction in pH levels of water to 3.7, resulting in toxic water that has serious biological effects [McCarthy and Humphries, 2013].

It has been reported that the sulphate concentration in Witbank dam exceeds 200 mg/L, which is above the recommended maximum concentration allowed in domestic water [McCarthy, 2011].

The mode of occurrence and association of mineral matter in coal provides crucial information that helps understand the formation of AMD. Pinetown *et al.* (2007) investigated the quantitative distribution of minerals and their potential impact on AMD of coals from Witbank and Highveld coalfields.

Low temperature ashing (LTA) and high temperature ashing (HTA) samples were prepared and studied to evaluate the distribution of mineral matter in coals. The net neutralizing potential (NNP) acid-base accounting method was adopted and used as a screening criterion to quantify the potential impact of AMD on the two coalfields. According to the study, it was found that the No. 4 upper and No.5 coal seams had the potential to cause AMD.

Other future impacts of AMD in SA include the deterioration of water quality of the Olifant's River, which may be fueled by unmined coalfields around the Olifant's catchments [McCarthy, 2011]. The longer term impact of AMD, particularly by the coal mining industry is expected to create severe damage in SA more than any other countries. It is understood that the problem will be aggravated by the geography, climate, population distribution and the scale of coal deposits found in SA [McCarthy, 2011].

1.3.2 Emissions from coal utilisation processes

Coal fired power plants are the major consumers of coal, and the major contributors of gaseous emissions, which have deleterious implications towards human health and the environment. The effect of gaseous emissions from coal combustion has seen most countries, including developing nations, setting stringent environmental laws and regulations to reduce gaseous emissions. The greenhouse gas emissions are enforced by the Kyoto Protocol, which was adopted in Kyoto, Japan in December 1997 at the United Nations Framework Convention on Climate Change (UFCCC). The global reduction targets were set at 5% below the 1990 levels, and this were to be achieved during the 2008-2012 period [Thitakamol *et al.*, 2007].

The amount of CO_2 emitted from coal fired power plants in SA were estimated at 340 Mt in 2006, making SA the 15th largest emitter of CO_2 globally [McCarthy and Humphries, 2013]. Other emissions include carbon monoxide (CO), sulphur oxides (SO_x), nitrogen oxides (NO_x), ash, particulate matter (PM), volatile organic compounds (VOCs), and trace elements (TEs). These emissions are associated with mineral matter rather that their maceral counterparts [Liu *et al.*, 2005].

During the pyrolysis stage, nitrogen present in coal volatilises and form compounds such as tar-N, HCN, NH_3, and N_2. The N-compounds formed release the three forms of nitrogen oxide, (NO, NO_2, and N_2O). The conversion of N-compounds to NO is dependent on coal rank [Wang *et al.*, 1994], and NO is the dominant form of NO_x released into the environment. The work by Hindmarsh *et al.* (1994) indicated that semifusinite tends to release more NO gas compared to other sub-group macerals. The adverse effect of the release of NO_x is the subsequent formation of acid rain, which is harmful to the environment.

Coal fired power plants are also the major producer of anthropogenic VOCs. The emitted VOCs account for approximately 37% of total anthropogenic emissions. Moreover, VOCs can easily react with NOx, forming photochemical smog, in the presence of strong sunlight, low wind and low humidity [Fernández-Martínez *et al.*, 2001].

1.3.2.1 Particulate matter (PM)

Particulate matter (PM) is a complex air pollutant, made up of a complex mixture of extremely small solid and liquid droplets of acids, organic chemicals, metals, soil or dust particles [United States Environmental Protection Agency, 2010]. Pulverised coal combustion is one of the major sources of PM found in the atmosphere [Ninomiya *et al.*, 2004].

Coal rank, type, particle size, oxygen content and mineral matter are some of the factors that determine the emission of PM into the environment [Wang *et al.*, 2008]. During coal combustion, PM is released into the environment in the form of dust or ash particles [Zhang *et al.*, 2006] causing adverse toxicological effects such as cardiovascular and respiratory diseases on human health [Schwartz *et al.*, 1996]. The deposition of PM into the lung system can cause respiratory ailments, chronic bronchitis, and fatal premature death [Hanapi and Dai, 2012].

Ninomiya *et al.* (2004) investigated the influence of particle size on PM emissions. The test was conducted in a constant environment, whilst the particle size of coals was varied. The findings showed that a decrease in particle size of coal led to an increase in the generation of fine PM_{10} (particle diameter less than 10 μm), $PM_{2.5}$ (particle size of 2.5 μm or less) and PM_1 (particles size of less than 1 μm).

The PM has a high probability of escaping without being captured by air pollution control devices (APCD). The APCDs such as electrostatic precipitators (ESP) and fabric filters are generally installed in power plants worldwide to control and reduce the amount of PM emissions emitted into the environment. An ESP operates by directing PM (<30 μm) in the flue gas onto electrically charged metal plates, whilst fabric filters (FF) collect PM by passing flue gas through a porous membrane. The collection efficiency of an ESP decreases with increasing particle size. The FF on the other hand is superior at controlling PM, and once the filter cake has formed, the efficiencies may reach 100% [Sager, 2013]. Both the ESP and FF are used in SA coal-fired power stations to control emissions [Dabrowski *et al.,* 2008].

1.3.2.2 Trace elements (TEs)

Coal contains potential toxic elements released into the environment via coal combustion processes. The toxic elements released into the environment via bottom ash, fly ash, or flue gas effluent streams are responsible for air, water, and soil contamination. However, it is important to note that the characteristics and composition of bottom ash and fly ash depends largely on the feed coal, and the combustion process.

Fly ash is an inorganic solid waste material made up of micro-sized, translucent spherical particles which consists mainly of alumina, silica, iron oxides, and unburnt carbon, with traces of hazardous elements such as As, Pb, Ba, and Hg. TEs concentrated in the fly ash and flue gasses are released through stacks, and frequently escape without being captured by the cleaning systems such as the ESP and scrubbers. Moreover, the ESPs display poor efficiency in removing Hg from flue gas, with only 30% removal efficiency of Hg. However, the wet flue gas scrubbers (FGCs) conditioning system used to remove SO_2, and NO gases together with FF have been successful in addressing Hg emissions into the environment [Dabrowski *et al.,* 2008].

In order to protect the environment, a number of regulations such as the clean air act, were adopted. These regulations have led to ongoing research related to the association of TEs in coal and fly ash. There is a wealth of research studies that focused on determining the mode of occurrence of TE in coals [Raask, 1985; Finkelman, 1994; Diehl *et al.*, 2004; Vejahati *et al.*, 2010; Riley *et al.*, 2012], and the studies showed that TEs are associated with both the organic and mineral matter in coals.

Trace elements associated with maceral matter are either organically bound, ionically bound or soluble in maceral pore moisture. The organically bound TEs are covalently or ionically bound to the organic matter as carboxylic acids, phenolic hydroxyl, mercapto, or imino groups. Carboxylic association of TEs in coal is common in brown coals and lignite coals [Gluskoter *et al.*, 1977; Swaine, 1992; Clarke, 1993; Laumb *et al.*, 2008], with a high concentrations of TEs associated with vitrinite maceral group. Figure 1-2 shows the association of TEs in coal, as described by Vejahati *et al.* (2010).

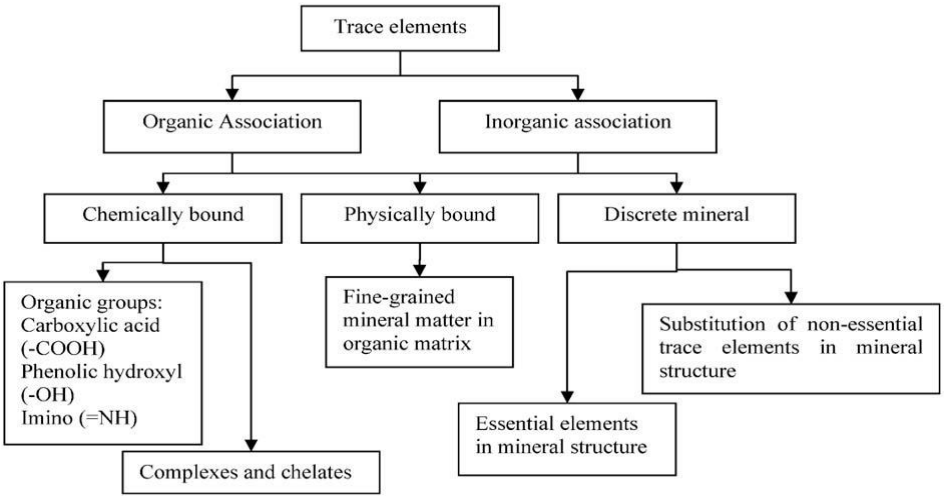

Figure 1-2: Association of trace elements in coal [Vejahati *et al.*, 2010]

The majority of TEs are associated with mineral matter, present either as discrete minerals, replacement ions in minerals, or adsorbed on mineral particles. Pyrite, kaolinite, and illite are the major minerals associated with TEs in coals [Davidson, 1996]. Heavy metal impurities such as lead (Pb), arsenic (As) and mercury (Hg) are hosted primarily in pyrite and marcasite minerals [Shirazi *et al.,* 1995]. Limic and Valkovic (1986) found that germanium (Ge), beryllium (Be) and boron (B) were strongly associated with organic matter, whilst B, Be, calcium (Ca), molybdenum (Mo), sulphur (S), strontium (Sr), and uranium (U) were associated with mineral matter in lower rank coals. Similar observations have been reported for South African coals [Wagner and Tlotleng, 2012].

1.3.3 Clean coal technologies (CCT)

Clean coal technology (CCT) is a broad term used to describe measures to improve coal quality, increase efficiencies, and reduce noxious gaseous emissions in the atmosphere. In view of the challenges discussed, a major drive towards producing ultra clean coals (UCCs) and implementing CCTs is progressing globally. The UCCs are treated coals with an overall ash content of less than 1wt. % [Jorjani *et al.,* 2011]. The UCCs are considered a possible solution towards achieving increased efficiencies and near zero non CO_2 emissions in coal conversion processes [Steel and Patrick, 2001; Wijaya *et al.,* 2011].

Generally, the physical beneficiation methods are not sufficient to produce UCCs because of poor washability characteristics of coals. Consequently, successive methods that utilises both physical and chemical approaches are used. In some cases, pure chemical leaching routes are selected as preferred methods of reducing ash content in coals.

Nonetheless, research studies have indicated that significant reduction of mineral matter content can be achieved by utilising chemical leaching methods [Wijaya *et al.,* 2011], whereby various chemical reagents such as caustic soda (NaOH), acids (HCl, HNO_3, H_2SO_4, HF), oxidising agents (H_2O_2, $FeCl_3$), and mixture of caustic soda and acids (NaOH/HCl/HF) are used in sequential leaching processes [Jorjani *et al.*, 2011]. Nabeel *et al*. (2009) used alkali-acid sequential leaching method to produce UCCs from low grade coals. The concentration of NaOH and H_2SO_4 and the stirring time were varied. Considerable degree of demineralization of up to 80% was obtained during the second stage, after alkali treated coal was demineralised with H_2SO_4.

Studies on burning UCC in gas turbine combined cycle (GTCC) and direct carbon fuel cell (DCFC) systems have reported net power generation efficiency of about 48% and 60%, respectively, whilst CO_2 emissions were reduced by up to 25-35% compared to conventional coal-fired power stations [Wijaya *et al.,* 2011]. However, despite the success to produce UCC, it has been reported that there is currently only one UCC technology used to treat Australian bituminous coals because the technology has not emerged as an economically viable process due to cost implications, and the corrosive nature of reagents used to demineralize coals [Wijaya *et al.,* 2011].

Clean coal technologies have emerged as the preferred approach to help reduce emissions and the carbon footprint. Some of the emerging CCT proposed towards future burning of coals include:

(i) oxy-fuel circulating fluidised bed combustion (CFBC),

(ii) intergrated gasification combined cycle (IGCC) technology,

(iii) oxy-fuel coal combustion (OFCC),

(iv) ultra-supercritical pulverised coal combustion (SCPCC),

(v) circulating fluidised bed combustion, and

(vi) post combustion CO_2 capture.

The oxy-fuel circulating fluidised bed combustion (CFBC) utilises pure O_2 to combust coal, producing CO_2 and H_2O in the flue gas stream [Buhre *et al.,* 2005]. The oxy-fuel technology was first introduced for co-firing of pulverised coals. The technology was classified as CCT because of improved efficiencies, low NO_x emission and the incorporation of in situ removal of SO_2 using sorbents. The advantage presented by the technology is its capability to combust coals that are not easy to burn in conventional pulverised fuel combustion.

The IGCC technology was identified as a potential CCT to advance future power generation in SA [Engelbrecht *et al.,* 2008] because of its high efficiencies, lower pollutant emissions, potential carbon capture and sequestration, capability to handle a variety of feedstock, and the ability to utilize by-products in various industries. Although CCTs can be beneficial in coal conversion processes an in-depth research and understanding of mineral matter is still a necessity [Matjie *et al.,* 2011; Matjie *et al.,* 2012].

Limited understanding of mineral matter has led to recurring problems such as slagging, fouling, bed agglomeration, degradation of refractory materials; syngas exit blockage, and defluidization in various types of gasifiers [Krishnamoorthy and Pisupati, 2015]. Coal characterisation is still deemed the ultimate first step towards addressing problems related to mineral matter in coal combustion and gasification processes, and often coal characterisation is used as the most important step towards adhering to stringent environmental legislation and attaining desired conversion efficiencies. As a result, more analytical approaches have been introduced and improved over the years, to resolve the underlying complexities presented by coals in conversion processes [Aktaş *et al.,* 1998; Ward *et al.,* 1999; Huggins, 2002; van Dyk *et al.,* 2006; Gupta, 2007].

The different analytical techniques have provided answers in three key research areas that involved elemental analysis, coal mineralogy, and inorganic speciation [Huggins, 2002]. A detailed discussion of the different analytical tools is presented in Chapter 4.

1.4 Motivation for research

South African coals are typically characterised by a high concentration of mineral matter in coals. Thus, the effect of mineral matter in coals is to be well understood, since knowledge of composition of mineral matter in coals has a large influence on equipment design, efficiency, coal quality, and emissions.

Despite the role played by mineral matter and coal quality in coal conversion processes, only a limited account of research on detailed characterisation of South African mineral matter in conversion processes is found in literature [Waanders *et al.,* 2003; van Dyk *et al.,* 2006; Mahlaba *et al.,* 2011; Matjie *et al.,* 2011; Matjie *et al.,* 2012; Matjie *et al.,* 2016; Everson *et al.,* 2013].

Characterisation of mineral matter depends largely on the availability of analytical tools. Although bulk analyses such as XRD, and XRF analyses are preferred, these techniques only give general information, without taking into consideration the complexity and heterogeneity of coals. The analyses treat coal as a homogenous material, significantly reducing the possibility of assessing the contribution and interaction of individual particles. However, coupling optical microscopes with mRs, and performing SPA-EPXMA, allow for direct characterisation of specific maceral and mineral matter over a small area of interest, with a spatial resolution of < 1 µm [Guedes *et al.,* 2010]. Comparing SPA-EPMXA to bulk analyses, it is apparent that the technique provides additional information such as particle size, and the association of mineral matter in coals.

The current work proposes to use mRs as an additional technique in conjunction with other complementary techniques such as SPA-EPXMA, FTIR, XRD, and coal petrography to characterise the complex make up of mineral matter. The use of SPA-EPMXA and mRs, as particle to particle techniques, will probe material on a micro scale. It is expected that probing coals on a microscopic level will address some of the challenges related to mineral matter in coals.

The mRs technique is considered one of the most rapid analytical tools used for the characterisation of materials in many fields of research [Michel *et al.,* 1996; Liem *et al.,* 2000; Smith and Dent, 2005]. The technique has advanced significantly over the past 35 years, and the arrival of the laser source has significantly improved the prospects of the technique [Smith and Dent, 2005]. The mRs technique provides structural information of material, with minimal sample preparation required. Unlike XRD, mRs can be used to investigate local molecular structure, and provide information of elemental speciation in a mineral.

The technique can identify elements of different oxidation state, crystallinity and mineral symmetry. Compared to FTIR, the mRs spectra are relatively narrow, making it easy to distinguish minerals in mixtures [Das and Hendry, 2011].

A systematic study of determination of elemental composition in coal using SPA-EPXMA will be used to characterise mineral matter. Chemical boundary classification (CBC) and principal component analysis (PCA) will be used as statistical packages to classify the different mineral groups and determine the mode of occurrence of mineral matter in coals. To the knowledge of the author, little work has been conducted, where CBC and PCA are used to study coals.

Khare *et al.* (2011) used a statistical approach to establish correlation between activation energy and properties of coals. Sharma *et al.* (2014) followed a similar approach, using hierarchical cluster analysis (HCA) and PCA to determine the origin, geochemical formation environment, and ash chemistry using geochemical and statistical parameters. Thus, previously gained knowledge based on CBC and PCA will be adopted, to determine elemental composition of raw coals, using SPA-EPXMA, and to establish the mode of occurrence, and association of mineral matter in SA coals.

The proposed approach to characterise mineral matter of selected SA coal samples has not been reported anywhere in literature. The knowledge gap identified led to the conceptualisation of this research work. Therefore, it is envisaged that this work will provide further understanding of coal mineral matter for application that can be transferred to CCT processes. Furthermore, improved coal characterisation is to benefit the beneficiation process, which will have enhanced effect on assessing environmental impact of coal and the by-products formed.

1.5 Research questions

Some of the research questions raised and addressed in the study are:

(i) Is there a need for multi-technique characterisation of mineral matter in coals?

(ii) How does a multi-technique approach benefit the coal industry?

(iii) What are the benefits of using mRs over traditional analytical techniques?

(iv) What are the possibilities of using mRs as an on-line technique?

(v) How does chemical composition of mineral matter in coals influence slagging, fouling and ash fusion behaviour in combustion processes?

1.6 Hypothesis

It is postulated that the application of multiple characterisation techniques, including mRs, will provide highly suitable technological information for accurate and complete determination of mineral matter in coals, and for monitoring coal quality.

1.7 Aim and objectives of the research

Given the relevance and need to understand mineral matter occurrence and distribution in coal, and to overcome the limitations presented by mineral matter, it is imperative to device characterisation methods that will help reduce the ambiguity presented by bulk characterisation methods. The main aim of this research work was to perform a comprehensive characterisation study of mineral matter, restricted to coals from different geological settings in SA. The work will involve fusing existing techniques and knowledge together with a novel approach that focuses on using mRs as the primary characterisation technique and SPA-EPXMA for elemental analyses.

The study is conducted to further elucidate the benefit of integrating advanced multi-techniques to characterise mineral matter in coals. The aim of this work was achieved through the following objectives:

- Review the present knowledge of mineral matter in SA coals.
- Determine major and minor elements in coals using XRF.
- Study mineral matter in SA coals using mRs in conjunction with other techniques such as SPA-EPXMA, coal petrography, XRD analyses, and FTIR spectroscopy.

- Establish the correlation between elemental composition and mineral speciation of mineral matter in SPA analysis using principle component analysis (PCA) and chemical boundary classification (CBC) methods.
- Use advanced characterisation techniques to characterise LTAs and HTAs.

1.8 Approach

To achieve the aim and objectives stated in Section 1.7, the research work was divided into three phases.

(i) Phase one: Characterisation of mineral matter in raw coal samples

The first phase of the study was conducted on four different South African coals. The three coals studied were obtained from three different coalfields, the fourth coal being a discard coal. The coal properties were determined by conducting proximate and ultimate analyses; XRF was used to determine ash chemistry, AFT was conducted on prepared coal ashes to determine slagging and fouling propensities of the coals. The SPA-EPXMA was used to determine elemental compositions of coals.

The mineralogical composition of the coals was determined by petrographic methods. Structural analyses were determined using XRD, FTIR and mRs techniques. Thermodynamic modelling using the FactSage package was use to predict high temperature phases.

(ii) Phase two: Characterisation of coal ashes

The second phase of the research was to isolate mineral matter from coal using low and high temperature ashing methods. The XRD, FTIR, and mRs techniques were used for structural identification of mineral matter in the LTA and HTA coal ashes.

(iii) Phase three: Data analyses and correlations

This phase of the work included pulling the data together and drawing up correlations for coal samples studied.

1.9 Layout of thesis

- *Chapter 1*: Introduces the concepts and discusses the motivation, research questions, hypothesis, aim, objectives, and approach of the research study.
- *Chapter 2:* A literature review on the geochemistry of coal, and the mode of occurrence and association of mineral matter with organic matter.
- *Chapter 3:* Provides a summary of the impact and the effect of mineral matter on coal utilisation processes.
- *Chapter 4:* Addresses the role played by analytical tools in coal studies, with an overview of the different characterisation techniques used within the coal industry.
- *Chapter 5:* Outlines the experimental procedures conducted to execute the objectives outlined in Section 1.7 of Chapter 1.
- *Chapter 6:* Presents the physico-chemical, elemental composition, thermodynamic modelling, petrographic and mineralogical analyses results obtained from the characterisation of raw coal samples, prepared LTA and HTA samples. The chapter also provides a consolidated discussion of the investigation.
- *Chapter 7:* This chapter presents the main findings and conclusions of the work. Recommendations are also suggested at the end of the chapter.
- A reference list is included at the end of the thesis, with raw analytical data included in the appendices.

CHAPTER 2: LITERATURE REVIEW

2.1 Introduction

This review chapter gives a broad overview of the geology and coal stratigraphy of SA coals. The makeup and chemical composition of coals, including the mode of occurrence, and association of mineral matter in coal, are also addressed in this chapter.

2.2 Geological setting of coal deposits in South Africa

Coal is broadly defined as a sedimentary fossil fuel rock formed from plant debris remains that were buried and exposed to enhanced temperatures and pressures, over a long period of time. Coals are classified according to their chemical structure and physical properties. These properties vary widely from one coal seam to the other and from one coalfield to the next throughout the world. Variations in coal properties are mainly due to the different conditions encountered within the depositional environments [Falcon and Ham, 1988].

The depositional environment have a direct influence on both the coal composition and coal quality (i.e. type, grade, and rank), and the economic value of the respective coal seam. In retrospect, the time of formation of coal plays an important role in the overall composition and conversion behaviour of coals.

South African coals were formed during the Permian age through to mid-Triassic age in the Gondwana Karoo Basin, under a climatic regime that changed from cold to cool to warm [Snyman and Botha, 1993]. The environmental conditions ranged from the lagoonal, marine deltaic, lacustrine deltaic, fluviodeltaic, and alluvial fan settings [Catuneanu *et al.,* 1998].

However, the deposits in southern Africa are believed to be primarily of deltaic and fluvial environmental settings [Cairncross, 2001]. A review of coal deposits in southern Africa is presented by Cairncross (2001), and the description of coal stratigraphy, coal seam, and coal quality is detailed in earlier work by Snyman and Botha (1993), and Smith *et al.* (1993), with the most recent studies conducted by Hancock and Götz (2014).

The formation of the Karoo Supergroup stratigraphy occurred during the early Permian and the late Permian age [Cairncross, 2001], due to glacial sedimentation, that lead to the deposition of the basal Dwyka Group. The end of glaciation, with the melting of ice, left behind a shallow sea. Clays and mud accumulated within the region, forming the Lower Ecca group, whilst the Upper Ecca group was formed by alluvial plain deposits, occurring in a warmer climate. As a result, the early Permian coals are characterised by sandstone, whilst the late Permian coals are associated with mudstones [Cairncross, 2001].

The Molteno formation was deposited into the central part of the basin where debris fans concentrated. The periodic floods due to glacial wet season resulted in the formation of coarse grained deposits. The sediment of coarse grained deposits together with aeolian sand dune deposits were preserved as the Clarens Formation. Lastly, the volcanic flow of the Drakensberg Group was formed at the end of the Karoo Supergroup Formation [Cairncross, 2001]

It is evident from the description of the different deposits, that SA coals experienced lateral and vertical regional differences, with diverse structural and sedimentary settings, and a wide range of plant communities, which included lycopids, shenopsids, marattialean ferns, glossopterids, and gangamopterids. The palaeoflora of the Vryheid Formation was more diverse than the preceding Dwyka [Glasspool, 2003].

The lithostratigraphy results summarised in Table 2-1 clearly show that the occurrence of the different formations/groups took place at different climate and geological times [Snyman and Botha, 1993]. The lateral regional differences, variable plant communities, changing climate, and geological time led to a diverse structure of coal maturation, organic composition, and mineral matter constituents throughout the different coalfields in the country [Falcon, 1986].

Table 2-1: Lithostratigraphy of the Karoo sequence in the main basin and inferred climate conditions [Snyman and Botha, 1993]

Formation/Group	Southern Facies	Northern Facies	Climate	Age
Drakensberg Formation		Flood basalt		Early Jurassic 187±7 Ma
Clarens Formation/Elliot Formation		Aeolian sandstone, Red mudstone and sandstone	Arid	Late Triassic
Molteno Formation		Sandstone, mudstone, minor coal		Middle Triassic
Beaufort Group	Greenish bluish grey sandstone	Carbonaceous shale, sandstone	Semi-arid	Early Triassic
Ecca Group	Grey to black shale, minor sandstone	Shale coal: Volksrust Formation Feldspatic sandstone Shale, coal: Vryheid Formation Shale: Pietermaritzburg Formation	Cool temperature to peri-glacial	Early Permian
Dwyka Formation	Tillite, varved shale: also drop stones	Tillite: Fluvio-glacial conglomerate	Glacial	Late carboniferous

The coal reserves in SA are widely spread over the Ecca group in the Karoo super-group stratigraphy, as indicated in Figure 2-1. The Ecca coal group constitutes over a third of coal reserves in the southern hemisphere. In SA there are 19 coalfields stretching over 700 km from north to south and 500 km from east to west. The coalfields are located in five provinces namely: Limpopo, Free Sate, Mpumalanga, Kwazulu-Natal and the Eastern Cape [Jeffrey, 2005].

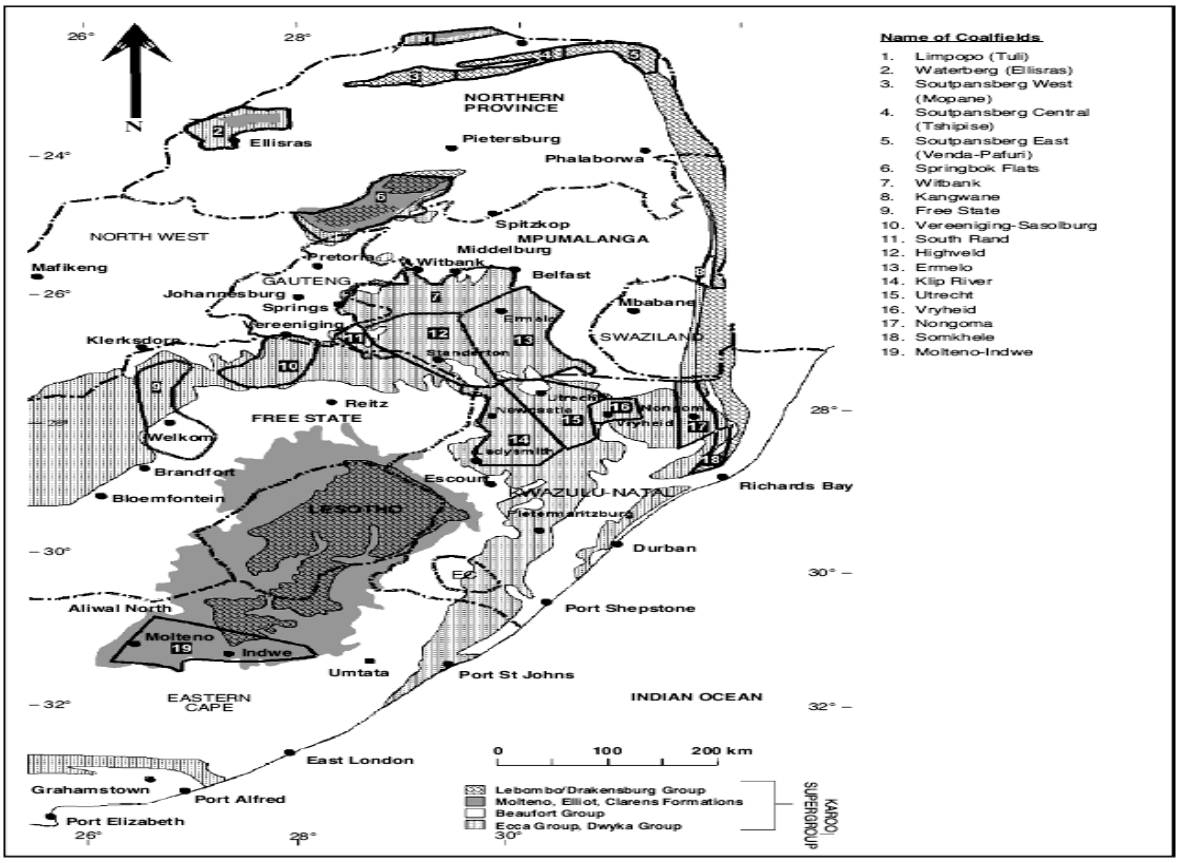

Figure 2-1: Map of coal deposition in South Africa [Jeffrey, 2005]

The main coal reserves of industrial importance are found in the central Karoo Basin, which includes the Witbank, Highveld, and Ermelo coalfields, located in Mpumalanga Province. Figure 2-2 gives a summary of the coalfield rankings based on production rate of the different coal mines. It can be seen Witbank coalfield is the largest producer of coal, with over 50% of the ROM produced from the coalfield. The Highveld coalfield is the second largest producer of coal in SA, producing approximately 21% of ROM [Xmp consulting, 2009].

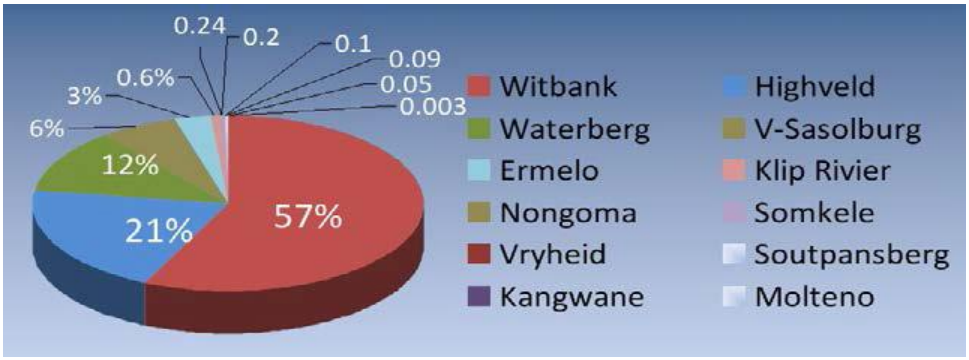

Figure 2-2: Coalfield ranking by ROM production [Xmp consulting, 2009]

2.2.1 Lithostratigraphies of South African coalfields

This section presents a discussion of the lithostratigraphy of coalfields that are of economic importance in SA.

- **Witbank coalfield**

The Witbank coalfield extends from Brakpan in the West through to Belfast in the East. Both the Witbank and the Highveld coalfields are characterised by numerous post-Karoo age dolerite sills and dykes, and rocks of the Vryheid Formation of the Ecca Group that cover most of the area. The coal seams are relatively shallow, and less than 200 m below surface [Jeffrey, 2005].

The sedimentological and coal petrographic studies based on seventy logged boreholes drilled on a 100 m × 50 m grid pattern provided data for the investigation of the Permo-Carboniferous Karoo sequence in the Witbank coalfield. The coalfield consists of 6 seams numbered in ascending order from No. 1 to No. 6. The No.1 seam is at the base of the sequence, and the No. 6 seam is at the surface of the coal mine [Holland *et al.*, 1989].

The coal seams formed in fluvial environment are characterized by thick and laterally continuous seams, with high inertinite content. The typical concentration of inertinite ranges from 20-80 wt. %, and the mineral matter content can be up to 25 wt. %. Coals that are formed in lower delta plain environment are comprised of thin and discontinuous seams [Holland *et al.*, 1989].

The Witbank coalfield produces a wide range of products. The No. 2 seam produces good quality export steam coal. The No. 5 seam consists of bright coal with thin shale and mudstone partings, and produces metallurgical coal. The low grade middlings from the No. 5 and No. 2 seam are utilised by Eskom for generating electricity. The No. 1 seam is the least economical, and consists mainly of lustrous to dull coal, with local shale and sandstone parting [Snyman, 1998; Jeffrey, 2005]. According to a study by Falcon (1986), the macro and micro-floral evidence pertaining to the geological area gives an indication that the No. 2, 3, and 4 coal seams accumulated in both postglacial dry and wet forest environments, whilst the No.1 coal seam accumulated in a paraglacial climatic setting.

- **Ermelo coalfield**

The Ermelo coalfield is situated east of the Highveld coalfield in Mpumalanga. The coalfield forms part of the Vryheid formation. The nomenclature used to describe the economical seams is A, B, C, D, and E. However, the large part of seam A has been eroded. The B seam is of low quality, and is comprised mostly of dull coals which contain fewer vitrain bands compared to the lower portion of C upper seam. The C seam is divided into the upper half and a lower half. The lower C seam is about 1.5 m thick and the most economical. The seam consists of bright coal, with ash content ranging between 13-18 wt.% [Horsfall, 1992]. The high grade steam coal from the lower C seam is exported. The C upper seam is of a lower quality, with no in-seam partings.

Coal from the D seam is of high quality, and has no clastic partings. The seam has a high concentration of vitrain, and minor durain bands. The E seam is of a fair quality. However, the potential to mine the seam is reduced southwards, because of the rich torbanite and shale contents [Jeffrey, 2005].

- **Highveld coalfield**

The Highveld coalfield is located in south eastern Mpumalanga Province. The width of the coalfield stretches over a 95 km distance, covering an area of about 7000 km^2. Highveld coalfield is the second largest producing mine in South Africa. The coalfield is made up of five seams (No. 1, No. 2, No. 3, No. 4, and No. 5) in the Vryheid formation. The No. 1 seam is thin and discontinuous. The No. 2 seam is about 1.5 to 4 m in thickness, with irregular shale partings. The No.2 seam consists of low grade bituminous coals with ash content between 22-35 wt. %, and a calorific value (CV) of 20-23 MJ/kg.

The No. 3 seam is thin, discontinuous and of poor quality. The No. 4 seam is about 1-12 m thick. This seam is continuous and the most economical within the Highveld coalfield. The sandstone parting separates the No. 4 upper seam, which is about 1 to 4 m thick. The No. 4 lower seam is about 4-12 m, thin and discontinuous. The No. 4A seam occurs above the No. 4 upper seam, and the No. 5 seam is about 1-2 m thick [Jeffrey, 2005]. Figure 2-3 shows the coal seam stratigraphy of Witbank, Highveld, Ermelo, and Kwa-Zulu Natal coalfields found in the main Karoo basin.

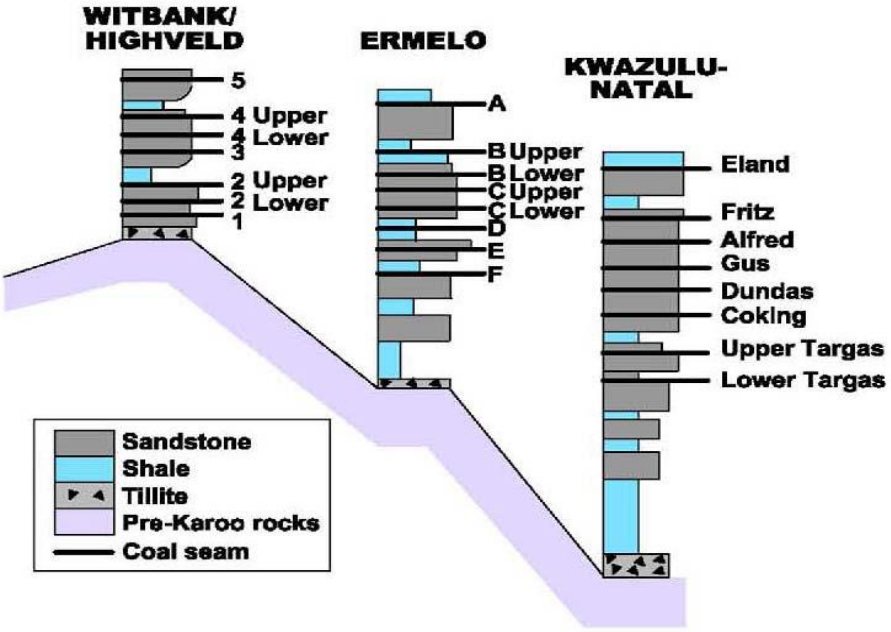

Figure 2-3. Diagrammatic representation of the coal seam stratigraphy and lithology in the main Karoo basin [McCarthy and Pretorius, 2009]

- **Waterberg coalfield**

There are distinct differences between coals from the Karoo and the outlying Karoo basins. Coalfields on the outlying Karoo basins (Waterberg, Springbok Flats, and Limpopo) are found in the Limpopo province. This outlying basin experienced a different depositional environment compared to the central Karoo Basin. The outlying deposits are faulted, as well as being intruded by dolerite.

The Waterberg coalfield is situated north-west of the Karoo basin. The formation of faults produced grabens, with shallow deposits, 500 m below surface. The geology of the Waterberg coalfield is made up of two formations, namely: the Vryheid and the Grootgeluk formation. The stratigraphy of the Waterberg coalfield is depicted in Figure 2-4. The Vryheid formation is about 55 m thick, made up of allochtonous 4 coal zones and 5 seams interbedded with sandstone and shale. The thickness of the seams ranges from 1.5 to 9 m.

The coal quality within the coal-mudstone sequence is increasing vertically up, from an ash content of 43 wt.% to 60 wt.% in the upper seam [Cairncross, 2001]. The Grootgeluk formation is made out of autochthonous 60 m thick seams. The carbonaceous mudstones are interbedded with thin coal seams.

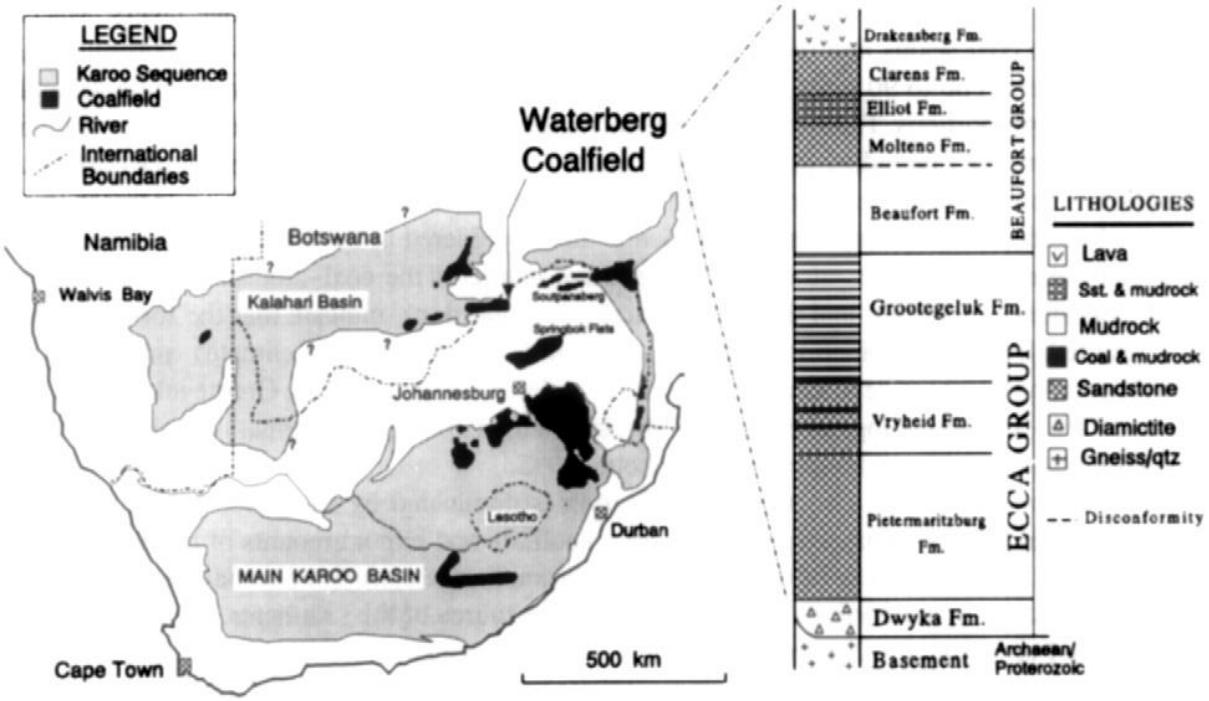

Figure 2-4: Stratigraphy of Waterberg coalfield [Wagner and Tlotleng, 2012]

The coal mined from the Waterberg coalfield is used primarily in steel production and power generation, supplying Matimba and the new Medupi power station. The coal that is deeply buried and unminable in the Waterberg coalfield is being explored for potential use as coalbed methane [Cairncross, 2001; Jeffrey, 2005].

The Waterberg coalfield is to be further explored for future supply of coal in southern Africa as resources in the Witbank/Highveld coalfields are being depleted; and currently there is only one producing mine (Grootegeluk) in the Waterberg area.

However, challenges related with mining coal in Limpopo province are a serious concern. Some of these challenges include water shortage in the province, environmental considerations, lack of infrastructure, and the complex geology of the coalfield [Jeffrey, 2005].

- **Free State and Kwa-Zulu Natal coalfields**

The Free State coalfields to the western side of the main Karoo Basin, are typically of lower rank, and inertinite-rich, when compared to the higher rank Kwazulu-Natal coalfields to the east, which contain anthracite and semi-anthracite, formed by higher geothermal temperatures and igneous intrusions. The higher rank anthracite coals are typically used as reducing agents in the production of titanium, ferrochrome, ferromanganese, iron, and steel in the metallurgical industry [Jeffrey, 2005].

The coal stratigraphy and composition of South African coalfields is quite vast, variable and of different coal quality. Table 2-2 gives a summary of the typical physico-chemical properties of some of the raw coals from the different coalfields within the Karoo Basin. For detailed discussions related to lithostratigraphy, and the geology of SA coals, the reader is requested to refer to Snyman and Botha (1993); Smith *et al.* (1993); Jeffrey (2005); and Hancock and Götz (2014) for further information.

Table 2-2: Typical analyses of raw coal for coalfields on the Karoo basin [Cairncross, 2001]

Locality (coalfield)	Seam	H_2O (%)	Ash (%)	VM (%)	CV ((MJ/kg)
Witbank	1	1.7	25.4	21.0	24.0
	2	5.3	23.3	21.5	21.2
	4	2.6	27.6	20.7	22.2
	5	2.5	13.1	32.0	28.7
Highveld	2	3.8	29.3	19.9	20.5
	4	2.5	27.9	20.2	21.9
	5	3.2	17.1	32.7	25.9
Mpumalanga	E	2.7	20.4	31.5	25.5
	D	2.5	23.0	26.7	24.0
	C	3.6	19.9	32.0	25.3
	B	2.8	29.5	23.7	21.1
Vereeniging	Composite	4.4	40.8	18.6	16.3
Free State	Bottom	5.6	27.7	21.4	20.5
Utrecht	Coking	1.6	9.1	23.8	31.4
	Dundas	1.9	10.3	28.3	30.2
	Gus	1.4	14.2	10.6	29.5
	Alfred	1.2	40.3	11.7	
Vryheid	Gus	2.1	16.5	20.8	28.9
Viefontein	Bottom	6.7	25.8	21.1	20.7
Koppies	1 and 2	4.5	32.6	21.0	18.7
Kroonstad	Bottom	4.0	39.1	21.2	17.2
Welkom	Bottom	4.5	36.7	20.5	16.7
	Top	3.9	34.1	21.8	20.7
	Dwyka	3.9	38.6	22.3	17.6

2.3 Coal chemistry and petrographic composition

Coal is a heterogeneous mixture formed by bacterial decomposition of peat, and made up of both the organic and mineral matter. Elements such as C, H, N, O, and S are the main constituents that make up the organic structure of coal, and are also referred to as the maceral matter. The term maceral was first proposed by Marie Stopes in the 1900s to describe the microscopic organic matter in coals [Stopes, 1935]. South African coals are typically characterised by low S, N, and P.

The different organic functional groups found in coal structure include hydroxyl, alkyl substituted aromatics, and heteroatomic rings, connected by methylene and ether linkage. The type and distribution of functional groups, aromacity, surface features, covalent and non-covalent cross links, and surface features are all related to coal rank, and determine physical and reactive properties of coal.

2.4 Maceral groups

The three main groups of macerals found in coals are: vitrinite, inertinite, and liptinite. Macerals are derived from terrestrial, lacustrine, and marine plant remains. The different organic matter are distinguished from one another on the basis of their physico-optical and technological properties [Falcon and Ham, 1988], and are classified by the International Committee for Coal and Organic Petrology (ICCP) classification system (1998).

2.4.1 Vitrinite maceral group

Vitrinite is the most abundant and reactive maceral group common in the northern Hemisphere coals. It originates from wood or bark, formed by successive processes of humification, biochemical, and geochemical gelification process, under aerobic conditions. The chemical properties of vitrinite found in low rank bituminous coals are rich in volatile matter, and have high hydrogen content.

The chemical structure of vitrinite is made up of aromatic compounds, with aliphatic peripheral compounds in lower rank coals. An increase in rank results in the loss of the aliphatic peripheral groups (OH, COOH, and CH_3), with the aromatic compounds becoming larger, and the structure more ordered. As a result, the carbon content and aromaticity increase with an increase in rank, and consequently the reflectance [Falcon and Ham, 1988; Smith and Smith, 2007].

Collonite, tellinite and pseudo-vitrinite are some of the sub-maceral groups of vitrinite. The amount of vitrinite is South African coals is variable, with an average concentration of about 40 wt. % [Falcon and Ham, 1988]. The positive correlation between vitrinite content and sulphur in coals of Vryheid Formation indicates that vitrinite has a higher sulphur content than inertinite [Roberts, 1988].

2.4.2 Liptinite maceral group

Liptinite is formed from spores, resin, algae, and cuticle remains. The liptinite macerals includes: cutinite, resinite, sporinite, alginate, suberinite, and liptodetrinite, named after the plant source from which the maceral is formed [Scott, 2002]. For example, cutinite is formed from leaves and needle-like cuticles, resinite from plant resin, sporinite is formed by spores, and alginate is formed by algal remains.

The structure of liptinite consists of aliphatic-aromatic compounds, with aliphatic side chains that are rich in peripheral groups. However, liptinite in lower rank coals is less aromatic than vitrinite, with smaller aromatic nuclei [Falcon and Ham, 1988]. Liptinite has a high yield of volatile matter, higher than vitrinite upon heating, producing bitumen and tar. When subjected to high temperatures, the aliphatic groups are lost, and the aromaticity increases, making liptinite more inert. As a result, it becomes difficult to distinguish between liptinite and vitrinite under the reflected light microscope in higher rank coal, as the shades of grey all converge to white.

SA coals typically have less than 10% liptinite, but reaches a maximum of 15%, with rare occurrence of alginate in coals formed in deeper waters [Falcon and Ham, 1988; Holland *et al.*, 1989; Snyman and Botha, 1993].

2.4.3 Inertinite maceral group

Inertinite, as the name implies, is considered to be more inert than other macerals; however, not all inertinite maceral groups are inert, but are also semi-reactive. The inertinite maceral groups are: fusinite, semifusinite, inertodetrinite, micrinite and sclerotinite.

South African coals are typically found to be inertinite-rich, with inertinite content greater than 55%, but ranging from 20 to 80% [Holland *et al.*, 1989]. A significant amount of inertinite found in SA coals is semi-reactive inertodetrinite [Snyman and Botha, 1993]. The low water table, due to slower rate of subsidence of peat swap, and oxidising conditions, are the result of the inertinite rich coals found in SA, which have been found to have similar characteristics across all Gondwana coals [Weeber *et al.*, 2000].

The inertinite macerals are derived from plant remains that are altered and degraded before deposition or at the peat accumulation stage [ICCP, 2001]. These macerals exhibit a high degree of aromatisation and condensation, compared to vitrinite and liptinite in low rank coals. The aromatic nuclei of inertinite maceral groups are much bigger and randomly orientated, with fewer and shorter aliphatic chains. The molecular structure of inertinite is characterised by low volatile matter and hydrogen contents. Table 2-3 summarises the different maceral groups found in carbonaceous materials, showing the different macerals with corresponding morphology, and respective origin.

Table 2-3: Macerals and group macerals recognised in hard coals [McCabe, 1984]

Group maceral	Maceral	Morphology	Origin
Vitrinite (Huminite)	Telinite	Cellular structure	Cell walls of trunks, branches, roots, leaves, etc.
	Collinite	Structureless	Reprecipitation of dissolved organic matter in a gel form
	Vitrodetrinite	Fragments of vitrinite	Very early degradation of plant and humic peat particles
Exinite (Liptinite)	Sporinite	Fossil form	Mega- and microspores
	Cutinite	Bands which may have appendages	Cuticles—the outer layer of leaves, shoots and thin stems
	Resinite	Cell filling, layers or dispersed	Plant resins, waxes and other secretions
	Alginite	Fossil form	Algae
	Liptodetrinite	Fragments of exinite	Degradation residues
	Fusinite	Empty or mineral filled cellular structure. Cell structure usually well preserved	Oxidized plant material—mostly charcoal due to burning of vegetation
Intertinite	Semifusinite	Cellular structure	Partly oxidized plant material
	Macrinite	Amorphous 'cement'	Oxidized gel material
	Inertodetrinite	Small particles of fusinite, semi-fusinite and/or macrinite	Redeposited inertinites
	Micrinite	Granular: rounded grains ~ 1 μm in diameter	Degradation of macerals, especially exinites, during coalification
	Sclerotinite	Fossil form	Mainly fungal remains

Variation in chemical and physical properties of macerals and coal rank influence combustion, gasification, hydrogenation, and pyrolysis processes [Stach *et al.,* 1982; Cloke *et al.,* 1997; Borrego *et al.,* 1997]. It is therefore important to understand the effect of maceral matter on conversion processes. However, since macerals are intimately associated with each other in coal, it can be challenging to access the effect of an individual maceral group. As a result, different separation methods (chemical fractionation, density separation, centrifuging) have been applied to better understand the structural characteristics and chemical reactivity of the individual maceral groups.

The two main macerals of interest that have been extensively researched for their respective roles in combustion processes are vitrinite and inertinite. Pyrolysis behaviour of vitrinite and inertinite was investigated by Zhao *et al.* (2011), using TG-MS and a fixed bed reactor. The study found that inertinite had a higher thermal stability and water yield, with lower tar and gas yields than vitrinite.

Sun *et al.* (2003) investigated the structural characteristics of Chinese Shemnu bituminous coal macerals during pyrolysis stage. The study showed that vitrinite chars had higher hydrogen and lower carbon content than inertinite chars when pyrolysis was conducted at the same temperatures. The vitrinite macerals had more aliphatic C-H, hydrogen bonding and lower aromaticity. An increase in temperature yielded a structure with more aromatic C-H, and a decrease in aliphatic C-H.

A study by Roets *et al.* (2015) indicated that acid washing had an effect on the pyrolysis products derived from a vitrinite-rich bituminous coal. The results further indicated that an acid washed coal produced low water and tar yield compared to a raw coal. The tar produced from the acid washed coal was more aromatic. From the study, it could be concluded that acid washing influenced pyrolysis products.

Van Niekerk *et al.* (2008) investigated the structural characteristics of inertinite-rich coals from the Highveld coalfield and vitrinite-rich coals from the Waterberg coalfield. From the study it was found that inertinite-rich coals were more ordered and aromatic than vitrinite rich coals. Chars derived from inertinite-rich and vitrinite-rich coals from SA coalfields showed that inertinite rich coals formed thick walled dense chars, whilst vitrinite derived chars were more isotropic, with increased surface area and micro pores [Roberts *et al.*, 2015].

2.5 Mineral matter in coal

Mineral matter is as a collective name that represents all the forms of inorganic components present in coal. Similar to organic matter, minerals are a product of a complex geological process that is related to the conditions of burial, including the source rock, lithology, temperature, pressure, pH, E_h, degree of weathering, migration of components within the seam, peat accumulation, and rank advance [Vassilev *et al.*, 2010]. The different mineral assemblages in run-off mines are present in varying quantities that range between 10-50 wt.% [Shirazi *et al.*, 1995]. These differences are due to varying depositional history and lithologies during coal formation. The inorganic matter is distributed and associated with coal in different forms, namely [Gluskoter, 1975; Ward, 2002]:

(i) dissolved salts,

(ii) discrete inorganic particles,

(iii) crystalline particles,

(iv) inorganic elements dissolved in pore water, and

(v) inorganic elements associated with organic matrix in coals.

2.5.1 Dissolved salts

Dissolved inorganic elements such as Na and Cl, are present in coal pores, and originate from surface or ground water around the peat swamp. Low rank coals such as brown coal typically consist of high moisture content, in which inorganic compounds or ions are dissolved. The inorganic compounds from vegetation plants include alkali and alkali earth metal cations, such as Na^{+}, K^{+}, Mg^{2+}, and Ca^{2+}.

These metal cations are present as salts of carboxylic acids in coals, replacing protons on oxygenated functional groups, phenolic hydroxyl, carboxylate, and esters. Dissolved anions may include Cl^{-}, HPO_4^{2-}, $H_2PO_4^{-}$, SO_4^{2-}, and OH^{-}. Inorganic elements forming chelates and organo-metallic complexes are common, particularly in low rank coals such as brown coal [Durie, 1961; Kiss and King, 1977; Kiss and King, 1979; Given and Miller, 1987]. TEs may be present as organo-metallic complexes.

2.5.2 Inorganic elements associated with organic matrix

The inorganic elements associated with organic matrix are either inorganically or covalently bound to the fuel matrix. The ionically bound elements are associated with oxygen containing anionic, organic functional groups such as carboxylic acids (- COOH) which can act as bonding site for metal cations (Na^{+}, K^{+}, Ca^{2+}). The organically bound non-metallic elements (S, P, and Cl) are covalently bonded to the organic matrix [Ward, 2002].

2.5.3 Discrete inorganic particles

Discrete minerals such as clays, sulphides, oxides, silicates and carbonates are the major mineral groups found in high rank coals [Vuthaluru and French, 2008]. Typically higher rank coals have low mineral matter contents, and subsequent low ash contents, whilst low rank coals are comprised of high mineral matter contents. The total amount of mineral matter present in coals determines the grade of coals [Falcon and Ham, 1988].

2.6 Formation of mineral matter in coals

Minerals in coals are formed at different times which define their origin. The three main origins of coals are syngenetic, epigenetic, and detrital [Mackowsky,1968]. Syngenetic mineral matter also referred to as inherent or included mineral matter originate from coal forming plants through a biochemical and physico-chemical process. Syngenetic mineral matter can be classified as early or late syngenetic mineral matter depending on the time the minerals were formed. The early syngenetic mineral matter formed during the early stages of coalification, shortly after the burial of the peat, when major compaction and solidification of coals has not taken place. The late stage syngenetic mineral matter was formed during the humification-gelification stages of coal, at the advanced stage of peat formation. The late stage syngenetic mineral matter was formed as a result of chemical reactions between the environment and coal constituents.

Syngenetic mineral matter is finely dispersed and closely associated with organic matter in coals [Ward, 2002]. As a result, syngenetic mineral matter is generally difficult to beneficiate. Primary syngenetic precipitates include siderite nodules, microcrystalline aggregates of pyrite crystals, and infilling pore compounds such as kaolinite, quartz, carbonates, sulphates, clays, and phosphate minerals.

Epigenetic minerals, also known as adventitious, extraneous, or excluded mineral matter, are found in coal fissures, and void infillings. The epigenetic minerals were deposited into coal cleats or fractures after coal compaction. Typical mineral matter formed by epigenetic mineralisation includes clays, silica, calcite, dolomite, ankerite, siderite, pyrite, marcasite, apatite, dawsonite, illite, and chlorites [Ward, 2002].

Epigenetic mineral matter is typically large and easily liberated during beneficiation and milling of coals. Figure 2-5 show images of epigenetic modes of occurrence of different minerals in coals.

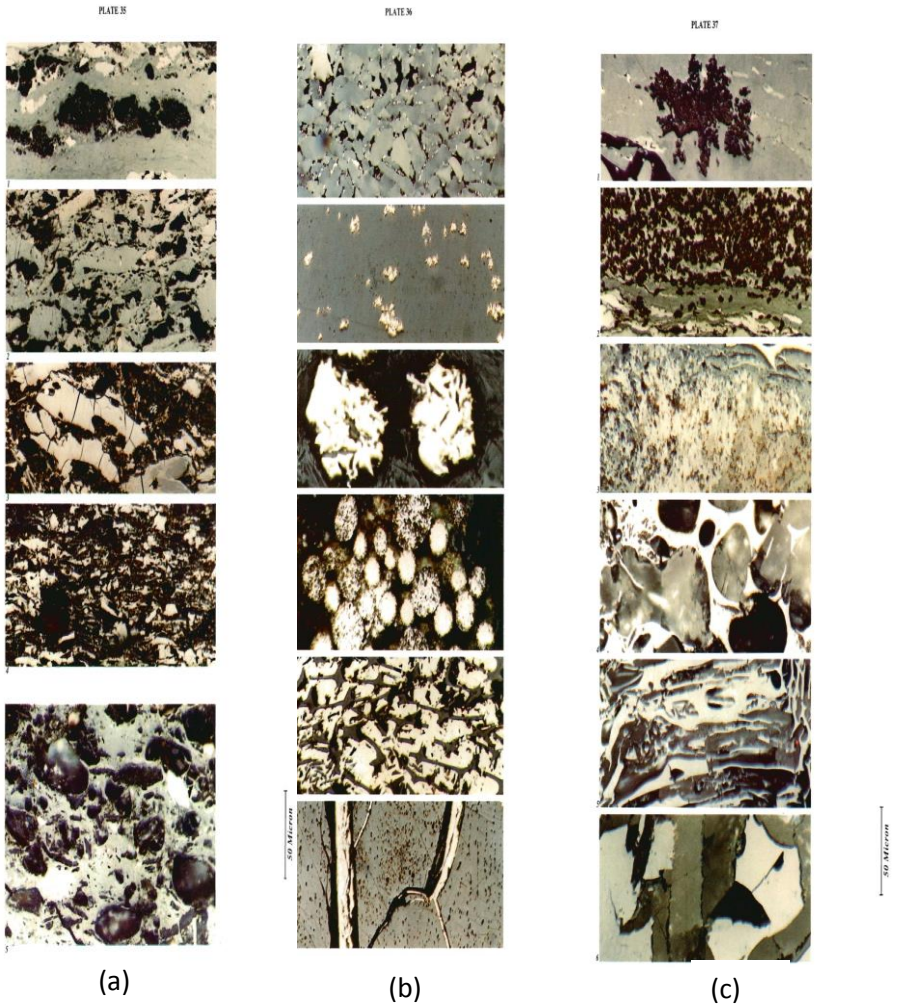

Figure 2-5: Forms of main mineral groups in coals: a) silicates, b) pyrite, c) carbonates [Falcon and Snymann, 1986]

Detrital minerals were deposited into the peat by either moving water, wind, or introduced by epiclastic and pyroclastic processes. Fragments of quartz, feldspar, irregular bands of clay minerals, and tonsteins are of detrital origin, and intimately mixed with organic matter [Ward, 2002].

The genesis of mineral matter can be associated with coal rank. Typically, low rank coals and coal ashes are enriched with moisture, volatile matter, ash, H, N, O, S, MgO, CaO, and SO_3. The high rank coals on the other hand are enriched with fixed carbon, SiO_2, Al_2O_3, Fe_2O_3, K_2O, Na_2O, and TiO_2.

2.7 Mode of occurrence of mineral matter in coals

The mode of occurrence describes the manner in which elements are chemically bound in coals. Knowledge about the mode of occurrence helps determine the association of mineral matter in coals. The mineralogical information can be extended to helps predict the fate of minerals in conversion processes, and assess environmental impact of mineral matter [Raask, 1985; Vassilev *et al.*, 1995; Gupta *et al.*, 1999, Ward, 2002]. For example, alkali species (Na and K), are the main cause of ash related problems in downstream parts of boilers such as fouling, slagging, and corrosion. Understanding their mode of occurrence can help in devising solutions to minimise their impact. A number of studies have been undertaken to understand the mode of occurrence of minerals in coals [Vulthara and French, 2008; Everson *et al.*, 2013].

Van Dyk *et al.* (2005) used chemical leaching methods to determine species-specific information on ash fusion temperature (AFT). López and Ward (2008) studied the composition and mode of occurrence of mineral matter in Colombian coals using low

temperature ashing (LTA), X-ray diffraction (XRD), and the results were compared to information derived from ash chemistry and Mössbauer spectroscopy studies.

Common methods such as sequential leaching and density fractionation are used to determine the mode of occurrence of different elements in coals. Advanced methods use computer aided techniques such as computer-controlled scanning electron microscopy (CCSEM) and Quantitative evaluation of minerals by scanning electron microscope (QEMSCAN). Sequential leaching methods use various solutions such as water, ammonium acetate and acids, to determine the affinity of minerals in coals and establish if minerals are organically bound, water soluble, or associated with minerals such as clay, carbonate, or sulphides.

Water soluble salts such as halite (NaCl) and thenardite ($NaSO_4$) are readily removed by treating coal in water. Ammonium acetate is used to extract exchangeable cations (Mg, Ca, K, Na) bound to functional groups such as carboxylic acid, phenol hydroxyl, carboxylates, and ether. Discrete particles are removed by treating coals with acids. An acidic environment is desirable for the solubilisation of metal ions [Khan *et al.*, 2002; Seferinoğlu *et al.*, 2003].

Elements recovered from acid treatment are organometallic complexes and traces of calcite and dolomite that could not be extracted by the ammonium acetate solution. However, HCl cannot effectively remove chelated cations from the organic matter because of the high stability of the complexes [Buruah *et al.*, 2003]. Silicates and minerals such as quartz and pyrite are not leached out, but remain in the insoluble residue.

Float-sink methods are established on separating mineral matter and organic matter coal fractions on the basis of the difference in densities between the organic (approximately 1.3 g/cm^3) and inorganic matter (an estimated average of 2.7 g/cm^3). However, physical methods are not effective in separating coals with low mineral matter content, or mineral matter that is

finely dispersed within the organic coal matter [Paulson *et al.,* 1972; Murkherjee and Borthakur, 2001; Querol *et al.,* 2001].

Table 2-4 presents some of the common elements found in coals and their associated mode of occurrence. For a full list of elements, the reader can consult the comprehensive list prepared by Finkelman (1982).

Table 2-4: Probable mode of occurrence of selected elements [Finkelman, 1982]

Element	Mode of occurrence
Al	Clay, feldspar, some organic association
As	Solid solution in pyrite
Ca	Calcite, organic association, sulphates, phosphates, silicates
Cl	Organic association
Cr	Clays
Mg	Clays
P	Phosphates
Si	Quartz, clays, silicates
Fe	Pyrite, siderite, sulphates, oxides, organic association
Na	Organic association, clays, zeolites, silicates
Zn	Sphalerite

Chemical leaching has limitations with undesirable implication in coal processes. Treating coals with acids could lead to possible structural changes which may influence the behaviour of coal in gasification processes. In some occurrences, the removal of Ca and Mg could affect combustion processes by reducing the reactivity of coal [Jenkins *et al.*, 1973].

Although sequential leaching and density fractionation methods are still popular, the processes are generally labour intensive and time consuming [Saikai and Ninomiya, 2011].

Other methods that are preferred to determine mode of occurrence of minerals in coals include the use of advanced analytical tools as stated earlier.

The CCSEM is an advanced technique used to assess the distribution of minerals in coals. The technique allows for simultaneous measurement of chemical composition, mode of distribution of minerals, and particle size distribution on individual particles [Liu *et al.,* 2005]. The technique has been recently developed to solve ash deposition problems. Matjie *et al.* (2011) used an integration method of single particle analysis, bulk techniques and ash chemistry to understand the behaviour of coal mineral matter in a gasification process. From the work it was concluded that the use of these techniques and understanding the mode of occurrence of mineral matter improved the basis of evaluating ash forming processes.

2.8 Mineral groups in coals

Mineral matter has 44 species that belong to various groups of silicates, carbonates, sulphates, sulphides, oxides, hydroxides, and to a lesser extend chlorides, biogenic minerals and lastly, the organic minerals. Ward (1989) compiled a list of some of the different major and minor mineral matter found in bituminous coals and these are summarised in Table 2-5.

Table 2 - 5: Major minerals identified by various authors in bituminous coals as summarised by Ward (1989)

Mineral groups	Chemical formula
Silicates	
Kaolinite	$Al_2Si_2O_5(OH)_4$
Illite	$KAl_2(AlSi_3)O_{10}(OH)_2$
Montmorillonite	$Na(AlMg)Si_4O_{16}(OH)_2$
Chlorite	$(MgFeAl)_6(AlSi)_4O_{10}(OH)_8$
Quartz	SiO_2
Chalcedony	SiO_2
Feldspar	$KAlSi_3O_8$
Carbonates	
Calcite	$CaCO_3$
Siderite	$FeCO_3$
Dolomite	$CaMg(CO_3)_2$
Ankerite	$Ca(Fe,Mg)CO_3$
Aragonite	$CaCO_3$
Sulphides	
Pyrite	FeS_2
Marcasite	FeS_2
Sphalerite	ZnS_2
Galena	PbS
Chalcopyrite	$CuFeS_2$
Sulphates	
Gypsum	$CaSO_4.2H_2O$
Barite	$BaSO_4$
Anhydrite	$CaSO_4$
Coquimbite	$Fe_2(SO_4)_3.9H_2O$
Szomolnokite	$FeSO_4.H_2O$
Natrojarosite	$NaFe_3(SO_4)_2.(OH)_6$
Thernadite	Na_2SO_4
Bassinite	$CaSO_4.1/2H_2O$
Celestite	$SrSO_4$
Phosphates	
Apatite	$Ca_6F(PO_4)_3$
Goyazite	$SnAl_3(PO_4)_2(OH)_5.5H_2O$
Other Minerals	
Anatase	TiO_2
Boehimite	$AlO(OH)$
Hematite	Fe_2O_3
Goethite	$Fe(OH)_3$
Zircon	$ZrSiO_4$

Minerals such as illite, kaolinite, quartz, calcite, pyrite, dolomite, siderite, with traces of microcline, illite, smectite illite, mixed-layer clays, analcime, plagioclase, marcasite, anatase, aragonite, ankerite, rhodochrosite, alunite, jarosite and gypsums have been identified in South African coalfields [Snyman and Botha, 1993], and the respective mineral groups are discussed in the subsequent sections.

2.8.1. Silicate minerals

Clays are the most abundant minerals found in coals worldwide, constituting over 60% of the total mineral matter in most bituminous coals [Raask, 1985]. These minerals are also the major ash contributors [Spears, 2000]. Clay minerals are the characteristic minerals formed in soils and sediments by both the diagenetic and hydrothermal alterations of the rock, and mostly described as hydrous alumina silicates.

Clay mineral structures consist of planes of cations arranged in tetrahedral sheets or octahedral sheets, where cations are surrounded by neighbouring oxygen and hydroxyl groups. The difference in the arrangement of layers is used to classify the different clay minerals. Layered silicates are called phyllosilicates, and kaolinite is the simplest 1:1 phyllosilicate clay mineral with one tetrahedral sheet and one octahedral sheet. Clay minerals such as mica, smectite, chlorite and illite consist of 2:1 layer minerals of 2 tetrahedral sheets and one octahedral sheet. Figure 2-6 illustrates the basic 1:1 structure of kaolinite clay mineral, showing the inter-layer and inner layer hydroxyl groups.

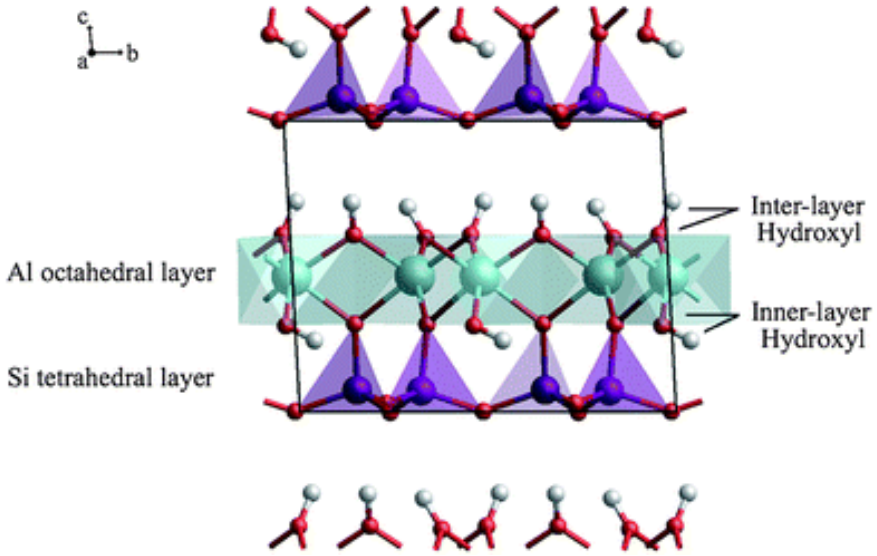

Figure 2-6: Layered structure of kaolinite showing inter and inner layer hydroxyl groups [Sperinck *et al.*, 2011]

Clay minerals consist primarily of silica, alumina and water, and small quantities of Fe, alkalies, and alkali-earth minerals [Nayak and Singh, 2007]. Common clays found in coals are: kaolinite ($Al_2Si_2O_5(OH)_4$), illite ($KAl_2(AlSi_3)O_{10}(OH)_2$), montmorillonite $Na(AlMg)Si_4O_{16}(OH)_2$, chlorite ($(MgFeAl)_6(AlSi)_4O_{10}(OH)_8$), and illite-montmorillonite mixed-layered clays. Kaolinite is the most abundant clay found in Gondwana coals with Southern Hemisphere coals typically having a higher concentration of kaolinite over illite [Gaigher, 1980]. However, the illite content in coals increases with an increase in coal rank. For example, kaolinite decreases and illite increases as coal rank advances for South African coals [Vassilev *et al.*, 1996]. Mixed-layer clays may also occur in high rank coals. Clay minerals occur as dispersed mineral grains, nodular masses, lenticles, and are also found in bands [Kemezys and Taylor, 1964].

2.8.1.1 Kaolinite

Kaolinite ($Al_2Si_2O_5(OH)_4$) is abundant in coal deposits formed by slow sedimentation, where climate conditions are humid and hot. Kaolinite is a layered silicate clay mineral which forms mainly due to decomposition alteration of rocks such as sandstone, which starts in an acidic environment, solubilising the feldspar type compounds and then precipitates out as the pH gradually increases to more neutral systems. The diagenetic alteration of pre-existing illite, montmorillonite, feldspars, muscovite, aluminosilicates minerals and pyroclastic glasses could also lead to the formation of kaolinite [Vassilev *et al.*, 2010].

2.8.1.2 Illite

Illite ($KAl_2(AlSi_3)O_{10}(OH)_2$) mineral is commonly found in alkaline brackish or marine depositional environments. The montmorillonite clay mineral ($Na(AlMg)Si_4O_{16}(OH)_2$) and chlorite ($(MgFeAl)_6(AlSi)_4O_{10}(OH_8)$ are found to be unstable in marine environments, leading to the transformation of montmorillonite into illite and chlorite in the presence of potassium (K) and magnesium (Mg) ions.

Weathering and hydrothermal changes can lead to the transformation of muscovite and K-feldspars and form illite minerals. Illite content generally increases with an increase in coal rank [Gaigher, 1980]. High rank coals in the Kwazulu-Natal coalfields have a higher concentration of illite clay minerals [Snyman and Botha, 1993] concentrated along bedding planes or associated with vitrinite [Falcon and Snyman, 1986].

2.8.1.3 Chlorites

Chlorites $(Mg, Fe, Al)_6(Al, Si)_4O_{10}(OH)_8$ are generally rare in coals because they are usually unstable in peat forming environments. Chlorites are of authigenic and epigenetic origin. Alkali chlorites are found in shales and underclays associated with coal seams. A high concentration of chlorite in high rank coals is formed as a result of chloritisation. Alkali chlorides occur in trace amounts in bituminous coals.

2.8.2 Silica minerals

Quartz is one of the most common oxide minerals found in coals. Quartz can have a detrital, authigenic or epigenetic origin. Quartz and kaolinite found in SA coals are frequently associated with inertodetrinite, indicating their detrital origin [Snyman and Botha, 1993]. The forms of detrital quartz range from rounded particles, to angular fragments and minute grains of less than 2 μm in size [Falcon and Snyman, 1986]. The rounded quartz grains are introduced into the peat swamp by water, while angular fragments are transported into the peat swamp by wind. The fine crystalline quartz infilling cells or pores of organic matter are of authigenic or epigenetic origin. Authigenic quartz originates from aqueous solutions during early stages of diagenesis.

2.8.3 Carbonates

Carbonate minerals have been identified as the second most abundant mineral in British and Australian coals [Kemezys and Taylor, 1964; Raask, 1985]. The different types of carbonates that form are calcite, aragonite, siderite, dolomite, and ankerite.

However, the composition of carbonates found in coals has a complex chemistry, because the compounds formed are in a solid solution state [Gluskoter, 1975]. Carbonate ions are derived from organic matter by biological activity or ground water movement in coal bearing strata.

Calcite ($CaCO_3$) is deposited in fresh water or under marine environments. An environment high in $Mg^{2+/}Ca^{2+}$ ratio favours the formation of ankerite ($CaMg(CO_3)_2$) over calcite [Garcia-Vallès *et al.,* 1993]. Conditions that are favourable for the precipitation of calcite are low partial pressure of CO_2 and a highly alkaline environment. Carbonate minerals can have an authigenetic, detrital or biogenic mode of occurrence.

Authigenetic carbonates are most commonly found in sub-bituminous coals. Syngenetic calcite occurs as individual grains, lenses, or cell in-fillings. The syngenetic calcite is commonly found as cavity fillings, whilst epigenetic calcite is found as cleat fillings [Renton, 1982]. The epigenetic calcite, which precipitated as a recrystallization product of the low temperature hydrothermal process, occurs as vein infillings. The epigenetic calcite and dolomite are abundant in coals near intrusive bodies, as a result of hydrothermal changes from igneous materials.

Siderite ($FeCO_3$) mineral is formed in environments where the concentration of sulphate ions is low. Therefore, the presence of syngenetic siderite indicates an acidic fresh water environment, due to the interaction between Fe and CO_2 in the absence of sulphate minerals. Siderite is associated with calcite in coals of freshwater origin. Siderite and dolomite are formed during the epigenetic stages of coal formation, whilst calcite and ankerite are formed during the late syngenetic stages of coal formation. Siderite occurs as nodules and in-fillings. Siderite that occurs as small nodule is of a syngenetic origin [Gould and Smith, 1979].

During maturation, metallic ions of Mg, Ca, and Fe found in coal are taken up into solution. The interaction of these ions with CO_2 and H_2O precipitates out carbonates that are redeposited inside cleats. Carbonate-filled cleat fissures are considered secondary carbonates, since they are formed after the formation of cleats.

The mode of occurrence of dolomite is authigenetic, and to a lesser extends detrital. The diagenesis of dolomite results from the transformation of calcite or aragonite. The formation of dolomite is favourable in environments where there is a high concentration of Mg, in warm and saline environments. Querol *et al.* (2001) indicated that the marine influenced coals tend to have a low concentration of dolomite when compared to non-marine coals.

Calcite is the most common form of carbonates, and siderite is the second most common carbonate found in coals. Van der Spuy and Willis (1991) used XRD to characterise mineral matter in South African coal from the Witbank coalfield. In the study, aragonite was found as one of the dominant carbonate minerals found in Witbank coals.

2.8.4 Sulphides

The three major forms of sulphur identified in coals are organic, pyritic, sulphate salts, and elemental sulphur [Calkins, 1994]. The organic sulphur is present as thiolic, sulphidic and thiophenic structures in the organic matrix of coal [Domazetis *et al.,* 2006]. Large quantities of thiol and disulphide sulphurs are found in low rank coals, whilst thiophene is common in high rank coals [Yani and Zhang, 2009].

Coals influenced by marine conditions have a high concentration of iron sulphides. Iron-bearing minerals found in coal are in the form of pyrite (FeS_2), pyrrhotite ($Fe_{(1-x)}S$), or marcasite (FeS_2). Marcasite has the same chemical composition as pyrite, but different mineralogical structure, morphology, and thermodynamic properties; marcasite is orthorhombic, whilst pyrite has a cubic structure.

Marcasite is metastable relative to pyrite, forming more stable phases at higher temperatures. The formation of pyrite and marcasite is controlled by sulphur speciation and pH of the solution in the environment.

Marcasite is the dominant phase at pH below 5, in the presence of neutral polysulphides, which are metastable in acidic environments. Pyrite precipitates out in mildly acidic to basic solutions [Murowchick and Barnes, 1986]. It is understood that the formation of pyrite in coals is associated with marine conditions due to activities of sulphur depositing bacteria, the reduction of ferrous sulphate by organic matter and the precipitation of ferrous sulphide by the interaction of hydrogen sulphide from plant decay [Nayak, 2013]. Pyrite is the most common sulphide mineral found in coals [Gray, 1978] and the main source of SO_x and harmful TEs emitted in coal conversion processes. Other forms of sulphide minerals reported in small quantities include chalcopyrite ($CuFeS_2$), sphalerite (ZnS), arsenopyrite (FeAsS), pyrrhotite ($Fe_{(1-x)}S$, and galena (PbS) [Calkins, 1994].

Pyrite is found in coals in a variety of morphologies and size. Figure 2-5 shows the different morphologies of pyrite found in South African coals [Falcon and Snyman, 1986]. Typical morphologies of pyrite are framboids, isolated euhedral crystals, non-spherical aggregates of euhedral crystals, irregular shapes, and fracture in-fillings [Roberts, 1988]. The framboidal and isolated euhedral pyrite are found in most coals, including low sulphur coals.

The typical size of framboids range between 100-200 µm in size, with individual crystallites of 0.1-2 µm. Marcasite occurs in three morphologies, namely: radial crystalline clusters, framboids or euhedral crystals, and massive crystals [Querol *et al.,* 1989]. Marcasite rarely occurs as cleat filling. The cell in-filling structure within coal replacing macerals is common in coals with a sulphur content greater than 1 wt. %.

Sulphides are either of a syngenetic or epigenetic origin. Primary (syngenetic) pyrite originates from the replacement of plant tissue micropores and macropores from biochemical decay. Syngenetic pyrite occurs as framboids, and isolated euhedral crystals. The presence of syngenetic pyrite is an indication of the formation of coals under marine conditions [Ward, 2002]. However, syngenetic pyrite can also be found in lacustrine environments, where there is no involvement of seawater, but sulphate-rich lake waters or sulphate-rich underground water. The epigenetic pyrite cleat fillings are related to marine conditions. It is important to note that the size, morphology, and the organic association of pyrite in coals affect the ease of liberation of the mineral during coal beneficiation [Frankie and Hower, 1985].

Marcasite of late syngenetic origin occurs as radial and spheroidal crystalline aggregates. Secondary (epigenetic) or redeposited pyrites, and to a lesser extend marcasite, are characterised by precipitates of euhedral and massive morphologies in fissure or cracks [Querol *et al.,* 1989].

2.8.5 Sulphates

The presence of sulphate sulphur in coal is less common in fresh coals, but found in partially weathered coals [Yani and Zhang, 2009]. The concentration of sulphates in coals are generally low, ranging from 0.01-0.05 wt. %, on a dry basis [Given and Yarzab, 1979]. Common sulphates found in fresh coals are gypsum ($CaSO_4.2H_2O$) and barite ($BaSO_{4)}$.

These minerals are mainly of epigenetic origin, occurring as long prismatic crystals or crack infilling [Vassilev and Vassileva, 1996]. Sulphides are easily oxidised, and form from some of the hydrated sulphate minerals found in coals such as szomolnokite ($FeSO_4 \cdot H_2O$), rosenite ($FeSO_4 \cdot 4H_2O$), melanterite ($FeSO_4 \cdot 7H_2O$), coquimbite ($Fe_2(SO_4)_3 \cdot 9H_2O$), roemerite ($FeSO_4.Fe_2(SO_4)_3 \cdot 14H_2O$), jarosite($(Na,K)Fe_2(SO_4)_3(OH)_6$), and halotrichite ($FeAl_2(SO_4)_4 \cdot 22H_2O$) [Chou, 2012]. Bassinite ($CaSO_4.{}^1/_2\ H_2O$) is commonly identified in LTA as an artefact [Ward, 2002].

2.8.6 Phosphates

Apatite ($10CaO.3P_2O_5.H_2O$) (calcium phosphate) is the most common phosphate mineral found in coals. Other phosphate minerals found in coals include gorceixite ($2BaO_3.3Al_2O_3.2P_2O_5.7H_2O$) and goyazite ($2SrO_3.3Al_2O_3.2P_2O_5.7H_2O$). The concentration of P in coals is generally low, with an average concentration estimated at 500 ppm [Ward *et al.*, 1996]. The average concentration of P_2O_5 in SA coals is approximately 0.2 wt. %. However, the concentration can be as high 2.4 wt. % [Snyman and Botha, 1993]. The concentration of P in Mpumalanga coalfields is variable from one seam to the other. The mode of occurrence of P is either organically (disseminated in coal macerals) or inorganically bound (cell infillings and cleats), with detrital and authigenetic origin [Vassilev and Vassileva, 1996]. Coarse grained crystals of phosphate minerals with particle size greater than 10 µm are of detrital origin.

2.8.7 Oxides and other minerals

Other oxides and minerals found in minor quantities or present as accessory minerals in coals include Fe-oxides, (i.e. hematite and magnetite), Ti-oxides, (rutile, brookite, and anatase), and goethite. Ti has been cited as a primary cause of deactivation of supported Co-Mo

hydroliquefaction and hydrodesulfurization catalysts [Garcia and Martinez-Tarazona, 1993]. Fe hydroxides and iron sulphates are considered to be weathering products that formed during prolonged storage or formed as a result of low temperature ashing [Vassilev *et al.*, 1996].

2.9 Chapter summary

Coal is one of the most important commodities driving the SA economy, with an estimated 55 billion tonnes of economical coal reserves. The major coalfields are found in the central basin, located in the provinces of Mpumalanga, Free State, Gauteng, Eastern Cape, and Kwa-Zulu Natal province. Coal parameters such as grade, rank, and type are largely influenced by the climate, the geography of peat forming swamps, basin tectonics and differential subsidence. SA coals formed in the Gondwana Karoo Basin experienced climate conditions different from the northern hemisphere coals, making SA coals quite distinct from their counterparts. The varying geological and environmental conditions that existed throughout the Karoo Basin led to the formation of characteristic inertinite-rich coals, with a wide range of coal products, ranging from thermal, metallurgical, and steam coals. The formation of various types of mineral matter is dependent of the pH-Eh of the environment and the bacterial life associated with the enclosed environment. Typically, SA coals used in coal conversion processes are low rank coals with high ash content.

Common mineral matter found in SA coalfields includes clays, sulphides, oxides, silicates, phosphates, and carbonates. Kaolinite and quartz are the most abundant minerals matter found in SA coals. The mode of occurrence and association of the different mineral matter can be variable, and this can have an impact on overall performance of mineral matter in coal conversion processes. The role of mineral matter and the impact of mineralogical structure in coal processes are discussed in more details in Chapter 3.

CHAPTER 3: THE EFFECT OF MINERAL MATTER IN COAL UTILISATION PROCESSES

3.1 Introduction

This chapter focuses on the effect of mineral matter on coal utilisation processes. The review evaluates ash related problems, whereby different phase transformations, ash transportation mechanisms, ash deposition structures, and predictive tools are discussed.

3.2 Coal conversion processes

Coal combustion, carbonisation, and conversion are the three major industrial processes that are categorised as coal utilisation processes, with coal combustion being the major process of the three. The coal combustion process involves burning of coal under oxidising environments to liberate thermal energy used in the electricity power plants to generate steam. The carbonisation process involves heating coal in the absence of air, to produce metallurgical coke, and lastly, the conversion processes (hydro-liquefaction and gasification), transform coal into gaseous or liquid fuels products, also known as synthetic fuels.

During coal conversion processes, minerals undergo thermal decomposition, fusion, disintegration, and agglomeration [Chakravarty *et al.,* 2015]. Some of the reactions that are related to the transformation of mineral matter include oxidation-reduction, decomposition, dehydration, dehydroxylation, destruction, polymorphic transformation, volatilization, condensation, dissolution, melting, recrystallization, vitrification, solid-phase interactions, and combined reactions [Vasileva and Vassilev, 2005].

The partitioning of mineral matter during coal conversion depends on the association, chemical and physical characteristics, as well as combustion conditions. Extraneous and inherent mineral charged into the conversion chamber undergo both chemical and physical degradation, under either oxidising or reducing environments. However, these minerals experience different thermal history that lead to their chemical degradation process. For example, excluded minerals are likely to experience fragmentation, fusion, and chemical reaction prior to solidification [Krishnamoorthy and Pisupati, 2015].

Fragmentation of excluded minerals may occur due to factors such as thermal shock and rapid gas evolution during decomposition, thus leading to the formation of fine ash particles. Thermal shock due to sharp temperature gradients within a particle can lead to the development of strong stresses within the particle, whilst rapid gas released can lead to internal pressure built-up that could lead to fragmentation [Krishnamoorthy and Pisupati, 2015].

Transformed extraneous minerals produce coarse ash particles ranging from 10-90 μm in size. The particle size of these ashes is influenced by the type of coal, and the combustion conditions the coals are exposed to. However, the composition of ashes formed by extraneous mineral matter is somewhat similar to the original composition of mineral matter in coals.

Inherent mineral matter (carboxylic, phenolic, hydroxyl groups, metalloporphyrins, and organo-metallic compounds) associated with organic matter and water soluble inorganics (water soluble salts and inorganic substances in the pores and surface of the coal) experience high temperatures and may coalesce during burnout of the parent char particle. The coalescence of mineral matter results in an increase in the ash particle size, and change in the chemistry of the particle [Krishnamoorthy and Pisupati, 2015].

At high temperatures under reducing environments, included minerals will transform into tiny ash nodules within char pores [Ragland and Baker, 1987]. The transformation of inherent mineral matter is governed by condensation and fragmentation. The fragmented mineral matter is characterised by a bi-modal size distribution of particles that contribute to the formation of fly ash.

Figure 3-1 shows the ash transformation mechanism of extraneous and inherent mineral matter that is subjected to high temperatures during combustion. From the schematic illustration, it is seen that inorganic compounds transform into aerosols, ash particles, and gaseous species [Tomeczek *et al.*, 2002].

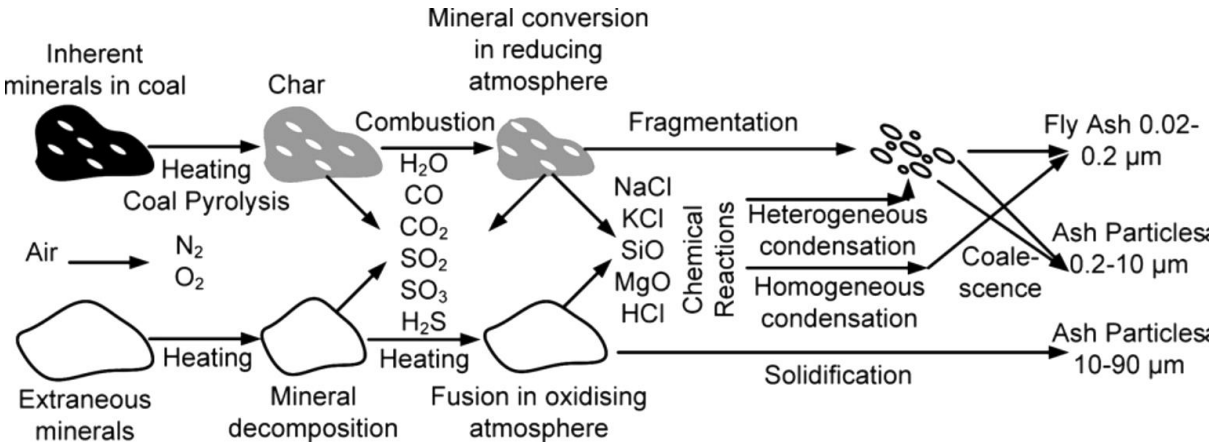

Figure 3-1: Ash formation mechanisms during coal combustion [Tomeczek and Palugniok, 2002]

The transformation of mineral matter and slag formation are important properties that provide information regarding the suitability of coals for either combustion or gasification processes [Zhang *et al.*, 2011; Matjie *et al.*, 2011].

Extensive research was directed towards understanding the transformation of mineral matter in gasification processes. Matjie *et al.* (2011) investigated the sintering and slagging behaviour of mineral matter in a gasification process, using XRF, QEMSCAN, and XRD. Soundarrajan *et al.* (2012) characterised mineral matter using ash yield measurements, XRF,

XRD, CCSEM, and Mossbauer spectroscopy Hai-tao *et al.* (2015) used XRD and FTIR to investigate phase transformation of minerals in direct coal liquefaction under gasification atmosphere, and Mössbauer spectroscopy to study the iron bearing minerals that contribute to phase transformation. Other studies used differential thermal and thermogravimetric methods.

O'Gorman and Walker (1973) investigated the thermal behaviour of individual mineral matter in four coals of different ranks using thermogravimetric (TG) and derivative thermogravimetric (DTG) methods. The phase transformation of mineral matter at high temperatures, under nitrogen atmosphere are summarised in Table 3-1, and discussed in subsequent sections.

Table 3-1: Differential thermal analysis (DTA) data for minerals occurring in coals-determined under a nitrogen atmosphere [O'Gorman and Walker, 1973]

	Endothermic effects		**Exothermic effects**	
Mineral	Peak temperature range (°C)	Interpretation	Peak temperature range (°C)	Interpretation
Kaolinite	100-120	Release of adsorbed water	950-1000	Phase transformation to γ-Al_2O_3 and nucleation of mullite
	500-600	Dehyroxylation		
Illite	50-150	Release of interlayer water	940-950	Phase transformation to spinel phase
	370-620	Dehyroxylation		
	850-900	Lattice destruction		
Montmorillonite	100-150	Release of interlayer water	900-920	Phase transformation to spinel phase
	600-730	Dehyroxylation		
	850-900	Lattice destruction		
Prochlorite	550-750	Decomposition of brucite layer	860-900	Formation of olivine $(Mg, Fe)_2SiO_4$
	750-820	Dehydration of talc layer		
	820-860	Dehydration		
Mixed-layer illite-montmorillonite	50-150	Release of adsorbed and interlayer water	900-950	Phase transformation
	450-590	Dehyroxylation		
	600-650	Lattice destruction		
	950-1000	Decarbonation		
Calcite	710-950	Decarbonation		
Dolomite	740-800	Decarbonation		
	815-910	Decarbonation		
Siderite	425-610	Decarbonation		
Quartz	570	Quartz inversion		
Gypsum	100-150	Dehydration	350-370	Phase transformation γ-$CaSO_4 \rightarrow \beta$-$CaSO_4$
	150-200	Dehydration		

3.2.1 Transformation of clay minerals

The loss of OH structural groups from clay minerals results in rearrangement of the mineralogical structure, releasing water of crystallisation, following an endothermic reaction at temperatures between 100°C and 120°C [Given and Yarzab, 1979].

Clay minerals become dehydrated at temperatures above 550°C, following a dehydroxylation process described in Equation 3-1 [Gray, 1978]. It is at these high temperatures where structural changes lead to the formation of an amorphous phase called metakaolinite. The metakaolinite phase remains stable only up to temperature around 925°C.

$$Al_2O_3.2SiO_2.2H_2O \rightarrow 2H_2O + Al_2O_3.2SiO_2 \qquad Equation\ 3-1$$

Further dehydration processes on metakaolinite lead to the deformation of the crystal lattice, mass loss, and subsequent chemical decomposition of metakaolinite into aluminosilicate. The overall effect of endothermic reactions involved in the decomposition of clay minerals lead to the reduction in calorific value of pulverised coals [Falcon and Ham, 1988; Shirazi *et al.*, 1995; Spears, 2000]. However, at higher temperatures (between 950°C and 1000°C), aluminosilicates undergo an exothermic reaction, transforming into aluminosilicates liquid, following the reaction indicated in Equation 3-2.

$$2(Al_2O_3.2SiO_2) \rightarrow SiO_2 + 2Al_2O_3.3SiO_2 \qquad Equation\ 3-2$$

Upon solidification of molten aluminosilicates, aluminosilicate glass with mullite ($Al_6Si_2O_{13}$) and cristobalite (SiO_2) are formed, as described by the reaction shown in Equation 3-3 [O'Gorman and Walker, 1973; Gupta *et al.*, 1998]. At this point, the two phases, $Al_6Si_2O_{13}$ and SiO_2 co-exist together until temperatures are above 1500°C, where $Al_6Si_2O_{13}$ exists as the only stable phase [O'Gorman and Walker, 1973].

$$2Al_2O_3.3SiO_2 \rightarrow SiO_2 + 2(Al_2O_3.SiO_2) \qquad Equation\ 3-3$$

The presence of mullite and cristobalite in a melt can be interpreted in two folds. The high temperature mineral phases can be an indication of addition of fluxing agents such as Na_2O, K_2O, CaO, and alkali carbonates or it can indicate the absence of low melting species that causes ash fusion [Krishnamoorthy and Pisupati, 2015].

The presence of iron accelerates the formation of mullite. Potassium on the other hand has an opposite effect, retarding the formation of mullite. The presence of elements such as potassium, iron, and calcium oxide lower the melting point of eutectic mixtures, giving rise to the formation of silicate glasses at temperatures below 1300°C [Gupta *et al.,* 1998].

3.2.2 Transformation of carbonate minerals

Calcium (Ca) is either organically bound or associated with mineral matter. The behaviour of Ca is strongly dependent on its mode of occurrence. Ca in the form of carbonates influence ash behaviour (sintering, clinkering, fouling and fusing) in gasification and combustion processes [Matsuoka *et al.,* 2002]. In conversion processes, carbonate minerals loose CO_2 during combustion and decompose at temperatures ranging from 810-1100°C and form CaO agglomerates, following a reaction described in Equation 3-4. The CaO formed, can either react with sulphurous gases (SO_2 and SO_3) to form sulphates, as described by Equations 3-5 and 3-6, or react with alumina-silicate slag.

$$CaCO_3 \rightarrow CaO + CO_2 \qquad Equation\ 3-4$$

$$CaO + SO_3 \rightarrow CaSO_4 \qquad Equation\ 3-5$$

$$CaO + SO_2 + \frac{1}{2}O_2 \rightarrow CaSO_4 \qquad Equation\ 3-6$$

The interaction of CaO with atmospheric water leads to the formation of portlandite ($Ca(OH)_2$), the metal oxide can also react with metakaolin to form anorthite ($CaAl_2Si_2O_8$), gehlenite, and gehlenite ($Ca_2Al_2SiO_7$) [Van Dyk *et al.,* 2006; Hai-tao *et al.,* 2015].

3.2.3 Transformation of iron-containing minerals

Iron bearing minerals (pyrite, siderite, jarosite), particularly pyrite (FeS_2) have been considered the major contributor towards slagging propensities of coals [Reid, 1984; Groves *et al.*, 1987; Waanders *et al.*, 2003]. Studies, including AFT tests have confirmed that the presence of Fe in coal lowers temperature, whilst the presence of Fe^{2+} lower the viscosity of aluminosilicates melts. Therefore, extraneous pyrite play a role in slag deposit initiation, whilst inherent pyrite captured by aluminosilicates influences viscosity.

In coal conversion processes, FeS_2 loses sulphur at 300°C, following an endothermic reaction described in Equation 3-7, and transforms into pyrrhotite ($FeS_{(1-x)}$) [Groves *et al.*, 1987]. $FeS_{(1-x)}$ is sticky, thus initiating slag deposition on coal conversion units.

$$2FeS_2 \rightarrow 2FeS_{1-x} + S_2 \qquad Equation\ 3-7$$

The oxidation rate of $FeS_{(1-x)}$ depends on sulphur vapour generated inside the particles and the concentration of O_2. In general, when $FeS_{(1-x)}$ is oxidised, it forms iron oxide (FeO) as indicated in Equation 3-8.

$$FeS_{1-x} + \frac{3}{2}O_2 \rightarrow FeO + SO_2 \qquad Equation\ 3-8$$

However, in the presence of a high concentration of oxygen, further oxidation will occur, resulting in the formation of hematite (α-Fe_2O_3) at temperatures of about 800-900°C [Thiessen *et al.*, 1936; Groves *et al.*, 1987].

The presence of iron bearing minerals such as wustite, fayalite, hercynite, and cordierite leads to the initiation and growth of deposits in combustion environment. However, the abundance of these phases is dependent on temperature and ash chemistry [Hai-tao *et al.*, 2015].

Zhang *et al.* (2011) investigated the behaviour of Fe-bearing minerals [Wustite (FeO); almandite ($3FeO.Al_2O_3.3SiO_2$), and fayalite ($FeO.SiO_2$)] in ash. The results showed that the sintering behaviour of coals was influenced by the different oxidation states of Fe (Fe^{2+}/ Fe^{3+}) in combustion processes.

3.2.4 Transformation of organically-bound mineral matter

Although Fe-bearing minerals are the major source of slagging in boiler tubes [Reid, 1984; Groves *et al.*, 1987], the presence of organically bound elements (S, Cl, and Na) in low-rank coals may vaporise and condense at later stages onto coal ashes or deposits. Condensation of the organically bound elements may lead to corrosion. These elements act as fluxing agents, lowering the melting temperature of refractive silicates.

3.3 Slagging and fouling deposition mechanisms

Mineral reactions and phase transformation of either included or excluded mineral matter lead to the formation of molten deposits on the walls of conversion units. The ash deposits on conversion units presents major operational problems in coal conversion processes. Slagging and fouling are the two most common deposits encountered in coal–fired boilers, gasifiers, heat exchangers, and other coal conversion units.

Slagging is the formation of sintered or molten deposits on the walls of boilers in the radiation section, at temperatures between 1300°C and 1600°C. It is commonly found that slag formation is initiated by fluxing agents (Na_2O, CaO, Fe^{2+}, and MgO) that react with alumina-silicates or chlorides, subsequently reducing AFT [Van Dyk *et al.*, 2009].

Deposition of mullite, cristobalite, iron oxides, anhydrite, anorthite, Ca-silicates and amorphous materials reduces absorption heat in furnace, which lead to an increase in the exit gas temperature. The deposits that form reduce thermal performance and efficiencies of the equipment, and aggressive deposition of molten slags can lead to a complete shutdown of the equipment.

Soot blowers which utilise high pressure jets of air, steam or water are used to remove the deposits. However, soot blowing is not always effective in removing deposits that have strongly adhered to walls of the boiler, because excessive blowing can cause erosion damage to the equipment, and corrosion may occur beneath the deposits formed [Wee *et al.*, 2005].

Fouling deposits form in post combustion environments, on heat exchanger surfaces, where flue gas and suspended fly ash cools down [Hatt, 1990]. Figure 3-2 shows a schematic presentation of fouling deposit. The two main types of fouling are the low temperature fouling (LTF) and the high temperature fouling (HTF). The LTF occurs within the temperature ranges of 400-900°C, whilst HTF occurs at 900-1300°C.

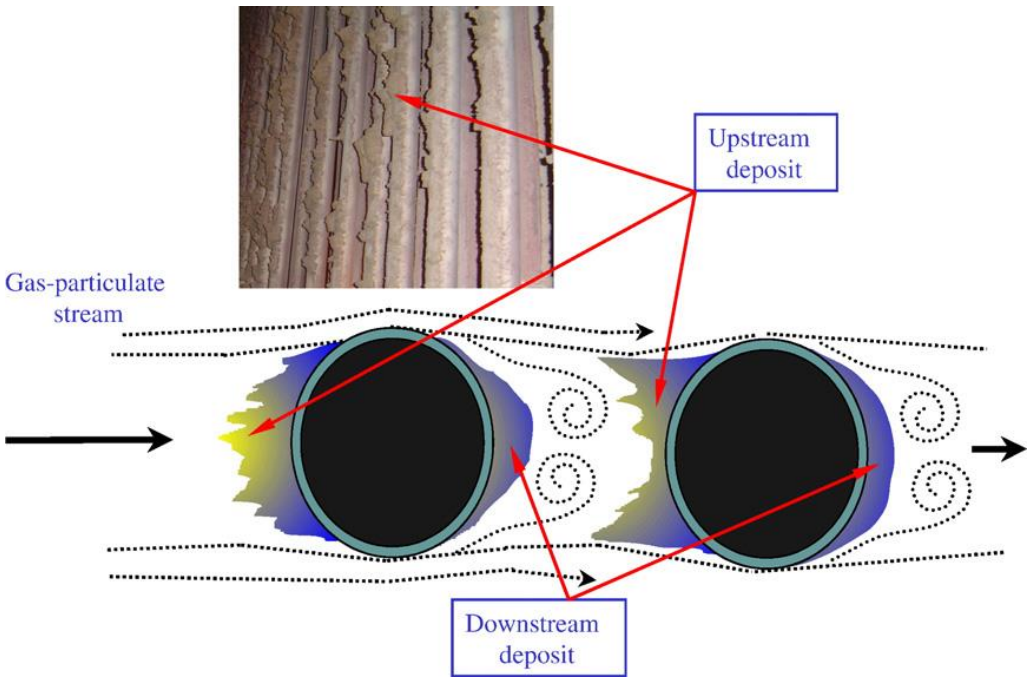

Figure 3-2: Fouling deposit on tubes in convective pass [Ma *et al.*, 2007]

The fouling mechanism involves condensation of previously volatilised flame species present in the flue gas. As a result, the deposits that form are often composed of condensed alkali salts, which provide a sticky surface, and trap other non-sticky particles [Vuthulura and French, 2008; Krishnamoorthy and Pisupati, 2015]. Fouling is common in low rank coals because of the high sodium concentration found in these coals [Vuthulura and French, 2008].

Coals that contain high quantities of Ca will readily form LTF deposits. Once the Ca particles are deposited, they are sulphated and form $CaSO_4$. The sulphated Ca can significantly add to the mass of the deposit and increase the deposit strength. The presence of alkali and alkali earth metals promote HTF.

Factors that influence slagging and fouling propensities include mineral matter particle size distribution, composition, and boiler operating conditions, such as boiler load, air to fuel ratio, gas temperature, and soot blowing patterns [Wee *et al.,* 2005]. The degree of slagging and fouling varies throughout the boiler, and is mostly affected by local combustion environment, which influence characteristics of ash deposits formed on heat transfer surfaces.

3.3.1 Ash particle transport mechanisms and ash deposits

The transportation mechanism of ash particles onto heat transfer surfaces can be classified according to the size of particles that are being transported. The three main mechanisms of importance are diffusion, thermophoresis, and inertial impaction.

- **Diffusion** is the transportation of gas particles of less than 1 μm, due to local concentration gradient. There are three types of diffusion mechanisms which describes the movement of particles to the surface. The Fick diffusion mass transport results in molecules moving to the surface due to concentration gradient present.

Brownian diffusion describes the haphazard movement of small particles, and Eddy diffusion describes diffusion due to turbulent flow effects [Babat *et al.*, 2011].

- **Thermophoresis** is the transportation of small particles (<1 μm) due to thermal gradient from hot gases to cooler heat transfer areas. The thermophoresis transportation mechanism is generally relevant at very low deposition rates. For example, the deposition will occur when boiler tubes are new or clean. Inertial impaction is a process which involves large particles (usually greater than 5-10 μm) of sufficient size and density to come out of the air flow patterns around the tube and stick to surfaces of a tube or deposit. Eddy impaction involves the transportation of particles from one region to the next due to the difference in charge between the particle and heat transfer areas. The transportation of particles less than 10 μm follows the thermophoresis and electrophoresis mechanism, whilst large particles follow the inertial impaction mechanism.
- **Inertial impaction** is the most important transporting mechanism for large particles of an average diameter greater than 10 μm. Volatile enriched particles that are less than 1 μm are transported by diffusion mechanism.

The four types of slag deposits formed in coal conversion processes are classified as either metallic, amorphous, vesicular, or sintered [Unsworth *et al.*, 1988; Hatt, 1990]. The deposit characteristics depend on temperature and operating conditions inside the conversion unit. The metallic slag is usually associated with the combustion of pyrite rich coals. The amorphous (bound) glassy deposit is comprised of assimilated ash particles. The versicular deposit consists of amorphous slags, which trap bubbles that give the slag a sponge like appearance, whilst the sintered slag deposit consists of partially fused ashes. Figure 3-3 gives a description of the different slag deposits that are formed in boiler tubes during coal combustion.

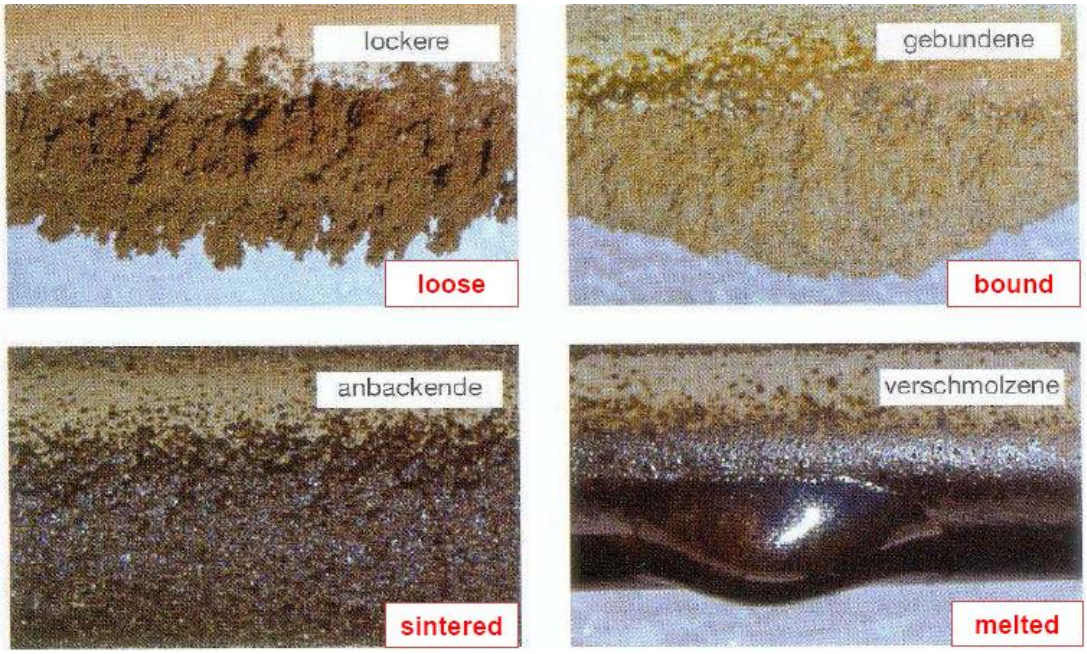

Figure 3-3: Loose, bound, sintered and melted slag deposits that are typically found in boiler tubes [Hatt, 1990]

3.3.2 Prediction of ash deposition in coal conversion processes

A number of methods have been developed to evaluate slagging and fouling propensities of coals in conversion units. The main approaches used to predict slagging and fouling includes:

(i) empirical methods,

(ii) laboratory tests,

(iii) mechanistic modelling approach, and

(iv) computational fluid dynamics (CFD) modelling.

Most industrial practices are still using the traditional empirical approaches that are based on ash chemistry, viscosities, and AFT parameters, to determine slagging and fouling indices. Studies have shown that slagging depends on the combined effect of forming liquid phases, temperature and the ash loading [Lawrence *et al.*, 2008].

The mechanistic approach uses advanced indices that include mineralogical data from Computer Controlled Scanning Electron Microscope (CCSEM) and chemical fractionation tests to study slagging and fouling propensities in coal [Wall, 1992; van Alphen, 2007]. The CFD use models that calculate both the thermal and aerodynamic conditions in the combustion chamber. A combination of computational fluid dynamics, thermodynamic and viscosity model present a more accurate estimation of slagging temperatures [Krishnamoorthy and Pisupati, 2015]. FactSage and viscosity models give information on slag viscosity, whilst computational models provide information regarding particle temperature and particle trajectory inside a gasifier. Nonetheless, for the purpose of this research work, only the ash deposition indices and AFT will be discussed.

3.3.2.1 Ash deposition indices

Coal ash chemistry and mineralogy are the two most important factors used for selecting coals; mainly because of the impact coal ash have in coal conversion processes. The major and minor oxides (SiO_2, MgO, CaO, P_2O_5, SO_3, Al_2O_3, TiO_2, Fe_2O_3, Na_2O, and K_2O) that represent the amounts of elements in coal are used to formulate ash deposition indices that can be used as predictive tools to determine slagging and fouling propensities, and to evaluate coal quality in coal-fired boilers and gasifiers [Winegartner, 1974; Reid, 1984]. The oxides can be classified as acidic (SiO_2, Al_2O_3, and TiO_2) or basic (Fe_2O_3, CaO, MgO, K_2O, and Na_2O).

A number of indices have been proposed for coals, and coal blends. Over the years, deposition indices have been modified and tailored for specific coals, and to determine slagging and fouling propensities of biomass [Wang and Massouri, 2013]. The typical indices

used include; the base-acid (B/A) ratio, silica/alumina (SiO_2/Al_2O_3) ratio, iron /calcium (Fe/Ca) ratio, and silica percentage.

The indices summarised in Table 3-2 give the degree or severity, and acceptable limits for both slagging and fouling propensities in conversion processes [Lawrence *et al.*, 2008].

Table 3-2: Summary of key empirical correlations for slagging and fouling [Raask, 1985]

Index	**Formula**	**Slagging or fouling propensity**			
		Low	Medium	High	Severe
Slagging propensity					
Base-Acid Ratio	$\frac{B}{A} = \frac{Fe_2O_3 + CaO + MgO + K_2O + Na_2O}{SiO_2 + Al_2O_3 + TiO_2}$	<0.4 or > 0.7		0.4 to 0.7	
Slagging factor	$\frac{B}{A} \times Sulphur\ in\ coal$	<0.6	0.6- 2.0	2.0- 2.6	>2.6
Iron-calcium ratio	$\frac{Fe_2O_3}{CaO}$	<0.3 or >3.0	0.3- 3.0		
Iron plus calcium	$Fe_2O_3 + CaO$	<10%			
Silica percentage	$\left(\frac{SiO_2}{SiO_2 + Fe_2O_3 + CaO + MgO}\right) \times 100$	72-80	65-72		50-65
Fouling propensity					
Fouling factor	$\frac{B}{A} \times Na_2O\ in\ the\ ash$ (%)	<0.2	0.2- 0.5	0.5-1.0	>1.0
Sodium content	Na_2O % *in the ash for bituminous ash*	0.5	0.5-1.0	1.0- 2.5	>2.5
	Na_2O % *in the ash for lignitic ash*	<2.0	2-6.0	6-8	8.0

The B/A ratio equation expressed in Table 3-2 is one of the most common index used to predict slagging potential for coals of all ranks and types [Su *et al.*, 2003]. The B/A ratio take into account the influence of basic oxides with low melting point and acidic oxides with high melting point. According to the classification and criteria given in Table 3-2, coals with B/A ratio between 0.4 and 0.7 have low AFT, and high slagging propensity [Wang and Massouri, 2013]. Coals with low slagging propensities will have a B/A ratio < 0.4 or > 0.7, whilst an ideal coal composition will have a B/A ratio below 0.11. The fouling index takes into account

the effect of Na_2O because coals with high amount of Na have a high tendency to form deposits in conversion units [Vuthaluru and French, 2008].

Patterson and Hurst (2000) investigated the suitability of using bituminous Australian coals in a gasifier. From the study it was observed that the silica ratio < 80 were required for entrained-flow gasifiers, whilst silica ratio < 70 were ideal for fixed bed reactors.

Fluxes are generally used for coals with high silica ratios. The use of fluxes can be minimised by adjusting the SiO_2/Al_2O_3 ratio to ranges between 1.6 and 2.0. Table 3-2 shows that coals with low slagging propensity have a silica percentage between 72 and 80, whilst coals with high slagging propensity have a slagging index between 50 and 65 [Raask, 1985].

The interaction between iron and calcium form low melting eutectics, that lowers the AFT, and favour slag deposition. Lowered fusibility is observed when the Fe/Ca ratio is between 0.3 and 3, subsequently leading to medium to high slagging propensity. Low slagging propensities is observed when the Fe/Ca ratio is less than 0.3 or greater than 3. Various researchers have concluded that CaO, FeO, and SiO_2 can be used as indicators of ash fusion properties [Patterson *et al.,* 1994]. However, the CaO content of the ash should be between 5-40 wt.%, whilst Fe_2O_3 should be below 6 wt.% [Akar and İpekoğlu, 2007].

The developed deposition indices are highly subjective to a particular type of coal, and their application is limited because these indices do not take into account the boiler design or the operating conditions. Moreover, the ash composition does not reflect the true interactions between mineral particles during combustion [Lawrence *et al.,* 2008]. Therefore, the deposition indices overlook the complex chemistry of mineral matter which includes among other factors, the mode of occurrence and association of mineral matter in coals. As a result,

indices can be used only as a guide, and caution should be exercised when reporting indices based on ash chemistry [Vuthaluru and French, 2008].

3.3.2.2 Ash fusibility and ash flow temperature (AFT)

The ash fusion temperature (AFT) is an important and widely accepted index used to predict slagging and fouling in gasifiers and boilers [Vuthaluru and French, 2008]. The AFT test is designed to simulate coal ash behaviour under oxidising or reducing conditions. The test is based on observing four characteristic temperatures as the shape of coal ashes change with increasing temperature. The change in shape occurs as a result of deformation, shrinkage and flow. Figure 3-4 shows the ash fusion standard test measuring method.

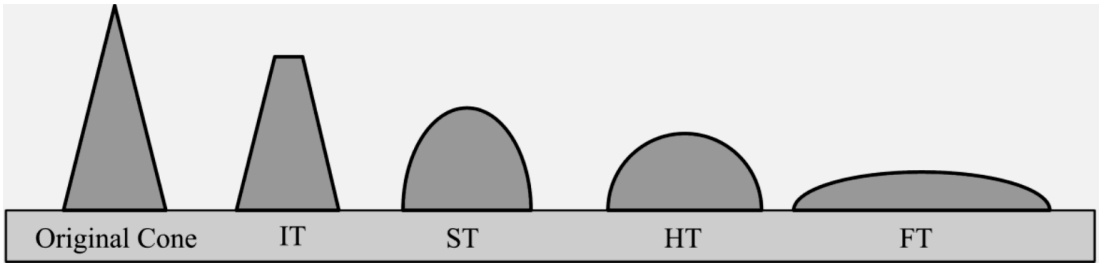

Figure 3-4: Ash fusion standard method for the determination of fusion behaviour of ashes (following the ISO 540 standard) [Akar and İpekoğlu, 2007]

The four temperatures measured during the AFT test are the initial deformation temperature (IDT/DT), an onset of sintering, whereby the sample begins to lose its original shape, softening temperature (ST), hemispherical temperature (HT), at which the sample reaches the shape of half a sphere, and the fusion temperature (FT), where the ash becomes completely molten. In summary, Ash fusion temperature (AFT) is the temperature at which the ash in coal begins to soften, flow and fuse [Weeber *et al.,* 2000]. The AFTs indicate temperature ranges at which bulk ash chemistry may start to deposit on heat absorbing surfaces, but does not give actual temperatures at which melting start. An optimal FT < 1400°C and up to

1500°C is acceptable in reducing environment. However, caution should be exercised if the coal sample has high ash content and FT below 1260°C.

Although the AFT test together with depositional indices are still used for quick screening, accessing slag viscosity, flux requirements and determining the suitability of coal in combustion and gasification processes [Patterson and Hurst, 2000], the test can be subjective and unreliable with poor reproducibility since the results are based on the operator's observation [Jin *et al.,* 2009]. The AFT results reported from different laboratories can vary by a temperature difference of 20-100°C [Özbayoğlu and Özbayoğlu, 2006]. Moreover, the laboratory test cannot accurately predict conditions inside a gasifier [Van Dyk *et al.,* 2006].

3.3.2.3 Correlation between ash chemistry and AFT

A number of investigations have been carried out to establish a correlation between ash chemistry and AFT [Özbayoğlu and Özbayoğlu, 2006; Van Dyk, 2008; Han-xu *et al.,* 2008; Lawrence *et al.,* 2008; Liu *et al.,* 2013; Chakravarty *et al.,* 2015]. Liu *et al.* (2013) reported CaO, Fe_2O_3, and SiO_2/Al_2O_3 ratio as the main chemical compositional identifiers that influenced AFT. Increases in basic oxide compositions reduce the AFT of coals.

As mentioned earlier, over and above the correlation between ash composition and AFT, different analytical techniques are being used to characterise mineral matter and gain understanding on fusion characteristics of coal ashes. For this reason, full knowledge of transformation of mineral matter in coal is paramount to the determination of ash fusion characteristics. Analytical techniques can be used to determine the relationship between ash fusibility and chemical composition of minerals in coal.

Some of the techniques used to predict slag phases include scanning electron microscope, energy dispersion X-ray spectroscopy, thermogravimetric analyses, CCSEM, FTIR, Mossbauer, Electron probe micro analysis, XRD, XRF, and thermodynamic computer package FactSage [Oliviera *et al.,* 2011; Krishnamoorthy and Pisupati, 2015].

3.4 Chapter summary

Mineral matter plays an extensive role in conversion processes. The association of mineral matter within the organic matrix influences the interaction and transformation of mineral matter. The transformation of mineral matter at high temperatures leads to slagging, fouling, erosion, and corrosion, which could lead to reduced thermal efficiencies and downtime of equipment. The three most undesirable minerals responsible for slagging and fouling are pyrite, carbonates, and illite. The presence of both Fe and Ca lowers temperatures, forming low melting eutectics. Understanding the mode of occurrence of mineral matter in coal structures can help reduce the effect of slagging and fouling in conversion processes, and this has been elucidated by various studies that investigated the relationship that exist between coal properties and overall combustion behaviour. However, information provided by the different analyses based on ash chemistry have become inadequate, as a result, various predictive modelling tools that closely simulate real conditions have been developed to determine slagging propensities of coal.

A multiple technique approach has been proposed by various researchers to understand the effect of mineral matter on conversion processes. In order to characterise and understand mineral matter various analytical techniques can be used. Some of the different techniques commonly used to characterise the organic and mineral matter in coals are discussed in the next chapter.

CHAPTER 4: REVIEW OF CHARACTERISATION TECHNIQUES USED TO DETERMINE MINERAL MATTER IN COALS

4.1 Introduction

South African coals are characterised by high ash content. The presence of mineral matter in coals is generally undesirable as highlighted in Chapter 3. Therefore, detailed characterisation of mineral matter with respect to particle size distribution, chemical composition, mode of occurrence, association, textural, and structural morphology is required for proper assessment and selection of coals in utilisation processes [Kimura, 1998; Ruan and Ward, 2002].

It is becoming a necessity to fully characterise mineral matter in coals because of the stringent specification requirements of raw coals, need to optimize conversion processes and maximize profit [Cook, 2000]. Although conventional methods such as proximate and ultimate analyses, calorific values, and ash chemistry are still useful, these methods fall short to fully predict the performance of coals in conversion units [Falcon and Ham, 1988].

Over the years it has been suggested that a multi-technique approach should be adopted to increase the knowledge on the behaviour of mineral matter in conversion processes. Full understanding and characterisation of mineral matter relies on the use of various analytical tools that will best describe the composition and structural morphology of coal, and to relate these properties to coal conversion processes [Martinez-Tarazona *et al.*, 1992].

It was not until recently, that there has been growing interest towards the use of advanced techniques to characterise coals [Ward *et al.*, 1999; Vassilev and Vassileva, 2009]. Comprehensive reviews on analytical tools for characterising mineral matter are presented by Ward (2002), Huggins (2002), and Vassilev and Tascón (2003).

These reviews highlight traditional techniques used for the determination of major, minor and TEs in coals, namely: inductively coupled plasma-atomic emission spectroscopy (ICP-AES), inductively coupled plasma mass spectroscopy (ICP-MS), and X-ray fluorescence (XRF) spectroscopy; the study of bulk mineralogical composition using X-ray diffraction (XRD); automated techniques such as scanning electron microscope (SEM) analyses; and more advanced techniques such as computer controlled scanning electron microscopy (CCSEM) or quantitative evaluation of minerals by scanning electron microscopy (QEMSCAN). These techniques allow for an in-depth evaluation and understanding of mineral matter in coals.

Research work focusing on detailed characterisation of mineral matter has improved significantly, mainly because of the availability of advanced micro analytical techniques [Bandopadhyay, 2010; Silva *et al.*, 2012]. The fast growing micro-analytical techniques have presented possibilities to solve technological challenges associated with mineral matter.

Most recent studies have shown that an integrated and holistic approach of using advanced techniques is critical in advancing the knowledge on mineral matter in coals. A study by Matjie *et al.* (2011), focusing on the behaviour of coal mineral matter in sintering and slagging ash in gasification processes highlighted the importance of determining bulk chemistry, mineralogy, mode of occurrence and association of mineral matter in coals using multiple techniques. In the study, XRF, SEM, XRD, QEMSCAN were used to characterise raw coals, coals ashes and density fractionated samples. It was found that integration of the different techniques provided more insight in the evaluation of ash that formed in gasification process.

Silva *et al.* (2012) characterised mineral matter and evaluated the environmental potential impact of sulphate minerals using techniques such as optical microscope, SEM-EDS,

confocal microscopy, mRs, and thermodynamic modelling simulations. In the investigation, it was found that the multi-analytical approach was beneficial in identifying mineral phases that helped explain the mechanism of sulphide oxidation.

As discussed previously, CCSEM, together with chemical fractionation methods, is used for quantitative determination of abundance, and association analyses of mineral matter in coals, and to study surface morphology of coal samples. Another approach of determining mineral matter in coals involves the use of recalculation of bulk chemical analyses using chemical quantitative phase analysis methods [Ritz and Klika (2010)]. Tickner and Roach (2004) investigated mineral matter content in coals by using Compton profile analysis via XRF, with most recent work reported by Perdikatsis (2013) on lignite samples. The study showed that XRF analyses using the Compton Effect can rapidly determine the concentration of mineral matter in an unknown sample, without ashing the sample.

Advanced techniques have helped to shape the present and future of coal usage, and the understanding of mineral matter in coals. To date, CCSEM is considered an ideal technique that characterises mineral matter in coals, and solve ash deposition problems [Gupta *et al.*, 1998; Zhang *et al.*, 2002; Saikai and Ninomiya, 2011]. The advantages presented by the technique include the ability to conduct particle to particle analyses, that helps elicit information pertaining to the association and mode of occurrence of minerals and organic matter analysed. However, most recent studies have shown that there is a growing interest and an inclination towards using multiple advanced techniques to characterise and understand coal behaviour [Manoj and Kunjomana, 2010; Oliviera *et al.*, 2011; Soundarrajan *et al.*, 2012].

Soundarrajan *et al.* (2012) used a multiple technique approach to determine ash yields. The analyses such as XRD, XRF, CCSEM, and Mossbauer were used to characterise mineral

matter in coals. Many other researchers used similar approaches to investigate the effect of mineral matter on conversion processes [Babat *et al.,* 2011; Matjie *et al.,* 2011; Oliviera *et al.,* 2011; Saikia and Ninomiya, 2011; Matjie *et al.,* 2016].

Oliviera *et al.* (2011) used multiple techniques to understand the Fe-bearing minerals that influenced slagging and fouling, found in coals from the Jorge Lacerda power plant in Brazil. Silva *et al.* (2012) used the multi-analytical approach to determine the association of mineral matter in coals. In the study, complex and diverse phases were identified. The multiple technique approach highlighted and addressed the complexity and heterogeneity of mineral matter in coal samples, and emphasised a need for a holistic approach to studying mineral matter, which will help in further development of various models used to predict slagging and fouling propensities of coals, among other properties. Matjie *et al.* (2016) used conventional and advanced techniques to determine mineral matter and elemental composition of individual macerals of Highveld coals.

Therefore, it can be said that the main purpose of a multi-technique approach is to fully understand processes and mechanisms taking place in conversion process, and to eliminate problems associated with mineral matter in downstream processes.

It is beyond the scope of this work to discuss all the possible analytical techniques used within the coal industry to characterise the organic matter and mineral matter in coals. This chapter discusses some of the major analytical tools that are used in the study to address the objectives of the research work. The analytical techniques discussed include coal petrography, XRD, FTIR, mRs, XRF, and SPA-EPMXA.

4.2 Coal petrography

Petrology is a branch of geosciences that was introduced in the early 20th century. Coal petrography, a subset of petrology, is a fundamental technique used to characterise whole coals, coal lithotypes, macerals, coal blends, chars, coke, fly ash and mineral matter in coal [Cloke and Lester, 1994]. Marie Stopes contributed significantly towards the nomenclature characterisation of the various coal components in the 1940's [Stopes, 1935].

Petrographic analyses involve microscopic evaluation of polished blocks of coal using reflected light under oil immersion. Petrographic techniques have gained importance in the determination of:

(i) Coal type (maceral composition);

(ii) Maceral and mineral matter association in coal (microlithotypes);

(iii) Shape and morphology of organic components and textural relationships between mineral matter and macerals, and;

(iv) Vitrinite reflectance, an indicator of coal rank (addressing the metamorphic transformation of macerals).

In addition to the factors listed above, it is also possible to detect oxidation, intergrowths, porosity, internal reflections, optical isotropy and anisotropy, coal to coke transformation, predict Hardgrove grindability and extend of mineral liberation [Gray, 1991]. Petrographic studies are based on qualitative and quantitative determination of macerals by conducting a point count (by volume) on polished blocks under a light microscope equipped with an oil immersion objective lens. The petrographic blocks are prepared according to the SABS ISO Standard 7404-part 2. In determining the relative abundance of macerals in coals, the maceral

that is observed on the crosshair under the eye piece is classified and counted, as per SABS ISO 7404-part 4.

Petrographic composition (i.e. maceral type and mineral matter) influences the ignition process, reactivity and the overall process efficiency in conversion processes [Cloke and Lester, 1994]. Petrographic analyses, together with geochemical analyses of coals and coal seams are useful in predicting combustion behaviour [Gentzis *et al.,* 1996], and provide useful information that can be used for mine exploration [Orheim *et al.,* 2007]. Thus, coal petrography is used to establish the applicability of coal in conversion processes [Korwin-Kossakowski *et al.,* 1990]. Méndez *et al.* (2003) studied the influence of petrographic composition and its influence on combustion reactivity. Their findings indicated that a mixture of macerals and minerals are favourable, and subsequently lead to improved reactivity. López and Ward (2008) used petrographic methods to determine the mode of occurrence of mineral matter in Colombian coal samples.

Although petrographic studies have paved way towards the understanding of coal geology and coal geochemistry, it is also important to highlight some of the challenges related to the use of the technique. Petrography is time consuming and involves sample preparation, and requires a skilled petrographer to analyse the coals. The low resolutions from the optical microscope make it difficult to analyse finely disseminated minerals or particles less than 10 μm in size [Gluskoter, 1975].

4.3 Characterisation of inorganic and mineral matter in coals using XRD technique

X-ray diffraction is an analytical tool used for bulk analysis of crystalline materials, and provides crystallographic information and unit cell dimensions of a particular crystalline material. The technique is based on the interaction of the constructive interference of monochromatic X-rays with the crystalline materials. The powder X-ray diffraction (PXRD) technique has been used as a characterisation tool within the coal industry since 1920s, and it is amongst the well-established and most highly developed techniques used to identify mineral matter and organic matter in coals [Rao and Glukoster, 1973; Lin and Guet, 1990; Ward *et al.*, 2001].

Qualitative analyses of organic matter structural parameters such as the degree of ordering, interlayer spacing, d_{002} and crystalline size, $L_{a,}$ are structural parameters studies for evaluating the structural properties of coal. However, there are limitations with regard to the use of PXRD as an analytical tool, which include the low detection limits of composition of compounds present below 1 wt. %, change in diffractogram characteristics caused by ionic substitution, grain preferred orientation of minerals such as mica and clays, different absorption characteristics of X-rays by various minerals in mixtures, overlapping of peaks, crystallite size, and the inability to characterise amorphous phases [Schoening 1982; Ward, 1999; Ruan and Ward, 2002; Vassilev and Tascón, 2003].

The initial use of XRD on coal was purely on a qualitative and semi-qualitative basis. Semi-qualitative analyses were obtained by measuring the relative intensities of the main diffraction peaks, to identify individual mineral phases [Vassilev *et al.,* 1997]. As much as the technique was used successfully as a characterisation technique for mineral matter, the inability to quantitatively characterise mineral matter, due to the presence of amorphous matter in coals was a limiting factor.

Recent advances allowed for quantitative and direct determination of mineral matter in coals using Rietveld methods [Ward and Taylor, 1996; Matjie *et al.,* 2016]. Quantitative analyses are dependent on good sample preparation to produce an accurate diffraction pattern. For quantitative analyses, both the peak intensity and the peak position must be accurate for one to extract accurate results. A number of methods were developed for quantitative analyses of crystalline materials, and the intensity equation is one of the methods commonly used. Peak intensities indicate the total scattering from the different planes within the crystal structure, and could serve as an indication of the amount of phases present.

The Rietveld method is the most accurate method used for quantitative analysis of mineral phases [Hutton and Mandile, 1996]. An internal standard is used to calibrate the scale factors used by the program. A normalized fit is conducted when an internal standard is not used.

Quantitative analyses using SIROQUANT^{TM}, developed by Taylor (1991), is a computer program based on Rietveld refinement methods. SIROQUANT has received much attention [Hutton and Mandile, 1996; Lu *et al.,* 2001, Ward *et al.,* 2001; Ural, 2007] mainly because the quantitative analyses provide more knowledge about crystalline mineral matter compared to other quantitative methods available [Ural, 2007].

Despite shortcomings presented by the technique, previous studies have shown that there has been significant success and improvement in characterising mineral matter in coals. Quantitative analyses of clay minerals using SIROQUANT have been reported by various authors. Ward *et al.* (1996) have applied SIROQUANT technique for the determination of mineralogical analysis of a wide range of sandstones and clay minerals from Australian coal basin strata. Other studies involved characterising mineral matter in low temperature ash from various Australian coal samples [Ward and Taylor, 1996].

Successful work carried on characterisation of mineral matter using SIROQUANT has shown that there is a good correlation between quantitative analysis of mineral matter using XRD and chemical composition methods.

Clay minerals are the most abundant minerals found in coal, and the most difficult to identify, thus ethylene gycol is commonly used to collapse the expendable lattice structure for easy identification [Wilson, 1987; Ruan and Ward, 2002]. Some of the inherent challenges related to quantitative analysis of clay minerals include compositional variation, variable degree of structural order or disorder, and the preferred orientation of clay minerals in powdered samples.

4.4 Elemental analyses of coal

The X-ray fluorescence (XRF), neutron activation (NA), atomic absorption spectrometry (AAS), inductively coupled plasma optical emission spectrometry (ICP-OES) and inductively coupled plasma mass spectrometry (ICP-MS) are destructive methods that require sample digestion or fluxes to determine elemental composition of major, minor and trace elements, in coal samples. Although the ICP analyses have been considered the ultimate method for assessing TEs in coals [Davidson, 1996], only the XRF technique will be discussed in this review. TEs determination is beyond the scope of this investigation.

4.4.1 X-ray Fluorescence (XRF) spectroscopy

X-ray Fluorescence spectroscopy is a fast, routine technique, widely used for determination of qualitative and quantitative elemental composition of materials in various research areas, including geological, environmental, biological and industrial studies [Gupta, 2007].

The technique depends on fundamental principles that are common to instruments that operate from the basis of the interaction between electron beams and X-rays, such as SEM-EDS and X-rays.

Quantitative analysis is dependent on calibration of the instrument with standards that have a similar composition to the sample of interest. The characteristic energies of the fluorescent X-rays are recorded with an X-ray detector to determine individual elements; the two main analytical techniques used are the wavelength dispersive X-ray fluorescence (WDXRF) and the energy dispersive X-ray fluorescence (EDXRF) spectrometer.

In coal studies, whole coals and coal ashes are analysed using XRF spectrometer. The samples, fused in a borate glass, are bombarded with primary X-rays from an X-ray tube with high melting point Cr or W targets. The Cr and W targets are generally used for coal ashes because these elements are found in low concentrations in coal samples [Huggins, 2002]. Evan *et al.* (1990) studied eight Argonne Premium coals using both EDXRF and WDXRF to analyse ash and whole coal samples. In the study, the accuracy of the EDXRF was estimated at ± 5% for the determination of TEs, while the accuracy of WDXRF was estimated between 2-5% for major elements for whole coals.

Some of the advantages presented by the technique in coal analysis include:

(i) good detection limits below 1 ppm,

(ii) easy sample preparation when compared to wet method analyses such as ICP,

(iii) full automation of the equipment allows for multiple sample analysis at a time.

The limitations of the technique are:

(i) poor sensitivity for detecting TEs when compared to ICP-MS technique

(ii) light elements such as C, H, N, and O are difficult to detect, and

(iii) for accurate quantitative analysis, the technique requires the use of standards that are close in composition to that of the coal sample.

4.4.2 Electron microprobe analyses (EPMA)

Electron probe microanalysis (EPMA) is a non-destructive micro-analytical technique used in coal studies. Materials are characterised by detecting X-ray characteristics of elements when the sample is exposed to a focused electron beam. Electron Probe Microanalysis (EPMA) in combination with energy dispersive spectrometry (WDS) is capable of quantifying different elements. High energy electrons are focused on the sample, and the characteristic X-ray radiations are generated as a result of the interaction between the electron beam and the irradiated sample. For quantitative measurements, a wavelength is selected and the monochromatic radiation is diverted to a counter. The intensity is then translated into concentration, by comparing the composition of an unknown sample to a known standard, using the ZAF method [Ward and Gurba, 1998]. The three constituents of the matrix are Z, which is the atomic number correction; A is the absorption correction, and F the fluorescence correction. The ZAF method is described by Equation 4-10.

$$\frac{W_j^u}{W_j^{std}} = \frac{I_j^u F_{z,j}^u F_{A,j}^u F_{F,j}^u}{I_j^{std} F_z^{std} F_A^u F_F^u} \qquad Equation\ 4-10$$

Where, indices, u, and std refer to the unknown sample and the standard sample.

The F_Z, F_A, F_F corrects the differences in atomic number, absorption, and secondary fluorescence in the standard and unknown sample [Ward and Gurba; 1998]. Quantitative analyses using the ZAF method are calculated on the basis and assumptions that the intensities of both the standard and unknown sample are collected under identical experimental conditions.

Analyses using EPMA can be performed on flat surfaces, and single point data measurements [Ward, 1999]. However, a large population of sample would be required to obtain statistically meaningful data. Analyses can be performed on a population of anything between 100 and 4000 particles. The large amount of data received from EPMA analyses can be refined and reduced using statistical methods. The analysis of large population of data is made possible because of the automation of the technique, which improves both the accuracy and acquisition time. The technique can be used to determine particle size, elemental chemical composition and mineral association with organic matter in coals [Gupta, 2007].

Ward and Gurba (1998) used the technique to study the occurrence and distribution of organic sulphur in coals from the Gunnedah Basin. EPMA with an automated image analyser (AIA) can be successfully used for rapid determination of mineral matter in coal. A study by Shirazi *et al.* (1994) highlighted the fact that the method is reliable for the direct determination of mineral matter in coal, by providing accurate results, compared to indirect methods. Most recently, Matjie *et al.* (2016) used electron microprobe together with conventional techniques to characterise mineral matter and individual macerals.

4.5 Fourier Transform Infra-Red (FTIR) spectroscopy

Fourier Transform Infra-red spectroscopy is one of the most popular techniques used to characterise both the crystalline and amorphous matter in coals [Bosman, 1983; Li *et al.,* 2008], since both the macerals and mineral matter absorb within the infrared region [Rochdi and Landais, 1991; Saikai *et al.,* 2007]. Other materials characterised by FTIR include kerogens, and sediments in organic geochemistry. The vibrational spectroscopic investigations yield useful information such as hydration characteristics, interlayer cations, and moisture content, particularly in clay minerals [Saikai *et al.,* 2010]. Ideally, FTIR can be used to observe changes in aliphatic, aromatic, and inherent minerals such as loss of water, with increasing temperature. This is valuable information that can be used to understand processes such as coal carbonisation, fluidity and coal oxidation [Cole-Clarke and Vassalo, 1992].

The transmittance and reflectance micro-FTIR spectroscopy is sensitive to structural changes, due to the oxidation of coals, stretching bonds of aromatic rings and carbonyl functional groups, and oxidation of whole coals and individual macerals [Mastalerz and Bustin, 1993; Cloke *et al.,* 1997]. The technique is capable of discriminating between a raw coal and treated coals, by studying the functional groups, and fingerprint region. As a result, the technique was found to be an ideal tool to characterise chemical functional groups of coal macerals [Chen *et al.,* 2012], coal chars and liquefaction products.

There has been an increasing appreciation for the use of micro-FTIR to study mineral matter in coal. Early work on characterisation of mineral matter using FTIR was conducted by Estep *et al.* (1968) and Painter *et al.* (1978). The major challenge of characterising coals is due to the interference between functional groups of organic matter, and mineral matter. As a result, better characterisation of mineral matter is conducted on LTAs [Painter *et al.,* 1978].

The mineral matter identified in the study was kaolinite, quartz, gypsum, calcite, illite, montmorillonite, and pyrite, among other minerals [Painter *et al.*, 1978; Shepherd *et al.*, 1986].

Baruah *et al.* (2003) investigated the mode of occurrence of organically and mineral bound elements from LTA samples prepared from Assam coals, India, using FTIR techniques. In the analyses, mineral matter such as calcite, siderite, gypsum, jarosite, kaolinite, chlorite, and pyrite were identified. Findings from the study further elucidated that both XRD and FTIR were more comprehensive, and gave more insight about the nature of bonding of mineral matter found in the coals.

Han-xu *et al.* (2008) used FTIR to study ash melting behaviour of coals from China. The aim of the work was to understand properties that influence performance of coals in gasification. The study was used to correlate AFT, chemical composition, mineralogical phases, and functional groups by linking AFT to location and transmittance of different absorption peaks. The Si-O-Si absorption bands at 1080 cm^{-1} and 476 cm^{-1} of coal ashes with low AFT were shifted to high and low wavenumbers respectively. The asymmetric broad band at 900-1200 cm^{-1} was related to low AFT, whilst the symmetric band corresponded with high AFT.

Although Jenkins and Walker (1978) considered IR spectroscopy to be the promising technique to characterise mineral matter in coal, the developments in the use of FTIR showed that the technique was of less significance in studying mineral matter in coals, because the technique is best suited for specific identification of specific minerals, particularly clays [Farmer, 1974], quartz, and carbonates [Ritz and Klika, 2010].

Qualitative and quantitative analysis of mineral matter in coal can prove challenging, mainly because of the presence of organic matter [Rochdi and Landais, 1991]. Similar challenges were reported by Martinez-Tarazona *et al.* (1992). However, the least square fitting methods can be used to resolve the problem.

4.6 Micro Raman Spectroscopy (mRs)

Raman spectroscopy is an analytical technique that probes materials on a microscopic level by measuring the changes in the vibrational energies from a sample that is illuminated by monochromatic light (laser) to excite molecules. The excitation energy changes the state of molecules from the ground state to a virtual state. The excited molecules return to a different energy state after emitting a photon. The scattered light is emitted either elastically or inelastically, causing an increase or a decrease in frequency of the emitted photon, which will differ from the excitation wavelength.

The Raman spectrum is characteristic of a specific material, with shifts giving energy and providing information such as the chemical bonds, and molecular composition about the phonon modes that are described by vibrational, rotational and other low frequency modes. Factors that control the quality of the Raman spectra are the type of laser, power of the laser, and the accumulation time. Lapuerta *et al.* (2011) studied the effect of these parameters on soot products. The presence of fluorescence in the analyses involving Raman spectroscopy generates a background that makes it difficult to resolve any underlying peaks. Possible ways of addressing fluorescence in the analyses is to bleach the samples by exposing samples to longer laser exposure times, subsequently reducing the effect of fluorescence.

The laser is used as the beam of monochromatic light to excite the molecules and produce a Raman spectrum for a material. The monochromatic light must be stable, with low background emission. The probes collect the scattered photons, filtering out the Rayleigh scatter and direct the Raman scatter to the spectrograph. The Raman scattered photons are separated by wavelength using a transmission grating and then passed on to a detector, which records the intensity of the Raman signal at each wavelength. The data is then plotted as the Raman spectrum.

Information that can be extracted from a Raman spectrum includes:

(i) band position which gives chemical bonds, composition of a material, phase transformation, polymorphs, hydrates, non-hydrates, and molecular confirmation;
(ii) band shift gives information pertaining to grain size, coherence length, stress and temperature;
(iii) band asymmetry which gives information regarding possible defects in a material, and along grain boundaries, and lastly;
(iv) band width, will tell if the material is ordered or disordered.

The advantages that make the mRs techniques attractive include:

(i) minimal or no sample preparation;
(ii) structural changes observed and detected accurately because of high resolutions;
(iii) the size of the laser allows for a small area to be analysed; and
(iv) the vibrational spectrum from 50 to 4000 cm^{-1} can be observed in a single recording instrument.

However, the performance and efficiency of micro-Raman spectroscopy can be affected by factors that can limit the application of the technique. Such limitation can include:

(i) the weak Raman effect for Raman inactive materials,

(ii) intense laser radiation can destroy the sample that is being analysed,

(iii) the detection must be sensitive and highly optimised,

(iv) Fluorescing materials can be difficult to characterise.

4.6.1 Application of Raman spectroscopy within the coal industry

Similar to FTIR, mRs can be used to determine structural properties or composition of coal, and the two spectroscopic methods are complementary. The technique can probe a material on a molecular level, at high spatial resolutions, providing information on the crystallinity of a material, (i.e. degree of ordering or disorder), symmetry, phase transformation, hydrates, non-hydrates, and molecular confirmation. Moreover, the technique does not rely on the crystalline structure of the molecule like XRD and is therefore sensitive to amorphous compounds too, unlike XRD. The use of Raman spectroscopy is becoming more attractive, because the instruments are now portable, and execute results faster, with high spatial resolution, and reproducibility. The technique has a wide range of applications in industries such as pharmaceutical, ceramics, art, forensic sciences and materials characterisation [Michel *et al.,* 1996; Liem *et al.,* 2000; Smith and Dent, 2005].

Infrared (IR) and nuclear magnetic resonance (NMR), Transmission Electron Microscope (TEM), XRD, and mRS are techniques used to study structural order of carbonaceous material. However, mRs remains the best possible technique to study carbonaceous materials [Beyssac *et al.,* 2003], because of its sensitivity to change in structural disorder [Mennella *et al.,* 1995].

The mRs is used extensively for characterisation of various carbonaceous materials such as coals, inorganic inclusions, char, fly ash, anthracite, kerogens, graphite, diamonds, and the determination of char reactivity [Nakazimo *et al.,* 1974; Johnson *et al.,* 1986; Wagner *et al.,* 1989; Jehlička and Beny, 1992; Quirico *et al.,* 2005; Zaida *et al.,* 2007; Guedes *et al.,* 2010; Silva *et al.,* 2012] because of its sensitivity to structural disorder. Raman spectral parameters such as intensity ratio, $R = \frac{I(D)}{I(G)}$ and the coherence length, $L_{a,}$ are used to determine structural and phase information of carbonaceous materials.

Initial mRs studies of carbonaceous materials were first reported by Tuinstra and Koenig (1970), where graphite (a highly ordered structure) was studied. A single shift on the Raman spectra of the first ordered graphite was observed at 1580 cm^{-1} wavenumber, also referred to as the G-band. The peak is due to the E_{2g2} vibrational mode. The peak at 1380 cm^{-1} occurs in poorly structured carbonaceous materials, and is referred to as the D-band. It was concluded that the D-band was due to structural defects, which affects the crystalline symmetry [Tsu *et al.,* 1977]. In addition to the G and the D band, other peaks are observed in the first order and second order spectrum. The 1150 cm^{-1} peak is associated with sp^3 or mixed sp^2 - sp^3 bonding, which are the active sites in carbon. The second order spectrum is generally more sensitive to the deformation than the first order peak, as indicated in Figures 4-1 and 4-2.

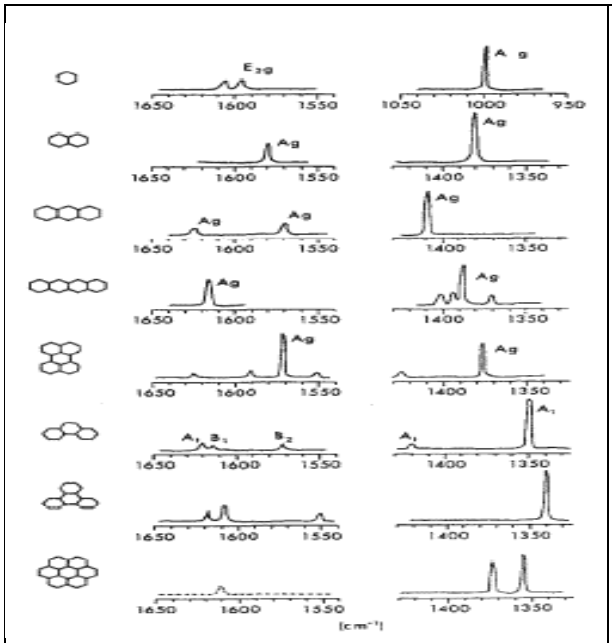

Figure 4-1: Raman spectra of condensed aromatic hydrocarbons [Nakazimo *et al.*, 1974]

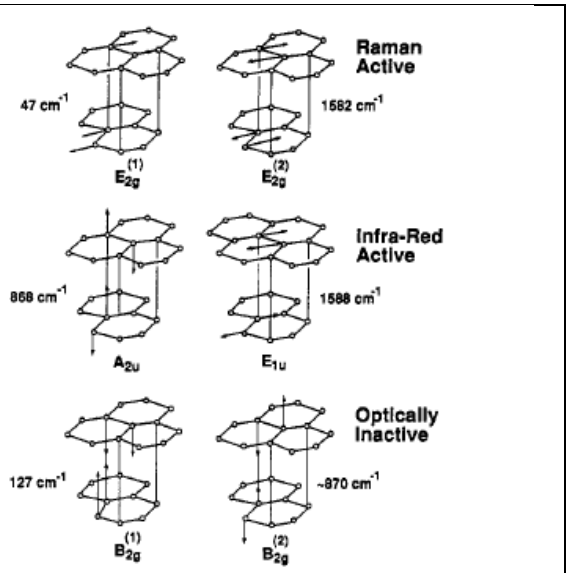

Figure 4-2: Vibrational modes for single crystal graphite [Wang *et al.*, 1990]

The use of Raman spectroscopy as a characterisation tool for identification and structural analysis of minerals has been recognized since 1975, and the technique was first introduced in the cement industry by Bensted since 1974 [Bensted and Varma, 1974].

However, an increase in the use of the technique on cementitious material, including fly ash, metakaolin, Portland cement, and calcium sulfoaluminate gained popularity when the instrumentation and the software packages were improved, with intentions of overcoming weak Raman signals that were obtained from analysing cementitious materials [Potgieter-Vermaak *et al.*, 2006]. There has been a growing interest in using the technique to study minerals [Potgieter-Vermaak *et al.*, 2011; Mernagh and Trudu, 1993; Coleyshaw *et al.*, 1994] with the point counts providing information regarding mineral abundance, association, grain size, etc. Furthermore, variability of mineral composition and discrimination of polymorphs can be deduced from Raman analysis. Mineral groups with their respective characteristic spectral regions are summarised in Table 4-1.

For example, carbonates have their respective characteristic Raman fingerprint within the 1030-1130 cm^{-1} region, whilst sulphide minerals vibrate at frequencies below 500 cm^{-1}.

Table 4-1: Mineral groups identified in Raman spectroscopy

Mineral group	Spectral region (cm^{-1})
Carbonates	1030-1130
Sulphates	950-1100
Phosphates	900-1100
Oxides	640-780; 200-400; 1300
Sulphides	Below 500
Tectosilicates	240-300; 425-545
Layer silicates	650-780; 800-1150
Orthosilicates	800-1000

Over 1000 minerals have been positively identified using Raman spectroscopy and the data is found in various libraries worldwide. Little work has been conducted to study mineral matter in coal, with fluorescence being a serious disadvantage and limitation in mRs techniques. As stated earlier, this project applies this technique to characterize major mineral matter in selected coal samples, and considers prospects of using the technique on-line, with the ultimate aim of improving combustion efficiencies.

The ability to characterise both mineral matter and organic matter using the same instrument will have economical value to coal characterisation in general. The non-destructive nature of the technique allows for direct characterisation of in-situ coals, at a spatial resolution of 1µm. This provides unaltered and detailed information about coal origin, association and heterogeneity better than bulk measurements analyses [Chen *et al.*, 2012]. Furthermore, the instant results would allow for the necessary downstream process changes, and thus mRs technique is currently gaining popularity within the coal industry. The obvious advantage of using mRs technique is the ability to characterise the sample without preparing the sample.

4.7 Scanning Electron Microscope (SEM) and Computer Controlled Scanning Electron Microscope (CCSEM)

Scanning electron microscopy, equipped with an energy dispersive X-ray analysis (EDX), is a powerful tool that has been widely used over the past 20 years to characterise mineral matter. Similar to the optical microscope, the SEM analyses are based on observation of mineral matter in coals. The SEM-EDX provides information on maceral-mineral matter association, grain morphology and mineral intergrowths, and the determination of included and excluded mineral data of individual particles [Gupta, 2007]. The coupling with the EDX allows for compositional analyses on components of interest. The Computer Controlled Scanning Electron Microscope (CCSEM) is an advanced SEM technique, boosted with backscatter electron detector, digital beam control, an ultra-thin window energy dispersive X-ray detector for better imaging and analysis of low-Z elements, and analysing mineral matter. The CCSEM gives more information compared to conventional SEM-EDX technique.

The technique allows mineral matter to be analyse on a particle to particle basis, and particles as small as 0.5 μm in size can be resolved using the technique [Saikai and Ninomiya, 2011]. The equipment has the capability to analyse both the crystalline and non-crystalline mineral matter. The technique is helpful in predicting char fragmentation, ash deposition behaviour [van Dyk *et al.,* 2009] and the extend of coal beneficiation [Strasheim *et al.,* 1988].

The QEM*SEM is an automated image analysis system, coupled to a SEM. QEM*SEM uses backscattered electron (BSE) and EDX signals from SEM to create an image across the sample. The QEM*SEM was first developed by Gottlieb *et al.,* (1991). The image of the pixel information derived from BSE and EDX gives information about the chemistry, and association of components under the electron beam.

The QEM*SEM gives detailed information over a large scan area, rather than on a few points, as it is the case with SEM and optical microscopy. The computer is used to monitor stage movement of the sample and the electron beam, and also collects and analyses the data of about 100 000 points at relatively high speeds. Thus, QEM*SEM is complementary to the electron probe micro-analyser.

The statistical information obtained from the technique gives mineral volume fractions, size distribution, shape parameters, mineral association, and the degree of mineral liberation [Creelman and Ward, 1996]. The study on various coals by Creelman and Ward (1996) showed that there was a good correlation in quantification of mineral matter, particularly, quartz and siderite when using QEM*SEM analyses and chemical analysis data. In the study it was concluded that QEM*SEM was more detailed in terms of characterising mineral matter in coal and performed better when compared to the conventional petrographic methods [Creelman and Ward, 1996].

Wigley *et al.* (1997) studied a series of coal samples from various deposits across the world. The aim of the study was to characterise particle size distribution of mineral matter in pulverised coals. The findings of the study concluded that mineral matter in South African coals were more organically bound, compared to Northern hemisphere coals studied. Research studies have also applied QEMSCAN as a detailed technique to understanding the effect of mineral matter on gasification and combustion processes [Matjie *et al.*, 2011; Saikai and Ninomiya, 2011].

Saikai and Nimomiya (2011) used the CCSEM to investigate the distribution of heterogeneous mineral matter in Assam pulverised coals. From the study, major and minor minerals were identified. The particle size distribution (PSD) of included minerals was found

to be fine and these included minerals had an effect on the reactivity of coal samples. The mode of occurrence of major inorganic matter was also associated to the different mineral matter. The advantages presented by QEMSCAN technique has contributed significantly towards progression in clean coal technology. For example, Beér *et al.* (1992) used mechanistic models to predict slagging and fouling, and in the study CCSEM data was used as input to the model.

4.8 Chapter summary

From literature studies it was observed that indirect determination of mineral matter is not adequate in characterising mineral matter in coal. This creates a need for a holistic direct approach in accessing mineral matter in coals to understand their behaviour and overall impact on the environment. However, despite the extensive amount of work that has been conducted to date, little is still understood or known about mineral matter.

This could be attributed by the fact that most advanced characterisation methods have not been fully explored, and more work is still to be done. The literature to date suggest that the combination of various techniques (including traditional routine-based as well as new macro- and microanalysis techniques) are to be considered for characterisation of raw coal and ashes, to establish their behaviour and characteristic properties in respective conversion processes. Most of the literature described here used a compendium of techniques but none that the author is aware of used all the above mentioned techniques to characterise the mineral matter in coal. In this research, proximate analysis, ultimate analysis, AFT, petrography, mRS, FTIR, XRD, SPA-EPMXA, and XRF will be used to characterise coals.

CHAPTER 5: EXPERIMENTAL PROCEDURE

5.1 Introduction

Laboratory based analyses were conducted to address the objectives proposed in Section 1.6. In the study, coals were investigated following two different routes. The initial stage of the work was to determine the physico-chemical properties of coals, which included proximate and ultimate analyses, ash chemistry, ash fusion temperature, elemental analyses, and structural properties of mineral matter in coals. The second stage of the research work was to characterise the mineral matter, with less interference from the organic matter. This was achieved by driving off the organic matter at low and high temperatures, producing LTA and HTA samples. The analytical techniques used to characterise mineral matter is outlined in Table 5-1. A schematic lay-out of the analyses conducted is presented in Figure 5.1. The primary objective of the work was to use mRs as the primary analytical tool, complemented by other techniques.

Table 5 - 1: Characterisation methods conducted on raw and ash samples.

Samples	Analytical methods
Raw coals	Proximate, Ultimate, XRF, AFT, SPA, Petrography, XRD, FTIR, and mRs.
Low temperature ashes	XRD, FTIR, and mRs
High temperature ashes	XRD, FTIR, and mRs

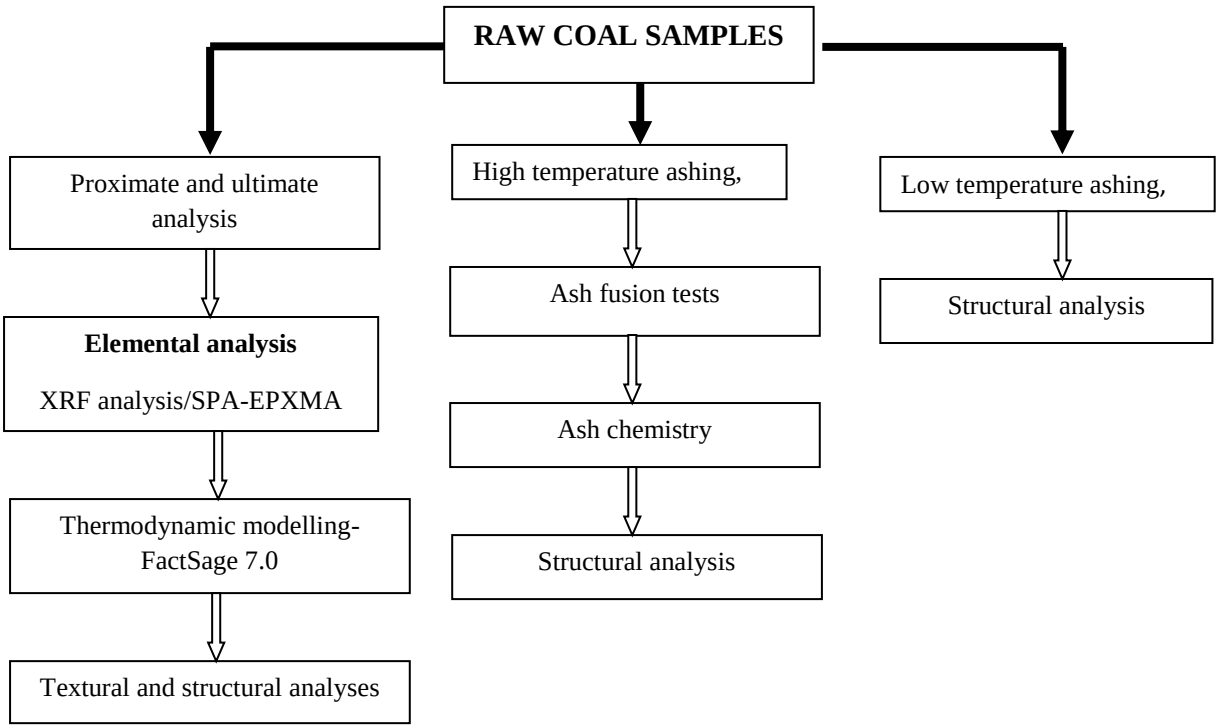

Figure 5-1: Experimental work overview

5.2 Geographical overview of the coals studied

Coals studied were selected from three different coal mines situated in different geological settings. The intention was to obtain coals with a varying mineralogical signature. A total of 4 coal samples were selected for the study, all being medium rank C-bituminous coals, and identified as coals A, B, C and D. Due to concerns regarding confidentiality, the exact location of the samples cannot be revealed. However, a broad overview of location and geological background of South African coals is provided in Section 2.2 (Figure 2-1). Sample C, a discard coal was included in the investigation because of the high ash content (> 60 wt. %). The typical composition of a South African discard coal has a high ash content (10-70%), low calorific value (8-26 MJ/kg), low volatile matter (8-30%), and high sulphur (0.8-8%) content.

5.3 Sample preparation

Sample preparation is important and critical for obtaining a representative coal sample, and for subsequent analyses. Cone and quartering was conducted to obtain a representative sample from the as-received raw coals. A Retsch ZM 200 mill was used to pulverise the samples to the desired particle size, as required by a specific test or analyses. The mill speed was set at 6 000 rpm. The particle sizes obtained from the mill were classified, using sieve sizes ranging between 150 and 1000 μm in size. Samples were split using a riffler to obtain respective particles sizes for ashing (LTA and HTA) and characterisation.

5.4 Proximate analyses

The four parameters determined by the proximate analyses are fixed carbon, volatile matter, ash content, and moisture content. An in-house Perkin Elmer Simultaneous thermal analyser (STA) 6000 was used to determine proximate analysis of raw coals from an in-house thermo-gravimetric (TGA) method. A representative sample was pulverised to -150 μm particle size. A sample mass of approximately 15 mg was pre-weighed inside an alumina crucible, and then heated under nitrogen gas flowing at the rate of 14 ml/min. The coal was heated at 50°C/min to 110°C and held at that temperature until a constant mass was reached. The sample was further heated to temperatures up to 900°C at a rate of 50°C/min. Nitrogen gas was then switched to oxygen. The oxygen gas was introduced at the rate of 14 ml/min. The oxygen gas was introduced to aid combustion.

Surface moisture was calculated by taking the difference in mass between the initial sample mass and the stable mass at 110°C. Volatile matter is derived from organic matter and mineral matter. Organic matter volatiles include gases such as CH_4, CO_2, CO, N_2, and hydrocarbons.

These volatiles influence the ignition temperature and combustion characteristics of coals. The sources of volatile matter derived from mineral matter include CO_2 from carbonate minerals, SO_x from pyrite and water of crystallisation from clay minerals. The volatile matter content gives an indication of the gaseous phases found in coals. Thus, during the analysis, volatile matter is represented by the mass loss between the stable sample mass at 110°C and stable mass at 900°C. Residue is presented by the mass percentage remaining after all the carbon is burnt off at 900°C in air [Falcon and Ham, 1988]. The analyses were repeated three times in each case, to check for consistency and repeatability of results.

Fixed carbon is the carbon solid residue that remains once all volatile matter is driven off [Falcon and Ham, 1988]. The fixed carbon content gives an indication of the heating value of coals. Fixed carbon content was calculated by taking the difference from 100% of total surface moisture, volatile matter and the ash residue contents. Inherent moisture is the water that remains entrained in coal pores and fissures after all the surface moisture has been removed. Ash content is the residue that remains after all the organic matter has been driven off during combustion.

5.5 Ultimate analysis

Carbon, (C), and hydrogen (H) are the major combustible elements found in coals. The typical nitrogen (N) content in coal samples generally varies between 1-2%. The oxygen content helps with the ignition of coal samples, and it is generally inversely proportional to the C-content.

Coal samples were submitted to ALS, Witbank for ultimate analyses. ASTM D5373 was followed, for the analyses of C, H, N, and O (by difference). The coal samples were also

analysed for the forms of sulphur (total sulphur, organic sulphur, and pyritic sulphur). ASTM D 4239 was followed for the determination of sulphur and the different forms of sulphur.

5.6 Forms of sulphur

Sulphur is one of the most problematic elements found in coals. The abundance of sulphur in coal is variable, ranging from 0.5% to 5 wt.% of total sulphur [Chou, 2012]. Coals with sulphur content of less than 1 wt. % are classified as low sulphur coals. Coals with sulphur concentrations ranging from 1% to 3% are classified as medium sulphur coals, and coals with sulphur content greater than 3 wt. % are classified as high sulphur coals. The three forms of sulphur in coal are pyritic, organic and sulphate sulphur (S_{sulp}). Pyritic sulphur (S_{pyr}) is determined by calculating the amount of pyrite extracted by nitric acid. Organic sulphur (S_{org}) in coals is difficult to determine, and thus, ASTM methods are used to determine organic sulphur, by calculating the difference between the total sulphur and the sum of pyritic and S_{sulp}.

5.7 Ash fusion temperature (AFT)

The four samples were submitted to SABS Commercial (SOC) LTD Mining and Minerals labs in Witbank for analyses. The test was conducted following the ISO 540 method. The standard method is designed to simulate the behaviour of coal ash under either oxidising or reducing environments.

5.8 X-ray fluorescence (XRF) analyses of coal ash samples

Pulverised (-212 µm) coal samples were submitted to SABS Commercial (SOC) LTD Mining and Minerals labs in Witbank for analyses. The samples were ashed according to the ISO 1171:1997 standard method.

Coal ashes were subjected to XRF analyses, for the determination of chemical composition of 10 major and minor elements (Al, Mg, Ca, Si, Fe, S, Na, K, P and Ti) present in coal samples. The composition of major and minor elements is reported as oxides.

5.8.1 Preparation of pellets

Fused beads were prepared by mixing approximately 1 g of coal ash samples with 9 g of fusion flux (Lithium borate [$Li_2B_4O_7$]) and fused inside a platinum crucible at 1050°C using M4 Fluxer Claisse, as described in the ASTM D3682 method. The molten mixture was poured into a mould to form a pellet of approximately 1 mm thickness. The dispersion of mineral species in glass allows for homogeneous distribution of elements, and improved determination of major and minor elements [Suarez-Fernandez *et al.*, 2001]. The bottom surface of the bead was bombarded with primary X-rays for chemical analyses, with SARM 19 from Mintek used as a reference material.

The XRF analyses were conducted on a wavelength dispersive Thermo Fischer Scientific instrument. The current was set at 80 mA, and the voltage at 30 kV. The spectrometer has scintillation (SC) and flow proportional (FPC) detectors and LiF220, PET, LiF, analysing crystals. Detectors are used to convert X-rays into electronic signals, which can be used to determine energy and intensity emitted from the sample. Characteristic energies of fluorescent X-rays were determined individually and quantitative analyses were obtained by

measuring the intensity of characteristic lines of the elements, using WIN XRF software. The detection limit of the instrument was set at 0.8 ppm. The elements were reported as oxides.

5.9 FactSage modelling

Computer assisted thermodynamic modelling of phase equilibria was used to predict possible high temperature phases that could form at high temperatures between 1100°C and 1400°C. The FactSage (7.0) thermochemical modelling software in combination with Fact PS, FT-oxid, and SGTE solution databases were used to predict possible reactions and equilibrium slag, gas and oxide phases. The thermodynamic equilibrium calculations of the four samples were conducted in a temperature range from 1100°C to 1400°C, and atmospheric pressure. The initial inputs to the modelling programme were the ash oxide composition of the coals determined by XRF analyses.

5.10 Electron Probe X-ray Microanalysis (EPXMA)

Single particle analyses using EPMA were conducted on raw coals and ashed samples (LTA and HTA). The purpose of the analyses was to determine the abundance and association of minerals in the investigated samples. The samples were submitted to Manchester Metropolitan University, (UK), for analyses. Approximately 1 mg of milled coal sample of particles size less than 20 µm in size was suspended in acetone. The suspension was filtered on a 47 mm nuclepore filter with 0.4 µm pore size using a polycarbonate Sartorius filter holder. Whatman filter paper was placed under the nuclepore filter to enhance a homogeneous distribution of particles. A part of the filter paper was mounted on a double sided tape on a clean plastic plate and fitted into the microprobe sample holder.

The low-Z (Z<11) and high-Z elemental composition of the particles was analysed with electron-induced X-ray spectrometry, performed on an electron probe X-ray micro-analyzer (EPXMA, JEOL 733, Tokyo, Japan) coupled to an atmospheric ultra-thin window X-ray detector (Oxford, Abingdon, UK). The acceleration voltage, beam current, and X-ray accumulation time were set at 10 kV, 1 nA, and 10 s (automatic mode)/20 s (manual mode), respectively. In order to minimise the loss of volatiles, particles were cooled to liquid nitrogen temperature. Between 100 and 500 particles were analysed. Over 60% of the particles analysed were below 2 μm in size, with an average particle size of approximately 0.5 μm. About 30% of particle size analysed was between 2 μm and 5 μm, and approximately 10% of the particles above 20 μm in size.

Automatic detection and X-ray analysis of the particles where achieved by an in-house program that is based on back-scatter images. The X-ray spectra were processed using AXIL software for both EDXRF and EPMA. For EPMA, quantitative calculations of the particle composition (including light elements such as C, N and O) were performed using a recently developed method based on iterative Monte Carlo simulations. In order to establish the mode of occurrence of major elements in raw coal and coal ashes, statistical correlation method of cluster analysis and factor analysis were performed.

A multivariate technique was used to reduce large data generated from the analyses. The statistical technique used was based on compositional similarities and relative abundance of elemental composition in coal and ashed samples. The purpose of clustering analysis was to group similar elements together.

Chemometrics employs mathematical tools to process large data. Clustering analysis is a common chemometric method, based on mathematical algorithms, and frequently used to

characterise aerosol particles in groups according to their chemical similarities. However, clustering interpretation is based on the experience of the user, and therefore introduces some degree of subjectivity. The chemical classification method, based on chemical boundary condition (CBC) is an easier approach to characterising single particle components into various classes. This work followed CBC outlined by Kandler *et al.* (2007) because of the common mineral groupings of materials investigated.

The criteria used in the study are based on mineralogical criteria, with elemental ratios based on the stoichiometry of pure substances. Elements considered for the clustering analyses included 16 elements (C, N, O, Na, Mg, K, Al, Si, P, S, Cl, Ca, Ti, Cr, Mn, and Fe), and the particles were clustered into 11 different classes of iron-rich, titanium-rich, carbonates, other calcium-rich, gypsum, halite, quartz, silicates, sulphate-silicate mixtures, sulphates and others.

The gypsum class contains all particles with a formula related to $CaSO_4.XH_2O$. The iron-rich class contains all the particles with iron oxide and hydroxides. The silicate class contains all the aluminium silicates and quartz. The class classified as other, contains all other particles that have mineral characteristics but not satisfying the boundary conditions of the mineral classes.

Principal Component Analysis (PCA) was applied to the dataset to find the association between elements. The PCA technique extracts Eigen values and vectors from the covariance values of the original matrix to measure the association variance.

5.11 Petrographic analyses

Polished sections were prepared for petrographic analyses. The blocks were prepared by mixing coal samples prepared to -1000 μm with IMP cold mounting resin. The samples were left for 24 hours to set. The blocks were polished in a series of steps on the Stuers TegraForce-1 polishing machine to a 0.05 μm finish, as per SABS ISO standard 7404-2.

Maceral group analysis (including mineral matter) was conducted following SABS ISO standard 7404-part 4. The main maceral groups (namely vitrinite, inertinite, and liptinite) were sub-divided, and the main petrographically observable mineral groups (namely silicate, pyrite, carbonates) were also recorded. A more detailed petrographic analysis focusing on the mineral matter, mode of occurrence, and morphology was developed for the purpose of this research.

This analyses was also point count based, recording 500 particles per sample. All petrographic analyses were undertaken by Prof. Wagner at the University of the Witwatersrand using a Leica DM 4500P reflected light microscope with oil immersion lens at a magnification of 500X. Petroglite software and an automated stage was used for point counting. Photomicrographs were taken on a Zeiss Universal petrographic microscope with Axiovision software.

5.12 Powder X-ray Diffraction (PXRD) analyses

Powder X-ray diffraction was used to determine the quantitative composition of the phases and multiphase mixtures of mineral matter present in coals and coal ashes using a Bruker D8 diffractometer, housed at the University of the Witwatersrand. The instrument uses Cu-Kα radiation as the excitation source with the instrument generator settings at 40 kV and 20 mW.

Samples were scanned from 5° 2θ to 90° 2θ at a scan rate of 0.02 2θ. The X'Pert HighScore software package was used for qualitative analyses of diffractograph patterns obtained. Minerals were identified by reference to the ICDD powder diffraction file. Quantitative analyses of mineral phases in the raw coal and LTA were performed by SIROQUANT^{TM}, commercial interpretation software written by CSIRO, based on the Rietveld XRD analysis technique.

The mineralogy of each LTA sample was analysed by PXRD using a Phillips X'pert diffractometer with Cu- Kα radiation source, and the minerals present identified by reference to the ICDD Powder Diffraction File. Quantitative analyses of mineral phases in the LTA were made using SIROQUANT™, commercial interpretation software written by CSIRO [Taylor, 1991] based on the Rietveld XRD analysis technique.

The clay fraction (less than 2 μm effective diameter) of each sample was isolated by ultrasonic dispersion in sodium hexametaphosphate (Calgon) and subsequent settling. The clay fraction was investigated further by X-ray diffraction of oriented aggregates, using glycol and heat treatment. The relative proportions of the different clay minerals in this fraction for each sample were determined by the method of Griffin (1971). The inferred chemical composition of the ashes expected from each sample, calculated from the mineral abundance and assumed mineral compositions, is given Appendix F.

5.13 Fourier Transform Infrared (FTIR) analyses

Transmission FTIR measurements of coals and coal ashes were recorded at room temperature on a Vortex 70 FTIR instrument housed at the University of the Witwatersrand, School of Chemistry and at Manchester Metropolitan University, (UK), equipped with an attenuated

total reflectance (ATR) stage. A background scan was collected by the spectrometer, before any samples could be analysed. Powered samples were then placed on the diamond and an arm lever applying a constant torque was used to ensure that the contact with the spectral window is constant throughout. In order to improve noise to signal ratio, 128 scans were collected at a resolution of 2 cm^{-1}, and averaged. The spectral range collected in the transmittance mode was set at 500-4000 cm^{-1}. The Opus software was used to interpret and manipulate the data. An inbuilt spectral library was used to identify components that made up the coals.

5.14 Micro-Raman Spectroscopy (mRs) analyses

The mRs technique was used in the study to determine the structural composition of mineral matter (MM) in coals. The mRs analyses were conducted on powdered samples and polished blocks that were prepared for petrographic analyses. The reason for analysing both prepared blocks and powdered samples was to see the effect sample preparation would have on Raman analyses, since it has been reported that no sample preparation is required for mRs techniques. All the acquired Raman spectra were measured at room temperature using a Bruker SENTERRA spectrometer. The analyses were performed at the University of the Witwatersrand (Wits) and at Manchester Metropolitan University (MMU). The instrument was equipped with a monochromatic (Nd: YAG laser) laser, filter system, Olympus optical microscope and a thermo-electrically cooled charge-coupled device (CCD) camera.

Continuous wave laser energy at a wavelength of 532 nm (green light) was used as the excitation source. The laser power was set at 10 mW to prevent the sample from degrading; however, the power was varied depending on the size of mineral viewed under the microscope. An Olympus 20X objective was used to focus on the sample and the analysed

sample could be viewed on the computer in the video measurement screen of the OPUS software. The instrument was equipped with a microscope stage that moves the sample in the x and y directions. The sample was focused by increasing the depth of the image focal plane. Spectral accumulations were obtained at the integration time that was varied between 10 and 50 s, at an instrument resolution of 3-5 cm^{-1}. The spectral range selected for the analysis was from 50-2750 cm^{-1}. The instrument was calibrated using the 520 cm^{-1} shift silicon wafer before measurements. The system photomultiplier records the signal of the illuminated analysed spot. The recorded Raman spectra was analysed using the OPUS 6.5 software package for data analysis. In order to validate the results, about 100 spots were measured on each individual sample.

5.15. Low temperature ashing (LTA)

Gluskoster (1965) introduced a low temperature ashing (LTA) method which used oxygen plasma to drive off organic matter in the coal structures. In LTA process, the organic matter is driven off leaving behind ash. The LTA gives a close representation of mineral matter in its least altered state [Gluskoter, 1975; Miller *et al.*, 1979; Vorres, 1986].

The LTA samples were prepared at CSIRO, Australia. A representative sample of particle size below 150 µm was subjected to low temperatures (120°C) using oxygen-plasma IPC 4-chamber asher, as outlined in Australian Standards 1038, part 22. The mass percentage of LTA was determined, and the mineralogy of each LTA fraction was characterised by XRD technique. Other analyses conducted on the prepared LTA samples included SPA, FTIR, and mRs analyses.

5.16 High temperature ashing (HTA)

High temperature ashing was conducted at the University of the Witwatersrand. Ashing was performed by placing a pulverised coal (-150 μm) of a known mass in a boat alumina crucible. The sample was placed inside a muffle furnace. The heating rate was set at 50°C/min and the samples heated to temperatures of about 815°C. The coal samples were held at the temperature for an hour. After complete combustion, ashes were collected and weighed. High temperature ashes were analysed using XRD, FTIR, and mRs techniques.

CHAPTER 6: RESULTS AND DISCUSSION

6.1 Introduction

This chapter presents results obtained from the characterisation of the four South African raw coals, and their low and high temperature ashes, following experimental methods discussed in Chapter 5. The results are structured and presented in four parts:

(i) The physico-chemical properties of raw coals discussed include the proximate and ultimate analyses, and ash chemistry. Indices based on ash chemistry results and AFT's are used to evaluate the slagging and fouling propensities of coals.

(ii) The petrographic results of maceral and mineral matter of raw coals are discussed.

(iii) The structural analyses of raw coals, LTA and HTA determined by XRD, FTIR, and mRs are presented and discussed.

(iv) The last section presents elemental analyses results of coals using single particle analyses.

6.2 Physico-chemical analyses of raw coals

The physico-chemical properties evaluated for the four coal samples are proximate and ultimate analyses, forms of sulphur, ash chemistry, and AFT analyses. These parameters are commonly used to assess the application of coals in conversion processes.

6.2.1 Proximate and ultimate analyses of coals

The proximate analyses give an indication of the amount of moisture, volatile matter, fixed carbon and ash content in coals. The ultimate analyses reports the elemental composition of major elements (C, H, O, S, and N) making up the organic component of coal.

Table 6-1 provides the proximate, ultimate analyses, and forms of sulphur results of the four coal samples investigated in this study. Proximate and ultimate analyses were conducted on an air dry basis (adb). The proximate analysis results show that the moisture content of the four coals ranged from 2 to 4 wt.%. Volatile matter ranged from 13 to 20 wt. %, and low volatile matter was reported for coal C. The low ash content of approximately 23 wt. % reported for coal D is usually desirable in coal conversion processes. The proximate and ultimate results are comparable with results reported in literature, and therefore are characteristic of typical South African coals [Everson *et al.*, 2013]. Physico-chemical results can be attributed to the deltaic and fluvial environmental settings of South African coalfields [Cairncross, 2001].

Table 6 - 1: Proximate, ultimate analyses and forms of sulphur (wt. %) of selected South African coals (air dry basis)

	Coal A	Coal B	Coal C	Coal D
Proximate analysis (wt. %)				
Moisture	2.4	4.3	2.0	4.3
Volatile matter	18.5	22.4	13.9	20.5
Ash	40.1	26.6	68.3	22.6
Fixed carbon	39.0	46.7	15.8	53.6
Ultimate analysis (wt. %)				
C	75.2	73.2	57.7	75.1
H	4.5	4.7	5.9	4.6
N	1.7	1.9	1.6	1.9
O (by diff)	17.0	18.0	26.7	17.8
S	1.6	2.2	8.1	0.6
Forms of sulphur (wt. %)				
Pyritic	0.1	0.2	0.3	0.1
Sulphate sulphur	1.2	1.8	7.6	0.4
Organic sulphur	0.2	0.2	0.3	0.2

However, coal C reported the highest ash content (68 wt.%), and in fact cannot be classified as a coal. The results imply the sample is enriched with mineral matter. The ash content reported for coal C is as expected, since the sample is a discard coal.

A plot of the relationship of the data between organic matter and mineral matter was statistically evaluated using Microsoft Excel. Figure 6-1 shows a correlation between carbon and ash, as determined from proximate and ultimate analyses data. The plot showed a linear relationship between carbon and ash content of coals, with a regression coefficient (R^2) of 0.83. The results implies that coal samples with a high carbon content, will typically have low ash content, and the opposite is also true. This trend is as expected, and in agreement with the proximate and ultimate results of the investigated coals. The correlation further implies that the carbon content can be predicted in coal samples with a reasonable degree of accuracy if the ash content is known, and vice versa.

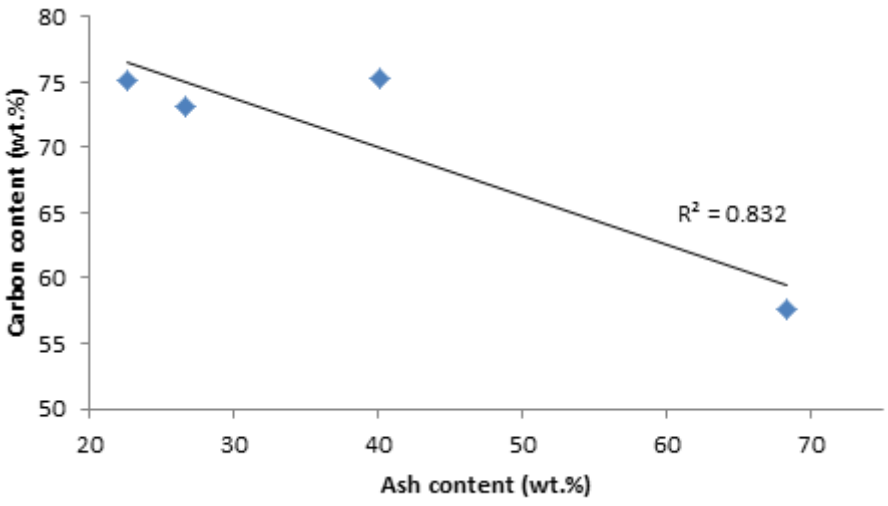

Figure 6 – 1: Correlation between carbon and ash content

6.2.2 Forms of sulphur

The three forms of sulphur identified in coals samples are: sulphide sulphur (mostly pyrite), sulphate sulphur, and the organic sulphur. Generally, pyritic sulphur and organic sulphur make up the bulk of the total sulphur (Chou, 2012). Coals that are enriched in organic sulphur, with a concentration ranging between 4 and 11 wt. % are classified as superhigh-organic sulphur coals, and these coals are found in special depositional environments (Dai *et al.*, 2008b; Chou, 2012). In this study, the concentration of organic sulphur was relatively low, with concentrations ranging from 0.18 to 0.29 wt. %. The concentration of the organically bound (S_{org}) and pyritic sulphur (S_{pyr}) was low, with concentrations ranging from 0.06 – 0.3 wt. %. The results are typical of South African coals, since the average sulphur content in SA coals is generally below 2 wt. % [Cairncross and Cadle, 1988]. Roberts (1988) investigated the relationship between macerals and sulphur of Permian coals of the Vryheid formation in SA, and the findings from the study illustrated that there was a strong correlation between sulphur (organic and pyritic), and vitrinite. However, the relationship between vitrinite and sulphur was not investigated in this study.

The % total S (ultimate analyses) reported in Table 6-1 is the summation of the different forms of S (both the organic and the inorganic sulphur found in the samples), and the sulphur content ranged from 0.6 wt. % to 8 wt.%. The amount of sulphur, organic sulphur in particular, is usually low in coal, and coals used in combustion processes will commonly have total sulphur concentration ranging between 0.5 and 3 wt. % (Laban and Atkins, 2000).

It is observed that sulphate sulphur is relatively high in all coals samples, contributing over 60% towards total sulphur in the coals, with the highest concentration of sulphate sulphur reported for coal C.

The presence of high sulphate amounts in coal C could be attributed to possible oxidation of the sample during storage. The occurrence of sulphate sulphur is rare in fresh coals, but commonly found in partially weathered coals (Yani and Zhang, 2009; Chou, 2012).

Weathered products found in coals include minerals such as szolnokite [$FeSO_4 \cdot H_2O$], rosenite [$FeSO_4 \cdot 4H_2O$], coquimbite [$Fe_2(SO_4)_3 \cdot 9H_2O$], roemerite [$FeSO_4 \cdot Fe_2(SO_4)_3 \cdot 14H_2O$], jarosite [$(Na,K)Fe_3(SO_4)_2(OH)_6$], and halotrichite [$FeAl_2(SO_4)_4 \cdot 22H_2O$] (Chou, 2012).

The presence of S_{pyr} is an indication of marine influence, whereby pyrite formed as a result of bacterial reduction of SO_4^{2-} in pore waters either during or after deposition [Chou, 1990]. The S_{org} indicates a syngenetic contribution from fluids and high sulphate content. The concentration of S_{org} was relatively equal in all coals, although the S_{pyr} was variable, with coal D reporting the lowest concentration of about 0.06 wt. %.

Sulphur is undesirable, as it could lead to the formation and large emissions of SO_x, and subsequent acid rain which forms due to the interaction between SO_2 and moisture in the atmosphere. A high concentration of S_{pyr} could influence slagging and fouling propensity in coals, and as discussed in previous chapters, S_{pyr} is a major contributor of AMD.

6.2.3 Relationship between ash chemistry and mineralogy of coals

Coal ash chemistry is an important factor in coal characterisation processes, because the ash chemistry is used to identify mineral matter in coals, and the results can be used to further understand ash fusibility of coals. The XRF analyses were performed on coal ashes prepared at 815°C to estimate quantitative elemental composition of 12 major and minor elements in the coal samples. The major and minor oxides of major elements are presented in Table 6-2.

Table 6-2: Nominal ash oxide analyses of major and minor elements as determined by XRF

Elements (wt. %)	Coal A	Coal B	Coal C	Coal D
CaO	0.45	0.80	7.53	3.46
MgO	0.19	0.47	2.35	1.95
K_2O	0.32	0.83	0.77	0.26
Na_2O	0.16	0.24	0.66	0.26
Fe_2O_3	2.11	6.35	5.61	3.23
TiO_2	2.90	1.61	1.89	1.90
Al_2O_3	42.00	28.70	23.80	36.10
SiO_2	49.30	57.90	45.10	45.5
Cr_2O_3	0.01	0.01	0.02	0.01
MnO	Nd	0.01	0.02	0.04
SO_3	0.07	0.63	9.85	3.96
P_2O_5	0.40	0.24	0.86	0.98
Total	**97.84**	**97.79**	**98.46**	**97.65**

The ash analyses assume coal to be a homogeneous matter. Moreover, the analyses do not unambiguously identify the form of mineral present in coal. Nonetheless, Figure 6-2 shows possible relationships that can be drawn between ash oxides and mineral matter found in coals. From Figure 6-2, it can be seen that ash oxide composition can indicate possible combinations that can be used to predict the presence of minerals in coals. For example, the concentration of SiO_2 can indicate the possible presence of quartz, and other clay minerals such as kaolinite, illite, and montmorillonite, etc.

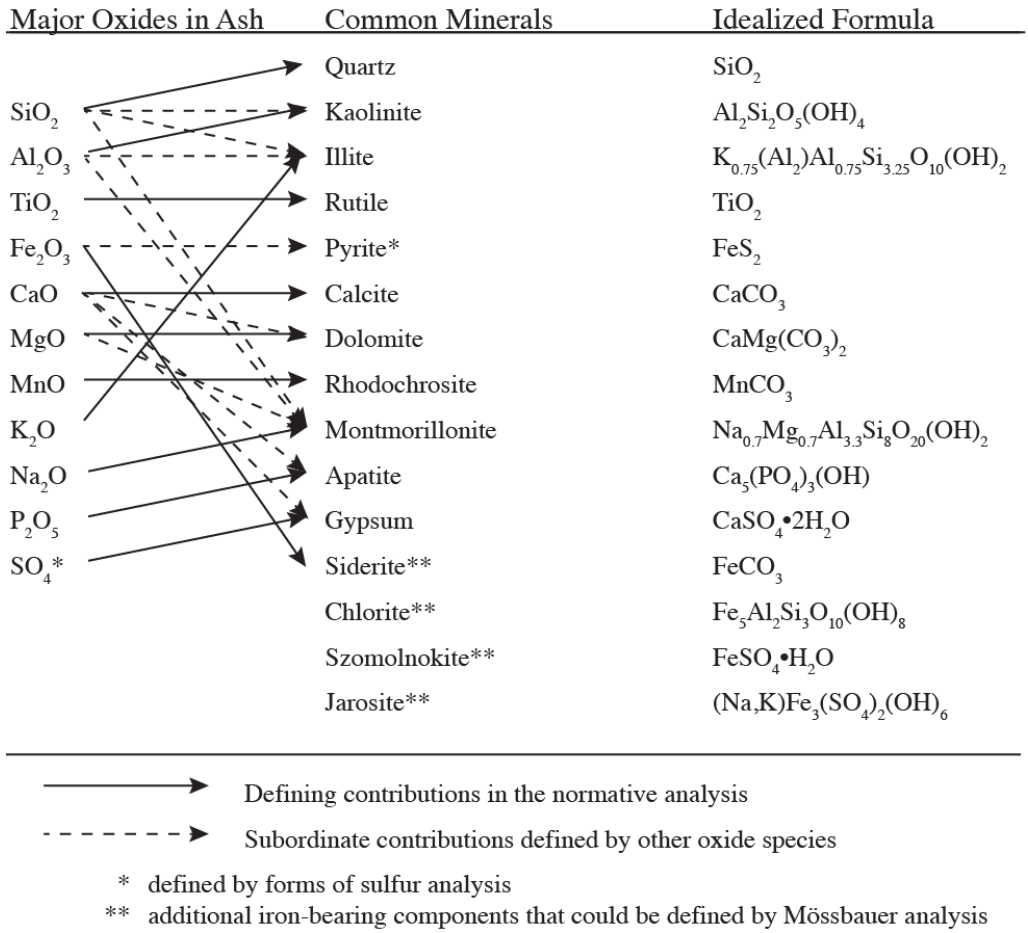

Figure 6-2: Oxides composition and the respective association with mineral matter [Huggins, 2002]

From the ash chemistry analyses presented in Table 6-2, it is observed that Al_2O_3 and SiO_2 are the major oxides present in all the samples investigated. Si in coals occurs mostly as quartz and clay minerals, whilst Al is primarily found in the form of clay minerals [Saikai and Ninomiya, 2011]. Thus a high concentration of Al_2O_3 and SiO_2 found in coal ashes is an indication that clays and silicates are the dominant mineral matter in the studied samples.

The SiO_2: Al_2O_3 ratio and other geochemical indicators can be found in Table 6.3. From the geochemical indicator results, it can be observed that coals A and D have a SiO_2: Al_2O_3 ratio close to the kaolinite theoretical value of 1.18 [Dai *et al.*, 2011], and this suggests there is no alumina rich mineral other than kaolinite in these samples.

A higher SiO_2/Al_2O_3 ratios reported for coals B and C suggest some of the free SiO_2 reported to quartz. Vassilev *et al.* (1997) classified coals with high Al and Si content to be of detrital origin. The accumulation of detrital clay minerals in coal deposits could be due to hydrothermal alteration of volcanic rocks.

Calcium in coal samples can be present in the form of carbonates such as calcite, dolomite, ankerite and fluorapatite. From the results presented in Table 6-2, it was noted that coal C had the highest concentrations of both CaO and MgO reported at 7.53 wt. % and 2.35 wt.%, respectively. The lowest concentrations of CaO and MgO were reported in coal A, at the concentrations of 0.45 wt. % and 0.19 wt. %, respectively. The presence of CaO and MgO can be associated with calcite and dolomite minerals. The wt. % ratio of Ca: Mg was greater than 1, confirming the presence of dolomite in all coal samples. In this case the association of Ca with clay minerals is neglected, since most of the aluminosilicates (calcium aluminosilicates, gehletite, and arnothite) are high temperature products. The presence of fluorapatite could not be confirmed by the XRF technique because the instrument has low detection limits and therefore cannot detect fluorine (F).

Amongst the four coal samples investigated, coal B reported a high concentration of Fe_2O_3 (6.35 wt.%), suggesting the presence of pyrite mineral. Although pyrite is considered to be the major source of Fe, other sources of Fe that have been reported in coals are due to the presence of minerals such as illite, goethite, jarosites, and siderite. It is to be noted from this work that the Fe: S weight % ratio was high for coals A and B, and relatively low for coals C and D. Pyrite could not be assigned to coals C and D. The results further suggest that the iron existed as either carbonate ($FeCO_3$) or sulphate ($FeSO_4$) mineral.

A high concentration of K_2O (0.83 wt.%) was observed in coal B, whilst a high concentration of Na_2O (0.66 wt.%) was reported for coal C. The high concentrations of K and Fe could suggest coal B has experienced glauconisation, which is the transformation process whereby mica is transformed into glauconite, which is an iron and potassium rich aluminophyllisilicate with a chemical composition of $(K,Na)(Fe, Al, Mg)_2(SiAl)_4O_{10}(OH)_2$. Glauconite is known to be of authigenic origin.

The presence of glauconite in the Witbank coalfield is evidence of marine conditions that prevailed during the coalification process [Le Blanc Smith, 1980; Cairncross and Winter, 1984]. However, other studies are not in agreement with conclusions by Cairncross and Winter (1984), but suggest the formation of glauconite and glauconitic mica to be due to non-marine sediments, whereby alluvial and paleo environments are responsible for the formation of glauconite. Therefore, the presence of K and Na are due to the detrital K and Na bearing silicates from the source area.

Titanium (Ti) in coals is present as a polymorph of rutile, anatase, and/or possibly brookite, with rutile as the most common and stable mineral found in coals. Anatase (TiO_2) is found in minor quantities in most SA coals, with concentration ranging from 1 and 2 wt. % [Roberts, 1991; Matjie *et al.*, 2016]. From the results presented in Table 6-2, coal A constituted a high concentration of TiO_2 (2.9 wt. %), whilst coal B had the lowest concentration of TiO_2 reported at 1.61 wt. %. TiO_2 is soluble in acidic solutions and can be precipitated out with kaolinite.

The SO_3 concentration represents the S in coal samples. From the result, concentration of SO_3 was high in coal C (9.85 wt. %), and it was also clear that the SO_3 concentrations obtained from XRF analyses followed a similar trend observed from the analyses of the different forms

of sulphur presented in Table 6-1. Furthermore, the Ca: S weight % ratio suggests the possible presence of gypsum in the investigated coals, and a significant amount of gypsum is expected in coal A.

In this study, the results show that the average concentration of P_2O_5 across the different samples was 0.62 wt. %, with coal D reporting the highest concentration of P_2O_5 (0.98 wt. %) relative to the investigated samples. Studies by Willis *et al.* (1991) indicated that the average P_2O_5 content in SA coals was about 0.2 wt. %, and generally increased towards the top of a coal seam.

Therefore, it can be considered that the concentration of P_2O_5 is within the concentration limits of SA coals. The presence of P_2O_5 suggests a possibility of the occurrence of phosphate minerals such as apatite in coals B, C, and D.

6.3 Ash classification

The chemical and mineral matter classification of coals was first introduced by Vassilev *et al.* (1995). The purpose of ash classification was mainly to assess operational problems associated with coals. The classification was based on studying high temperature ash (HTA) of 43 samples prepared from coals of variable geological history, mineralogy and ash yield. The classification system is based on 3 ternaries derived from ash chemistry. Ash deposits can be classified according to mechanical, thermal or chemical composition. The four main types of ash identified by the classification system are sialic, calsialic, ferrisialic and ferricalsialic ashes.

A similar approach was adopted in this work to determine the relationship between ash chemistry and the classification of coals. The different coals are labelled by letters, A, B, C

and D as indicated in Figure 6-3. From the results presented in the figure, coals A and B are classified as high acid sialic ashes, whilst coal D was classified as medium acid sialic ash.

The sialic ashes are typical of high rank bituminous coals and to a lesser extend subbituminous coals. The sialic ash is characterised by high fixed carbon, C, Si, Al, Ti, detrital/authigenic index, ash fusion temperature, quartz, kaolinite, Fe, Al hydroxides, siderite, and goyazite. Elements and minerals such as Fe, S, sulphate sulphur, montmorillonite, calcite, pyrite, marcasite, and gypsum are found in low concentrations.

The coals are characterised by high abundance of detrital minerals. The high acid coals have an abundance of quartz, kaolinite, whilst the medium acid coals have small amount of authigenic minerals [Vassilev and Vassileva, 2009].

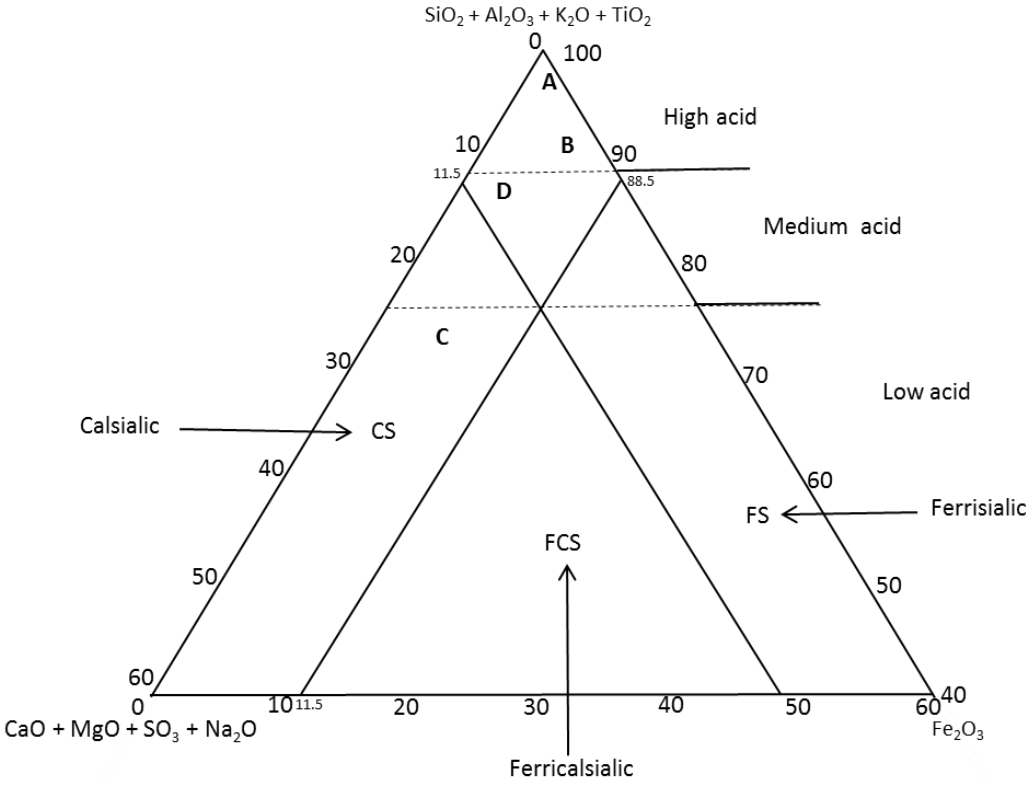

Figure 6-3: Ash classification system of investigated samples

Coal C was classified as calsialic type ash. The calsialic type ash has a medium to low acid affinities. The classification of these coals is common with bituminous coals, and to a lesser extends subbituminous coals and lignite. The calsialic type is characterised by high values of volatile matter, moisture, Ca, sulphate sulphur, Mg, Ti, Na, kaolinite, monmorillonite, K-feldspar, Fe and Al-hydroxides, spinels, brushite, calcite, dolomite, ankerite, and barite. The coals have an abundance of minerals of authigenic origin such as carbonates, and to a lesser extent, sulphides, sulphates, and detrital clay, mica, quartz, and feldspars [Vassilev and Vassileva, 2009].

The study by Matjie *et al.* (2012) showed that calsialic ashes were most likely to give rise to slagging and fouling. It can be drawn from the observations by Matjie *et al.* (2012) that coal C could be susceptible to slagging and fouling propensities.

6.4 Geochemical indicators used to predict slagging and fouling propensities

The geochemical, slagging and fouling predictive indices are based on ash chemistry, ash fusion temperature, and viscosity. These indices are widely used in industry for coal selection and designing of boiler and gasifier. However, it is important to note that ash deposition indices only takes into account the chemistry of coal ashes, and not necessarily the mineralogy nor the mode of occurrence of mineral matter found in coals [Vuthalura and French, 2008]. Although the indices are important for decision making, they are limited by the complexities involved in coal conversion environments [Vamvuka *et al.*, 2009].

Equations 6-1 to 6-4 were used to calculate the predictive indices [Vassilev *et al.*, 2010], and the corresponding results are presented in Table 6-3.

$$Silicon\ percentage = \frac{SiO_2 \times 100}{SiO_2 + Fe_2O_3 + CaO + MgO} \qquad Equation\ 6-1$$

$$Base - acid\ (\frac{B}{A})\ ratio = \frac{Fe_2O_3 + CaO + MgO + Na_2O + K_2O}{SiO_2 + Al_2O_3 + TiO_2} \qquad Equation\ 6-2$$

$$(DAI) = \frac{SiO_2 + Al_2O_3\ + K_2O + \ Na_2O + TiO_2}{Fe_2O_3 + \ MgO + CaO + SO_3} \qquad Equation\ 6-3$$

$$Iron\ index = \ Fe_2O_3 \times \left(\frac{B}{A}\right) \qquad Equation\ 6-4$$

Table 6-3: Ash deposition, slagging and fouling predictive indices of the investigated coals

Ash deposition indices	Coal A	Coal B	Coal C	Coal D
Si percentage	95.00	88.00	74.00	84.00
Base-acid	0.03	0.10	0.24	0.11
DAI	33.60	10.80	2.90	6.70
Si/Al	1.17	2.02	1.89	1.26
Fe/Ca	4.69	7.94	0.75	0.93
Fe index	0.06	0.64	1.35	0.36

6.4.1 Silicon (Si) ratio

The slagging propensity can be classified according to the Si percentage in coals, as expressed by Equation 6-1. The slagging propensity is classified based on the Si ratio percentage index as low, medium or high. The Si percentage between 72% and 80% has low slagging propensity. Medium slagging propensity is observed when the ratio is between 65% and 72% and a high slagging propensity result when the silicon ratio is between 50% and 65% [Lawrence *et al.*, 2008].

The silicon percentage of coals investigated in this study ranged between 74% and 95% as shown in Table 6-3. The lowest Si percentage is reported for coal C, and the highest Si percentage of 95% is reported for coal D. Based on the results obtained from the Si-ratios of the coals, it can be anticipated that the coals will have low slagging potential. According to reports by Patterson and Hurst (2000), the recommended Si percentage for entrained-flow

gasifiers should be less than 80%. Therefore, according to the trend of Si percentage, the coals are ideal to be used in conversion processes, without serious concerns about slagging.

6.4.2 Base-acid (B/A) ratio

The B/A ratio is a parameter used to establish the correlation between ash fusibility and coal composition [Van Dyk *et al.,* 2005]. The B/A ratio is the relationship between basic and acidic oxides, as indicated in Equation 6-2. The acidic compounds found in coals are associated with SiO_2, Al_2O_3, P_2O_5, and TiO_2. The basic compounds reduce the melting point of slag, whilst acidic compounds tend to increase fusion temperatures, with Al_2O_3 having the strongest acidic effect [Van Dyk *et al.,* 2005]. Therefore, a high proportion of basic component to acidic components lowers the probability of slagging.

An acidic environment formed under non-marine depositional conditions tends to cause slagging whilst a basic environment causes fouling in coal conversion processes (Pearson, 1980; Weeber *et al.*, 2000).

According to the predictions based on the B/A ratio, coals with low slagging propensities would have a ratio below 0.4 or greater than 0.7. Severe slagging and fouling propensity occurs when the indices range between 0.4 and 0.7 [Su *et al.,* 2003; Wang *et al.,* 2013]. In this investigation the B/A ratio for all the samples is below 0.4, as shown in Table 6-3, suggesting the coals studied have a relatively low slagging propensity, as it was also predicted by the Si percentage.

The results obtained in the study, except for coal A are in agreement with findings by Matjie *et al.* (2012) who reported a B/A ratio that ranged from 0.1 to 0.3 for low-grade medium-rank C coal ashes that were prepared for a packed bed combustor.

6.4.3 Detrital-authigenic index (DAI)

The detrital-authigenic index (DAI) indicates the genetic relationship of mineral matter in coals, and slagging propensity. The index expresses the dominant detrital or authigenetic association of ash forming elements in coal [Vassilev *et al.,* 1996 a*;* Sharma *et al.,* 2014]. The DAI is expressed by HTA composition as indicated in Equation 6-3 [Vassilev *et al.,* 1997].

Typically, the DAI value greater than 8 indicates the detrital nature of mineral matter in coals, whilst the DAI value below 3 shows the authigenetic nature of mineral matter in coals [Sharma *et al.,* 2014].

Vassilev *et al.* (1996a) studied 43 coals from different coals seams around the world. The purpose of the study was to establish a relationship between coal rank (C^{daf}), minerals, chemical composition of coals with coal ashes. The study indicated that higher rank coals are associated with minerals of detrital origin, whilst low rank coals are associated with minerals of authigenetic origin. Therefore, detrital minerals tend to increase with increasing coal rank, and ash content.

The authigenetic minerals are characterised by a complex origin and transformation of minerals, whereby organically bound, ion-exchanged and pore water elements in low rank coals crystallize to form minerals in high rank coals [Vassilev *et al.,* 1996 a]. Typical authigenetic minerals include carbonates, sulphates, phosphates, and chloride minerals.

The highest detrital affinity is expressed by DAI>8, while DAI<3 indicates an authigenetic affinity of minerals [Sharma *et al.,* 2014]. From the results presented in Table 6-3, the DAI values ranged from 2.9 to 33.60. Coal A had the highest DAI (33.60), followed by coals B (10.8) and D (6.70), whilst coal C, which is at the borderline was characterised by authigenetic mineral matter with a DAI value of 2.9.

The low DAI value of coal C imply the ash is associated with authigenic minerals, since the coal is of low rank, with high ash content and low carbon content.

Studies conducted by Vassilev *et al.* (2010) classified Meghalaya coals with an average DAI of 4.33 as coals of allochthonous origin. This implies minerals were transported into the coal, possibly under the influence of tectonic forces.

As previously highlighted, DAI is related to coal rank, and is expected to decrease with increasing ash content. From the results depicted in Figure 6-4, DAI decreased with decreasing ash content for coals A, B, and D. Coal C behaved differently, not following a similar trend to that of coals A, B, and D. This behaviour can be attributed to the fact that coal C is a discard coal characterised by authigenetic minerals such as carbonates and phosphates.

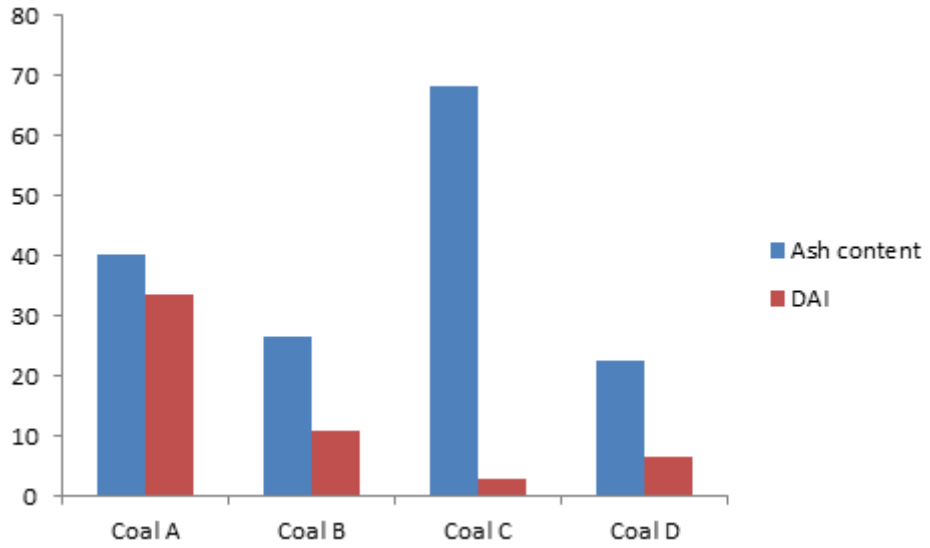

Figure 6-4: The relationship between ash content and DAI of the four investigated coals

The correlation between ash content and DAI was drawn for the three coals, with the exception of coal C. The discard coal was excluded in the correlation, because the ash content in the sample was due to the concentration of mineral matter during a beneficiation process, and does not represent the actual or original mineral matter found in the coal. Figure 6-5 shows the relationship between ash content and DAI of coals A, B, and D. the linear correlation coefficient (R^2) between ash content and DAI is 0.99.

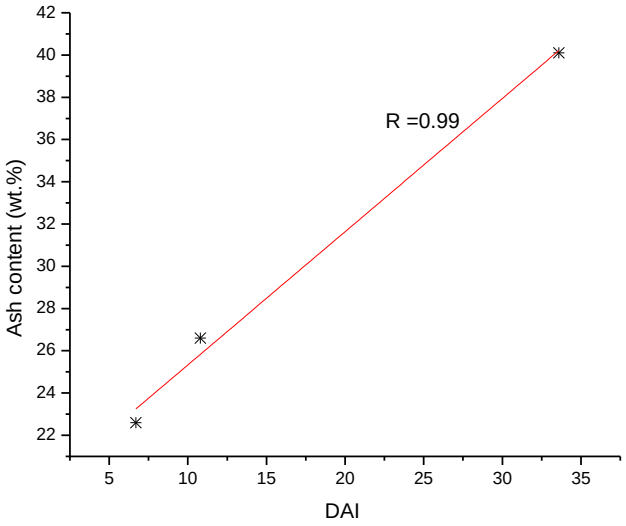

Figure 6-5: Relationship between detrital authigenic index and ash content of coal samples

Previous studies have reported a linear relationship between detrital mineral matter and ash content [Vassilev *et al.*, 1996 a]. However, the linear relationship between ash content and DAI does not apply to all coals. From the results, it was deduced that coals A, B, D were of detrital origin, because of the correlation between ash content and DAI values. The results are in agreement with findings by Vassilev *et al.* (1996 a).

Common detrital minerals in coals include quartz, kaolinite, illite, acid plagioclases, muscovite, rutile, apatite, Fe and Al oxyhydroxide. These minerals are found to be stable

during weathering and coalification processes. Some of the detrital minerals such as montmorillonite, biotite, pyroxene, amphibole, plagioclase, and K-feldspars undergo transformation, forming more stable minerals such as kaolinite, illite, chlorite, muscovite, and Fe-oxyhydroxide [Vassilev *et al.*, 1996 a].

6.4.4 Silica-alumina ratio

Silica (SiO_2) and alumina (Al_2O_3) are the major constituent elements found in coal ashes. The ratio between the two oxides can be used to calculate the silica-alumina ratio index used to predict the slagging and fouling propensities of coal samples [Liu *et al.*, 2013]. Shibakao (1972) found that the SiO_2: Al_2O_3 ratio can be variable throughout a seam, and the ratio is very much dependant on the chemical composition and mechanical erosion of rocks.

High values of the SiO_2: Al_2O_3 ratio and increased ash yield are an indication of coal formed under unstable conditions. Yudovich (1978) concluded that a high SiO_2: Al_2O_3 ratio and high ash yield is an indication of mountain peat-forming environments, dominated by mechanical erosion. The low SiO_2: Al_2O_3 ratio and a decrease in ash content are an indication of coals formed under stable conditions of deposition with low degree of tectonic movement [Vassilev *et al.*, 2011].

A low SiO_2: Al_2O_3 can be due to weathered products where leaching is predominant or due to high Al_2O_3 content. The high melting point of Al_2O_3 and its strong ionic bonds result with an increase in AFT, due to the formation of high melting corundum. As the SiO_2: Al_2O_3 ratio increase, weakly bonded low melting anorthite and gehlenite formed via a solid state reaction reduces the AFT, but only until a ratio of 1.5 is reached [Unsworth *et al.*, 1988; Liu *et al.*, 2013]. At higher SiO_2: Al_2O_3 above 2, the AFT changes slightly or remains constant [Liu *et al.*, 2013].

The results presented in Table 6-3 show that the SiO_2: Al_2O_3 ratio of the investigated coals ranged from 1.17-2.02, with coal B reporting the highest SiO_2: Al_2O_3 ratio. Coals with low deposition tendencies have a SiO_2: Al_2O_3 ratio of less than 0.31 or greater than 3. Therefore based on the results, the samples studied have low to medium tendencies to form slag deposits. From the results, it can be considered that coals A, B and D will have high AFT. Studies by Liu et al. (2013) reported that coals with low SiO_2: Al_2O_3 ratio have AFT higher than 1450°C.

6.5 Relationship between ash fusion temperatures (AFT) and coal chemistry

The different ash oxides formed from coal combustion influence the coal behaviour, and subsequently the melting temperature of fuel ashes. Ash fusion temperature (AFT) is the temperature at which material softens, and fuses together. The AFT tests are used to predict the slagging and fouling behaviour of coals ashes. The four temperatures reported from AFT tests are the initial deformation temperature (IDT), softening temperature (ST), hemispherical temperature (HT), and the flow temperature (FT). The IDT, ST, HT and FT of the investigated coals are summarised in Table 6-4.

Table 6-4: Ash fusion temperatures of the investigated coal samples

Ash fusion temperature (°C)	Coal A	Coal B	Coal C	Coal D
Initial deformation	+1500	+1300	+1500	+1500
Softening temperature	+1500	+1320	+1500	+1500
Hemispherical temperature	+1500	+1340	+1500	+1500
Fluid temperature	+1500	+1360	+1500	+1500

From the results, coals A, C, and D have high AFT values above 1500°C. The high AFT can be due to a high concentration of quartz and clay mineral found in SA coals. Snyman and Botha (1993) found that both quartz and clay have a tendency to increase AFT above the

temperature of about 1300°C, and this is an advantage for coals used for generating steam. Large quantities of SiO_2 result in the formation of strong covalent bonds, yielding a liquid phase with high viscosity and low deposition potential [Huang *et al.*, 1996; Laursen *et al.*, 1998; McLennen *et al.*, 2000]. Therefore, a high concentration of refractory minerals leads to high AFTs [Vassilev *et al.*, 1995].

Most Australian coals, similar to SA coals are characterised by AFT above 1500°C, correlated with high silica content, SiO_2: Al_2O_3 ratio, and low basic oxide content [Patterson and Hurst, 2000; Van Dyk *et al.*, 2006; Liu *et al.*, 2013]. The acidic component of ash (SiO_2, Al_2O_3, and TiO_2) increases the AFT of coal samples, because of the high softening temperature exhibited by the oxides, with Al_2O_3 having the most significant effect, due to its ion-oxygen attraction, and its high oxidation state [Van Dyk *et al.*, 2006].

A study by Weeber *et al.* (2000) investigated the mineralogical and petrographic factors that influenced AFT on the No.2 coal seam from Witbank coalfield, and it was concluded that the optimum AFT from coals within the Witbank coalfield was approximately 1400°C. Therefore it can be considered that SA coals in general have high AFT values. Usually, AFTs of about 1300°C and above are desirable to ensure slagging and fouling does not occur [Weeber *et al.*, 2000; Patterson and Hurst, 2000]. However, in cases where AFTs are above 1500°C addition of fluxes might be required.

The AFT results for the investigated coals are well within the expected AFT for SA coals. However, coal B showed a different behaviour from coals A, C, and D, reporting the lowest AFT relative to coals investigated, as seen from Table 6-4. The low AFTs recorded for coal B are attributed to the high Fe_2O_3 (6.35 wt. %) and K_2O (0.83 wt. %) content in coal B as reported in Table 6.2. It is apparent that the behaviour was also influenced by a high Fe/Ca

ratio of 7.94. However, it is noted that although the AFT was considerably lower than other coals, the propensity to form slagging for coal B is still relatively low.

High iron and potassium content usually lowers the slag viscosity, and coals with Fe_2O_3 content below 6 wt. % have low slagging tendencies [Wall *et al.*, 1998]. Findings by Van Dyk *et al.* (2009), Liu *et al.* (2013), and Chakravarty *et al.* (2015) concluded that the slagging propensity of coals was related to Fe content which lowered the AFT in coal samples, by reducing the melting point and viscosity of ash particles. The AFT of coal B decreased due to an increase in Fe_2O_3, SiO_2: Al_2O_3, and K_2O. However, it should be mentioned that K_2O does not always have an effect on AFT [Liu *et al.*, 2013], and this could also be attributed to the mode of occurrence of potassium in coals.

Another important factor that has an effect on AFT is the oxidation state of Fe in coal conversion processes. In a study by Weeber *et al.* (2000), it was found that there is a relationship between AFT and the form of Fe mineral found in coal samples. The slag viscosity was lowered in the presence of Fe^{2+}, because the Fe^{2+} iron and unsaturated O^{2-} form a chemical bond that destroys the network structure of high melting silicate, thus reducing slag viscosity [Waanders *et al.*, 2003; Oliviera *et al.*, 2011; Liu *et al.*, 2013; Hai-tao *et al.*, 2015].

Other major chemical compositions known to affect AFT are the base-acid ratio [Van Dyk, 2005], CaO, and the SiO_2: Al_2O_3 ratio [Liu *et al.*, 2013]. The AFT also decreases with an increase in CaO content, and the Si: Al ratio of up to 1.5. High Si/Al ratio above 2.0 does not have any significant effect on AFT. An increase in B/A ratio lowers slag viscosity, subsequently increasing the slagging potential [Wall *et al.*, 2008]. However, based on the results of the four coals investigated, there is no correlation drawn between AFT and the

base-acid, CaO, and SiO_2: Al_2O_3 ratio. Furthermore, it has been reported that the correlation between base-acid ratio and AFT is a poor indicator of slagging and fouling propensity [Akar and İpekoğlu, 2007].

Vassilev *et al.* (2011) reported that high AFT are related to increasing coal rank, high DAI values, and refractory minerals such as kaolinite, quartz, and Ti-bearing minerals, which are mostly detrital in nature, and a decrease in concentration of fluxing minerals such as carbonates, sulphides, sulphates, and phosphates. Therefore, lower AFT values are ascribed to lower rank coals, with lower DAI values and detrital minerals and an increased concentration of authigenic minerals.

Findings from this study did not conclusively draw any correlation to findings by Vassilev *et al.* (2011). Although coals C and D had low DAI of 2.9 and 6.7 respectively, the coals did not have low AFT. These findings suggest that coal composition; and most importantly, the mode of occurrence; have more influence on AFT than DAI values.

It can be said that high concentration of Fe_2O_3, SiO_2: Al_2O_3, and Fe: Ca ratio, lead to a decrease in AFT (as shown in Table 6-4) for coal B. Low AFT result with coal samples having a high propensity towards slagging. Su *et al.* (2000) examined slagging and fouling indices of 25 coals and coal blends. From the study, it was found that Fe: Ca ratio was the only index that could be used to positively predict the slagging propensity. On the other hand, Han-xu *et al.* (2008) added Fe_2O_3 as a fluxing agent to lower AFT in Liuer coal samples. The authors concluded that Fe_2O_3 content increased with a decrease in AFT. These observations confirm the results found in this investigation.

6.6 Thermodynamic equilibrium modelling-FACTSAGE

As already stated, although slagging prediction empirical indices are commonly used to predict slagging methods, the approach is not always reliable since the indices do not reflect the interaction between mineral particles during phase transformation [Van Dyk *et al.,* 2005; Lawrence *et al.,* 2008]. Thermodynamic modelling approaches have been developed to predict equilibrium phases at high temperatures.

A thermodynamic modelling package FactSage 7.0 was used to predict the different phases that might form at temperatures between 1100°C and 1400°C for coals A, B, C, and D. The XRF ash analysis compositions of the respective samples were used as initial inputs. The major phases predicted from the modelling package include mullite ($Al_6Si_2O_{13}$), feldspar ($KAlSi_3O_8$; $NaAlSi_3O_8$; $CaAl_2Si_2O_8$), corundum (Al_2O_3), immiscible slag phases, and cordierite ($Mg_2Al_4Si_5O_{18}$). From the results presented in Figures 6-6 to 6-9, it is evident that the coal samples studied would behave differently at high temperatures, mainly due to the difference in their chemical compositions.

From the results, mullite is predicted as the dominant mineral formed in coals A and D as shown in Figures 6-6 and 6-9 respectively. At high temperatures, kaolinite losses water of crystallization to form metakaolin which transforms into mullite. Therefore, the amount of mullite can be correlated with the amount of kaolinite found in raw coals and the slag phase [Van Dyk *et al.,* 2008]. Mullite in coal A was the major mineral matter present. This indicates the acidic nature of ashes in coal A, with refractory materials that increase temperatures above 1500°C. However, it was also noted that the concentration of mullite in coal D remained the dominant phase until complete transformation was observed as temperatures reached 1200°C, above which the concentration decreased slightly, and more slag phase was formed as a result of the reaction of cordierite and feldspars.

The ferromagnetic minerals such as cordierite and feldspar influenced slag formation. The partial melting of ferromagnetic minerals occur at 200-400°C [Huffman *et al.,* 1981]. Therefore the slag formed was expected to have high concentration of Fe.

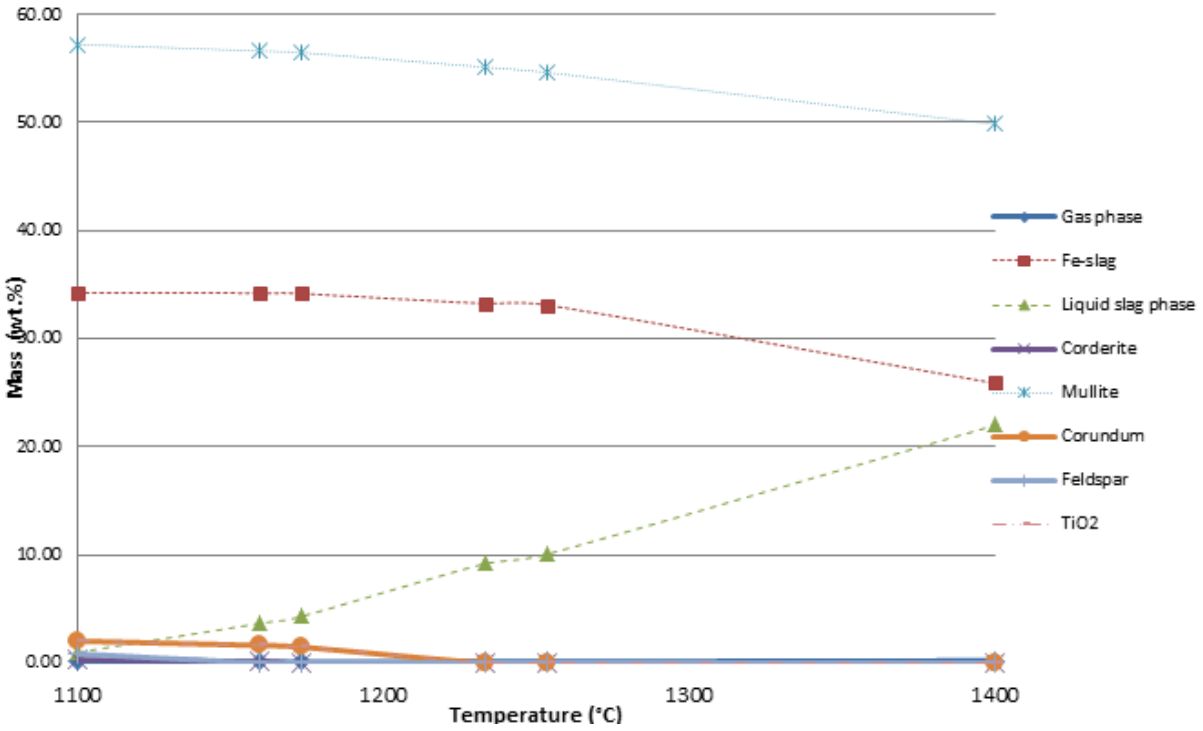

Figure 6-6: Predicted high temperature phases in coal A using FactSage thermodynamic modelling package

The Fe-slag phase was found to be the dominating phase in coal B. It is understood that the breaking down of corundum, corderite, feldspar, and mullite led to the formation of the liquid slag phase 2, which sharply increased at temperatures of about 1170°C until 1250°C. The significant drop in the concentration of slag 2 subsequently led to an increase of slag 1. The behaviour of coal B as shown in Figure 6-7 explains the low AFT reported for the sample. The sample reported the lowest AFT, which implies the coal formed a slag phase at relatively low temperatures compared to the rest of the coals studied. The ash composition of coal B lowered the AFT in favour of forming the slag phase.

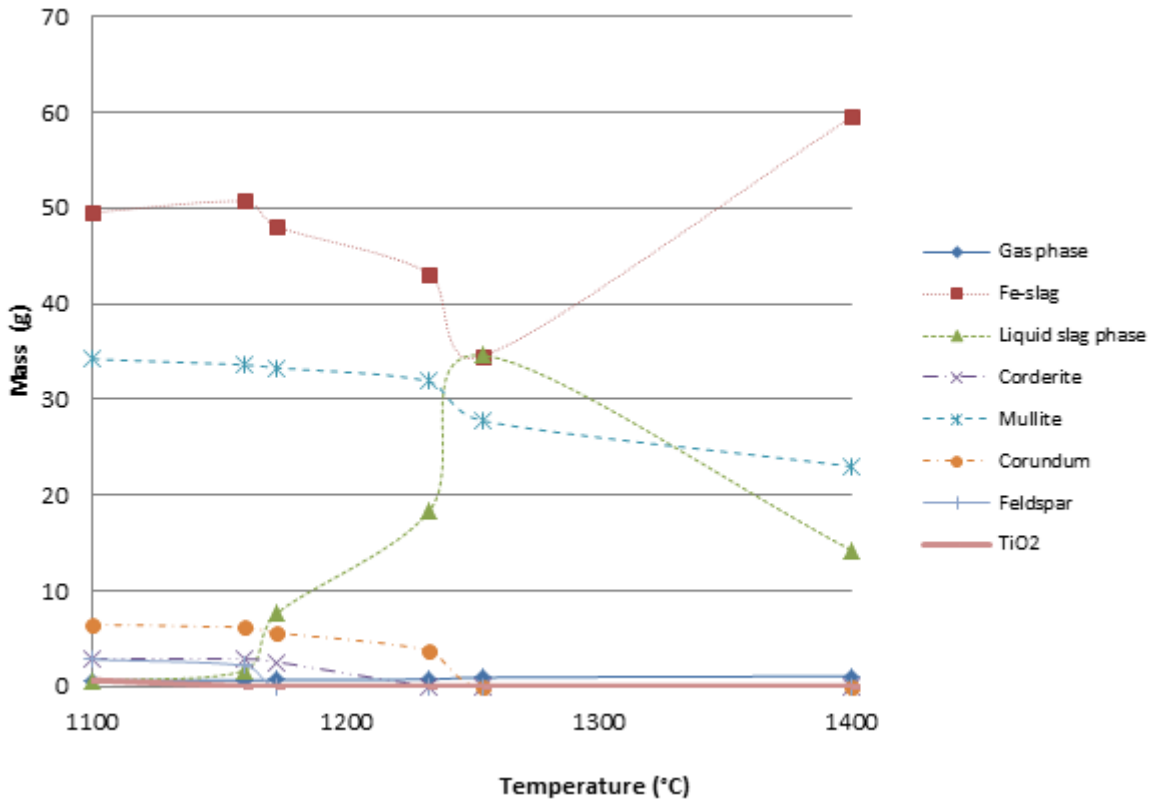

Figure 6-7: Predicted high temperature phases in coal B using FactSage thermodynamic modelling package

Anorthite ($CaAl_2Si_2O_8$) is a high temperature phase that form via a solid state reaction between alkali compounds, (i.e. Ca-containing species) and kaolinite [Raask, 2000; Spears, 2000]. The Ca containing species occur as calcite, dolomite, ankerite, and fluorapatite. Feldspars have a low melting temperature of about 1200°C as indicated in Figures 6-6 and 6-9. It was observed that feldspars were the dominating phase in coal C, which gradually decreased until the temperature reached 1330°C. The decrease in the composition of feldspar resulted in the formation of liquid slag [Van Dyk *et al.*,2008]. The concentration of mullite in coal C was relatively low compared to coals A, B, and D. The high concentration of feldspar could imply the coal had a significant amount of anorthite, which could be confirmed by the high Ca-content in coal ashes of coal C. The abundance of feldspar shows that silica activity was low in the transformation of coal C.

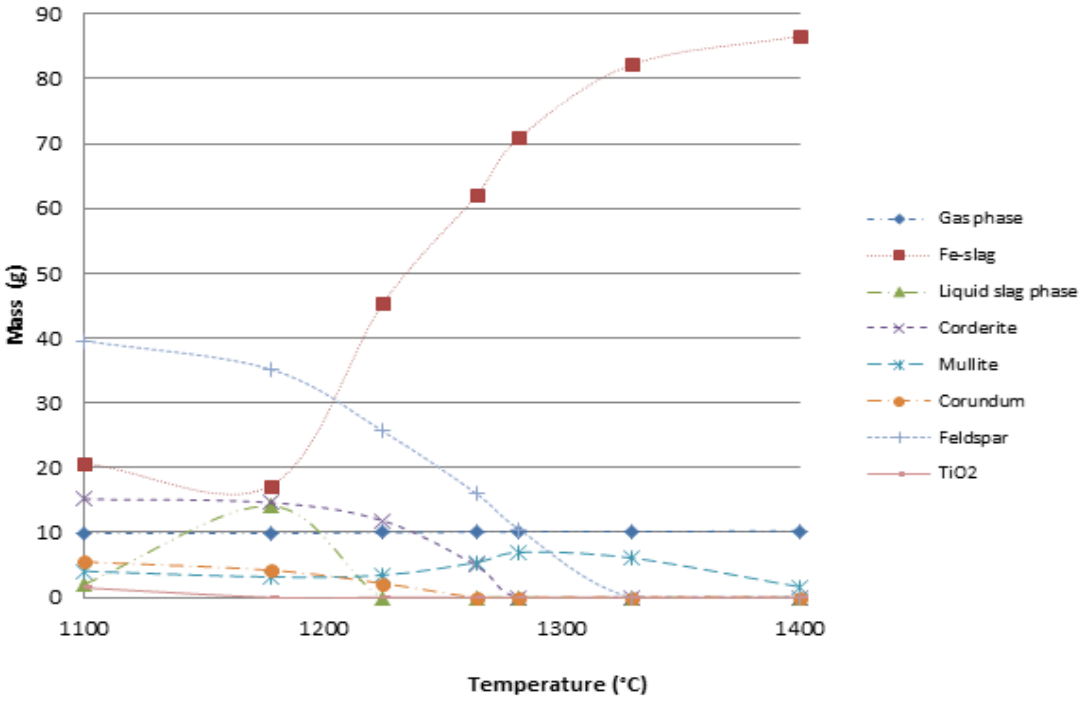

Figure 6-8: Predicted high temperature phases in coal C using FactSage thermodynamic modelling package

Liquid slag 1 is the main slag phase found in coal C, with a small amount of liquid slag 2. However, the second immiscible phase was completely transformed at 1225°C. It was anticipated that feldspar, corderite, and mullite were the phases that would undergo transformation to form more of slag 1 phase.

Significant amount of corderite and feldspar are predicted in coal D, whilst the concentration of mullite remains relatively constant with a decrease in temperature. From the behaviour depicted in Figure 6-9, it can be said that feldspar and corderite react to form the slag phase. The concentration of slag 1 started to increase at 1168°C, when a drop in the concentration in slag 2 was observed. The high temperature phases predicted are to be confirmed by XRD, FTIR, mRs, and SPA-EPXMA in subsequent sections.

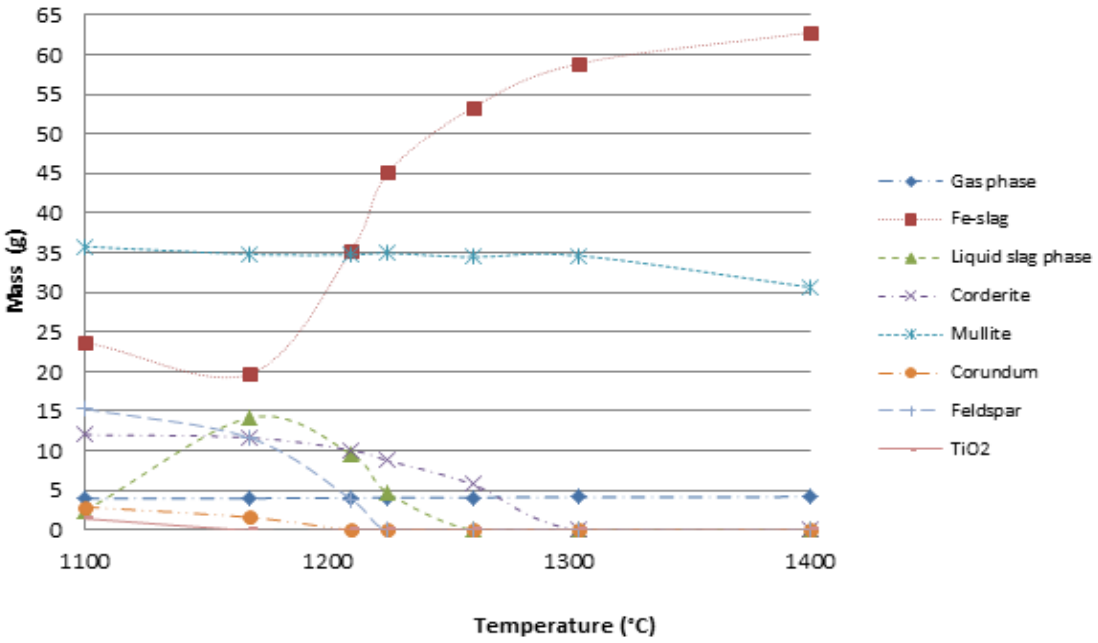

Figure 6-9: Predicted high temperature phases in coal D using FactSage thermodynamic modelling package

From the FactSage thermodynamic modelling, it can be concluded that both Ca and Fe contributed to the formation of the slag phase in coal samples. The mullite phase contributes to high AFT in coal samples.

6.7 Coal petrographic analyses of raw coals

As discussed in section 4.2, petrographic analyses involve microscopic evaluation of polished sample blocks under reflected light and oil immersion. It is important to determine petrographic composition of coals, since petrography can be used to predict the applicability of coal in various coal conversion processes, and understand the origin of coal. The petrographic studies focused on the determination of different macerals group, mineral matter composition, diagenetic features, and the morphology of various mineral matter in the samples. The abundance of organic matter and mineral matter was based on counting 500 points, and the results presented in volume percentage. The last section of the coal

petrography section draws the correlation between petrographic composition and coal ash chemistry.

6.7.1 Maceral group analyses

Macerals are derived from terrestrial, lacustrine, and marine plant remains. These macerals are distinguished from one another on the basis of their physico-optical, chemical, and technological properties [Falcon and Ham, 1988], and are classified by the ICCP classification system (1963, 1971, 1975, 1993) into three main groups: vitrinite, inertinite and liptinite. Petrographic photomicrographs of selected coal samples are shown in Figure 6-10.

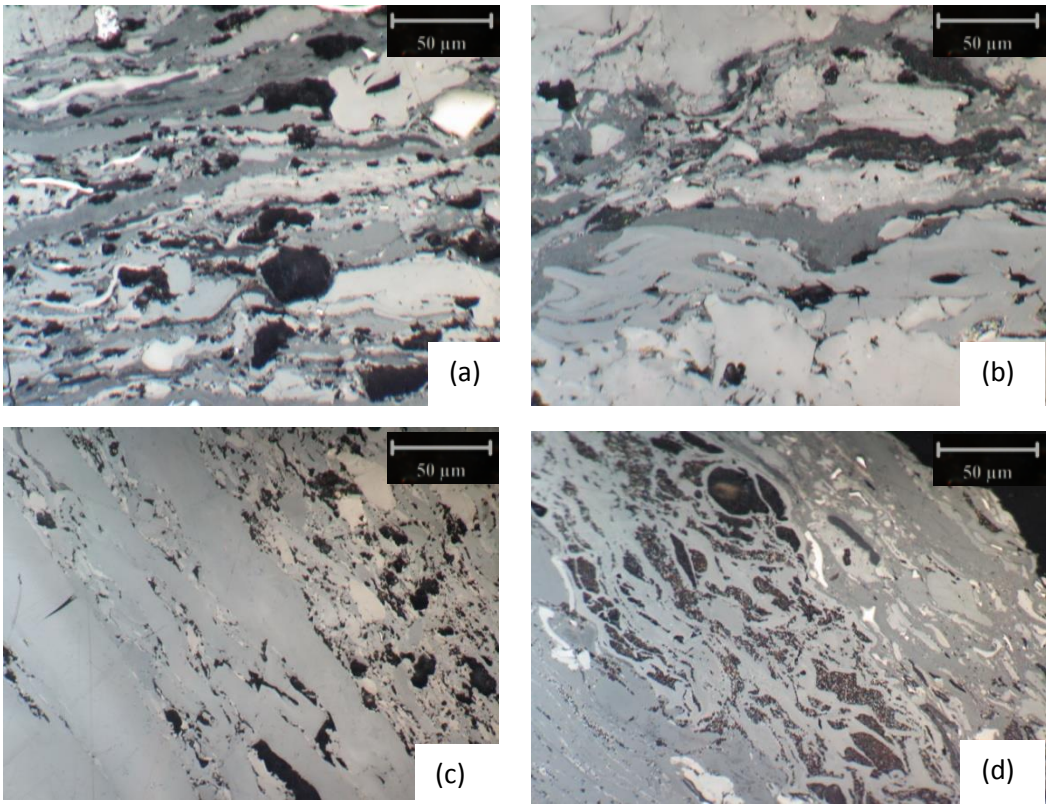

Figure 6-10: Examples of maceral composition in the bituminous South African coal samples; (a) Inertinite-rich with some vitrinite bands; (b) banded semifusinite at bottom, (c) carbonate minerals associated with organic matter (d) Centre: Flocculated clays contained in vitrinite (x500 magnification, oil immersion lens)

The petrographic analyses identified the composition and abundance of the major maceral groups (vitrinite, inertinite and liptinite) found in coal samples, with a summary of the results presented in Table 6-5. The detailed petrographic investigation of sub-maceral compositions of the various coal samples are presented in Table E-1 in Appendix E. As expected, these South African medium rank C bituminous coals are inertinite-rich, with the inertinite composition making up more than 75 vol.% on a mineral matter free (mmf) basis. The vitrinite and liptinite maceral groups are present in relatively low concentrations.

Table 6-5: Petrographic composition of macerals in South African coals (vol. %) mmf basis.

Maceral group	Coal A	Coal B	Coal C	Coal D
Vitrinite	5.00	20.8	4.10	10.7
Inertinite	90.8	75.5	84.3	79.7
Liptinite	4.30	3.80	11.6	9.60

6.7.1.1. Inertinite maceral group

South African inertinite-rich coals were subjected to aerobic, strongly oxidative environments, with the inertinite content typically decreasing from top to bottom of the coal seam [Falcon and Ham, 1988]. The increase in inertinite is due to the subsidence of the peat swamp over time, and the lowering of the water table. The coal samples investigated in this study are inertinite rich, with inertinite concentration ranging from 70-91 vol.% (mmf) as shown in Table 6-5. Coal A is characterised by high amount of inertinite (91 vol.%) mmf.

The maceral groups of inertinite (fusinite, reactive semifusinite, inert semifusinite, micrinite, macrinite, secretinite, and inertodetrinite) were identified in the samples at variable quantities. It was observed that inertinite comprised mainly of inert semi-fusinite and inertodetrinite as the most abundant macerals identified in the coals studied. Inertodetrinite concentrations were high in all the investigated coals, relative to inert semi-fusinite.

Similar observations on Highveld coalfield were reported by Hagelskamp and Snyman (1988) on low reflecting inertinite coals. The results were confirmed by Snyman and Botha (1993), and most recently by Everson *et al.* (2013). In their findings, inertodetrinite was the most abundant maceral, concentrated in the durain bands and partly in the clarain bands. Inertodetrinite is semi-reactive, formed from plant debris that were introduced into the peat during periods of flooding, and redeposited with clastic minerals in low lying swamps [Falcon, 1989; Snyman and Botha, 1993; Weeber *et al.*, 2000].

The dominance of inertodetrinite in coal samples is an indication of water transportation activities and re-deposition that took place during the formation of coals [Falcon, 1989; Weeber *et al.*, 2000]. Coal A reported the highest proportions of inertodetrinite and inert semifusinite, as depicted in Figure 6-11. The presence of fusinite, semi-fusinite, macrinite, and micrinite is an indication of forest fires during dry periods of coal formation. Generally, the coals consisted of very low concentrations of micrinite and macrinite.

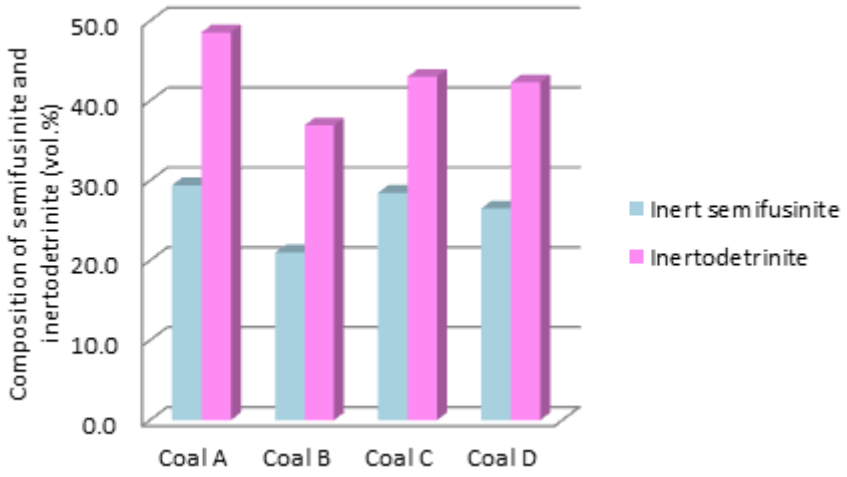

Figure 6-11: Comparison of inert semifusinite and inertodetrinite concentration in the coal samples

6.7.1.2 Vitrinite maceral group

Vitrinite is regarded as the reactive maceral in coals, and is common in Northern hemisphere coals, forming in anaerobic conditions. The vitrinite content in Southern hemisphere coals has an average composition of 40 vol. % [Falcon and Ham, 1998]. The vitrinite content in the investigated coal samples varied between 5 and 21 vol%, mmf, which can be considered typical of run-off-mine (ROM) SA coals.

Collotelinite (Table E-1) was the most abundant vitrinite maceral found in these coal samples, with coal B (9.7 vol.%, mmf) and coal D (7.3 vol.%, mmf) reporting the highest concentration of collotelinite. Coal A (3.2 vol. %, mmf) and coal C (4.1 vol. %, mmf) had the lowest concentrations of collotelinite. Vitrodetrinite (Table E-1) was the second most abundant vitrinite maceral found in the coals studied, with the highest concentration reported for coal B (10 vol. %, mmf). Other maceral groups, such as gelinite, pseudovitrinite, and corpogelinite, are present in relatively low concentrations.

6.7.1.3 Liptinite maceral group

The amount of liptinite present in all coal samples is relatively low compared to other maceral groups. Typically, South African coals have a low concentration of liptinite, ranging between 2 and 10 vol.% [Falcon and Ham, 1988], and generally below 5 vol.% [Snyman, 1989]. Thus, the liptinite content in coal C, with a composition of approximately 12 vol.%, (mmf.) can be considered to be high. High liptinite content leads to a high volatile matter and low fixed carbon content [Falcon and Ham, 1988].

Coal C had by far the highest amount of mineral matter and lowest fixed carbon contents (as indicated in Table 6-1); this suggests the liptinite was intimately bound with the mineral matter, since the sample is a discard coal. Sporinite was the dominant liptinite maceral identified in these coals, with a concentration of approximately 11 vol.% in coal C. Other macerals present in minor quantities included cutinite, resinite and the liptodetrinite.

It can be summarised that South African coals typically have high concentration of inertinite macerals as it has been reported previously. Typically coals from the Karoo basin have reported high concentrations of inertinite (up to 78%), moderate to low vitrinite (17-45%), and moderate to low liptinite content (2-11%). From this work, it can be seen that the dominating maceral groups are inert semifusinite and inertodetrinite, which is characteristic of SA coals [Everson *et al.*, 2013].

6.7.2 Mineral matter found in South African coals and their mode of occurrence

Petrographic evaluations allow for direct identification of mineral matter present in coal samples. However, only mineral matter visible at a magnification of X500 can be identified, thus making it difficult to identify finely distributed mineral matter. As discussed in previous sections, South African coals are typically low grade coals, with a relatively high ash content (up to 35 wt.%). This implies that a significant amount of mineral matter is present in SA coals, and this mineral matter are to be accurately classified and identified for one to understand their impact in downstream processes.

Mineral matter in South African coals can be classified into four main groups: clays, silicates, sulphides, and carbonates. The presence of these minerals was first identified by analysing the ash content. From ash chemistry, it was deduced that kaolinite, quartz, dolomite, calcite, and pyrite were present in coals.

The identification of these minerals was based on the assumption that coal is homogeneous. The detrital-authigenic index indicated that coals A, B, and D were detrital in nature. Although DAI calculation can be used to determine the detrital and authigenetic nature of mineral matter in coals, it is not easy to recognize the mode of occurrence of the minerals from ash chemistry.

Petrographic analyses were conducted to identify mineral matter and establish their association and mode of occurrence in coals. Mineral matter identified in the investigated coals are clays, sulphides, carbonates, quartz, oxides and a small fraction of mineral matter that was not identified petrographically. The petrographic analyses are compared to the ash composition results detailed in Section 6.2.3. The mineral matter composition for different coals is presented in Table 6-6. The detailed results of the petrographic mineralogical compositions can be found in Appendix E.

Table 6-6: Mineral matter composition in volume percent (organic matter free basis) of coal samples determined by petrographic point counting method

Mineral matter (Vol.%)	Coal A	Coal B	Coal C	Coal D
Silicates	39.9	22.1	71.0	47.1
Sulphides	13.3	10.4	6.1	7.8
Carbonates	8.7	22.9	1.8	9.8
Quartz	37.2	43.8	20.7	30.4
Other	0.9	0.8	0.3	2.0

6.7.2.1 Clay minerals

Clays are the major minerals found in South African coals [Falcon, 1988]. From the petrographic results presented in Figure 6-12, it can be observed that more than 50% of mineral matter in coals is present as clay minerals, with approximately 70 vol.% clay mineral content in coal C. The petrographic observations are in agreement with the ash chemistry results, whereby Al_2O_3 and SiO_2 are dominating elements in coals, indicating the presence of clay minerals.

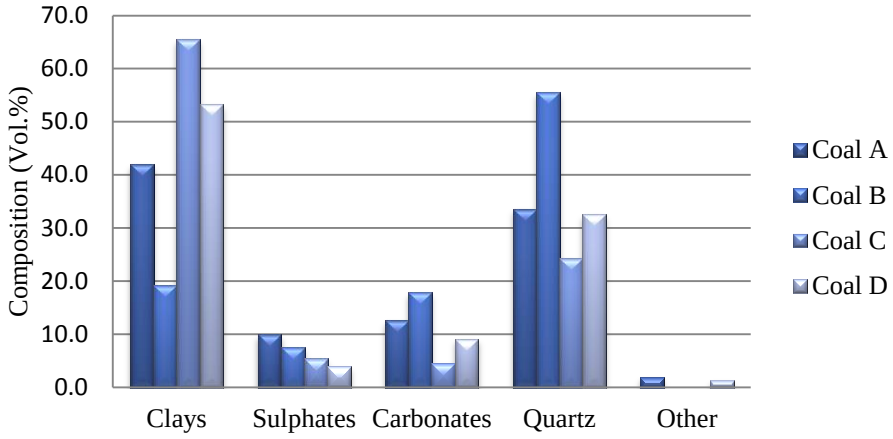

Figure 6-12: Mineral matter in coals as determined by optical microscopy [including organic matter]

The mode of occurrence of clay minerals found in South African coals is variable. Some of the clay minerals are dispersed in organic matter such as vitrinite (Figure 6-13), or present as veins or cell infillings. From this work, it was noted that kaolinite is present as a syngenetic and an epigenetic mineral matter, as indicated in Figures 6-13 (a) and (b), respectively. Syngenetic minerals are formed during the early stage of coalification, after deposition or by diagenetic degradation of pre-existing minerals. These forms of minerals exhibit crystal faces, and are intimately intergrown with other syngenetic minerals and are found in cell cavities. The epigenetic minerals are found in fractures or cleats, and bear no relationship to the inherent structure of coal.

The finely grained mineral matter occurs as infilling of vitrinite cell structure and other organic matter (Figure 6-13 b). Generally, most of the clay minerals identified were finely grained and associated with organic matter, or occurred as infilling in cell structures. The association of kaolinite with inertodetrinite indicated the detrital origin of the mineral in coal [Snyman and Botha, 1993], and these results are in agreement with the detrital-authigenetic index relationship derived from ash chemistry.

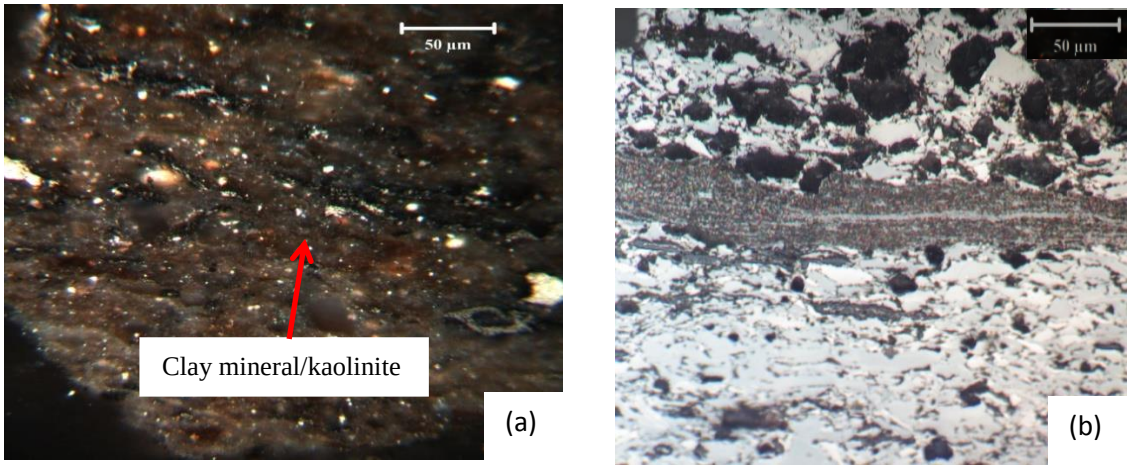

Figure 6-13: a) Disseminated syngenetic clay minerals b) Epigenetic kaolinite mineral deposited in organic matter (Magnification, X500, oil immersion lens, reflectance microscope).

6.7.2.2 Quartz

Quartz is the second most abundant mineral present in coal samples. Coals A, B, and C have the highest concentration of quartz (Table 6-6), with composition ranging from 20 vol. % to 44 vol.%, on a maceral free basis. The quartz found in the coals was of both syngenetic and detrital origin, mostly spherical, but also angular and liberated, with some particles showing internal reflection of rutile rods, as indicated in Figure 6-14 (a) and (b), respectively. The rounded quartz indicated a detrital origin, whereby the mineral was transported into coal peat at a later stage of coal formation by moving water or winds. The detrital quartz was mostly associated with clay mineral.

Quartz associated with organic matter is most likely to experience high temperatures during coal conversion, whilst quartz associated with clay minerals is expected to be liberated during beneficiation of coals.

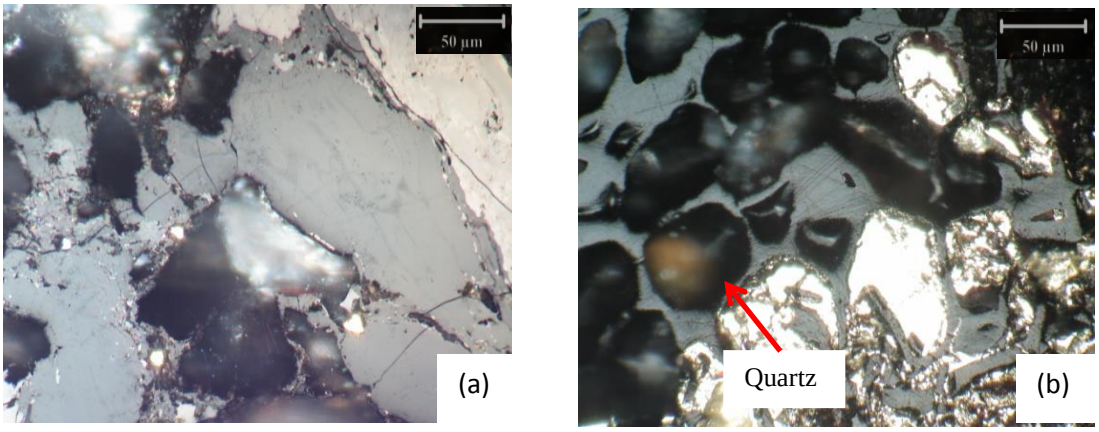

Figure 6-14: a) Authigenetic quartz with internal reflection, b) Rounded quartz and epigenetic pyrite infilling vitrinite structure. (Magnification, X500, oil immersion lens, reflected light).

6.7.2.3 Carbonates

The interaction and activity of CO_2, H_2O and elemental species lead to the precipitation of carbonate minerals [Garcia-Vallès *et al.*, 1993]. Carbonate minerals are typically of an authigenic origin in coals. Carbonates of syngenetic origin are common in sub-bituminous coals, and common carbonate minerals found in South African coals are calcite and dolomite [Snyman, 1989].

From the petrographic results, the carbonate mineral concentration ranged from 2.0-23 vol. % (maceral free basis). Coal B reported the highest concentration of carbonate minerals (23 vol. %), whilst coal C had the lowest concentration of carbonates (1.8 vol.%). From this account it is noted that there is a difference in the reporting of the carbonate minerals by petrographic methods and ash chemistry composition.

The difference in the reporting can be due to the fact that ash chemistry will report the total amount of elements that is either organically or mineral matter bound. Petrographic analyses as already stated, identify minerals that are visible at a magnification of X500. Moreover, the petrographic results are reported in volume percentage, and not in mass percentage. Therefore, it is anticipated that the two analyses will not reflect similar results.

The morphological structure of carbonates identified in these coals is shown in Figure 6-15 (a) and (b). The carbonate mineral was of an authigenetic origin, and associated with inertodetrinite.

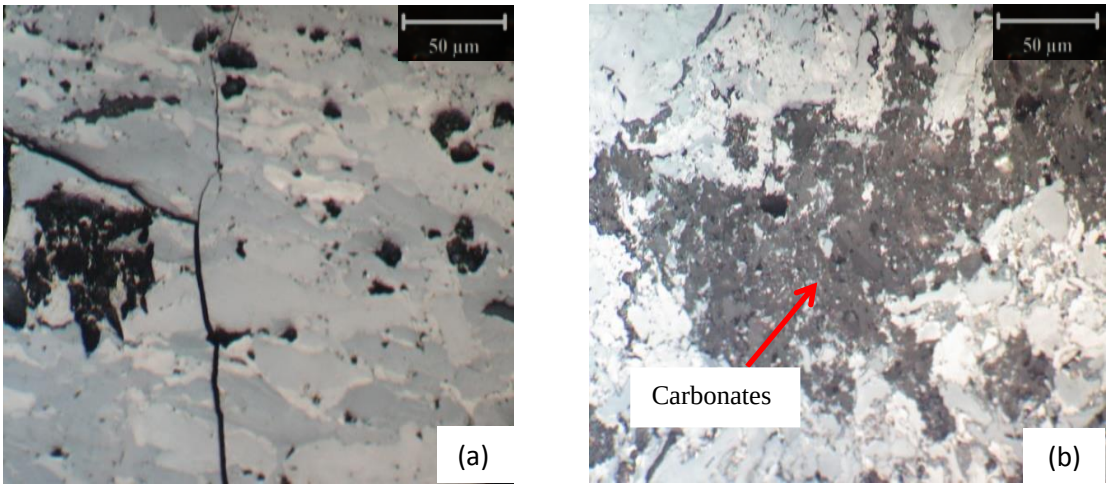

Figure 6-15: a) Carbonate-siderite mineral in inertodetrinite. b) Carbonates in organic matter (Magnification X500, oil immersion lens, reflectance microscope)

6.7.2.4 Sulphides

Pyrite is a common mineral that hosts sulphides in coals. Sulphides can be classified either as syngenetic or epigenetic. Syngenetic sulphides form during the early stages of peatification, the minerals are usually small in size and finely distributed throughout the coal structure. Conditions that favour the formation of pyrite are marine environments, which consist of high concentrations of sulphates and iron, under reducing and acidic environments [Querol *et al.*, 1989; Taylor *et al.*, 1998] and bacterial activities.

Pyrite intrusion into cell cavities is due to sulphur bearing aeolian and fluviatile during the early stages of the peat accumulation, precipitating out syngenetic pyrite [Weeber *et al.*, 2000; Falcon and Snyman, 1986]. Framboidal pyrite is syngenetic and is formed during early diagenetic process. Epigenetic pyrite is introduced into the coal after compaction. Contrary to syngenetic pyrite, these sulphides are larger and fairly coarse. The epigenetic pyrites form in conditions where there is enough reduced sulphur, dissolved cations, and formation sites such as cracks, cleats and cavities, where pyrite precipitates out. Coal D comprised of both syngenetic and epigenetic pyrite. However, generally the coal samples were comprised of epigenetic pyrite.

The petrographic composition of pyrite ranged from 6-13 vol.%. Coal C has the lowest concentration (6.1 vol.%) of finely disseminated pyrite mineral. The morphology of pyrite in the coal samples was variable, as depicted in Figure 6-16 (a)-(d). From the study, the most common mode of occurrence of pyrite was massive replacement, and the infilling of cell structure, cleats and fractures.

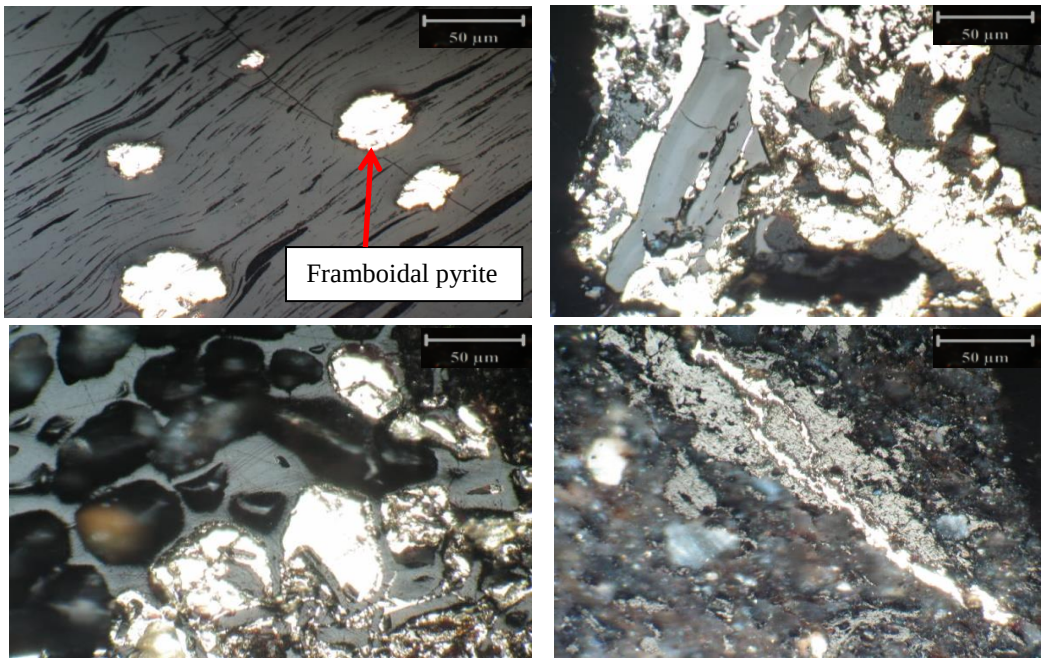

Figure 6-16: The different morphologies of pyrite in coals. a) Nodular syngenetic pyrite in vitrinite. b) Epigenetic cleat in-filling; c) Cell in-filling; and d) Pyrite lens in clay-rich particle. (Magnification X500, oil immersion lens, reflected light)

The detailed morphologies and mode of occurrence as determined by petrographic analyses are summarised in Table 6-7.

Table 6-7: Detailed analyses of mineral matter of the investigated samples (Vol. %) showing the mode of occurrence in coals

Mineral group	Mineral form (vol. %)	Coal A	Coal B	Coal C	Coal D
Clays	**Fine grained in organic matter**	**11.8**	**6.8**	**23.0**	**23.4**
	Fine grained infilling cell structure vitrinite	6.5	6.2	0.4	20.8
	Infilling cell structure other	1.1	3.4	1.6	5.2
	Fine grained association	0.0	0.0	0.0	2.6
	Association with quartz	**18.7**	**2.7**	**29.2**	**1.3**
	Liberated	3.8	0.0	11.1	0.0
Sulphides	**Finely distributed**	**0.0**	**0.7**	**0.0**	**0.0**
	Infilling cell structure other	**5.0**	**2.1**	**1.2**	**0.0**
	Infilling cleats / fractures	1.9	3.4	1.2	3.9
	Massive / replacement	**3.1**	**1.4**	**2.9**	**0.0**
Carbonate	Finely distributed siderite	0.0	0.7	0.4	0.0
	Siderite growths	**0.0**	**11.0**	**0.4**	**9.1**
	Infilling cell structure fusinite	1.5	0.0	1.2	0.0
	Infilling cell structure other	**0.4**	**3.4**	**1.2**	**0.0**
	Infilling cleats /fractures	10.7	2.1	1.2	0.0
	Calcite veins with twinning	0.0	0.7	0.0	0.0
Quartz	Associated with clays <10	21.8	8.2	13.6	0.0
	In organic matter	**11.8**	**41.8**	**10.7**	**31.2**
	Liberated	0.0	5.5	0.0	0.0
	With rutile rods	0.0	0.0	0.0	1.3

Based on petrographic studies, clay minerals occurred in various forms coals C and D were characterised by fine-grained clay minerals associated with the organic matter. Fine grained infilling cell structure of vitrinite is abundant in coal D. A significant amount of clay minerals in coal C, are associated with quartz, and some are liberated. A high concentration of liberated quartz in coal C is an indication that the minerals were originally epigenetic and were liberated during beneficiation.

Most of the carbonate occurred as siderite growth in coals B and D, and infilling cell structure and cleat/fracture. Carbonate minerals in coal A are characterised by infilling cleats/fracture. The mode of occurrence of quartz is mostly associated with organic matter or clay minerals. Majority of quartz, most especially in coal B is associated with organic matter, whilst a good proportion is associated with clay minerals in coal A. Quartz in coal D is also associated with rutile rods.

Pyrite minerals are dominantly present as infilling cleats or fractures. Infilling minerals have an epigenetic mode of occurrence. Pyrite occurring as isolated euhedral forms framboids, indicating the syngenetic origin of pyrite. Syngenetic pyrite formed as a result of a chemical reaction between H_2S generated from SO_4^{2-} by sulphate reducing bacteria and ferrous ions in the peat swamp (Kostova *et al.,* 1996, Chou, 1997, Dai *et al.,* 2002). The most common form of occurrence of pyrite is infilling cell structure/fracture and massive replacement, and less common as finely distributed mineral.

The mode of occurrence and association of mineral matter depends on the paleogeographic conditions that were pertinent during peat formation, and the subsequent coalification process, referred to as syngenetic minerals and successive epigenetic mineralisation due to

fluid inclusions. The mode of occurrence of mineral matter is likely to influence the combustion behaviour of different coals [Shirazi *et al.,* 1995].

6.8 Relationship between mineral matter determined by petrographic methods and ash content

The determination of ash content following ISO 1171 was used to estimate the amount of mineral matter in coals. The ash content was related to mineral matter that was determined from petrography. The relationship drawn between the two parameters is presented in Figure 6-17, showing a linear relationship, with a correlation coefficient (R^2) of 0.94, between mineral matter and ash content.

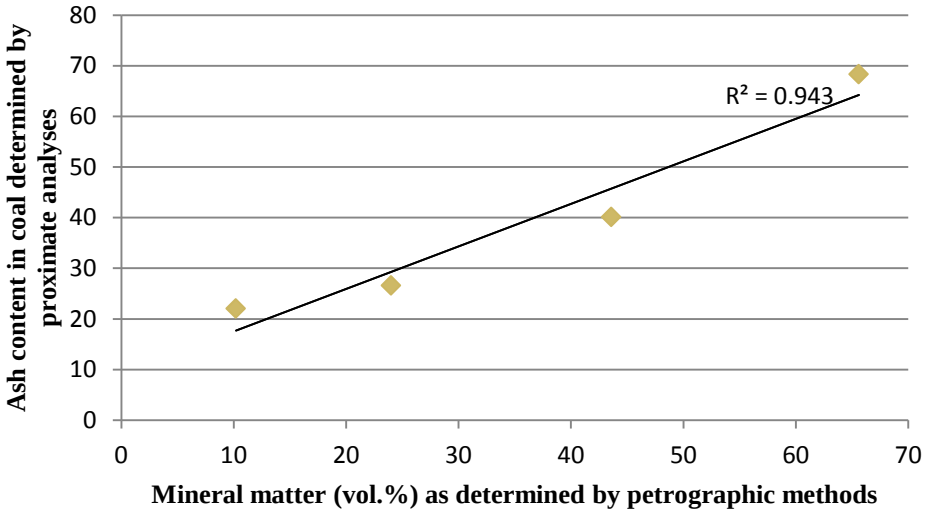

Figure 6-17: Relation between petrographically determined mineral matter and ash content

The use of petrographic methods was valuable in describing the different maceral groups, mineral matter, their association and mode of occurrence. From the analyses made to this point it can be summarised that the major mineral matter present in coals are clays, carbonates, sulphides, sulphates, and oxides, as were reported previously for SA coals [Everson *et al.,* 2013; Falcon and Ham, 1988; Matjie *et al.,* 2016].

A good correlation was drawn between ash content and mineral matter using proximate and petrographic analyses. However, both petrographic and proximate methods fall short in terms of providing detailed information in identifying, and describing mineral matter found in coals, particularly in cases where minerals are in low concentrations. A volume concentration of minerals ranging from 0.3 to 2 vol.% could not be identified, and the minerals were classified as other. Moreover, petrographic methods could not discriminate between minerals that belong to the same group. The next section of the report focuses on bulk structural analytical tools and point analyses that were used to characterise mineral matter in more depth.

6.9 Structural analyses of mineral matter in coals

A number of characterisation techniques are generally used to study both the organic structure and the mineral matter composition in coals. This section of the thesis focuses on the use of structural techniques such as XRD, FTIR, and mRs to characterise and understand the nature and mineralogical structure of mineral matter that occur as discrete minerals or organically associated with coal in raw, LTA and HTA samples. This section of the chapter will first consider bulk structural techniques, and lastly the single particle analyses method.

6.9.1 X-ray diffraction (XRD) analyses of raw coals

In order to determine the mineralogy of raw coals, the diffraction patterns were measured and collected over the scan ranging from 10° to 80°, and the obtained results are shown in Figure 6-18. The quantitative analyses of the four coals were computed using the Siroquant processing system. The Siroquant program generates a synthetic XRD pattern, and compares it to the observed XRD pattern. Scaling factors are then used to estimate the quantitative composition of the different minerals. The XRD results of raw coals determined by the Siroquant program are summarised in Table 6-8.

Comparing the four patterns of the investigated coals, it can be clearly observed that the different diffractograph patterns obtained showed the difference in mineralogy and crystallinity in all four coal samples studied.

According to the obtained results, it was observed that coal D, with a low mineral matter content, was highly amorphous, compared to the other three coals under investigation. The presence of amorphous carbon masked the diffraction pattern, forming a broad pattern between 18° and 30° scanning ranges. The amorphous nature of the coal can be attributed to the high carbon content, as it was previously reported from ultimate analysis results in Table 6.1, whereby the results indicated that coal D was a carbonaceous rich sample.

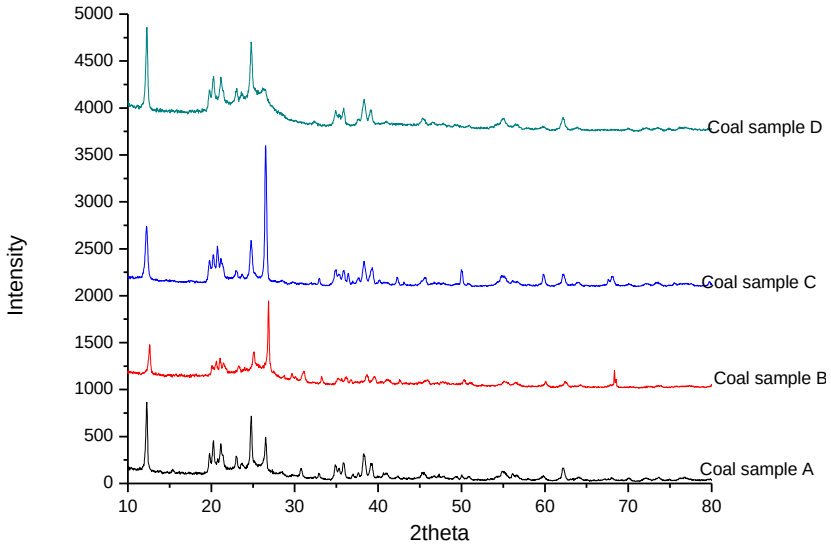

Figure 6-18: XRD diffractograph pattern of raw coal samples collected at room temperature

Major silicates, carbonates, sulphides, phosphates, hydroxides, oxides, and sulphates identified by XRD included quartz, kaolinite, calcite, aragonite, dolomite, pyrite, muscovite, alunite, gypsum, brushite, gorceixite, and anatase. In can be seen from the results presented in Table 6-8 that the major crystalline minerals present in coals are consistent with previous literature that conducted similar studies and identified mineral matter present in SA coals [Snyman and Botha, 1993; Pinetown *et al.*, 2007; Matjie *et al.*, 2016].

Table 6-8: Quantitative crystalline mineral matter composition for the coal samples after normative calculations based on XRD identification. Concentrations are expressed in weight %

Mineral	Chemical formula	Coal A	Coal B	Coal C	Coal D
Quartz	SiO_2	6.2	23.1	29.7	**1.2**
Kaolinite	$Al_2(Si_2O_5)(OH)_4$	78.4	47.8	60.5	**97.7**
Calcite	$CaCO_3$		2.7		
Aragonite	$CaCO_3$		1.1		
Dolomite	$CaMg(CO_3)_2$	4.2	11.4		
Pyrite	FeS_2	8.9	8.6	4.2	
Muscovite	$KAl_3Si_3O_{10}(OH)_2$		1.5	5.3	
Alunite	$KAl_3(SO_4)_2(OH)_6$		1.6		
Gypsum	$CaSO_4(H_2O)_2$		2.0		
Brushite	$CaPO_4(OH)(H_2O)_2$	1.4			
Gorceixite	$BaAl_3(PO)_4(PO_3OH)(OH)_6$	0.9			
Anatase	TiO_2		0.2	0.3	**1.1**
Total		**100.0**	**100.0**	**100.0**	**100.0**

Results presented in Table 6-8 show that the mineralogical composition of crystalline mineral matter in coals studied is mainly composed of kaolinite (Al_2 (Si_2O_5)$(OH)_4$) and quartz (SiO_2) as the dominant crystalline minerals for all coal samples investigated. Furthermore, it can also be seen that a large fraction of minerals found in coal D is in fact kaolinite. The concentration of kaolinite in coals varied between 47.8 wt. % and 97.7 wt. %.

The presence of other silicate minerals such as muscovite was not obviously observed with both XRF and petrographic evaluations. The identification of muscovite by XRD analyses indicates the importance of using structural technique such as XRD to confirm the presence of different clay minerals found in coal structures. However, it is important to notice that muscovite was not identified in all coal samples. Muscovite ($KAl_3Si_3O_{10}(OH)_2$) was found in coals B (5.3 wt.%) and C (1.6 wt.%).

Quartz (SiO_2), the second most abundant mineral found in coals was high in coals B (23.1wt.%) and C (29.7wt.%). According to the findings stated previously from the petrographic results, quartz was of detrital origin, and largely associated with organic matter.
The different carbonate minerals found in the coal samples were identified as calcite ($CaCO_3$), aragonite ($CaCO_3$), and dolomite ($CaMg(CO_3)_2$). All three carbonate mineral groups were identified in coal B. The sample had a nominal composition of dolomite at 12 wt. %. An investigation by Vassilev *et al.* (2010) found that South African bituminous coals from Witbank and Ermelo coalfields are rich in dolomite.

Dolomite is more prevalent in an environment where a high concentration of Mg and high salinity exists [Vassilev *et al.*, 2010]. Moreover, the transformation of either calcite or aragonite can also lead to the formation of dolomite minerals. The presence of dolomite in coals could be an indication of the arid conditions that prevailed during the coalification process.

The sulphide mineral identified in the coal samples was pyrite (FeS_2), identified in coals A, B and C. The compositions of FeS_2 are reported at 8.9 wt.%, 8.6 wt.% and 4.2 wt. % respectively. The presence of pyrite in coal D was relatively low, as expected, thus confirming the total sulphur results reported in section 6.2.2.

It is considered that although XRF and petrographic analyses indicated the presence of sulphide minerals in coal D, the minerals were not positively identified by XRD methods because of the detection limits of the instrument. Moreover, petrography is not a bulk analysis technique and hence can detect pyrite in individual particles.

The two sulphate minerals identified in coals are gypsum ($CaSO_4(H_2O)_2$) with a composition of 2 wt.%, and alunite ($KAl_3(SO_4)_2(OH)_6$) reported at a composition of 1.7 wt.%. The two phosphate minerals, brushite ($CaPO_4(OH)(H_2O)_2$) (1.4 wt.%) and gorceixite ($BaAl_3(PO)_4(PO_3OH)(OH)_6$) (0.9 wt.%) were identified in coal A. The presence of gypsum and brushite is an indication that calcium is not only present as a carbonate but as a sulphate and phosphate mineral.

The mode of occurrence of phosphorus can be associated with either organic or mineral matter [Swaine, 1990]. However, owing to the mineralogical analyses, it can be considered that the general bulk of phosphorus in coals is associated with mineral matter. The formation of gorceixite in coals is an indication of local pH that existed during the precipitation of alumina-phosphate mineral. Phosphate minerals are formed at low pH, due to chemical reaction between phosphate rich solutions, calcite and clay minerals. According to a study by Spears *et al*. (1988), phosphorus was released from plant decay, with elements such as strontium, barium, and lead. These elements were introduced into the coal peat by minerals from volcanic resources.

Anatase is usually found in trace amount in coals. A high composition of anatase (TiO_2) is reported for coal D. However, TiO_2 could not be detected in coal A, possibly because of the low detection limits.

In order to obtained detailed knowledge about the mineral matter, it was important to conduct bulk analyses on raw and ashed samples to gain more insight on the nature of mineral matter found in coals.

6.9.2 X-ray diffraction (XRD) analyses of low temperature ashes

The purpose of low temperature ashing is to drive off the organic matter and to accurately identify mineral matter without the interference of organic matter which can have an effect on mineral matter reported.

The mineral matter phases identified in LTA samples and the respective abundance of individual crystalline phase minerals was calculated and interpreted by making use of Siroquant and the results are summarised in Table 6-9. The XRD results show some similarities in composition between raw coals and LTA samples, which indicates the effectiveness of using LTA methods without altering the composition of minerals found in raw coals.

The major minerals (kaolinite and quartz) identified in LTA samples correlated well with results obtained from XRD analyses of raw coals. The results confirmed information derived from physico-chemical properties and petrographic evaluations of the coals.

Table 6-9: Mineralogy and ash composition of LTA samples based on XRD Siroquant analyses (wt. %)

Phases	LTA- A	LTA-B	LTA-C	LTA-D
Quartz	4.6	20.3	15.2	1.8
Kaolinite	79.2	47.3	63.7	93.5
Mica		2.7		
Illite		2.8	1.5	
Calcite		1.4		
Dolomite	2.7	7.6	1.0	
Pyrite	2.1	2.1	1.5	
Goyazite	0.9	1.4		
Bassanite		1.8		
Ash content	48.7	31.6	77.9	24.1

Finely distributed clay minerals of particle size below 2 µm were further interpreted by using oriented-aggregate XRD analysis. The results in Table 6-10 identified kaolinite as the major clay mineral in all LTAs, with concentrations ranging from 90-97 wt. %. Minor quantities of illite were present in LTAs C and D. The expandable mixed layer clays of irregular illite/smectite were identified in all LTA samples, with a high proportion of the clays reported for LTA-B (Table 6-10).

Table 6-10: Clay mineralogy of fractions less than 2 µm from oriented aggregate XRD analysis of low temperature ash samples

Sample name	Kaolinite (wt.%)	Illite (wt.%)	Expandable clays (wt.%)	Nature of expendable clays
LTA-A	96	0	4	Irregular illite/smectite
LTA-B	90	0	10	Irregular illite/smectite
LTA-C	91	6	3	Irregular illite/smectite
LTA-D	97	2	2	Irregular illite/smectite

Quartz is the second most abundant mineral found in LTAs, with LTA-B constituting the highest concentration (20 wt.%) of quartz. Comparing XRD result of raw and LTA samples, it was observed that there was a strong correlation between major minerals, particularly kaolinite and quartz. However, there was a deviation in the reporting of minor minerals. The concentrations of minor minerals reported by XRD analysis of raw coal were generally higher than the concentrations reported by XRD analysis of LTA samples. As a result, only the correlation between major minerals in raw and LTA samples was considered.

The results in Figure 6-19 show a good linear correlation coefficient (R^2 = 0.98) between major minerals (i.e. kaolinite and quartz) found in the raw coals and their derivative LTAs. The correlation is a good indication of the reporting of major mineral matter found in coals.

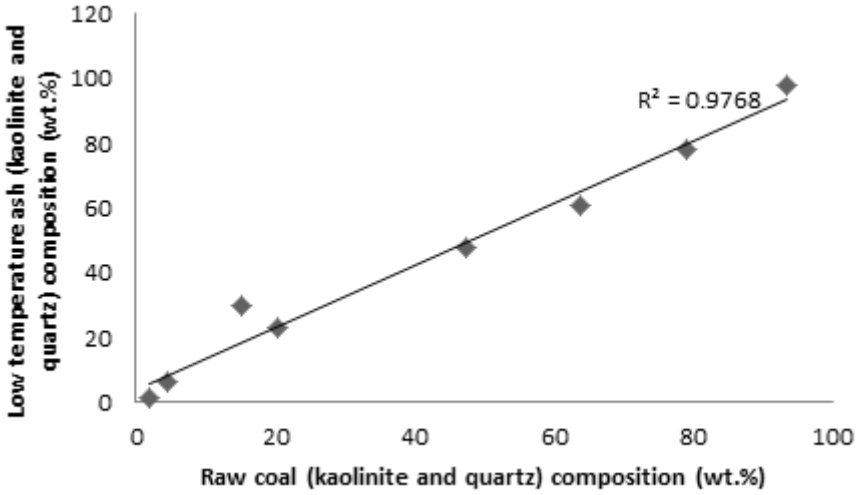

Figure 6-19: Correlation between kaolinite and quartz in raw coal and LTAs determined by XRD

Mineral matter present in minor quantities includes minerals such as dolomite, mica, illite, calcite, pyrite, goyazite, and bassanite. Goyazite ($SrAl_3(PO_4)(PO_3OH)(OH_6)$) was identified in LTA-A (0.9 wt.%) and LTA-B (1.4 wt.%), whilst bassanite ($2CaSO_4.H_2O$) was reported in LTA-B.

It has been reported previously that bassanite is a common artefact mineral that forms during LTA, due to the reaction between the organically bound sulphur and calcium [Ward, 2002], or due to the interaction between calcite and pyrite [Ward, 1989]. Another possible explanation for the formation of bassanite was proposed by Pearson and Kwong (1979) who suggested that bassanite was formed as a result of hydration of the ferrous sulphate product.

The dominant carbonate mineral identified in LTAs A, B, and C is dolomite. Calcite was identified in LTA-B, whilst pyrite was identified in LTAs A, B, and C. These results are consistent with reports by Vassilev *et al.* (2010), which suggests that dolomite is quite prominent in South African coals. Based on petrographic and XRD analyses of raw coals and LTAs, it is evident that coal B had significant amount of calcium that contributed to the reduction of AFT. These results are also confirmed by the ash chemistry inferred by XRD analyses of LTAs in Table 6-11.

Considerable differences exist in the ash chemistry results obtained from XRF analysis and those inferred by XRD Siroquant data. From the analysis, it can be seen that compositions reported by XRF are seemingly lower compared to results inferred by XRD. Nonetheless, it is important to note that the ash chemistry inferred by XRD methods allow for loss of hydroxyl groups from clay minerals, CO_2 given off during the decomposition of carbonate minerals, and the transformation of pyrite [Matjie *et al.,* 2016], which can bring about the difference in results.

Table 6-11: Inferred ash chemistry based on Siroquant data

Samples	LTA-A	LTA-B	LTA- C	LTA-D
SiO_2	54.89	59.73	61.91	55.29
Al_2O_3	40.52	28.86	34.93	44.35
Fe_2O_3	1.62	1.61	1.12	0.00
MgO	0.80	2.04	0.42	0.05
CaO	1.17	4.66	0.46	0.03
Na_2O	0.09	0.10	0.13	0.04
K_2O	0.56	1.31	1.03	0.24
P_2O_5	0.35	0.55	0.00	0.00
SO_3	0.00	1.14	0.00	0.00
Total	**100.00**	**100.00**	**100.00**	**100.00**

The results of ash composition determined by XRD are presented in Table 6-9. The results were correlated with ash composition determined by proximate analyses method using statistical tool in Microsoft Excel. Figure 6-20 shows a strong correlation between ash compositions determined by XRD and proximate analyses. From the results, it can be seen that there is a linear correlation coefficient of 0.98. From these analyses, it is noted that although the results are slightly different, there is an overall correlation between ash compositions determined by proximate analyses, petrography, and XRD. It seems most likely that there is a good agreement in results mainly because the analysis is on a bulk scale. Although bulk analysis considers the whole sample as a uniform unit, it is also noted that variations in reporting of results become apparent when coals are probed on a smaller scale.

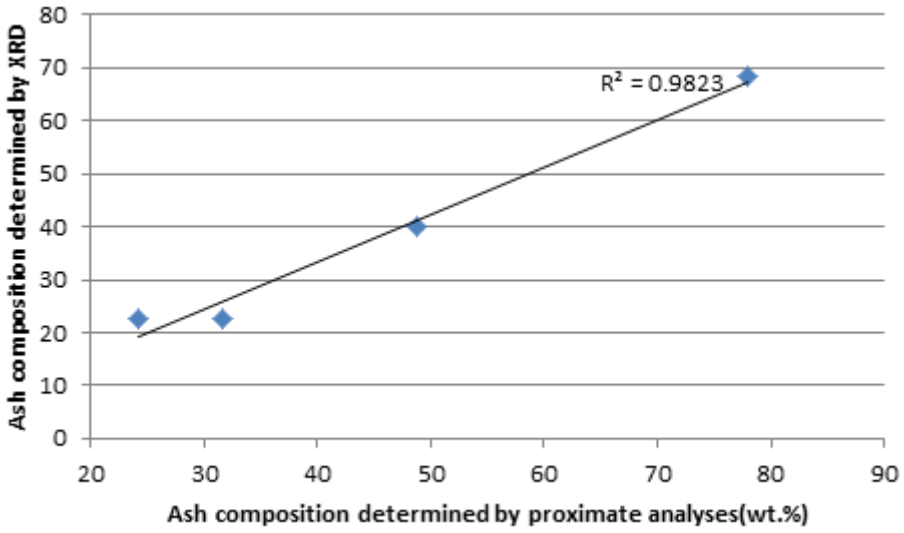

Figure 6-20: Correlation between ash compositions determined by XRD and proximate analyses

6.9.3 X-ray diffraction (XRD) analyses of high temperature ashes

The mineral matter in HTA samples identified by XRD included quartz, hematite, anhydrite, anatase, brookite, rutile and zircon as high temperature phases that formed at 815°C in air. The compositions of the different minerals are summarised in Table 6-12, and illustrated in Figure 6-21. The diffractograph of the different HTA samples are presented in Appendix F.

Table 6-12: X-ray diffraction (XRD) phases of high temperature ashes

Phases (wt. %)	HTA- A	HTA-B	HTA-C	HTA-D
Quartz	59.5	40.4	87.8	50.0
Hematite	6.9	19.0	6.6	11.4
Anhydrite	30.3	31.4	2.0	3.9
Anatase		0.5	1.6	14.8
Brookite	1.7	2.2	0.5	9.1
Rutile	0.4	1.1	ND	10.2
Zircon	1.1	4.6	1.5	0.6
Degree of crystallinity	51.0	34.0	64.0	22.7

The results show that quartz is the most dominant mineral in HTAs, with concentrations ranging from 40.4 wt. %. to 87.8 wt. %. Quartz is inert and therefore remains stable without undergoing phase changes at temperatures below 1000°C. Other dominant high temperature

phases formed included hematite and anhydrite. HTA-A and HTA-B constituted the highest amount of anhydrite, reported at 30.3 wt. % and 31.4 wt. % respectively.

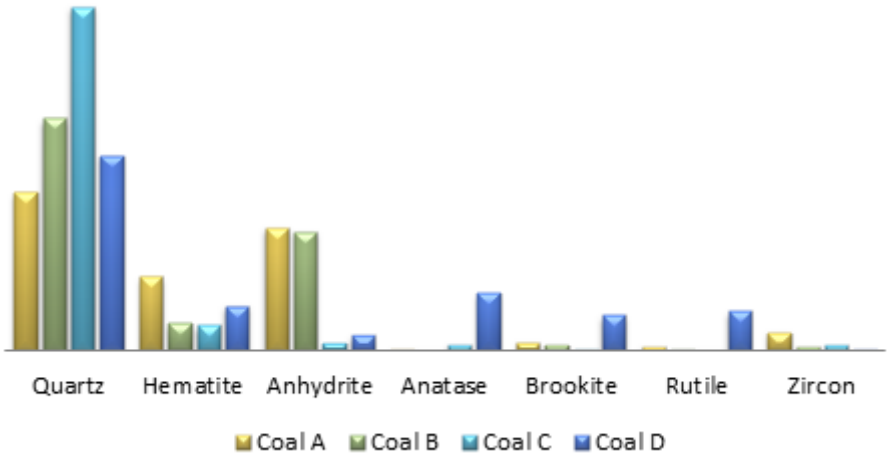

Figure 6-21: HTA XRD of the different high temperature minerals formed at 815°C

Anhydrite is a high temperature phase mineral, formed at high temperatures due to dehydration of gypsum, crystallization of pore water, and reaction between calcium and sulphur. The source of sulphur can be from organic matter, pyrite, or jarosite, whilst the source of Ca can be from carbonate minerals such as calcite, dolomite, ankerite, and fluorapatite [Vassilev *et al.*, 2003]. Dolomite was the main carbonate mineral identified in Coals A and B, and to a lesser extent calcite and aragonite (Table 6-8 and Table 6-9). The mode of occurrence of carbonates, particularly in Coal B is siderite growth, indicating the authigenetic nature of carbonates in the sample.

Pearson and Kwong (1979) proposed that anhydrite and hematite formed due to the oxidation reaction between FeS_2 and $CaCO_3$, as indicated by Equation 6-6.

$$4FeS_2 + 8CaCO_3 + 15O_2 \rightarrow 2Fe_2O_3 + 8CaSO_4 + 8CO_2 \qquad Equation\ 6-6$$

Kostakis (2011) described the formation of anhydrite as a reaction between CaO which is liberated when carbonate minerals decompose, forming gaseous phase (SO_2 and O_2) as indicated in Equation 6-7.

$$CaO + SO_2 + \frac{1}{2}O_2 \rightarrow CaSO_4 \qquad Equation\ 6-7$$

Hematite was identified as one of the major HTA minerals. Hematite is an oxidation product that is formed at high temperatures following the reaction between pyrite and oxygen, as indicated in Equation 6-8.

$$2FeS_2 + \frac{1}{2}O_2 \leftrightarrow Fe_2O_3 + 2SO_2 \qquad Equation\ 6-8$$

Pyrite is the common source of Fe that transforms into an amorphous Fe-containing glass and hematite in bottom ash produced in gasifiers (Waanders and Bunt, 2007). Petrographic and XRD analyses identified pyrite as the main source of Fe in raw coals; hence it is considered that iron bearing minerals in HTA are derivatives of pyrite.

The Fe-rich minerals in their Fe^{2+} state, and Ca-rich minerals interact at high temperatures and form low melting eutectic mixtures of temperatures of about 700°C, which lowers AFT [Han-xu, *et al.,* 2008; Kostakis, 2011; Van Dyk *et al.,* 2009]. Coal ashes with higher anhydrite content typically have lower AFT [Han-xu *et al.,* 2008]. Although the concentration difference between HTA-A, and HTA-B is marginal, it can be suggested that anhydrite identified in HTA-B had an effect on AFT results of the investigated coals.

The high concentration of hematite in HTA-B is also an indication that Fe lowered the AFT of the coal, as it was discussed previously. The HTA XRD results confirm conclusions drawn from slagging indices and thermodynamic modelling.

The amorphous phase in HTAs was due to partial dehydroxylation and decomposition of clay minerals such as kaolinite, forming poorly crystalline products [Vassilev *et al.*, 2003]. From the results, it was observed that an increase in ash content resulted with an increase in the degree of crystallinity. A strong correlation with regression of 0.88 was determined between ash composition and degree of crystallinity, as depicted in Figure 6-22.

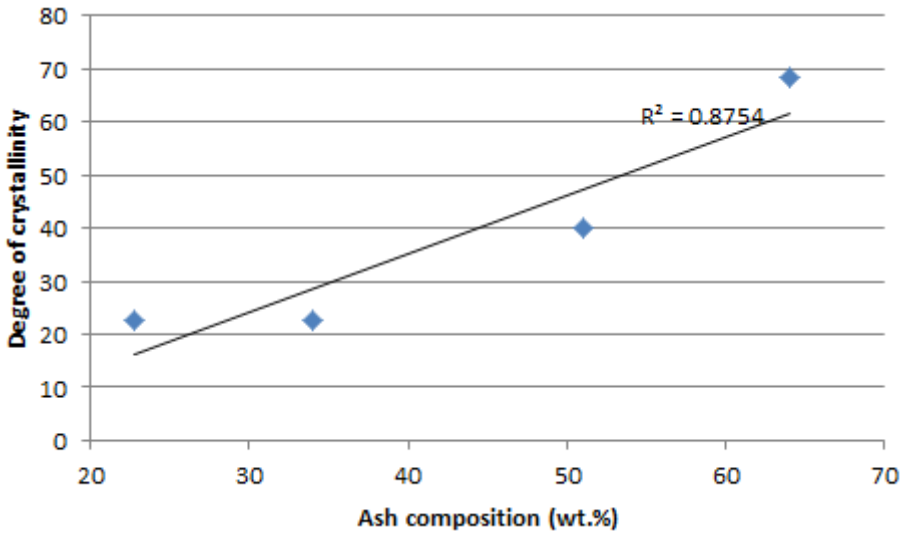

Figure 6-22: Correlation between degree of crystallinity and ash content

Rutile, anatase and brookite are minor elements in HTA, with high concentrations of the three polymorphs reported in HTA-D. As observed in XRD analyses of raw coals and LTAs, coal D had a high concentration of anatase. The formation of other phases such as rutile and brookite could be due to phase transformation of anatase to brookite. Comparing the composition of raw coals and HTA, it is noticeable that distinct phase transformation took place between mineral matter in raw coals and HTA samples.

6.9.4 Fourier Transform Infra-Red (FTIR) analyses of raw coals

The Fourier Transform Infra-Red spectroscopy (FTIR) was used to determine the structural composition of the raw coals. The FTIR spectra in the transmittance mode were collected over the mid-infrared (MIR) region (500-4000 cm^{-1}). Figure 6-23 depicts the typical spectrum that was obtained and observed for all the raw coals studied. The individual spectra for specific coals are presented in Appendix G. The infrared spectra observed were compared to data available in literature. The study by Saikai and Parthasarathy (2010) was conducted on clay mineral from Assam and Meghalaya, India, using both XRF and FTIR spectroscopy, and the work was used for attentive assignment of clay minerals found in coal samples. From the FTIR spectra in Figure 6-23, the OH vibrations typical found in kaolinite clays were identified, confirming the presence of kaolinite in coals.

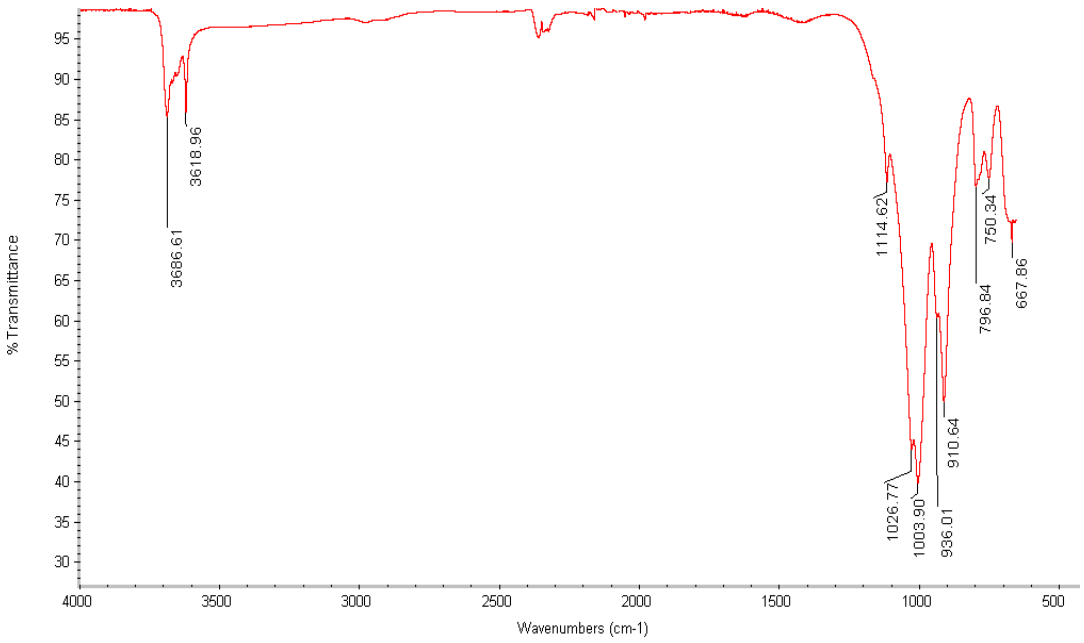

Figure 6-23: FTIR spectrum of kaolinite in raw coal A within the 500-4000 cm^{-1} spectral region

The results were also confirmed by fitting the kaolinite spectrum from the in-built spectral library of inorganic minerals. A list of peaks and their assignment are shown in Table 6-13.

Table 6-13: A summary of FTIR band position (cm^{-1}) identified in raw coals and theoretical kaolinite and muscovite [Saikai and Parthasarathy, 2010].

Theoretical kaolinite	Coal A	Coal B	Coal C	Coal D	Assignment
3670-56	3686	3687	3687	3686	Al---O-H
3645	3618	3619	3619	3618	OH stretching crystalline hydroxyl
1117-05	1115	1114	1115	1115	----------
1035-30	----------	----------	----------	----------	----------
Muscovite and quartz	1025	1026	1026	1026	Si-O stretching
1019-05	1004	1005	1003	1000	Si-O stretching
936	936	----------	936	----------	----------
918-09	910	912	910	910	OH deformation linked to Al^{3+} Mg^{2+}
800-784	788	797	796	788	
----------	749	750	750	750	----------
700-686	667	668	668	667	Si-O-Si bending
----------	658	660	659	----------	Si-O-Si bending

The FTIR peaks within the 500-1100 cm^{-1} spectral range and the doublet at 3695 cm^{-1} and 3620 cm^{-1} were assigned to clay minerals. A typical structure of kaolinite $Al_2Si_2O_5(OH)_4$ is described by four adsorption bands in the OH stretching region (3200-3800 cm^{-1}), with the bands positioned at 3695, 3670, 3650 and 3620 cm^{-1} [Vaculikova *et al.,* 2011].

Kaolinite in coals has two forms of crystallinity, the low crystalline detrital kaolinite and a highly crystalline neomorphic kaolinite. The highly crystalline kaolinite form due to in-situ leaching and re-precipitation processes that generally take place in peat swamps [Ward, 1989]. The interactions between precipitated alumina and silica in solution resulted in the formation of authigenetic and well-ordered kaolinite mineral [Ward, 2002].

O'Gorman and Walker (1971), assigned the characteristic bands at 3691 cm^{-1} and 3619 cm^{-1} to a crystalline form of kaolinite, whilst the two weak, out of phase vibrations at 3651 cm^{-1} and 3670 cm^{-1} were assigned to the poorly crystalline kaolinite [Farmer, 2000; O'Gorman and Walker, 1971].

The adsorption band at 3618 cm^{-1} is assigned to the inner hydroxyl, corresponding to H_2O vibrations and indicates the presence of water of crystallisation in clay minerals [Saikia and Parthasarathy, 2010]. The inner hydroxyl group is due to the bonding between a proton and oxygen that is also coordinated to Al^{3+} in an octahedral site [Kiros *et al.,* 2013]. Therefore, the results suggests that peaks observed at 3685 ± 1 cm^{-1} and 3617 ± 2 cm^{-1}, assigned to the OH stretching bonds are an indication of a crystalline kaolinite.

The peaks at 936 cm^{-1} and 910 ± 2 cm^{-1} wavenumbers are assigned to the OH deformation bands. The peak at 936 cm^{-1} was only identified in coals A and C. The presence of clays influences the increase of adsorption of OH bending at 910 cm^{-1} and the OH stretching band at 3695 cm^{-1}. However, reports have shown that the effect of clay minerals is most significant at the 910 cm^{-1} absorption band [Vaculikova *et al.,* 2011]. The Si-O stretching bands were assigned to peaks at 788, 795 and 796 cm^{-1}, and the Si-O deformation bands were assigned to peaks at 1000 ± 5 cm^{-1}. The peaks at 910 cm^{-1} and 1005 cm^{-1} could also be assigned to nacrite ($Al_2Si_2O_5(OH)_4$, a polymorph of kaolinite, because the peak assignment is similar to that of kaolinite [Russell, 1987].

The challenge presented by the FTIR technique was the overlap of adsorption bands between illite and smectite clays, which made it difficult to acquire well-defined peaks. Overlap between different clay minerals were observed in the investigation by Ekosse (2005). In the study, the overlap observed was due to the interference between smectite and muscovite at 797 cm^{-1} and 799 cm^{-1} adsorption bands, respectively. Based on findings by Ekosse (2005), it is possible to confirm the presence of smectite and muscovite minerals identified in coals B and C.

The absorption band at 1026 cm^{-1} was attributed to the presence of muscovite and quartz in the clay minerals, with quartz interference observed at 785-820 cm^{-1}. The characteristic feature of quartz is a doublet centred at 796 and 778 cm^{-1} [Ramasamy and Suresh, 2009]. Therefore, the υ (Si-O-Si) and the δ (Si-O) bands confirm the presence of quartz in coals [Nayak and Singh, 2007]. The interference of quartz and clay minerals indicates the association of the two minerals, thus confirming petrographic observation made about the association of clay minerals and quartz.

The major clay mineral was confirmed to be kaolinite. The FTIR spectrum of kaolinite was in good agreement with peak positions observed by Saikai and Parthasarathy (2010), except for a few peaks which could not be assigned in the investigation. Vibrational spectroscopy analyses provided useful information about the hydration characteristics, interlayer cations, moisture content in clays, and structural differences between clay minerals.

It was observed that clay minerals were also comprised of mixed layers of illite-smectite, muscovite and quartz, confirming XRD results of LTA samples. However, FTIR spectroscopy is not too popular in identifying mineral matter in coals, mainly due to the overlap of adsorption bands, and because few mineral matter compounds can be identified by the technique [Ritz and Klika, 2010].

Although FTIR can be mineral specific, subsequently placing a limitation to its application, it is observed that the technique has value in studying clay mineral composition. The technique can readily identify clay minerals relatively easy and faster compared to XRD analyses.

6.9.5 Fourier Transform Infra-Red (FTIR) analyses of low and high temperature ashes

A number of spectra were collected for the different coal ashes, and the spectra can be found in Appendix G. There was no distinct difference between FTIR spectra of raw coals and LTAs. Since similar spectra were obtained for raw and LTA samples, it was concluded that the minerals identified in raw coals were the same as minerals found in LTAs. These results further highlighted the fact that the presence of organic matter did not have any effect on the results. Therefore, it is not critical to perform ashing for FTIR analyses on coals because the technique can easily characterise both the amorphous and crystalline phases.

A representative spectrum of HTA sample is presented in Figure 6-24. The inbuilt spectral library was used to help identify the mineral matter in high temperature ashes. When comparing LTA spectra to HTA spectra, it was observed that significant changes in the coal mineral structures took place. The transformation of kaolinite could be noted and confirmed by the disappearance of the 3686 cm^{-1} and 3618 cm^{-1} peaks that were identified in raw coals and LTA samples. As discussed earlier, the peaks at 3686 cm^{-1} and 3618 cm^{-1} represented water of crystallisation in the clay minerals.

Other significant peaks in the frequency range 1000 cm^{-1} to 1200 cm^{-1}, that were attributed to silicate minerals, could not be identified in FTIR spectra of HTA samples. Furthermore, there was a noteworthy change in peak intensity from LTA and HTA samples within the 2000 and 2300 cm^{-1} spectral range. The DTA and TG studies conducted by Vassilev *et al.* (1995) on LTA found that the loss of water of crystallisation occurs at 110°C, following an exothermic reaction. Therefore, high temperature ashing resulted in new high temperature phases forming, and these phases were identified and confirmed by the appearance of new peaks on the FTIR spectra.

From the spectrum presented in Figure 6-24, it can be observed that the abundant mineral in HTAs is quartz, mainly because quartz remained unaltered at high temperatures, once again confirming the XRD results. The characteristic peaks of quartz are identified at 1091 cm^{-1} and 796 cm^{-1} peak positions, with a doublet peak at positions 778 and 796 cm^{-1}. The peaks are assigned to Si-O symmetrical stretching bands [Han-xu *et al.*, 2008]. The shoulder peak at 694 cm^{-1} is assigned to the Si-O bending vibrations, and the peak at 1082 cm^{-1} is due to asymmetric stretching due to the replacement of Al for Si [Buzgar *et al.*, 2013].

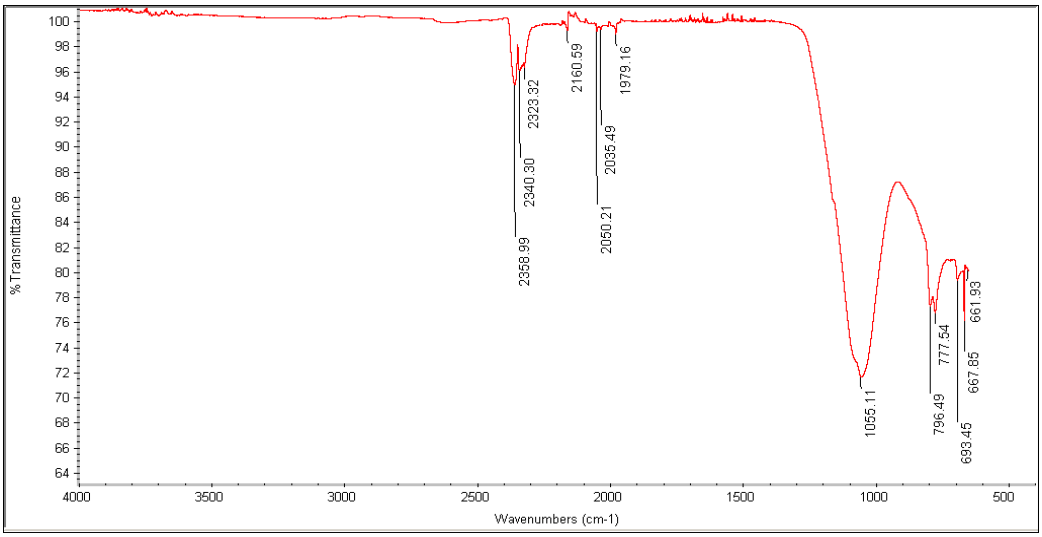

Figure 6-24: FTIR spectrum of high temperature ash of HTA-B

The FTIR spectrum of HTA-D, presented in Figure 6-25, shows an additional peak at 1091 cm^{-1}. Studies by Jin *et al.* (2009) assigned the peaks at 1090 and 790 cm^{-1} to mullite. This suggests that the dehydroxylation of kaolinite at temperatures above 550°C led to the formation of a stable, high temperature phase mullite and the amorphous glassy (SiO_2) phase.

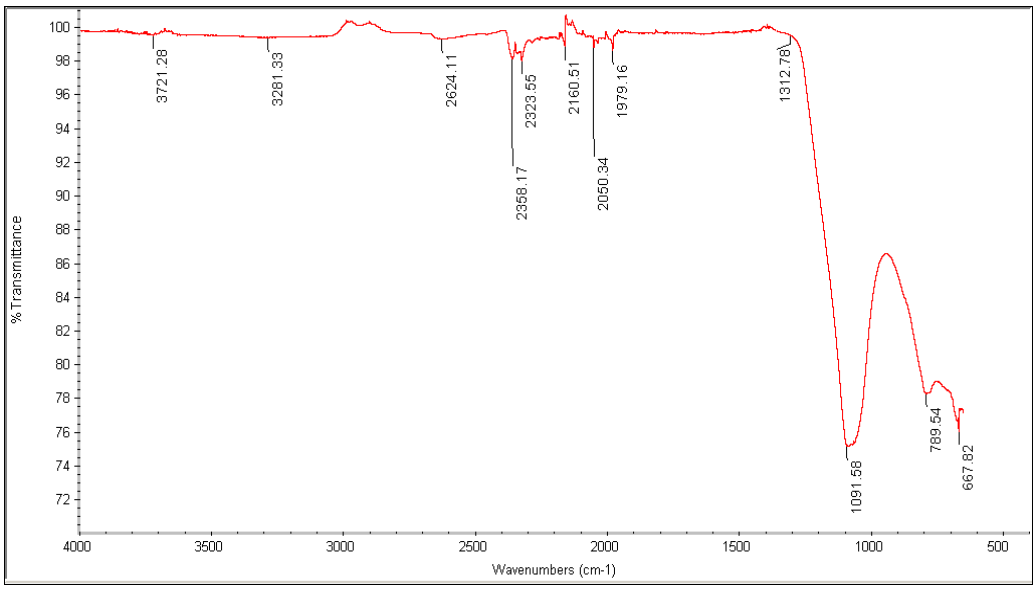

Figure 6-25: FTIR spectrum of high temperature ash of HTA-D

The formation of mullite could be as a result of Al_2O_3 reacting with SiO_2, following the reactions described in Equations 6-9 and 6-10 [Van Dyk *et al.*, 2009].

$$3(Al_2O_3 2SiO_2 2H_2O) \rightarrow 3(Al_2O_3 2SiO_2) + 6H_2O \quad ---------- Equation\ 6-9$$

$$3(Al_2O_3 2SiO_2 2H_2O) \rightarrow Al_6O_5(SiO_4)2 + 6H_2O \quad ---------- Equation\ 6-10$$

It is important to note that technological challenges such as sintering are initiated as a result of crystallization of anorthite and mullite [Matjie *et al.*, 2009; Van Dyk *et al.*, 2009]. The thermodynamic modelling using FactSage 7.0 predicted the formation of mullite at high temperatures, and from the analysis, it was apparent that the mullite phase contributed to slag formation at high temperatures.

6.9.6 Micro-Raman spectroscopy (mRs) analyses of raw coals

Micro-Raman spectroscopy (mRs), similar to FTIR and XRD analyses, is a structure specific analytical tool commonly used to characterise macerals in coals, with capabilities to detect changes in structural order. Correlation studies of Raman spectra and Raman parameters with carbon structures have been extensively explored. These studies related the first-order (G-bands) and second- order (D-bands) shifts with the degree of coalification or graphitisation in coals [Guedes *et al.*, 2010].

Although the technique has been widely used to characterise various inorganic minerals in other areas of research, the technique is not popular in characterising mineral matter in coals. The first published data on mineral matter in coals was reported by Green *et al.* (1983). Since then there has been random efforts to characterise mineral matter using mRs techniques.

This section presents results of mRs analyses of mineral matter in raw coals acquired from the SENTERRA instrument. Characterisation of the different mineral matter was performed by analysing 100 individual particles under the microscope at room temperature, within a spectral range of 100-1500 cm^{-1}. The various spectra were collected by varying instrument parameters, which included a variation of laser power and the exposure time. Only a few selected representative spectra are presented in this section. Major mineral matter identified in raw coals using mRs included oxides, sulphides, and carbonates.

Although kaolinite was the dominant mineral observed from previously discussed techniques such as ash chemistry, petrography, FTIR and XRD techniques, it proved difficult to identify clay minerals using mRs, due to the fluorescence nature of the clay minerals. According to findings and observations by Manoj and Kunjomana (2010), the clay minerals are more IR active and Raman inactive.

The challenge to identify clay minerals could also be attributed to the association of clays with organic matter, as a result, the mRs was not successful in identifying clays and hence, the discussion pertaining to clay minerals is excluded. Only sulphides, oxides, and sulphates are discussed in the subsequent sections.

6.9.6.1 Raman spectra of sulphides

The most common sulphide in SA coals is present in the form of iron-sulphide. The two polymorphs of iron sulphides commonly found in coals are pyrite and marcasite. However, because of the sensitive nature of the instrument, mRs can easily discriminate between the different polymorphs based on their characteristic bands.

Since sulphide minerals are good Raman scatters, it is therefore easy to characterise the minerals using the technique. From the investigation, it was observed that the Raman spectra of pyrite were dependent on the amount of power (energy intensity) illuminated on the pyrite particle. Generally, more than 50% of the power was used to acquire a good Raman spectrum without degrading the sample. The typical spectrum of the pyrite mineral acquired from coal samples is shown in Figure 6-26 (a). The spectrum shows the three characteristics peaks of an anisotropic pyrite structure. The assignment of the pyrite peaks is in accordance to the work by Mernagh and Trudu (1993), with major peaks displayed at 341 cm^{-1} and 374 cm^{-1} and a minor peak at 424 cm^{-1}.

The peak at 341 cm^{-1} was assigned to the E_g mode, the peak at 374 cm^{-1} was assigned to the A_g mode, whilst the peak at 424 cm^{-1} was assigned to the T_g mode. There was a slight shift in wavenumber of the reported spectra when compared to work reported by other researchers [Mernagh and Trudu, 1993; Voght *et al.*, 1983]. The shift in peak position could be attributed to the parameters such as laser power that were used in the investigation.

The mRs technique is quite sensitive to the presence of any structural impurities, and this was specifically observed with the Raman spectra depicted in Figure 6-26 (b). The spectrum showed that in addition to the major peaks commonly found in a pyritic structure, there was an additional sharp peak at 215 cm^{-1} and a broad peak at 278 cm^{-1}. According to the work by Mernagh and Trudu (1993), the additional peaks were attributed to the probable presence of elemental sulphur.

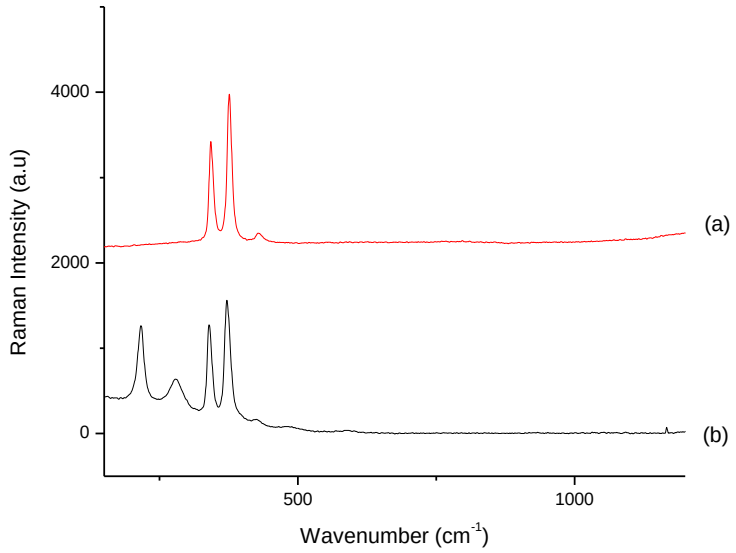

Figure 6-26: Raman spectra of sulphide minerals found in coal B in the wavenumber range 50-1500 cm^{-1} (Micro Raman, excitation 532 nm)

Over and above the three forms of sulphur (organic, pyritic, and sulphate) commonly found in coals, there is the fourth form of sulphur referred to as elemental sulphur. This fourth form of sulphur was first identified by Chatterjee (1942) in weathered Indian coals. The findings were validated by Richard *et al.* (1977), and later by White and Lee (1980). The analytical technique adopted to determine elemental sulphur was gas chromatography. However, it was highlighted that the detection limits of the technique presented challenges in terms of accurately detecting elemental sulphur in coals.

As a result, other techniques such as the electron capture detectors, sulphur selective flame photometric detectors and later the Hall electrolytic conductivity detectors, with better and improved sensitivity were used to characterise elemental sulphur [Ehrlich *et al.*, 1981].

Duran *et al.* (1986) found that the composition of elemental sulphur in samples provided by Illinois State Geological Survey, as determined by gas chromatography, was relatively high, at 5%, and suggested the sulphur in the coal was introduced after the coalification process, when the coals were exposed to air. Studies by Beyer *et al.* (1987) suggested microbial oxidation of pyrite lead to the production of ferric sulphate [$Fe_2 (SO_4)_3$], and the reaction between ferric ions and pyrite lead to the formation of elemental sulphur, as described by the reaction proposed in Equation 6-11.

$$2Fe^{3+} + FeS_2 \rightarrow 3Fe^{2+} + 2S \quad ---------- Equation\ 6-11$$

Findings by Stock and Wolny (1990) indicated that there was a direct relationship between elemental sulphur content and extend of weathering. The findings showed that an increase in the time of weathering led to an increase in the amount of sulphur content. Therefore, the study concluded that elemental sulphur was a by-product of pyrite weathering.

It is plausible that the two peaks observed in coal B (Figure 6-26 (b)) could be attributed to elemental sulphur, or possibly arsenopyrite. The detection of elemental sulphur is of significance and valuable insight in this regard, since previous studies have proved it is difficult to detect elemental sulphur. It is suggested that the possible association of pyrite with elemental sulphur in this study could be due to the weathering of pyrite, therefore agreeing with conclusions made by Stock and Wolny (1990). Other polymorphs of pyrite present in coals are marcasite and pyrrhotite. However, both marcasite and pyrrhotite are rarely found in SA coals.

6.9.6.2 Raman spectra of oxides

Coal in its as received state may contains different oxide minerals. The most common oxide found in coal is quartz. Other minerals present in minor quantities include minerals such as hematite, cristobalite, corundum, ilminite, chromite, rutile, anatase and brookite. The three main oxides identified in raw coals by the mRs technique included quartz, rutile, and anatase.

(i) Raman spectra of quartz

As noted previously in petrographic studies, the quartz found in coals was of a detrital origin, and associated with either inertodetrinite or kaolinite. Quartz was identified as the second most abundant mineral matter found in most coals as discussed and confirmed by ash chemistry analyses, petrography, FTIR and XRD.

The Raman spectrum of quartz in coal samples is presented in Figure 6-27. Although quartz is characterised by four A_1 symmetry Raman peaks [Denisov *et al.*, 1986] at 207, 356, 464, and 1085 cm^{-1} [Scott and Porto, 1967], only one peak at 462 cm^{-1} was observed. Other characteristic peaks were not resolved on the acquired spectrum. The peak at 462 cm^{-1} is characteristic of α-quartz, and the peak was assigned to the Si-O-Si stretching-bending A_1 mode [Kingma and Hemley, 1994]. Similar results are reported by Yin *et al.*, 2017, whereby quartz was identified in coal ashes. Accordingly, the mRs results confirmed the structure of the quartz in the investigated samples as an α-quartz, of authigenetic origin.

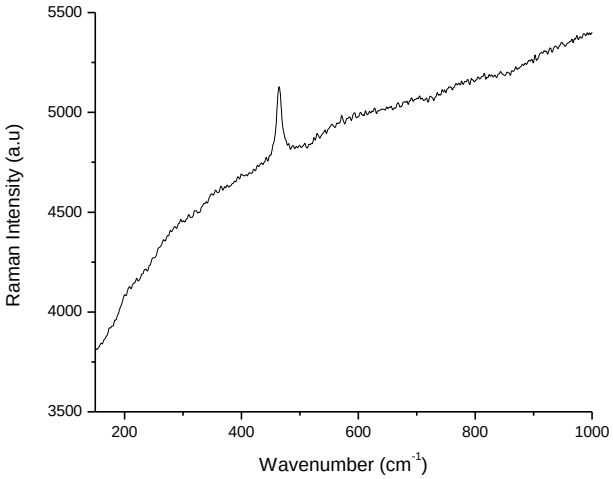

Figure 6-27: Raman spectra of quartz as observed using the 532 nm wavelength in the range 500-1500 cm^{-1} (micro-Raman, excitation 532 nm)

(ii) Raman spectra of anatase and rutile (TiO_2)

The three polymorphs of $TiO_{2:}$ rutile, anatase, and brookite, all have similar chemical composition, but different crystallographic structures. Rutile and anatase have a tetragonal structure, while brookite has an orthorhombic crystal structure. Rutile is considered the most stable form of TiO_2, whereas anatase and brookite are the metastable phases, which transform to form rutile.

Figures 6-28 (a) and (b) represent the acquired Raman spectra of anatase and rutile respectively. The micrograph on the right shows the dissemination of small bright particles of anatase in coal C. The two spectra show the different fingerprints of the two polymorphs and show how easily they can be discriminated, arguably without significant difficulties by the mRs technique.

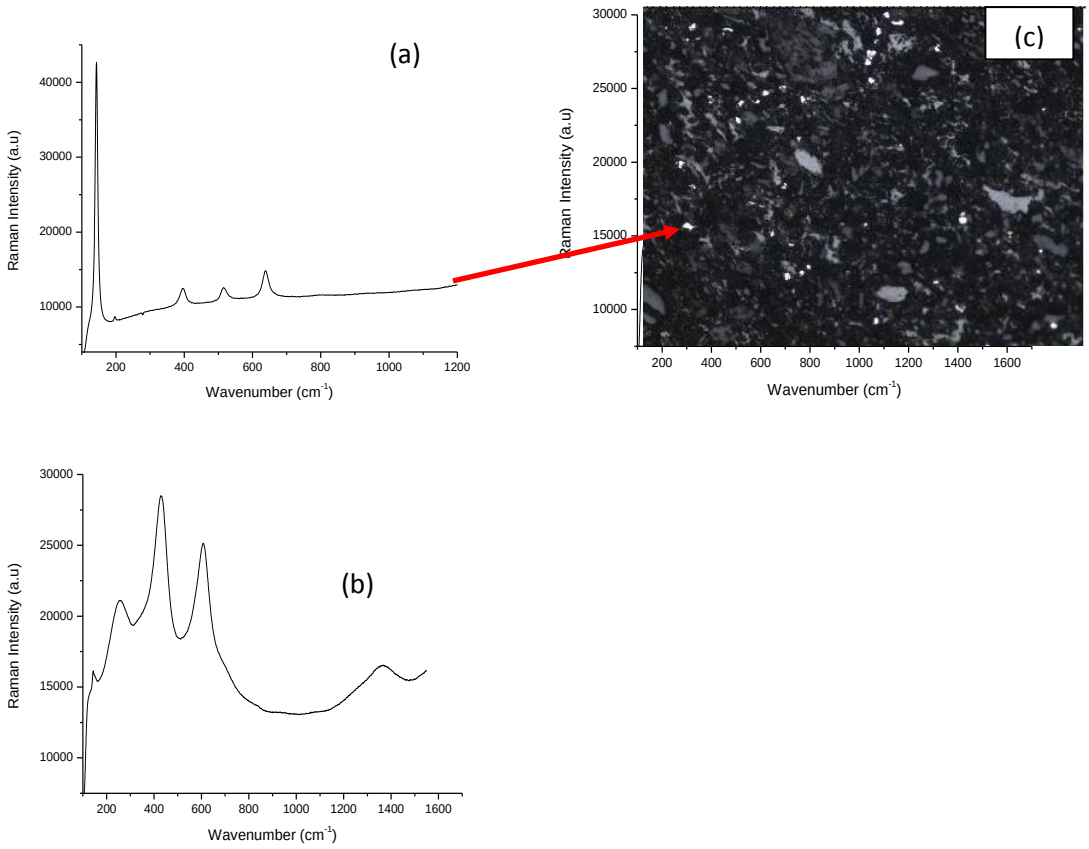

Figure 6-28: (a)Raman spectra of anatase (top) and (b) rutile (bottom) found in coal sample C in the wavenumber range 50-1500 cm^{-1} (Micro Raman, excitation 532 nm), (c) White anatase particles disseminated in coal A

According to the factor group analysis ($D_{4h}(I4_1/amd)$, anatase consists of six Raman active modes (A_{1g}, $2B_{1g}$ and $3E_g$), and three infrared active modes (A_{1u} and $2E_u$). The characteristic peaks of the Raman active modes of anatase are positioned at 144 cm^{-1} (E_g), 197 cm^{-1} (E_g), 399 cm^{-1} (B_{1g}), 519 cm^{-1} (A_{1g} and B_{1g}), and 639 cm^{-1} (E_g) in the first order Raman spectrum of TiO_2 single crystal [Memon *et al.*, 2013; Ohsaka *et al.*, 1979]. The rutile single crystal is comprised of four Raman active modes (A_{1g}, B_{1g}, B_{2g}, and E_g) [Ohsaka *et al.*, 1979]. The active modes of rutile were measured by Porto *et al.* (1967) at 143 cm^{-1} (B_{1g}), 447 cm^{-1} (E_g), 612 cm^{-1} (A_{1g}), and 826 cm^{-1} (B_{2g}). The assignment of anatase identified in coals was compared to Raman peaks of pure anatase studied by Mahdjoub *et al.* (2010), with the peak list and assignment presented in Table 6-14.

From the comparison of pure anatase (TiO_2) and the Raman spectrum acquired from the coal sample it can be noted that the coal spectrum corresponds to the Raman active modes of anatase. Furthermore, from results presented in Table 6-14, it can be noted that the Raman spectrum of anatase closely matched the results reported by Yin *et al.* (2017).

Table 6-14: Peak position (cm^{-1}) of vibrational modes of pure anatase and mineral matter in coal ashes [Mahdjoub *et al.*, 2010; Yin *et al.*, 2017]

Peak position (cm^{-1}) [This work]	Yin *et al.*, 2017	Mahdjoub *et al.*, 2010	Relative intensity	Width	Assignment
143	146	144 (vs)	46427	9.38	E_g
197	199	197 (w)	632	5.70	E_g
----------		320 (vs)	----------	----------	C
397	396	399 (s)	3294	20.26	B_{1g}
516	516	515 (m)	2234	20.63	A_{1g}
639	640	639 (m)	4569	20.46	E_g
----------		795 (w)	----------	----------	B_{1g}

The Raman spectra of rutile was characterised by three main broad peaks positioned at 267 cm^{-1}, 412 cm^{-1} and 604 cm^{-1}, with the main peak positioned at 412 cm^{-1}, and minor peak positioned at 144 cm^{-1}. These peaks were assigned and compared to a single rutile crystal, and the results are presented in Table 6-15 [Arsov *et al.*, 1991].

Table 6-15: Assignment of rutile spectra obtained from coal samples

This work (cm^{-1})	**Arsov *et al.* (1991) (cm^{-1})**	**Assignment**
144	143	B_{1g}
267	236	
412	447	E_g
604	612	A_{1g}
	826	B_{2g}

Previous studies by Betsch *et al.* (1991) assigned the weak peak at 144 cm^{-1} to the B_{1g} mode. However, the broad peak at 267 cm^{-1} has a different peak position to other previously

reported work. Arsov *et al.* (1991) identified this peak at 236 cm^{-1}, which is a considerable shift when compared to the observation made on coals investigated in this study.

Porto *et al.* (1967) assigned the broad band at 250 cm^{-1} to be a second order phonon. The peak at 412 cm^{-1} was assigned to the E_g mode. The 826 cm^{-1} peak assigned to the B_{2g} mode from the study by Arsov *et al.* (1991) was not observed in the acquired spectrum of coals. Nonetheless, the Raman spectrum of rutile was somewhat comparable and in agreement to the assignment based on previous research. The study further elucidated that the broadening of the Raman peaks at high temperature showed that a kinetic transition took place in the coal samples.

6.9.7 Micro-Raman Spectroscopy (mRs) analyses of low temperature ashes

The two Fe-minerals (lepidocrocite (FeO(OH)) and coquimbite ($Fe_2(SO_4)_3.9H_2O$)) and a sulphate anhydrite ($CaSO_4$) are identified in LTA samples. Figure 6-29 shows the Raman spectra of minerals identified. The anhydrite in LTA-B confirms the bassinite identified by XRD analyses of LTA, as stated in section 6.9.2.

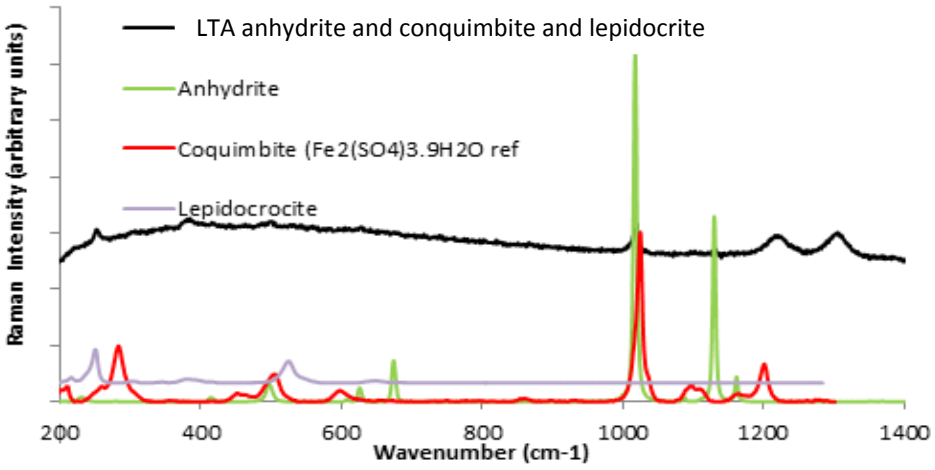

Figure 6-29: Raman spectra of LTA-B sample showing the presence of iron sulphate, iron hydroxide and calcium sulphate

The Raman peaks at 246 cm^{-1} and 520 cm^{-1} confirms the presence of lepidocrite (γ-FeO(OH)) in coal. According to a study by Hanesh (2009), the characteristic Raman peaks of lepidocrite can be found at 250, 348, 379, 528, and 650 cm^{-1}, with the most prominent peak identified at 246 cm^{-1} [Gehring and Hofmeister, 1994; Hanesch, 2009]. However, other peaks associated with lepidocrocite are not identified, probably because of the amorphous nature of coal, and the low laser power used to characterise the sample. The presence of carbon is indicated by the typical G band at 1311 cm^{-1}.

Although goethite (α-FeO(OH)) and γ-FeO(OH) have the same chemical formula and orthorhombic symmetry, their Raman spectra are different, thus making it easy to discriminate between the two minerals. The presence of γ-FeO(OH) is confirmed for the first time by mRs in LTA samples. The presence of γ-FeO(OH) mineral can be an indication of possible transformation of pyrite that took place in LTA samples.

Coquimbite is an iron sulphate mineral that is found as a secondary mineral in coals. The assignment of coquimbite in the LTA samples was based on the work by Frost *et al.* (2014). From the study, the peaks assigned to coquimbite are at 278 cm^{-1} and 1022 cm^{-1}. Frost *et al.* (2014) assigned the peak at 284 cm^{-1} as FeO stretching vibration, and the peak at 1025 cm^{-1} to SO_4^{2-} symmetric stretching mode. However, there is a slight shift with reference to the low frequency peak. The shift can be attributed to impurities and association between mineral matter and organic matter.

Generally coquimbite is not found in fresh coals, but in weathered and oxidised coal samples. The oxidation of pyrite mineral can form a number of sulphates such as coquimbite and jarosite which are responsible for AMD. Ward (2002) identified coquimbite as a possible

LTA artefact. The presence of coquimbite in this study could be due to the transformation of pyrite during low temperature ashing.

Based on the results obtained, it can be noted that pyrite mineral underwent a series of reactions and transformation during low temperature ashing. This transformation could only be observed from Raman analyses, and could not be identified by any of the analytical techniques discussed.

6.9.8 Micro-Raman Spectroscopy (mRs) analyses of high temperature ashes

This section presents results obtained from high temperature ashes prepared at 815°C.

6.9.8.1 Raman spectra of brookite (TiO_2)

The TiO_2 polymorph, brookite was first observed in high temperature ashes. The Raman spectrum of the polymorph is depicted in Figure 6-30. The work by Illiev *et al. (*2013) was used to assign the Raman peaks of brookite, with the respective Raman peaks tabulated in Table 6-16.

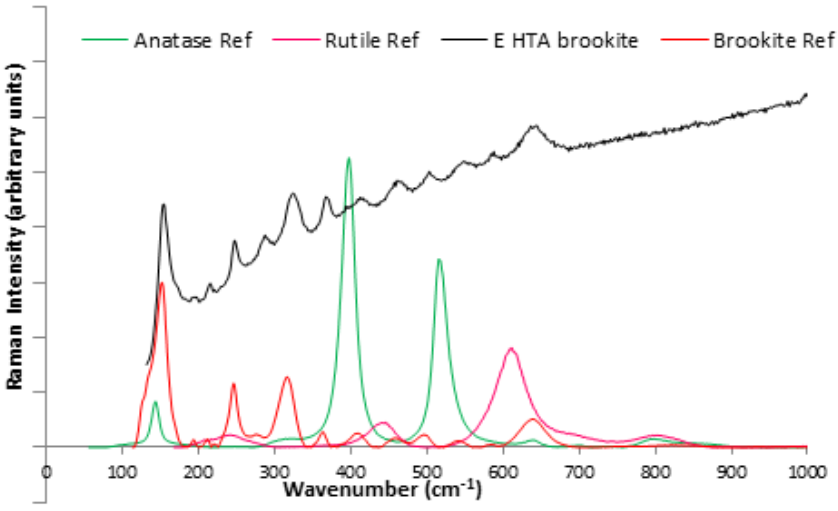

Figure 6-30: Raman spectra of a mixture of brookite, anatase, and rutile in HTA- D

Table 6-16: Raman peaks of brookite in HTA-D

This work	Illiev *et al.*, 2013	Assignment
157	152 (rutile, anatase)	A_{1g}
249	246 (brookite)	A_{1g}
286	Anatase	
321	324 (brookite)	A_{1g}
371		
411	412 (brookite)	A_{1g}
462	Quartz	
505	492 (brookite)	A_{1g}
545	545 (brookite)	A_{1g}
586		
646	640 (anatase)	A_{1g}

From the results presented in Table 6-16, it can be noted that the brookite Raman assignment by Illiev *et al.,* 2013 closely matches the Raman peaks in this study. Tompsett *et al.*, 1995 reported the seven A_{1g} mode of brookite at 125, 152, 194, 246, 412, and 640 cm^{-1}. In this study, additional Raman peaks were observed at 321 cm^{-1} and 545 cm^{-1}. These two additional modes are in agreement with findings by Illiev *et al.* (2013). The two peaks that were not assigned to TiO_2 polymorphs at 371 cm^{-1} and 586 cm^{-1} are attentively assigned to pyrite and apatite respectively. From the analyses, it is observed that rutile, anatase and brookite were in association with apatite, quartz and pyrite.

6.9.8.2 Raman spectra of chromite

Another mineral identified in HTA was chromite, with the Raman spectra depicted in Figure 6-31. Chromite ($FeCr_2O_4$) is an oxide mineral that belongs to the spinel group. Chromium is

one of the most toxic trace elements found in coals, particularly when it is in its hexavalent (Cr^{6+}) oxidation state. Therefore, the mode of occurrence of Cr and its valence state are important in combustion processes. It has been a challenge to establish the mode of occurrence of Cr. Nonetheless, several studies were able to determine the mode of occurrence of Cr using leaching methods.

Finkelman (1994) and Huggins *et al.* (2000) established that Cr is associated with both the organic and mineral matter. The association of Cr with mineral matter is with mineral groups such as clay, carbonates, oxides (hematite and chromite) and sulphides (pyrite) [Davidson, 2000], whilst in its elemental form, Cr is organically bound as Cr^{3+} in the coal structures.

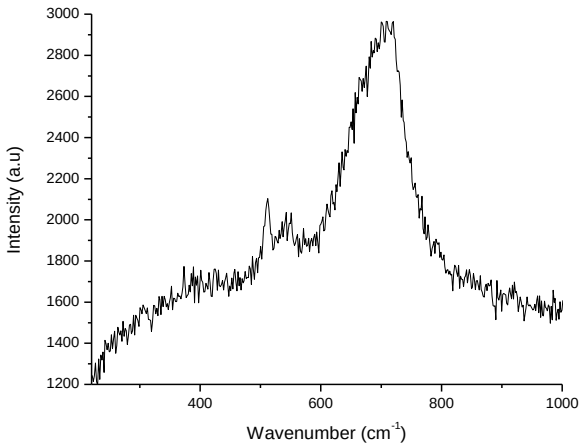

Figure 6-31: Raman spectra of chromite found in HTA-D

The prominent broad peaks at 700 cm^{-1} was assigned to the symmetric stretching vibration, (A_{1g}). The peak could be attributed to the presence of bonds of trivalent ions such as Cr^{3+}, Fe^{3+} and Al^{3+} with O_6 octahedral. The two minor peaks were assigned to F_{2g} and E_{2g} vibrational mode. It is deliberated that chromium in chromite is trivalent (Cr^{3+}) and associated with illite. These findings suggest that the deposits where the coals were formed contained Cr-bearing spinels [Reddy and Frost, 2005].

Table 6-17 compares the Raman spectra of chromite found in coal samples to the assignment of chromite based on literature. The bands observed at 500 cm^{-1}, 560 cm^{-1} and 700 cm^{-1} are in good agreement with the work from Reddy and Frost (2005), Chen *et al.* (2003), and Wang *et al.* (2004).

Table 6-17: Raman peaks (cm^{-1}) and assignment for $FeCr_2O_4$ spinel structure

This work	Reddy and Frost, 2005	Chen *et al.*, 2003	Wang *et al.*, 2004	Assignment
700	730	677	690	$A_{1g}(\nu_1)$
	445		520	$E_g(\nu_2)$
500	550	500	600	$F_{2g}(\nu_3)$
560	560	595	650	$F_{2g}(\nu_4)$
	195		445	$F_{2g\,(trans)}$
	218, 175, 160			Additional peaks

6.9.8.3 Raman spectra of hematite (Fe_2O_3)

Iron oxides are actually poor Raman scatters, and their peak positions are influenced by the laser power. Studies by de Faria *et al.* (1997) showed that an increase in laser power leads to a shift of Raman peaks to lower wavenumbers and subsequent increases in the bandwidth. However, high laser power results in the oxidation of minerals to more stable magnetite.

Hematite was the most common iron oxide that formed in high temperature coal ashes. Hematite appeared reddish brown in colour when viewed under the optical microscope. Figure 6-32 depicts the Raman spectrum of hematite as observed in HTA. Hematite belongs to the D_{36}^{6} crystal space group and the Raman spectra of hematite (α-Fe_2O_3) typically consist of seven phonon lines [de Faria *et al.*, 1997]. From Figure 6-32, it is shown that the six of the seven phonon lines expected in α-Fe_2O_3 were identified, with the Raman shift and assignment of characteristic peaks of hematite given in Table 6-18.

The seventh peak positioned at 1320 cm^{-1}, assigned to a two magnon (a collective spin movement) scattering has been reported in previous work by de Farai *et al.* (1997) and was not identified in the spectrum acquired in this work.

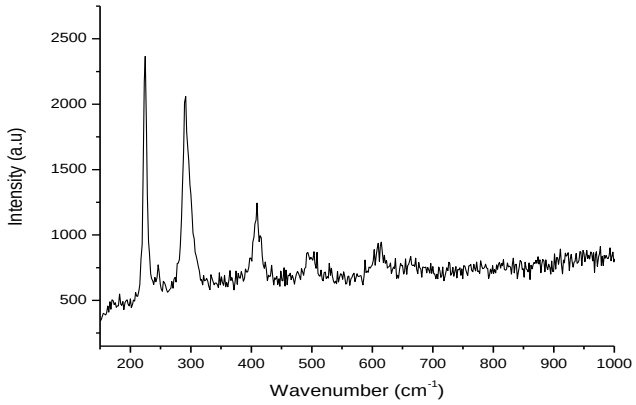

Figure 6-32: Raman spectra of hematite in HTA-D

The Raman spectrum of hematite showed strong peaks at 229 cm^{-1} and 295 cm^{-1}. The peak at 229 cm^{-1} was assigned to Fe-O stretching A_{1g} mode. The peak at 295 cm^{-1} was assigned to the Fe-O bending E_g mode. The minor peaks were identified at 414 cm^{-1}, 500 cm^{-1} and 615 cm^{-1} peak positions. The 414 $cm^{-1}$and 615 cm^{-1} peaks were assigned to the Fe-O bending E_g mode, whilst the peak at 500 cm^{-1} was assigned to the Fe-O A_{1g} stretching mode. These results are in agreement with published Raman data of hematite in the investigations by Legodi and de Waal (2007), de Farai *et al.* (1997) and other authors.

Table 6-18: Raman shift and assignment of hematite found in high temperature coal ashes [de Farai *et al.*, 1997; Jubb and Allen, 2010]

This work (cm^{-1})	Jubb and Allen, 2010 (cm^{-1})	de Farai *et al.*, 1997 (cm^{-1})	Assignment
229	229	226.7	A_{1g} (Fe-O sym stretching)
	249	245.7	E_g (Fe-O sym bending)
295	295	292.5	E_g (Fe-O sym bending)
	302	299.2	E_g (Fe-O sym bending)
414	414	410.9	E_g (Fe-O sym bending)
500	500		A_{1g} (Fe-O sym stretching)
615	615	611.9	E_g (Fe-O sym bending)
	660		A_{1g} (Fe-O sym stretching)

There have been controversial debates over the assignment of iron oxides, especially magnetite (Fe_3O_4) and different authors reported different Raman peaks to represent the different iron oxide phases. The Raman peak positions as identified by various researchers are summarised in Table 6-19 [de Farai *et al.*, 1997; Jubb and Allen, 2010]. From the discussions and observations made, the band at 660 cm^{-1} was identified as the characteristic peak of magnetite. Jubb and Allen (2010) attributed the weak peak at 660 cm^{-1} to the presence of residual magnetite and maghemite. The phase transformation of magnetite to form hematite is referred to as martitization. The transformation takes place at temperatures of about 400°C. As temperature increases, Fe_3O_4 is oxidised to a solid solution to form γ-Fe_2O_3 which transforms into α-Fe_2O_3. Therefore, from the analysis it can be seen that not all the Fe_3O_4 was transformed to α-Fe_2O_3.

6.9.8.4 Raman spectra of phosphates

Figure 6-33 shows the Raman spectrum of a phosphate mineral found in the coals. The characteristic features of the phosphate ion PO_4^{3-} with T_d symmetry is comprised of nine vibration modes, thus the expected vibration modes are the total symmetric stretching mode υ_1, double degenerate υ_2, triple degenerate asymmetric stretching mode υ_3, and the triple

degenerate bending mode υ_4. From the results, the acquired spectrum featured three main peaks. The two weak broad peaks observed at 428 cm^{-1} were assigned to the υ_2 PO_4 bending mode and the peak at 578 $cm^{-1}$was assigned to the υ_4 bending mode. The strongest peak at 964 cm^{-1} was assigned to the υ_1 PO_4 mode [Penel *et al.*, 1997].

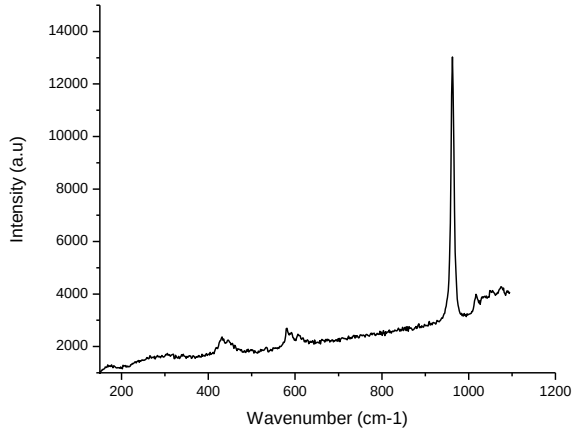

Figure 6-33: Raman spectrum of apatite as observed in HTA-A

Comparing the Raman peaks of apatite in coal to phosphates and hydroxyl vibration modes in the apatitic samples given in Table 6-19, it is noted that some of the peaks including the O-H stretching mode, (which can be found in the 3510-3650 cm^{-1} region) were not observed in the acquired HTA spectrum.

The spectrum was identified as hydroxyapatite [Ca_{10} $(PO_4)_6(OH)_2$]. The results are in agreement with observations made in XRD analyses of raw coal. The presence of hydroxyapatite in coal ashes suggest that brushite identified in raw coals underwent phase transformation at high temperatures, resulting in the formation of hydroxyapatite.

Table 6-19: Phosphate and hydroxyl vibration modes in apatitic [Penel *et al.*, 1997] and HTA-A sample

	Vibration frequency (cm^{-1})			
Vibration mode	**This work**	**Fluorapatite (FAp)**	**Hydroxyfluorapatite (FOHAp)**	**Hydroxyapatite (OHAp)**
PO_4 υ_1	964	965	963	965
PO_4 υ_2	428	432	431	433
		449	446	448
PO_4 υ_3				1029
		1034	1032	1034
		1042	1042	1041
		1053	1051	1048
		1061	1059	1057
				1064
		1081	1080	1077
PO_4 υ_4	578	581	580	580
		592	590	591
		608	606	607
		615	615	614
OH υ_1		3540	3540	
			3560	
			3570	3573

6.9.8.5 Raman spectra of anhydrite

The Raman spectra of anhydrite collected on coal ashes is presented in Figure 6-34 (i) and a mixture of anhydrite with hematite in Figure 6-34 (ii). The Raman band positions and assignments of anhydrite are summarised in Table 6-20.

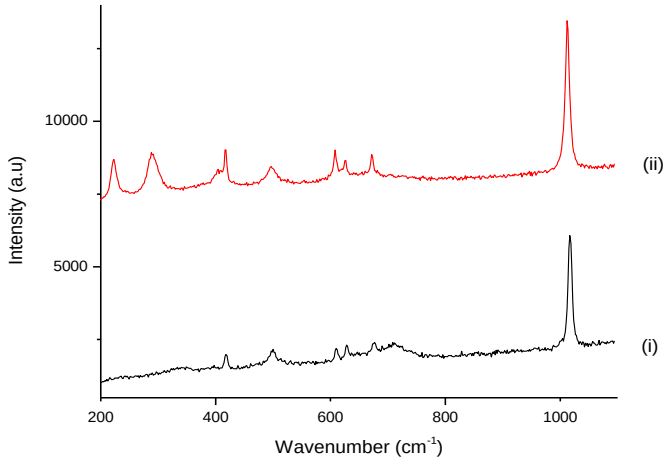

Figure 6-34: The Raman spectra of anhydrite mineral (i) and (ii) a mixture of anhydrite and hematite in HTA-A.

Anhydrite is characterised by its major peak at 1015 cm^{-1} assigned to the υ_1 SO_4^{2-} stretching vibration mode. The minor peaks are assigned to the SO_4 bending modes. The peaks at 417 cm^{-1} and 498 cm^{-1} are assigned to the υ_2, in plane bending, and the peaks at 623 cm^{-1} and 674 cm^{-1} are assigned to the υ_4, out of plane bending modes [White, 2009]. The assignment of anhydrite is in agreement with data from literature [White, 2009; Yin *et al.*, 2017].

Table 6-20: Anhydrite Raman band position (cm^{-1}) in HTA-B

This work	White, 2009	Yin *et al.*, 2017	Assignment
417	417	419	SO_4 bending (υ_2)
498	499	502	SO_4 bending (υ_2)
623	628	626	SO_4 bending (υ_4)
674	675	674	SO_4 bending (υ_4)
1015	1017	1017	SO_4 stretching (υ_1)
	1128	1129	SO_4 stretching (υ_3)
	1160	1162	SO_4 stretching (υ_3)

Figure 6-34 (ii) shows a mixture of hematite and anhydrite. The assignment of the different peak positions of the mixture are summarised in Table 6-21 [Yin *et al.*, 2017]. The Raman shifts below 300 cm^{-1} indicate the presence of hematite, whilst anhydrite was presented by peaks within the 400-1000 cm^{-1} range.

Table 6-21: Raman peak position of a mixture of hematite and anhydrite [Yin *et al.*, 2017]

This work	Hematite [Yin *et al.*, 2017]	Anhydrite [Yin *et al.*, 2017]	Assignment
225	226		Hematite
	244		
290	293		Hematite
	411		
420		419	Anhydrite
495	500	502	Anhydrite
606	609		Hematite
623		626	Anhydrite
670		674	Anhydrite
1014		1017	Anhydrite

6.9.8.6 Raman spectra of unknown white particle

The Raman spectra of a white particle identified in HTA-B is depicted in Figure 6-35. The intense peak at 1016 cm^{-1} was assigned to the υ_1 stretching vibrational mode of a sulphate ion. This could suggest the particle was anhydrite. However, there was uncertainty in the assignment of the peak at 462 cm^{-1}, which could be due to $FeSO_4$ or $BaSO_4$, or possibly quartz, depending on the crystal structure.

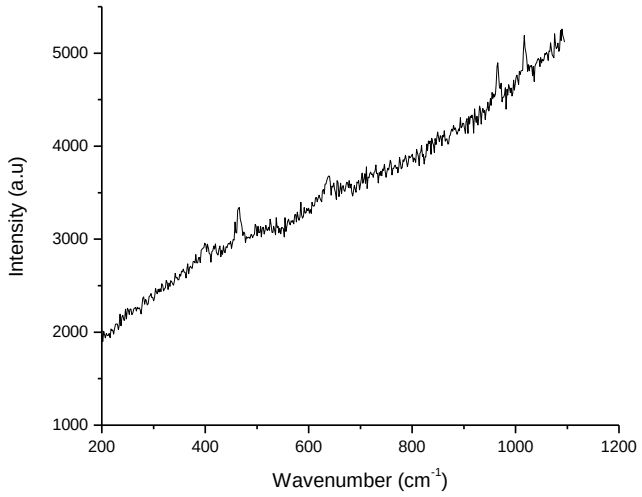

Figure 6-35: Raman spectra of an unknown white mineral particle identified in HTA-B

6.9.8.7 Raman spectra of mixture of minerals

Another mineral mixture identified in the HTA was a mixture of anatase and quartz, depicted in Figure 6-36. From the figure, it can be noted that the characteristic peak of quartz at the 465 cm^{-1} was the prominent peak in the mixture. Anatase appeared in various colour shades. In some instances it appeared white, and at times yellowish in the colour.

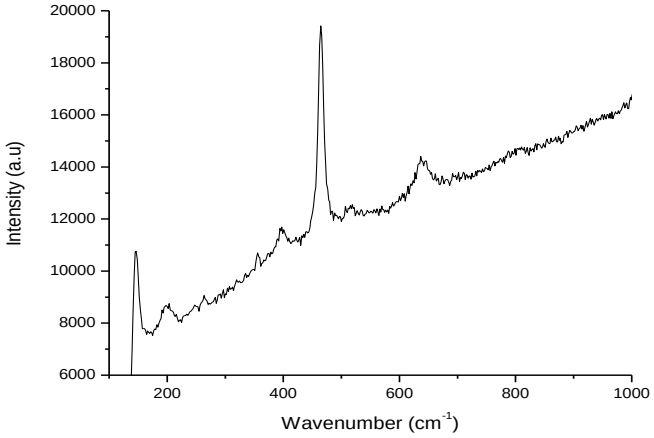

Figure 6-36: Discard coal, anatase associated with quartz in HTA-C

Other mixtures of minerals observed in high temperature ashes were a mixture of hematite and cristobalite, and a mixture of quartz and apatite. Figure 6-37 shows the Raman spectra of a mixture of anhydrite and aragonite.

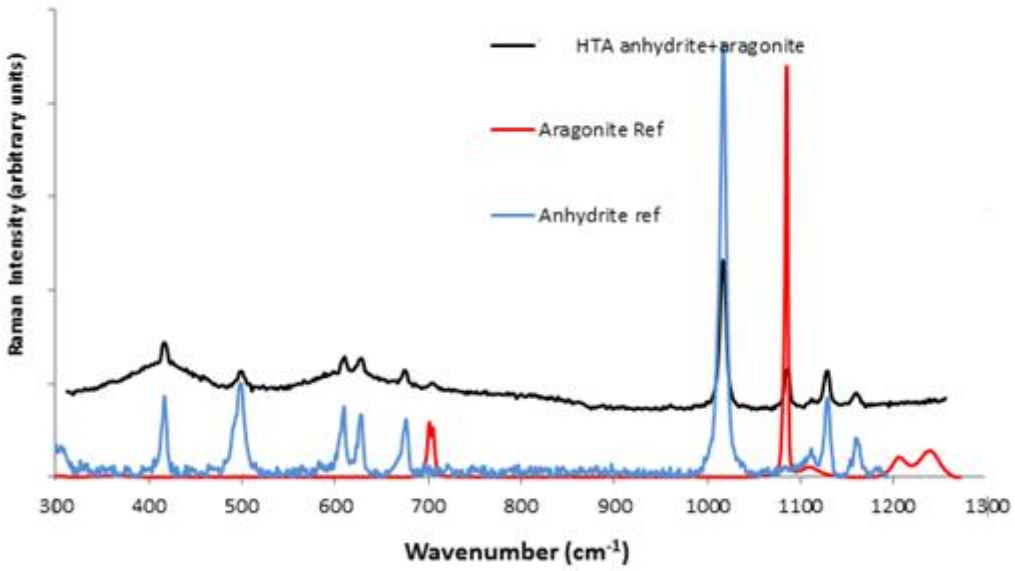

Figure 6-37: Raman spectra of a mixture of anhydrite and aragonite

The internal fundamental modes of vibration of carbonate ions of aragonite are found in the high frequency region. The peak at 705 cm^{-1} is assigned to υ_4 (A_g) in-plane bending vibrational mode, and the peak at 1085 cm^{-1} is assigned to the υ_1 (A_g) symmetric stretching vibrational mode of CO_3^{2-}. The mixture of anhydrite and aragonite indicates that not all the water of crystallisation was lost when the coals was subjected to high temperatures of 815°C.

Other high temperature mixtures of anatase (TiO_2), quartz (SiO_2), apatite ($Ca_{10}(PO_4)_6(OH)_2$), nepheline ($NaAlSiO_4$) and crednerite ($CuMnO_2$) are depicted in Figure 6-38. However, only the spectral reference of apatite, quartz and anatase are indicated in the figure. The rest of the spectral references can be found in Appendix H, Figure H-2.

According to Chen *et al.* (2015), the $CuMnO_2$ is a delafossite structure at high temperatures, with two Raman two active modes, the A_{1g} mode attributed to O-Cu-O vibration and the E_g vibration mode derived from the MO_6 octahedral structure. Therefore, the strong Raman active peak at 670 cm^{-1} is attributed to $CuMnO_2$ peak.

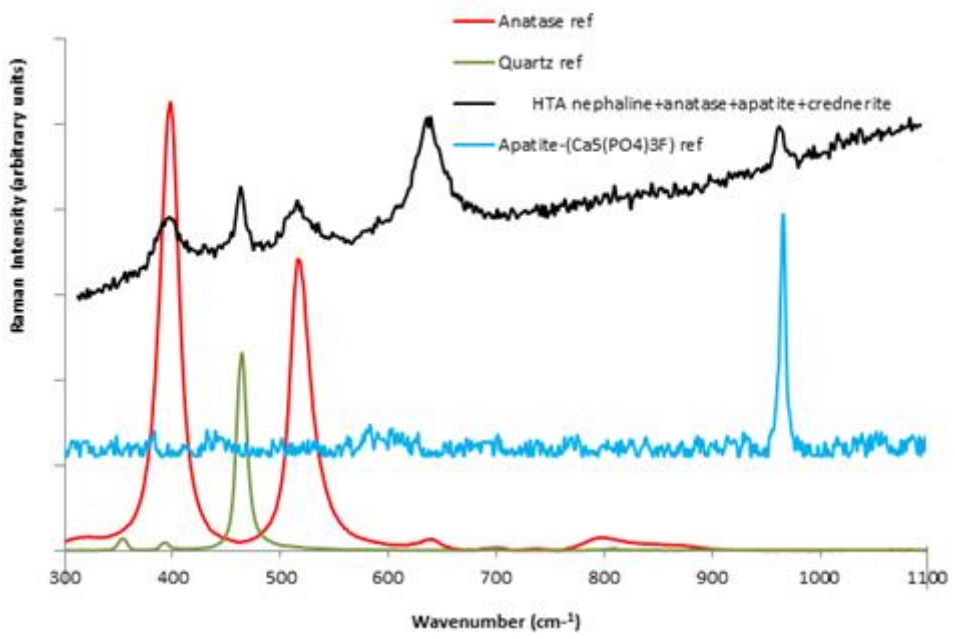

Figure 6-38: Raman spectra of HTA-B showing a mixture of anatase, quartz, nephaline, apatite, and crednerite

6.10 Single particle analyses (SPA) clustering

The reporting of ash oxide using XRF analysis is limited by the inability to accurately detect elements of an atomic number below Na (Z<11), and volatile elements such as Cl. Therefore, establishing mineral association and mode of occurrence in the raw coals by XRF analysis can be challenging. Although separation methods have been previously employed to determine the mode of occurrence of mineral matter in coals, studies have shown that these methods are also limited.

Microanalysis techniques such as CCSEM and EPMA have a far greater chance of addressing challenges related to the association and mode of occurrence of mineral matter in coals [Li *et al.*, 2007]. The single particle approach probes individual particles and allow for the determination of low Z elements, including boron. The SPA can probe particles of approximately 0.5 μm in size, which is a relatively high resolution compared to XRF analysis.

In this study a combined model of principal component analysis (PCA) and chemical boundary classification (CBC) was used to identify mineral matter in coals. The PCA model does not require prior knowledge of composition of minerals. For CBC modelling, statistical software (excel programme) based on chemical and phase boundaries approach by Kandler *et al.* (2007) was applied to assign 500 analysed particles into 11 classes.

6.10.1 Elemental abundance in raw coals

A total of 500 particles was analysed, and elements with weight composition greater than 5% were considered for species distribution. The elemental abundance of each element identified in coal samples (C, N, O, P, S, Cl, Na, Mg, K, Ca, Al, Si, Mn, Fe, Cr, and Ti) is presented in Table 6-22. Figure 6-39 provides a detailed overview of the elemental composition of the investigated coals.

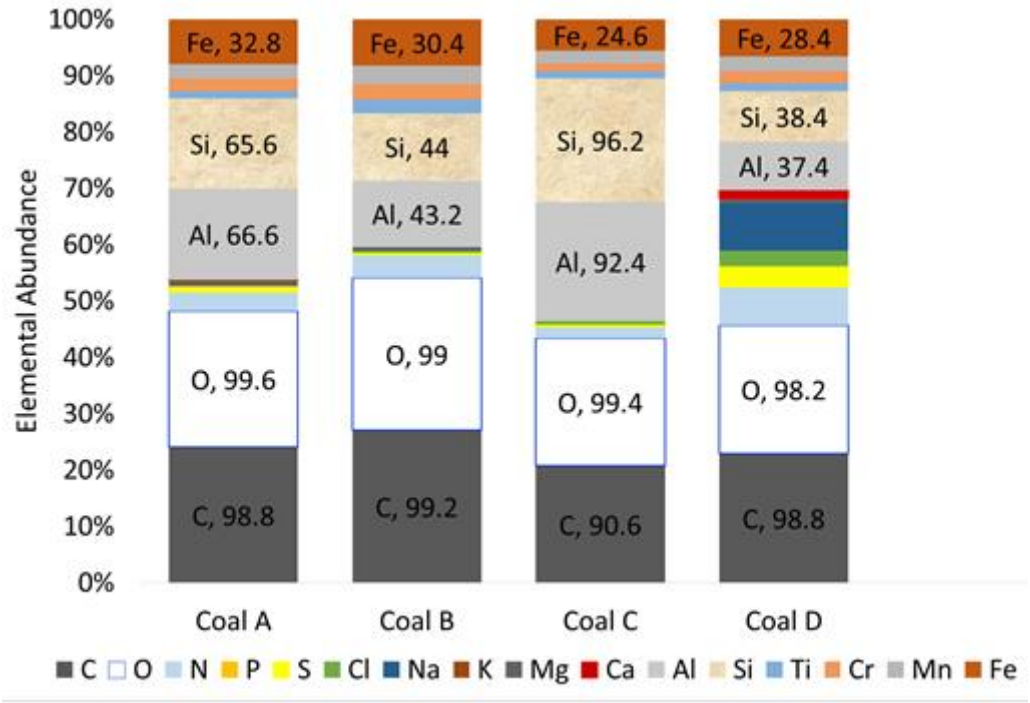

Figure 6-39: Elemental composition of raw coal samples

Table 6-22: Elemental abundance in raw coal samples

Elemental abundance (mol.%)	Coal A	Coal B	Coal C	Coal D
C	24.0	27.1	20.7	22.9
N	24.2	27.0	22.7	22.8
O	3.3	4.1	1.9	6.7
P	0.1	0.1	0.1	0
S	1	0.4	0.4	3.7
Cl	0	0.4	0.5	2.8
Na	0.1	0.1	0	8.4
K	0	0	0	0
Mg	1.1	0.5	0	0.7
Ca	0	0	0	1.5
Al	16.2	11.8	21.1	8.7
Si	15.9	12	22	8.9
Ti	1.3	2.3	1.2	1.4
Cr	2.3	2.8	1.4	2.2
Mn	2.6	3.3	2.2	2.6
Fe	8	8.3	5.6	6.6
Total	**100**	**100**	**100**	**100**

From the results it is observed that Al and Si are the most abundant elements. This is as expected, because XRF analyses on coal ash identified both Al and Si as abundant elements. However, it can be a challenge to assign the Al: Si ratio to the relevant clay mineral. Petrographic analysis indicated that clay minerals were of syngenetic and detrital origin. The XRD analysis classified the major clay minerals found in coals as kaolinite. The results were confirmed by FTIR.

Iron is the third most abundant mineral after Al and Si. From the aforementioned, Fe was associated with S, and pyrite was identified as the most dominant sulphide mineral. Pyrite was found in a wide range of morphologies, showing the syngenetic and epigenetic origin of coals. XRD confirmed the presence of pyrite in coals, whilst mRs identified FeS_2 to have an isotropic structure. However, XRD analyses on raw and LTA samples could not identify pyrite in coal D, probably because of low detection limits.

Other minerals present in minor quantities in coal D included Na, Cl, Ca, and S. The reporting of these elements, particularly Cl in coal D is significant since the element could not be detected by any of the techniques discussed, and was reported for the first time by SPA-EPXMA.

6.10.2 Principal component analysis

The principal component analysis (PCA) is commonly used to analyse data sets of high complexity by generating a new set of orthogonal variables and establish a link between the new data set [Sharma *et al.*, 2014]. The Eigen values are extracted from covariance matrix of the original variables, and used to measure associated variance.

Table 6-23 shows the varimax rotated component matrix obtained by PCA. From the table it is observed that there is a strong correlation between Mg, Ca, and Mn for component 1, which can be an indication of a carbonate mineral. Component 2 shows a strong correlation between Fe and S, which indicates the presence of pyrite mineral. Component 3 shows a strong relation between Na and P, these elements can be organically or inorganically bound. Component 4 shows a strong affinity of Ti, indicating probability of TiO_2 minerals. Component 5 indicates a probable association between Na and K, and lastly component 6 indicates an association between Si, S, Fe, and Mg.

Table 6-23: Varimax rotated component matrix of SPA data

	Component					
	1	**2**	**3**	**4**	**5**	**6**
Na	-.023	-.021	.936	-.019	.110	.017
Mg	.970	.077	.040	-.013	.003	.112
Al	-.338	-.365	-.062	.017	.008	-.855
Si	-.489	-.719	-.176	-.197	-.003	.376
P	.050	.013	.939	-.004	.092	.015
S	.015	.865	.015	-.062	-118	.201
K	-.047	-.028	.187	-.021	.976	-.006
Ca	.954	.055	.073	-.013	-.044	.109
Ti	-.033	-.010	-.023	.997	-.020	-.021
Mn	.828	.036	-.077	-.022	-.025	.063
Fe	.002	.858	-.088	.-013	.075	.182

The graphical plot of the correlation matrix was used to reduce the spread of data, and establish association of different minerals as indicated in Figure 6-40. The rotated component matrix gives a visual interpretation and association of mineral matter in coals. From the results, it can be deliberated that there is pyrite, clays, carbonates and oxide mineral in coal samples. The association of Mn with carbonates suggests a possible presence of rhodochrosite ($MnCO_3$), confirming ash chemistry results.

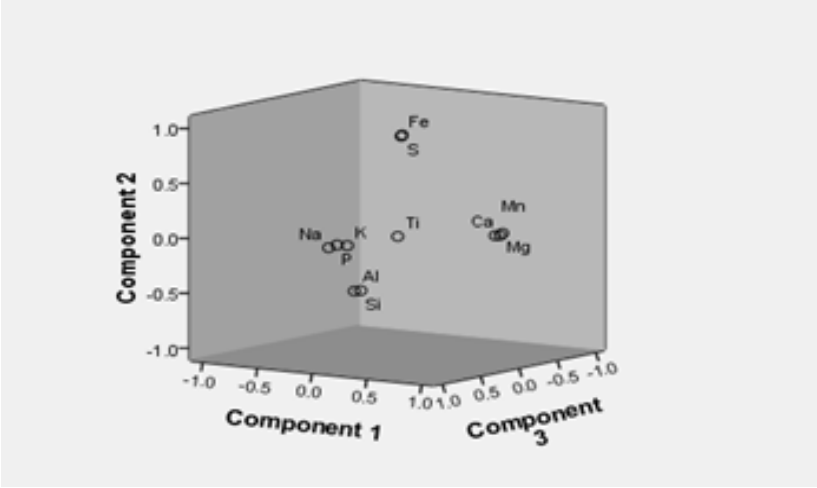

Figure 6-40: Rotated component matrix clustering of mineral matter in coal A

The rotated component matrix for coal B in Figure 6-41 further indicates the presence of alumina-phosphates. The XRD analyses of raw coal and LTA samples identified the two phosphates in SA coals as gorceixite and goyazite. Therefore, results extracted from PCA are in agreement with observations made by XRD results, where gorceixite and goyazite was identified in raw coal and LTA of samples A and B.

The phosphate minerals are associated with Ti, whilst Si occurs as quartz. The association of K and Al suggests the possible presence of feldspars (microcline, orthoclase and anorthite) and glauconite in investigated coals. Minor concentrations of mica were detected by XRD analyses of LTA samples. Therefore, the results suggest the presence of glauconite in the samples as predicted by PCA.

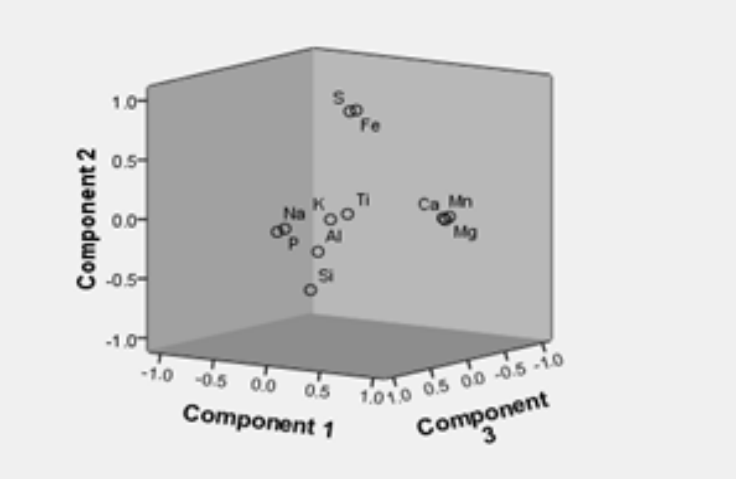

Figure 6-41: Rotated component matrix clustering of mineral matter in coal B

From the results it is observed that the association of elements is quite variable, and depends on the source of element and the environment at which the mineral were formed. Moreover, these results show that bulk analysis (ash chemistry analyses) are not fully descriptive and do not give the mode of occurrence of minerals, but depend on structural analytical techniques to confirm the compositions.

6.10.3 Chemical boundary classification (CBC)

The 11 mineral classes (Fe-rich, quartz, carbonates, silicates, gypsum, Ti-rich, sulphate silicate mixture, dolomite, sulphates, halites, other Ca-rich, other carbonaceous, not assigned) with their respective criteria used for CBC modelling are presented in Table 6-24.

Table 6-24: Clustering of different mineral matter using chemical composition and phase boundaries (Kandler *et al.*, 2007)

Class name	Criteria
Iron-rich	$\|Fe\| > 0.15$ and $Si/Fe < 1$ and $Ti/Fe < 1.33$
Titanium-rich	$\|Ti\| > 0.3$ and $Na/Ti < 1$ and $Mg/Ti < 1$ and $Al/Ti < 1$ and $Si/Ti < 1$ and $S/Ti < 1$ and $Fe/Ti < 1$
Carbonates	[$\|Ca + Mg\| > 0.5$ and $0.33 < Mg/Ca < 3$] or [$\|Ca\| > 0.5$ and $Mg/Ca < 0.33$ and $Si/Ca < 0.5$ and $S/Ca < 0.25$ and $P/Ca < 0.15$]
Other calcium-rich	$\|Ca\| > 0.25$ and $Si/Ca < 0.5$ and not in class carbonates or gypsum
Gypsum	$\|Ca + S\| > 0.5$ and $0.25 < Ca/S < 4$ and $Na/Ca < 0.5$
Halite	$\|Na + Cl\| > 0.5$ and $S/Na < 0.375$ and $S/Cl < 0.5$ and $Si/Cl < 0.5$
Quartz	$\|Si\| > 0.5$ and $Mg/Si < 0.2$ and $Al/Si < 0.2$
Silicates	$\|Si\| > 0.2$ and $Na/Si < 0.7$ and $Mg/Si < 1.33$ and $Al/Si < 0.33$ and $K/Si < 0.5$ $Ca/Si < 0.5$ and $Ti/Si < 0.5$ and $Fe/Si < 0.5$ and $\|P + S + Cl\| < 0.2$ and not in class quartz
Sulphate silicates mixtures	$\|Na + S + Mg + Al + Si + K + Ca\| > 0.7$ and $0.6 < S/Si < 2$
Sulphates	$\|S\| > 0.5$ and $Cl/S < 0.3$ and $Si/S < 0.5$ and $Fe/S < 0.5$ and not in class gypsum
Other	Not in other class

All elements ratios based on moles; $|X|$=total atomic content of element X relative to all other elements analysed (except C and O); $\|X\|$ total atomic content of element X relative to all other elements analysed (including C and O).

The results of mineral classification are presented in Figure 6-42, and from the results it can be noted that a large percentage of the minerals are silicate, particularly in coal C. Coal B is characterised by a high concentration of Fe-rich minerals. Significant amount of Fe-rich, and Ti-rich minerals were identified in coal B. Carbonates and gypsum were dominant in coal A, and halite and sulphate were high in coal D.

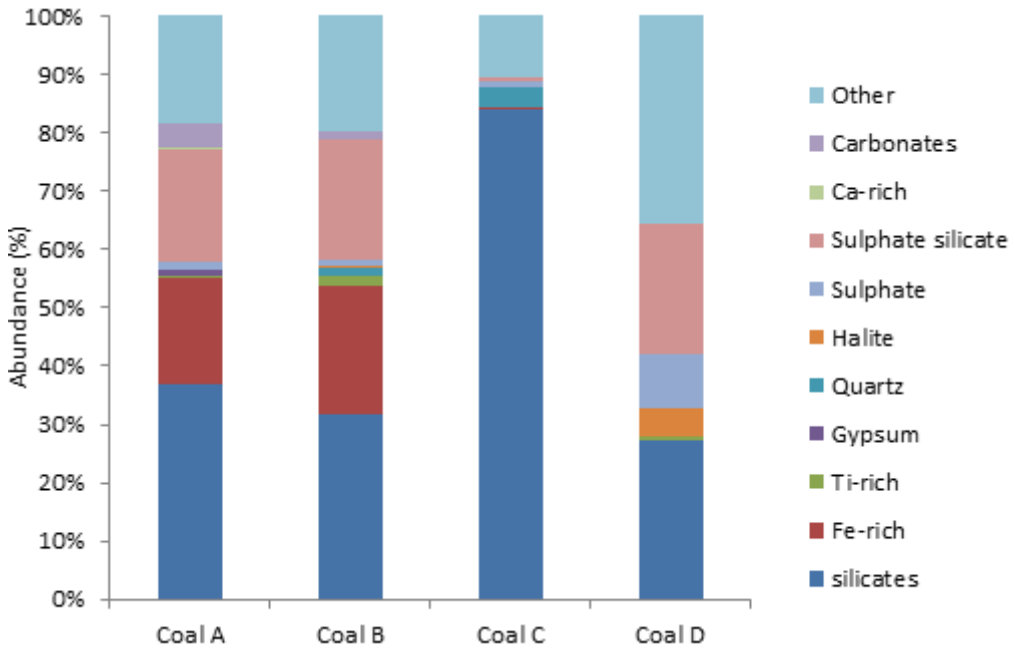

Figure 6-42: SPA clustering of mineral matter in coal using the chemical boundary classification method

To clarify the types of silicates in coals, the minerals were further classified into minor groups listed in Table 6-25 showing the abundance of each respective class.

Table 6-25: Minor groups of silicate minerals in raw coal samples

Minerals (mol.%)	Coal A	Coal B	Coal C	Coal D
Silicates	47.88	36.04	47.63	20.93
Silicate, Fe-cont	14.41	9.01	18.53	7.91
Silicate, Ti-cont	5.93	7.21	22.20	2.56
Silicate + Ti,Fe-cont	1.69	0.45	7.54	0.23
Silicate + S-cont	6.78	7.66	2.37	0.23
Silicate mix	5.72	8.33	0.22	12.79
Silicate mix Fe-cont	1.69	1.13	0.00	3.72
Silicate mix Ti-cont	1.06	4.50	0.00	6.28
Silicate mix S-cont	2.54	4.28	0.22	5.12
Sulphate silicate	0.42	0.90	0.22	7.67
Fe-rich, silicate containing	10.38	10.59	0.86	6.51
Fe-rich, Ti-rich	0.21	4.73	0.22	2.33
Other	0.21	0.90	0.00	14.19
Carbonaceous	0.64	2.93	0.00	5.35
Carbonaceous, S-rich	0.42	1.35	0.00	4.19
Total	100	100	100	100

From the results it is observed that pure silicates, Fe, Ti containing silicates were abundant in coal C. The Fe, Ti containing silicates indicates the possibility of clay minerals such as fayalite ($FeSiO_4$) and almandine ($Fe_3Al_2Si_3O_{12}$).

As discussed previously, coal D had an abundance of Na, Cl, S, and silicate minerals. It can be deduced that the sample will have halite and sodalite mineral. The Fe, Ti-rich mineral group indicates the presence of the ilmenite ($FeTiO_3$) mineral in coal B. Ti-containing minerals occur in areas that have been subjected to hydrothermal activity associated with volcanic activities or metamorphism. Other than pyrite being the dominant Fe-containing mineral, additional mineral that are present in minor quantities are identified by the SPA-EPXMA technique.

From the results it can be seen that most of the minerals were under reported by all the characterisation techniques. The use of SPA-EPXMA was instrumental in characterising and identifying minerals that would otherwise not have been identified. Some of the minerals identified by SPA are confirmed by XRD, FTIR, and mRs, and some were identified for the first time by SPA-EPXMA technique. Minerals identified by SPA-EPXMA include rhodochrosite, gorceixite, goyazite, anatase, quartz, feldspar, glauconite, ilmenite, almandine, fayalite, halite and sodalite.

It has been discussed that the lower AFT reported in coal B was due to the activity of Fe found in pyrite. However, the results presented by SPA-EPXMA suggest that the Fe^{2+} activity is not only due to pyrite, but also attributed to the presence of ilmenite in the sample, leading to the formation of slag phase at relatively low temperatures. It is postulated that Fe in silicates does not significantly impact on AFT. This speculation is supported by the fact that significant amounts of silicate, Fe-containing minerals were detected in coal C, but did not lower the AFT of coal C.

From thermodynamic modelling, it was observed that high concentrations of feldspar reacted at temperatures between 1100°C and 1200°C, resulting in an increase in the formation of the slag phase. The presumed presence of feldspars predicted by FactSage was supported by PCA analysis. Therefore, the SPA-EPXMA technique can be used to validate and confirm the thermodynamic predictions. Feldspars act as a fluxing agent, therefore it is expected that the presence of feldspar will reduce AFT.

It was reported earlier in the study that the chemistry of the melt phase can be related to coal composition. It was considered that the high mullite content in coals will have a correlation with the amount of kaolinite in coal samples.

Findings from SPA indicate that the high amounts of total silicates were reported in coal C. However, in the case of coal C, the FactSage predicted a low concentration of mullite, which means the correlation, was not valid in this instance.

It can be said that SPA-EPXMA was more detailed in characterising mineral matter, and more information was derived from the analysis. The SPA-EPXMA results not only did they confirm the bulk analysis results, but augmented on what was initially derived from bulk analyses. The results prove that SPA-EPXMA is a powerful technique that can be considered for analysis of coals and for thermodynamic modelling. Moreover, it can be considered an added advantage that the results are performed on raw coals; therefore, one can correctly identify the mineral matter in coal without having to perform mineral separation.

6.11 Discussion

Clean coal technologies, coal cost and quality, environmental consideration, sustainable development, growing economy, and governmental regulations are some of the issues faced by the coal industries today [Jeffrey, 2005]. This work was focused on addressing some of the challenges by understanding the mineralogical assembly of mineral matter of inertinite rich (medium rank C bituminous coal) samples. For this purpose, multiple techniques were used to evaluate the heterogeneity of mineral matter in coals. A novel approach was developed for the characterisation of mineral matter in selected SA coals from within the Karoo sequence. Multiple techniques such as XRF, SPA-EPMXA, petrography, XRD, FTIR, and mRs were used to characterise mineral matter.

Characterisation of raw coals

From the study, it was observed that the traditional physico-chemical analyses gave a broad picture of the type of coal. However, the analyses on their own did not provide a complete description or a true reflection of the nature of coals, nor did it give an indication of how the different minerals occurred or interacted in coal conversion processes. Nonetheless, the information derived from the physico-chemical analyses is still useful, most especially within the coal industry for selection and grading of coals.

Ash chemistry gave an indication of possible minerals present. However, the analyses did not identify nor give the speciation of specific minerals. Even so, based on the elemental composition, one could make an intuitive decision and extrapolate information using chemistry and molecular ratio, to identify possible mineral matter phases in coals. The ash chemistry and the mineralogy of the coal samples suggested clay minerals were the most dominant mineral matter present in all four coal samples. The results were later confirmed by petrography, XRD, FTIR, mRs and SPA-EPXMA techniques.

Petrographic analyses classified the main minerals into their respective groups without identifying specific minerals. Petrographic methods gave a general and broad characterisation by assigning minerals to different groupings. The minerals were identified and distinguished by their characteristic colours, and geological features. The analyses confirmed the presence and mode of occurrence of clays, carbonate, sulphides, and oxide minerals. Largely, the coals were of both syngenetic and epigenetic origin. The DAI index based on ash chemistry classified mineral matter found in coals A, B and D to be of detrital origin, whilst mineral matter in coal C was of authigenetic origin. The DAI index and ash classification were confirmed by the petrographic results, indicating the nature of coals in the study.

The mode of occurrence of mineral matter in coals is important because it is directly related to the behaviour of mineral matter. Therefore knowledge about the composition and distribution of mineral matter can be the most critical starting point for interpretation of potential application and effects of coals.

The disadvantage of petrographic analyses was the inability to discriminate between minerals. Moreover, one has to rely on the experience of the operator. The results obtained from petrographic analysis are reported in volumetric percentage. Therefore, one would need to know the true density of the different minerals to estimate the actual amount of mineral matter present. However, there was a good correlation between ash content reported by petrography and proximate analyses.

In order to have a true presentation and appreciation of the minerals found in coals, bulk and point particle analyses were considered. Furthermore, the coals were subjected to low and high temperature ashing. The purpose of ashing was to drive off the organic matter and analyse the samples without interference of organic matter.

The XRD studies on raw coal confirmed the presence of minerals such as quartz, kaolinite, calcite, aragonite, dolomite, pyrite, muscovite, alunite, gypsum, brushite, gorceixite, and anatase. The results are in agreement with findings by Matjie *et al.* (2006); Everson *et al.* (2013) and Pinetown *et al.* (2007) who studied some of SA coals. Matjie *et al.* (2006) identified kaolinite, quartz, calcite, dolomite, pyrite, feldspar microcline, muscovite, illite, rutile, anatase, apatite, Fe-oxide and siderite when characterising low rank bituminous coal used in gasification processes. Traces of microcline, illite, smectite-illite, mixed layers, analcime, plagioclase, marcasite, anatase, aragonite, ankerite, rhodochrosite, alunite, jarosite, apatite, crandalite, gorceixite, goyazite and gypsum have been reported in the No.4 lower seam in the Witbank and Highveld coalfields by Snyman and Botha (1993).

Although the list of minerals identified in this study was not exhaustive, it was clear that most of the minerals typically found in SA coals were identified. Most of the minerals were identified by SPA-EPXMA.

The XRD analyses on raw coals were also confirmed by XRD analyses of LTA samples. Although there were inconsistencies in the reporting of minerals found in raw coals and LTA samples, it was noted that there was a strong correlation in the reporting of major minerals, namely; kaolinite and quartz, with correlation coefficient of 0.98. Characterisation of clay minerals with XRD can be difficult due to factors such as compositional variations, variable degree of structural order, and preferred orientation. As a result, oriented aggregate XRD analysis was conducted to characterise clay minerals with particle size below 2 μm. The analysis confirmed the presence of other clay minerals such as illite, and illite/smectite expendable clays. However, these clay minerals were present in minor quantities. The results are in agreement with reporting by Matjie *et al*. (2016), for the determination of mineral matter of low grade, medium rank C coals from Highveld coalfield.

The clay assemblage in raw coal samples was further classified by FTIR. The FTIR peaks were attentively assigned to kaolinite, illite, muscovite, smectite and quartz. Kaolinite with characteristic peaks at 3691 cm^{-1} and 3619 cm^{-1} confirmed the clay to be well ordered and of authigenetic origin. Although XRD analyses confirmed the presence of muscovite in coal samples A and C, FTIR analyses was capable of confirming the presence of muscovite in all coal samples investigated. These findings highlight the limitations of bulk analyses and the detection limits of XRD over FTIR analyses.

The FTIR analyses of raw and LTA samples showed similar results. This could suggest special preparations such as low temperature ashing are not necessarily required when characterizing clay minerals in coals when using FTIR technique. These attributes from FTIR can be beneficial to coal characterisation, because time is always a concern in industry. Low temperature ashing can take days, and further classification is required in XRD analyses to characterise finely disseminate clay minerals of particle size less than 2 µm. FTIR proved to be relatively fast in charactering clay minerals, albeit the overlap of some of the characteristic peaks. The main disadvantage of FTIR was due to that the fact that the technique was mineral specific, since only clay minerals could be identified. In this case, the limitation was imposed by the spectral range of the instrument used.

Other minerals identified by the XRD technique included phosphate minerals. The presence of P_2O_5 was first reported in ash chemistry of coal samples. Phosphorus was assigned to minerals such as brushite ($CaPO_4(OH)(H_2O)_2$), and gorceixite ($BaAl_3(PO)_4(PO_3OH)(OH)_6$) in coal A. However, the LTA samples identified goyazite ($SrAl_3PO_4)(PO_3OH)(OH_6$) in coals A and B, and not gorceixite. The two minerals (gorceixite and goyazite) belong to the crandallite mineral groups, and can be difficult to differentiate. Aluminophosphates occur mostly as infilling in pore spaces and cell cavities of inertinite macerals. However, these minerals can also be associated with kaolinite and quartz [Ward *et al.,* 1996]. Apatite was later identified and confirmed by mRs in HTA. The occurrence of both apatite and goyazite mineral groups have also been report [Ward *et al.,* 1996]. This results show that the presence of carbonaceous materials can affect the reporting of mineral matter, hence it is generally preferred to subject coals to LTA before analysing with XRD.

The dominant sulphide mineral identified in coals was mostly anisotropic pyrite. The mRs technique could not identify clay minerals in coals. This was attributed to the fluorescent nature of clay minerals in coals, which complicated their identification. However, some of the minerals that are Raman active could be identified. The minerals identified in raw coals included pyrite, anatase, rutile, quartz, and jarosite. Quartz, which was reported as the second most dominant mineral matter by petrography and XRD was of detrital origin, and associated with clay minerals. The mRs technique identified its structure as the α-quartz. Additional information provided by the mRs technique showed that pyrite has an anisotropic structure.

An unusual distinctive feature was observed in one of the typical Raman spectra of pyrite in Coal C. The presence of an uncharacteristic peak indicated that pyrite in coal was not in its pure form. The peak was assigned to the possible occurrence of either elemental sulphur or arsenopyrite. The presence of elemental sulphur can be attributed to oxidation of sulphide minerals, whilst arsenopyrite can be attributed to the presence of trace elements. There is abundant evidence in literature that has correlated the association of pyrite to trace elements such as mercury, zinc, lead and arsenic [Swaine, 1990; Finkelman, 1994; Davidson, 1996]. The presence of jarosite in raw coals was evidence that oxidation took place in coal C.

Moreover, the technique was able to discriminate between the two polymorphs of TiO_2 minerals, (i.e. rutile and anatase). Consequently, the high spatial resolution of mRs analyses was able to identify and confirm the presence of TiO_2 in coal D, which could not be detected by XRD analyses. The mineral could not be identified because of low concentration of TiO_2 in coal samples.

The major challenge of using mRs was its inability to characterise clay minerals, which are considered to be the dominant phase in coals. This was attributed to the fluorescent nature of coal and the laser source used to characterise raw coals. The other disadvantage of using mRs was the topographic structure of mineral particles. Although sample preparation is not important in characterising samples with mRs technique, it was observed that mounting samples in resin did not help in charactering minerals particularly, fluorescent minerals, it was also noted that powdered samples proved to be challenging to characterise at times.

Single particle analysis (SPA) classified silicate minerals into various classes. Clay minerals were the most abundant minerals found in coal samples as indicated by ash chemistry, petrographic methods, XRD, and FTIR. However other groups of silicate minerals were identified and the garnets mineral group was the second most abundant mineral in coal samples. The common Fe-containing silicates included fayalite (Fe_2SiO_4), and almandine ($Fe_3Al_2Si_3O_{12}$). Traces of ilmenite ($Fe\text{-}TiO_3$) were identified in coal B, whilst trace of sodalite were detectable in coal D. Silicate containing Ti were dominant in coal C.

Coal D was characterised by silicate mix. From the analyses it was observed that not all clay minerals were characterised by bulk analyses. More detailed and descriptive nature of silicates was attained by SPA. The SPA gave more insight on mineral matter in raw coal far better than any technique that was considered for analysis. The results from SPA could be considered as somewhat the true representation of minerals in raw coals. There was no correlation drawn between ash chemistry and SPA-EPXMA results, because the state of the sample was altered for ash chemistry analyses, and the technique assumes ash to be homogeneous, whilst SPA-EPXMA took into account the heterogeneity of the coal particle. Although XRF is highly relied upon in many coal applications, the technique simply gives one an indication of expected compositions and not the actual compositions.

A noteworthy observations made with regard to SPA was the identification of halite and sodalite in coal D. The presence of these minerals gives one an indication of the type of environment the coals were subjected to during coalification. Although most of the coals were influenced by hydrothermal and volcanic activities, it is noticeable that coal deposits were subjected to environments where the salinity of ground water was high. This explains the high concentrations of dolomite as it was observed with the investigated coals [Vassilev *et al.,* 2010]. These findings once again indicate the benefit of using SPA for coal characterisation.

Another remarkable finding by SPA was the abundance of S, Ca, and Na detected in coal D. The CBC analysis showed that the high abundance of S in coal D was associated with sulphates and sulphate silicates. Hence pyrite was present in minor quantities relative to the coals investigated. These results show clearly that if the coal chemistry is not closely supervised, one can easily assume that sulphur is associated with iron to form pyrite, which was not the circumstance for coal D. It is interesting to note that this identification could not have been possible, since these observations were not obvious with conventional bulk analysis.

Although Cr was not assigned to any mineral group, chromite was identified by mRs in HTA-D. This is an indication of the importance of using a structural technique. In this case, even though the mineral was not classified, its existence could nonetheless be confirmed.

Comparing ash chemistry analysis to SPA-EPMXA, it was easily noticeable that SPA-EPMXA is more suitable to characterise mineral matter. The technique is capable of analysing elements of small atomic and particle size in their unaltered state. The elemental composition analyses using SPA-EPMXA proved to be ideal since the technique was capable of identifying some of the minerals that were not identified by any of the techniques used.

The PCA and clustering of different elements gave an in-depth knowledge of the association of the different elements in coals. The results were more detailed compared to ash oxide chemistry of coals.

Bulk analyses fell short in terms of identifying minerals present in raw coals. Overall the minerals identified by bulk analyses were under reported. This gives a glimpse of the challenges of understanding the behaviour of mineral matter in combustion processes, considering the fact that these approaches are still used to explain complex processes. Insufficient information is generally used to understand boiler and gasification conditions.

Nonetheless, not all minerals could be assigned by the CBC method. The unassigned minerals did not fit into the criteria set to determine the mineral phases. A significant proportion of minerals in coal D are not assigned to any mineral. This is an indication that the boundary classification can be revised so that as many minerals as possible can be classified.

The challenge presented by the SPA-EPXMA is the large amount of data to be mined from X-ray analyses of individual particles. Although the approach is supervised and more reliable, it is laborious and time consuming making the interpretation a daunting task.

Table 6-26 gives a summary of the different minerals identified by the different techniques. From the summary, it can be extracted that some of the minerals could be easily identified by all techniques. However, every technique had its advantages and limitations.

Table 6-26: Mineral matter identified in raw South African coals

Minerals (raw coal)	Ash chemistry	Petrography	XRD	FTIR	mRs	SPA
Silicate minerals	Kaolinite Quartz Mica	Kaolinite Quartz	Kaolinite Muscovite Quartz	Kaolinite Illite Muscovite Smectite Quartz	Quartz	Kaolinite Chlorite Quartz Alunite Fayalite Almandine
Oxides, Hydroxides	Anatase		Anatase		Rutile Anatase	Anatase Ilmenite
Sulphides	Pyrite	Pyrite	Pyrite		Pyrite Pyrrhotite Marcasite	Pyrite
Phosphates			Brushite Gorceixite			Brushite Gorceixite goyazite
Sulphates			Gypsum Alunite			Gypsum Dolomite Calcite Sodalite
Carbonates	Calcite/Dolomite	Calcite/Siderite	Dolomite Calcite Aragonite			Rhodochrosite
Salts						NaCl

Characterisation of low temperature ashes

The three techniques used to characterise low temperature ashes were XRD, FTIR, and mRs. From the discussion above, it was stated that there was a slight difference in the results reported by XRD and FTIR on raw coals and LTA samples. However, it was established that an artefact was formed when LTA samples were prepared. It is presumed that calcium reacted with sulphur to form a sulphate mineral, bassinite.

The analysis of LTA by mRs alluded to the possibility of additional reactions taking place to form artefacts in LTA. The secondary oxidation products identified in LTA included lepidocrite (γ-FeO(OH)), coquimbite ($Fe_2(SO_4)_3.9H_2O$, and anhydrite ($CaSO_4$).

These minerals were not detected in LTA samples, but were evident in mRs analyses. The only artefact identified by XRD was bassinite. From the results it can be confirmed that sulphur reacted with both Ca and Fe in LTA to form sulphate minerals, and oxides.

Although LTA analyses are considered to be a true representation of mineral matter, the phases that are identified and information brought forth by mRs analysis shows that there is an element of error in the reporting of LTAs, hence the inconsistencies, especially with the reporting of minerals that are present in minor quantities.

Despite the fact that LTA has been accepted as the best approach to selectively isolate mineral matter from coal, the approach seems to be suitable for major minerals, as it is the case with other bulk analyses. Hence there was a good correlation in the estimation of mineral matter by proximate analysis, petrography and LTA analysis. These implications show that for one to fully understand coal, it must be analyses in its unaltered state. Therefore, methods that do not require organic matter to be isolated should be sought after.

Table 6-27 gives a summary of the different minerals identified by the aforementioned techniques to characterise low temperature ashes.

Table 6-27: Mineral matter identified in low temperature ashes

Minerals (LTA)	**XRD**	**FTIR**	**mRs**
Silicate minerals	Kaolinite, Muscovite, Illite Quartz	Kaolinite, Muscovite Smectite, Illite, Quartz	
Oxides, Hydroxides	Goyazite		Lepidocrite
Sulphides	Pyrite		
Phosphates	Brushite, Gorceixite		
Sulphates	Bassanite		Anhydrite, Coquimbite
Carbonates	Dolomite, Calcite		

Characterisation of high temperature ashes

Ashes generated from high temperatures were analysed in the same manner as LTAs. From the analyses it was noticed that some of the mineral matter underwent phase transformation. The process of dehydroxylation was first observed in FTIR results. The observation was confirmed by a decrease in intensity of the infrared bands assigned to the inner hydroxyl group at 3618 cm^{-1}. and 3686 cm^{-1}. The TGA studies by O'Gorman and Walker (1973) indicated that the dehydroxylation process starts from 500°C until 600°C. The product that was formed after dehydroxylation was an amorphous metakaolinite [Cheng *et al.,* 2012], which further transformed to mullite at higher temperatures. The FTIR technique identified mullite and quartz as high temperature minerals that formed in the prepared ashes.

Minerals identified by XRD analysis included anhydrite, quartz, hematite, rutile, anatase and brookite. Quartz was identified as the most dominant mineral, with anhydrite being the second highest mineral reported in HTAs. It was expected that quartz will not undergo any phase transformation because of the temperatures (815°C) the samples were subjected to. Anhydrite was formed as a result of dehydration of sulphate minerals, presumably gypsum.

Most of the minerals that formed in HTA were identified by the mRs technique. The minerals identified included quartz, hematite, magnetite, marcasite, pyrrohotite, anatase, rutile, brookite, anhydrite, cristobalite, nepheline, aragonite, chromite, crednerite, and gypsum. The mRs analysis of HTA showed that HTA was quite heterogeneous in nature, this was noticeable since different mixtures of phases in HTA were identified by the technique. The association of mineral matter plays a significant role in determining the type of slag that forms. Although HT-XRD is used in modelling the behaviour of ashes at high temperature, the technique is still a bulk analysis, and therefore disregards the particle to particle

interactions. Table 6-28 gives a summary of the different minerals identified by different techniques in HTAs.

Table 6-28: Mineral matter identified in high temperature ashes

Minerals (HTA)	**XRD**	**FTIR**	**mRs**
Silicate minerals		Mullite, Quartz	Quartz, Nepheline
Oxides, Hydroxides	Hematite, Zircon Brookite, Anatase Rutile, Quartz		Rutile, Anatase, Brookite, Hematite, Magnetite, Chromite, Crednerite
Sulphides			Pyrite, Pyrrhotite, Marcasite
Phosphates			Apatite
Sulphates	Anhydrite		Gypsum, Anhydrite
Carbonates			Aragonite

From the results it was deduced that mRs was quite suitable for characterising high temperature ash. mRs is not a bulk technique, and therefore, one can control and identify key minerals of interest in the samples.

However, it should also be emphasised that fluorescence is a serious challenge with the mRs technique. Nonetheless, the author is of the view that information derived from mRs and SPA could be used together with thermodynamic models to validate slagging and fouling propensities, and understand the behaviour of minerals at high temperatures.

Slagging and fouling propensities

Slagging and fouling indices, AFT, together with thermodynamic modelling were used to predict slagging propensities of investigated coals. The high temperature phases that are predicted to form include mullite, feldspar, corderite, TiO_2, corundum, immiscible slag phases and gases. From the modelling results, it was observed that mullite was estimated to be high in Coal A. The presence of mullite was confirmed by FTIR analyses of HTA samples. The predicted high concentration of the slag phase in Coal B confirms the low AFT

reported for the sample. Information drawn from the deposition indices indicated that lower AFT reported by coal B was attributed to high concentration of Fe. The results were confirmed by XRD and SPA. This distinctively proved that Fe reduced the melting temperature of eutectics in coal. The observations are in line with what has been reported in literature. The relationship that is drawn between ash composition, ash indices, and AFT indicate that Fe and Ca play a significant role in the slagging and fouling propensity. Pyrite, dolomite, and ilmenite proof to be the minerals responsible for slagging in SA coals investigated.

The limitation of geochemical indicators commonly used to determine the propensity of slagging and fouling in coals were also observed. For example, DAI has been proven to influence slagging. However, there was no correlation between DAI and AFT in this study. Only the Si/Al ratio, Fe/Ca ratio, and Fe content could be related to AFT. Thus the high acid sialic coal B was found to be susceptible to slagging and fouling.

However, it is common that highly basic ashes will be most susceptible to slagging and fouling [Vassilev and Vassileva, 2009]. It is considered that Ca also contributed to the lowering of AFT.

The high clay mineral matter content tends to lower the basicity of coals and the subsequent increase in AFT to temperatures above 1300°C. Similar observations were made by Snyman and Botha (1993) and Bunt *et al.* (2012), whereby coal samples with high clay mineral contents had high AFTs. In their studies, it was also observed that there were minimal changes of AFT with increasing clay mineral content. This behaviour was attributed to the refractory nature of clay minerals. Thus, it is expected that the AFT of coals A, C, and D was relatively high, and this can be explained by the high concentration of clay minerals, with

contribution of sulphate minerals in coal D. The concentration of clay minerals was confirmed by XRF, SPA-EPMXA, petrography, and XRD.

Although thermodynamic models can be used to predict phases, it is important to understand that the input data is equally important. Since thermodynamic modelling depends on input data and equilibrium reached, every effort is to be made to make sure that realistic predictions are achievable. Ideally thermodynamic modelling should not be used separately. Van Dyk *et al.* (2009) found that coupling thermodynamic data with advanced characterisation tools such as high temperature X-Ray diffraction (HT-XRD) provides better insight into mineral interactions and slag formation in gasifiers. In this study, it is observed that mRs can be of value to better understand phase transformations taking place at high temperatures.

It was observed that most of the mineral phases that occurred in HTA were quite heterogeneous, and reported to the slag phase. The mRs technique was capable of discriminating between mixtures that would have been unnoticed with bulk techniques.

The SPA-EPMXA analyses provided more information and insight on the morphology and elemental concentration of elements in coals. Thus, the results obtained from SPA-EPMXA could be understood to provide a true reflection of elemental composition, without inducing any structural or elemental alterations. It is therefore considered that knowledge obtained from SPA-EPMXA and mRs in conjunction with FTIR and XRD techniques can proved to be helpful in understanding phase transformations taking place at high temperatures.

The mRs and SPA-EPMXA allow for high spatial resolution identification of individual elements. This further confirms that both SPA-EPMXA and mRs can easily identify minerals that are present in minute quantities or minerals that are present in a finely disseminated

morphology. However, with mRs, this will only apply if the mineral to be identified is Raman active. The limitation of bulk analysis is reflected by under reporting or exclusion of minerals such as Cl, which are critical in slagging and fouling behaviour of coals. Halite in the form of NaCl or other compounds can exist in the molten phase individually or through formation of eutectic mixtures [Krishnamoorthy and Pisupati, 2015]. The mRs technique was able to detect nepheline ($NaAlSiO_4$) in HTA. This could suggest the sodalite underwent transformation at high temperatures, releasing chloride ions.

Nonetheless, the use of mRs and SPA-EPMXA introduces a new outlook towards increasing knowledge and understanding of coal in conversion processes. The author is of the view that mRs and SPA-EPMXA will be able to characterise the amorphous glass phase, thus giving a good indication of the behaviour of mineral matter and their interaction at high temperatures. Using SPA data as inputs for thermodynamic calculations will improve the modelling of high temperature phases.

This unique and novel approach to gather detailed information about the mineral composition in coal has not been applied to SA or any other coals previously and constitutes a contribution to the field of study. It is quite evident from the most recent work on the determination of mineral matter and elemental composition in SA coals [Matjie *et al.,* 2016] that more knowledge is still required to address challenges in coal conversion processes. Hence the use of mRs and SPA is a step in the right direction towards achieving goals for clean coal technology.

Moreover, the results presented show emphasises on the need for multiple approach studies of mineral matter in coals, as it has been proposed over the years [Stefaniak *et al.,* 2009; Jung *et al.,* 2014; Kumar and Rajmunar, 2014; Matjie *et al.,* 2016]. The use of a multiple technique study distinctively provided a deeper understanding of mineral matter, which could not be

met by a single technique approach, and put into perspective a clearer picture of mineral matter present in coals. The study showed the capabilities and synergy of the different techniques, and valuable information derived from elemental, spot, and bulk analyses of the coal samples investigated. The combination of techniques worked well in terms of characterising mineral matter, since more information was derived from the different techniques combined, compared to results obtained from one technique. The insight provided about the nature of minerals in coal through a combination of SPA-EPMXA and mRS is unrivalled by any other technique or combination of techniques, and can be considered as a new novel contribution made by this investigation. Nevertheless, it remains important that the limitations of each technique are kept in mind.

6.12 Chapter summary

The limited understanding of transformation of mineral matter, and subsequent challenges in coal conversion processes, calls for a comprehensive characterisation of mineral matter in coals. An advanced multiple technique approach has been adopted to address some of these challenges. This chapter presented results obtained from characterisation of mineral matter in SA coals. This was achieved by studying raw coals, LTAs, and HTAs. The principal minerals identified in SA coals included clays, carbonates, sulphides, sulphates, oxides, and hydroxides. The dominant minerals include kaolinite, quartz, pyrite, calcite, dolomite, rutile, and gypsum. The presence of the minerals was confirmed by the various techniques used in this study.

Ash chemistry compositions were used to determine the mineral matter present in coals and to calculate slagging indices. The correlation between ash chemistry and AFT indicated that Fe and Ca influenced the behaviour of coals at high temperatures. Therefore, minerals such as

carbonate and pyrite should be evaluated before the samples are subjected to conversion processes. However, thermodynamic modelling, supported by characterisation techniques are recommended to help predict slagging and fouling propensities in conversion processes.

Clustering of SPA-EPXMA results gave an insight on the abundance and types of mineral matter found in coals. The clustering and PCA were able to put into perspective the elemental compositions by assigning the elements to mineral groups. The analyses were able to report the presence of halite. This was made possible because of high resolutions by the technique. Some of the mineral groups identified by SPA-EPXMA were confirmed by bulk and structural analyses, and in some cases, PCA analysis was put to use to determine the association of minerals in coals, which proved to be valuable.

Comparing ash chemistry to SPA-EPMXA, it was noted that the technique is a closely monitored characterisation method that proved to carefully describe the association of element on a particle to particle basis. The advantage offered by the technique shows that the classification using this approach is more realistic when compared to ash chemistry analysis. Unlike ash composition, which assumes a homogenous ash, SPA-EPMXA exploits the heterogeneous nature of coal particles and gives the true composition of elements.

Overall, the techniques were complimentary to one another in characterising coals fully. More information could be derived when using multiple techniques compared to using one or two techniques. Petrographic analyses gave a broad overview of the mineral matter present in coals. Structural techniques identified the mineral groups classified by petrographic methods. The mRs and XRD techniques easily discriminated between different polymorphs, albeit at different limits of detection. However, no single technique was able to characterise all mineral matter in coals. FTIR was valuable in characterising clay minerals in coals. The mRs

technique proved to be ideal for studying and understanding high temperature transformations. The descriptions and observations of these high temperature transformations by mRs has not been previously described, particularly in SA coals, and is a new contribution to knowledge in the field of study.

Characterisation of individual particles, demonstrated that single particle analyses offers a realistic analyses of materials. Moreover, the application of mRs and SPA-EPMXA can prove to be useful in determining probable mechanisms of formation of high temperature mineral phases. In this study, it was demonstrated that combining SPA-EPMXA, FTIR, mRs, XRD, petrography, and ash chemistry was a worthwhile approach to studying mineral matter in coals.

The knowledge obtained of the mineral matter in coal in this study is unrivalled by any other study previously conducted on SA coals, and especially the confirmation of high temperature phases transitions can prove very useful in dealing with slagging and fouling cases.

However, there were drawbacks related to the techniques, mainly due to detection limits. For example, an optical microscope is ideal to characterise mineral matter that is above 20 µm in size. Moreover, the technique relies on the knowledge of the observer. Thus, the analyses are based on level of experience of the operator. Structural analysis on the other hand can be better understood in depth when techniques such as XRD, FTIR and mRs are used. Nonetheless, the observations made showed that these structural analytical techniques presented advantages and disadvantages.

The XRD technique works well when the composition of materials is above 5 wt.%. In cases where concentrations were below detection limits, mineral matter could not be detected. Therefore, when selecting analytical techniques, one should first identify the need for the

analyses and the intended information that is to be acquired. Nevertheless, the combination of the techniques improved the understanding and knowledge of the coal structures.

Notably, the use of multiple techniques such as XRD, FTIR, mRs, and SPA-EPMXA is unrivalled by any other technique or combination of techniques, and can be considered as a new novel contribution made by this investigation. These findings answers and confirm hypothesis of this research work. Table 6-29 gives a summary of the different mineral matter identified by different techniques. The advantages and limitations of the techniques are also presented.

Table 6-29: Summary of the different techniques

Analytical technique	Petrography	FTIR	mRs	XRD	SPA-EPXMA
Raw coals	Major mineral matter: Kaolinite, quartz: Minor mineral minerals: carbonates, sulphates, and sulphides	Major mineral matter: Kaolinite, smectite, muscovite, illite and quartz	Pyrite, anatase, rutile, quartz, jarosite and calcite.	Clays, carbonates, phosphates, oxides,	Kaolinite, rhodochrosite, microcline, orthoclase, glauconite, fayalite, almandine, ilmenite, anatase, halite, sodalite
Low temperature ashes	----------	Kaolinite, quartz, smectite,illite	Lepidocrite, anhydrite, coquimbite	Similar to raw coals	
High temperature ashes	----------	Quartz, mullite	Hematite, anatase, rutile, brookite, apatite, anhydrous, magnetite, zinc sulphate, chromite,quartz, mixture of mineral matter	Hematite, quartz, zircon, rutile, brookite, anatase, anhydrite	
Advantages	Identify the different morphologies of mineral matter, their origin and association in coals.	Easily characterise clay minerals in coals.	Can resolve close particles, and easily detect mixtures of different mineral matter, no sample preparation is required. Fast execution of results, gives detailed structural information of minerals, easily discriminate between polymorphs	Discriminate between polymorphs	High resolutions, analyses particles of less than 0.5 in diameter. Can identify a wide range of minerals
Limitations	Cannot resolve particles less than 1µm in size, requires a skilled operator.	Limited to analysing clay minerals, overlapping of peaks could make it difficult to identify other mineral matter present.	Fluorescence nature of kaolinite, close control of laser power to avoid burning the sample, topography of the sample can make it difficult to get a good spectrum	Bulk technique, cannot analyse particles below 1 wt.%	Can be restricted by chemical boundary criteria

CHAPTER 7: CONCLUSIONS AND RECOMMENDATIONS

As discussed in Chapter 1, the coal industry is faced with serious challenges to meet soaring energy demands, improved efficiencies, and adhere to stringent legislation. For sustainability of coal reserves, to meet energy demand, and to achieve the emission restrictions, CCTs seem to be the viable option to revolutionise the coal industry, and ultimately change perceptions surrounding coal conversion processes. The successful inception of CCTs will result in processes operating at higher efficiency targets, and consequently, reduced emissions of hazardous greenhouse gases, TEs, and PM. Nonetheless, it is apparent that a comprehensive understanding of mineral matter using characterisation techniques must be a primary focal area of interest before investing in expensive technologies.

The objectives of this research work were to quantitatively and qualitatively characterise raw coals and coal ashes using the proposed multiple techniques, and evaluate how the multiple technique approach helps to better understand mineral matter. The adopted approach involved studying mineral matter on an elemental basis using XRF and SPA-EPMXA. The results were correlated with analytical techniques such as petrography, XRD, FTIR and mRs.

The following research questions posed in this study were addressed, and the main findings of this work are summarised as follows:

(i) Is there a need for multi-technique characterisation of mineral matter in coals?

The results computed from the generated data provided evidence and confirmed there is a greater need for the coal industry to adopt the multiple technique approach over a single technique approach. From the results, holistic information can be obtained from elemental analyses, physical properties and the bulk analyses.

Elemental analysis using EPXMA on single particles showed the different associations of mineral matter, identifying some of the elements that could not be identified by alternative analytical tools. Coal petrography can be used to gain an overall overview of mineral matter, their organic and inorganic association, and the rank of coal. The XRD and FTIR analyses remain the ideal techniques to characterise clay mineral matter in coals. The mRs technique was able to identify mineral matter such as pyrite, anatase, rutile, carbonates, and quartz in raw coals.

Analyses of coal ashes were conducted to study and understand mineral matter without the interference of the organic matter in coals. The findings showed that effect of removing organic matter using low temperature ashing methods were beneficial in the XRD analyses. However, analysing LTA's using mRs did not introduce any significant improvement on the mRs analyses compared to raw coals. This could be due to the high kaolinite content in LTA samples, which caused fluorescence. The XRD analyses on the HTA have revealed an abundance of glass phases, which were amorphous in nature. The results further elucidated the reactions and phase transformation that took place at around 815°C. Characterisation of HTA using mRs showed that the phases formed are not single homogenous phases, but mixtures of different high temperature minerals.

(ii) How does a multi-technique approach benefit the coal industry?

The use of multiple technique approach addresses both environmental and technological challenges presented by mineral matter. Knowledge of mineral matter in coals can help predict behaviour of mineral matter in conversion processes.

(iii) What are the benefits of using mRs over other analytical techniques?

The mRs technique is sensitive to structural defects and structural deformation. The ability to characterise the different mixtures in coal ashes provided an insight concerning the interaction of mineral matter at high temperatures. This interaction was not displayed by any other technique. This was an indication that the technique can be easily adapted to study and understand the different combustion products. Moreover, integration of various analytical techniques presented improved the basis for evaluating ash forming processes. The application of mRs and SPA-EPMXA can prove to be useful in determining probable mechanisms of formation of high temperature materials, and provide additional information not obtainable with any other single technique or combination of techniques.

(iv) What are the possibilities of using mRs as an on-line technique?

Using mRs as an on-line technique proves to be challenging. This is mainly due to the amorphous nature of coal, fluorescence mostly due to clay minerals, topography, and heterogeneity of the complex structure. The different minerals do not all give a good Raman spectrum at the same laser power, therefore the power has to be adjusted accordingly. However, high laser power has the potential to destroy the sample. These challenges diminish the possibilities of mRs applications as an on-line technique, most especially for an amorphous and heterogeneous structure like coal.

(v) How does mineral matter influence coal behaviour in coal conversion processes?

From the study, it can be concluded that elemental and structural composition of coal influences the behaviour of coals. For example, sulphur in the form of pyrite influence AFT, whilst organic sulphur will contribute to the formation of SOx.

Understanding the form in which elements are present and the mineralogical structure they are associated with will help elucidate the overall impact, and remedial measures that will be necessary to minimise the effect of such mineral matter in combustion processes.

From the investigations, the following conclusions based on the study were reached:

- The use of SPA-EPMXA together with optical and structural techniques such as petrography, FTIR, XRD, and mRs offers novel characterisation capabilities that are not possible when using one conventional analytical technique.
- From the study it was observed that the use of multiple techniques contribute greatly to a holistic understanding of a heterogeneous material such as coal. Using multiple techniques will not only minimise the effect presented by limitations of each technique, but also reduce the errors presented by each single technique.
- This study elucidated the capabilities of using mRs. The mRs will benefit the coal industry in investigating high temperature conversions.
- A significant advantage of mRs over FTIR and XRD is that information on mineral phases of interest can be attained directly.
- It was relatively easy to study the transformation that the clay mineral, kaolinite, undergoes when exposed to high temperatures, using FTIR. Although the technique was successful in characterising the different types of clay minerals, there were limitations displayed by the technique. The major limitation of using FTIR was the inability to identify most of the mineral matter found in either raw coals or coal ashes. Thus, it was necessary to use techniques such as XRD, petrography, and mRs to fully characterise mineral matter in coals.

- The mRs technique could not positively identify kaolinite, despite previous documented work, where mRs was used to characterise clay minerals [Michaelian, 1986]. The challenge of using mRs was mainly due to weak Raman signals by clay minerals, fluorescence and photodegradation of samples. As a result, the technique could not positively identify kaolinite, which was presumed to be the dominant mineral matter, as detected by various other techniques.
- The mRs technique proved to be suitable in characterising HTA samples. From the analyses, it was possible to characterise the different mineral mixtures and discriminate between various polymorphs. The other advantage presented by the technique was the rate at which results were acquired. Although sample preparation was not important with mRS, it was observed that surface topography could influence the Raman intensity. Again, close power control was necessary, to avoid damaging the samples.
- The optical microscope proved to be ideal for characterising mineral matter, maceral matter and association of mineral matter in coals with micro-structural resolution greater than 20 nm.
- The use of XRD, mRs, FTIR and thermodynamic modelling can be a useful tool to study phase transformations taking placing in coal conversion processes.
- High concentration of pyrite, calcium and silica content, increases the propensity of coals to form slagging and fouling.
- Pyritic sulphur has more influence and effect on slagging propensity than any other form of sulphur.
- The slagging and fouling parameters are largely dependent on the compositional structure and morphology of minerals of interest.

- Continuous development should be undertaken to improve ways of characterising mineral matter in coals.

7.2 Recommendations

The research work presented an area of knowledge that still needs further development to achieve sustainable gains, and achieve desired efficiencies and emission targets. With the endless improvement of the different techniques available on the market, the characterisation of coals should be easier, faster and more comprehensive. Moreover, the information derived from the characterisation of coals should be easily translated into the functional prediction of coals in conversion processes.

The following are suggested recommendations derived from the present study, and to be considered for future work:

- The use of multiple technique present avenues that help in understanding mineral matter, thus it is suggested in order to understand mineral matter, more techniques can be incorporated, including microscopic studies, which could assist in characterising mineral matter and TE and their mode of occurrence without performing selective leaching methods.
- Due to the amorphous nature of coal, it is suggested that a combination of techniques should be selected in such a way that the amorphous matter in coal and the crystalline matter are adequately characterised separately.
- Due to the heterogeneous nature of coals, predictive models used for slagging and fouling propensities should use inputs from all techniques that give more information about the combustion process, such that the predictions are more accurate.

- Consider using FT-Raman spectroscopy, since it has been reported that the technique minimises fluorescence in clay minerals, thereby subsequently, improving the signal to noise ratio, and reducing the effect of degradation of samples.
- The possible combination of SPA-EPXMA, CCSEM, HT-XRD, and mRs in fouling and slagging investigations could fruitfully be further exploited.
- Use mRs to characterise slag and ash that formed under combustion or gasification operating conditions.

8. References

Akar, G., İpekoğlu, Ü (2007), Relationship between ash fusion temperatures (AFT) and coal mineral matter in some Turkish coal ashes, The Journal of Ore Dressing, Vol. 9, Issue 17, pp 33-39.

Aktaş, Z., Karacan, F., Olcay, A., (1998), Centrifugal float-sink separation of fine Turkish coals in dense media, Fuel Processing Technology, Vol. 55, pp 235-250.

Arsov, L.J.D., Kormann, C., Plieth, W., (1991), Electrochemical synthesis and in-situ Raman spectroscopy of thin films of titanium dioxide, Journal of Raman Spectroscopy, Vol. 22, pp 573.

Arvelakis, S., Vourliotis, P., Kakaras, E., Koukios, E.G., (2001), Effect of leaching on the ash behaviour of wheat straw and olive residue during fluidized bed combustion, Biomass and Bioenergy Vol. 20, Issue no. 6, pp 459-470.

Attalla, M., Morgan, S., Riley, K., (2004), Trace element deportment in combustion processes, Cooperative research centre for coal in sustainable development (CCSD) Report 50, pp 128.

Baafii, E.Y., Ramanif, R.V., (1979), Rank and maceral effects on coal dust generation, International Journal of Rock Mechanics and Mining Sciences, Vol. 16, pp 107-115.

Babat, S., Maier, J., Scheffknecht, G., Stein-Brzozowka, G., Miller, E., (2011), Deposition behaviour of a bituminous coal in a large pulverized fuel power plant, Proceedings of International Conference on heat exchanger fouling and Cleaning, June 05-10, Crete Island, Greece, pp 156-163.

Baker, L., (2015), The evolving role of finance in South Africa's renewable energy sector, Geoforum, Vol. 64, pp 146-156.

Bandopadhyay, A.K., (2010), A study on the abundance of quartz in thermal coals of India and its relation to abrasion index: Development of predictive model for abrasion, International Journal of Coal Geology, Vol. 84, pp 63-69.

Baruah, M.K., Kotoky, P., Borah, G.C., (2003), Distribution and nature if organic/mineral bound elements in Assam coals, India, Fuel, Vol. 82, pp 1783-1791.

Benson, S.A., Sondreal, E.A., Hurley, J.P., (1995), Status of coal ash behavior research, Fuel Processing Technology, Vol. 44, pp 1-12.

Bensted, J, Varma, S.P., (1974), Some applications of infrared and Raman spectroscopy in cement chemistry, Cement Technology, Vol. 5, Issue 5, pp 440-442.

Betsch, R.J., Park, H.L., White, W.B., (1991), Raman spectra of stoichometric and defect rutile, Materials Research Bulletin, Vol. 26, pp 613-622.

Beyer, M., Ebner, H,G., Assenmacher, H., Figge, L., (1987), Elemental sulphur in microbiologically desulphurized coal, Fuel, Vol. 66, pp 551-555.

Beyssac, O., Goffé, B., Petitet, J., Froigneux, E., Moreau, M., Rouzaud, J., (2003), On the characterization of disordered and heterogeneous carbonaceous materials by Raman spectroscopy, Spectrochimica Acta Part A, Vol. 59, pp 2267-2276.

Beér, J.M., Sarofim, A,F., Barta, L.E., (1992), From properties of coal mineral matter to deposition tendencies of fly ash-a modeling route, Journal of the Institute of Energy, Vol 65, pp 55-62.

Borrego, A.G., Alvarez, D., Menéndez, R., (1997), Effects of inertinite content in coal on char structure and combustion, Energy and Fuel, Vol. 11, pp 702-708.

Bosman, R., (1983), Determination of the inorganic matrix of coal ash from an atmospheric fluid-bed boiler by FTIR analysis, Fuel, Vol. 62, pp 1009-1012.

Buhre, B.J.P., Elliot, L.K., Sheng, C.D., Gupta, R.P., Wall, T.F., (2005), Oxy-fuel combustion technology for coal fired power generation, Progress Energy Combustion Science, Vol. 31.pp 283.

Bunt, J.R., Waanders, F.B., Schobert, H., (2012), Behaviour of selected major elements during fixed-bed gasification of South African bituminous coal, Journal of Applied Pyrolysis, Vol. 93, pp 85-94.

Buzgar, N., Apopei, A.I., Buzatu, A., (2013), Characterization and source of Cucuteni black pigment (Romania): vibrational spectrometry and XRD study, Journal of Archaeological Science, Vol. 40, pp 2128-2135.

Cairncross, B., Winter, M.F.W., (1984), High-constructive lobate deltas in the Lower Permian Vryheid Formation, Rietspruit, South Africa, Transactions of the Geological Society of South Africa, Vol. 87, pp 101–110.

Cairncross, B., Cadle, A.B., (1988), Palaeoenvironmental control on coal formation, distribution and quality in the Permian Vryheid Formation, East Witbank Coalfield, South Africa, International Journal of Coal Geology, Vol. 9, Issue no.4, pp 343-370.

Cairncross, B., (2001), An overview of the Permian (Karoo) coal deposits of southern Africa, Journal of African Earth Sciences, Vol. 33, pp 529-562.

Calkins, W.H., (1994), The chemical forms of sulfur in coal:a review, Fuel, Vol. 73, No. 4, pp 475-484.

Catuneaunu, O., Hancox, P.J., Rubidge, B.S., (1998), Reciprocal flexural behaviour and contrasting stratigraphies:a new basin development model for the Karoo retroarc foreland system, South Africa, Basin Research, Vol. 10, pp 417-439.

Chakravarty, S., Mohanty, A., Banerjee, A., Tripathy, R., Mandal, G.K., Basariya, R., Sharma, M., (2015), Composition, mineral matter characteristics and fusion behavior of some Indian coals, Fuel, Vol. 150, pp 96-101.

Chatterjee, N.N., (1942), Free sulphur in some weathered tertiary coal specimens of India, Quarterly Journal of Geological, Mining and Metallurgical Society of India, Vol. 14, pp 1-7.

Chen, M., Shu, J., Xie, X., Mao, H., Natural $CaTi_2O_4$ structures $FeCr_2O_4$ polymorph in the Suizhou meteorite and its significance in mantle mineralogy, (2003), Geochemica et Cosmochimica Acta, Vol. 67, pp 3937-3942.

Chen, H.Y., Lin, Y.C., Lee, J.S., (2015), Crednerite-$CuMnO_2$ thin films prepared using atmospheric pressure plasma annealing, Applied Surface Science, Vol. 338, pp 113-119.

Chen, Y., Mastalerz, M., Schimmelmann, A., (2012), Characterization of chemical functional groups in macerals across different ranks via micro-FTIR spectroscopy, International Journal of Coal Geology, Vol. 104, pp 22-33.

Chen, T., Yan, B., Lei, C., Xiao, X., (2014), Pollution control and metal resource recovery for acid mine drainage, Hydrometallurgy, Vol. 147-148, pp 112-119.

Cheng, H., Liu, Q., Yang, J., Mac, S., Frost, R.L., (2012), The thermal behaviour of kaolinite intercalation complexes-A review, Thermochimica Acta, Vol. 545, pp1-13

Chou, C., (2012), Sulfur in coals: A review of geochemistry and origins, International Journal of Coal Geology, Vol. 100, pp 1-13.

Clarke, L.B., (1993), The fate of trace elements during coal combustion and gasification: an overview, Fuel, Vol. 72. No. 6, pp 731-736.

Cloke, M. Lester, E., (1994), Characterization of coals for combustion using petrographic analysis: a review, Fuel, Vol. 73, No.3, pp 315-320.

Cloke, M., Gilfillan, A., Lester, E., (1997), The characterization of coals and density separated coal fractions using FTIR and manual and automated petrographic analysis, Fuel, Vol. 76. No. 13, pp 1289-1296.

Cole-Clarke, P.A., Vassallo, A.M., (1992), Infrared emission spectroscopy of coal, Fuel, Vol. 71, pp 469-470.

Coleyshaw, E.E., Griffth, W.P., Bowell, R.J., (1994), Fourier Transform, Raman spectroscopy of minerals, Spectrochimica Acta, Part A, Vol. 50A, pp 1909-1918.

Creelman, R.A., Ward, C.R., (1996), A scanning electron microscope method for automated, quantitative analysis of mineral matter in coal, International Journal of Coal Geology, Vol. 30, pp 249-269.

Dabrowski, J.M., Ashton, P.J., Murray, K., Leaner, J.J., Mason, R.P., (2008), Anthropogenic mercury emissions in South Africa: Coal combustion in power plants, Atmospheric Environment, Vol. 42, pp 6620-6626.

Dai, S., Li,D., Chou, C., Zhang, Y., Ren, D., Ma, Y., Sun Y., (2008), Mineralogy and geochemistry of boehimite-rich coals: new insights from the Haerwusu surface mine, Jungar coalfield, Inner Mongolia, China, International Journal of Coal Geology, Vol. 74, pp 185-202.

Dai, S., Ren, D., Zhou, Y., Chou, C., Wang, X., Zhao, L., Zhu, X., (2008b), Mineralogy and geochemistry of a superhigh-organic-sulfur coal, Yanshan Coalfield, Yunnan, China: Evidence for a volcanic ash component and influence by submarine exhalation, Chemical Geology, Vol. 255, pp 182-194.

Dai, S., Wang, X., Zhou, Y., Hower, J.C., Li, D., Chen, W., Zhu, X., Zou, J., (2011), Chemical and mineralogical compositions of silicic, mafic, and alkali tonsteins in the late Permian coals from the Songzao Coalfield, Chongqing, Southwest China, Chemical Geology, Vol. 282, pp 29–44.

Das, S., Hendry, M.J., (2011), Application of Raman spectroscopy to identify iron minerals commonly found in mine wastes, Chemical Geology, Vol. 290, pp 101-108.

Davidson, R.M., (1996), Trace elements in coal, Energeia, Vol. 7, no. 3, pp 1-5.

Davidson, R., (2000), Modes of occurrence of trace elements in coal-Results from an international collaborative programme. CCC/36 IEA Clean Centre, London, UK.

De Farai, D.L.A., Venâncio Silva, S., de Oliveira, M.T., (1997), Raman micro-spectroscopy of some iron oxides and oxyhydroxides, Journal of Raman Spectroscopy, Vol. 28, pp, 873-878.

Demirbas, A., (2005), Potential application of renewable energy sources, biomass combustion problems in boiler power systems and combustion related environmental issues, Progress in Energy and Combustion Science, Vol. 31, pp 171-192.

Denisov, V.N., Mavrin, B.N., Podobedov, V.B., Sterin, K, E., (1986), A study of the non-symmetry of the hyper-Raman tensor in α-quartz using two frequency excitation, Optics Communication, Vol. 60, No. 1-2, pp 95-98.

De Vito, M.S., Rosendale, L.W., Conrad, V.B.,(1994), Comparison of trace element contents of raw and clean commercial coals, Fuel Processing Technology, Vol. 39, pp 87–106.

Diehl, S.F., Goldhaber, M.B., Hatch, J.R., (2004), Modes of occurrence of mervury and other trace elements in coals from the warrior field, Black Warrior Basin, Northwestern Alabama, International Journal of Coal Geology, Vol. 59, Issue 3-4, pp 193-208.

Domazetis, G., Raoarun, M., James, B.D., Liesegang, J., Pigram, P.J., Brack, N., Glaisher, R., (2006), Analytical and characterization studies of organic and inorganic species in brown coal, Energy and Fuel, Vol. 20, pp 1556-1564.

Duran, J.E., Mahassay, S.R., Stock, L.M., (1986), The occurrence of elemental sulphur in coals, Fuel, Vol. 65, pp 1167-1168.

Durie, R.A., (1961), The inorganic constituents in Australian brown coals: III Morwell and Yallourn brown coals, Fuel 40, pp 407-422.

Eckert, M., (2012), Max von Laue and the discovery of X-ray diffraction in 1912, Annalen der Physik, Vol. 524, Issue no. 5, pp A83-A85.

Ehrlich, B.J., Hall, R.C., Anderson, R.J., Cox, H.G., (1981), Sulfur detection in hydrocarbon matrices. A comparison of the flame photometric detector and the 700A Hall TM electrolytic conductivity detector, Journal of Chromatographic Science, Vol. 19, Issue 5, pp 245-249.

Ekosse, G.E., (2005), Fourier Transform Infrared Spectrophotometry and X-ray diffractometry as complementary techniques in characterising clay size fraction of kaolin, Journal of Applied Science and Environmental Management, Vol. 9, Issue 2, pp 43-48.

Engelbrecht, A,D., North, B.C, Hadley, T.D., (2007), Investigation into the gasification characteristics of SA power station coals, 24th Annual International Pittsburg Coal Conference, Johannesburg, South Africa, 11-14 September, pp 21.

Engelbrecht, A,D., North, B.C, Hadley, T.D., (2008), Clean coal technology: Gasification of South African coals, Industrial Fluidization South Africa (IFSA), Johannesburg, South African Institute of Mining and Metallurgy, pp188-202.

Estep, P.A., Kovach, J.J., Karr. Jr. C., (1968), Analytical Chemistry, Vol. 40, no. 2, pp 358-363.

Evans, J.R., Sellars, G.A., Johnson, R.G., (1990), Analysis of eight Argonne Premium coal samples by X-ray fluorescence spectroscopy, Energy Fuels, Vol. 4, pp 440-442.

Everson, R., Koekemoer, A., Bunt, J., Neomagus, H., Schwarz, C., (2013), Detailed characterization of South African high mineral matter-inertinite-rich coals and density

fractions and effect of reaction rates with carbon dioxide: Macerals, microlithotypes, carbominerites and minerals, South African Journal of Chemical Engineering, Vol. 18, No.1, pp 1-16.

Fabiańska, M.J., Kruszewska, K.K., (2003), Relationship between petrographic and geochemical characterisation of selected South African coals, International Journal of Coal Geology, Vol. 54, pp 95–114.Falcon, R.M.S., (1986), The coalfields of southern Africa: an introduction, Mineral deposits of Southern Africa, Vol. II, Geological Society of South Africa, Johannesburg, pp 1879-1899.

Falcon, R., Snyman, C., (1986), An introduction to coal petrography: Atlas of petrographic constituents in the bituminous coals of Southern Africa, The Geological Society of South Africa, Review paper, No. 2, pp 27.

Falcon, R.M.S., (1989), A brief review of the origin, formation and distribution of coal in Southern Africa. In: Anhaeusser and Maske (Editors), Mineral deposits of Southern Africa, II, Geological Society of South Africa, pp 1879-1899.

Falcon, R., Ham, A.J., (1988), The characteristics of Southern African coals, Journal of the South African Institute of Mining and Metallurgy, Vol. 88, no.5, pp 145-161.

Falcon, R.M.S., (1989), Macro-and micro factors affecting coal-seam quality and distribution in southern Africa with particular reference to the No. 2 seam, Witbank coalfield, South Africa, International Journal of Coal Geology, Vol. 12, pp 681-731.

Farmer V.C., (1974) The layer silicates. *Infrared Spectra of Minerals* (V.C. Farmer, editor), Mineralogical Society, London. pp. 331-363.

Farmer, V.C., (2000), Transverse and longitudinal crystal modes associated with OH stretching vibrations in single crystals of kaolinite and dickite, Spectrochimica Acta Part A: Molecular and Biomolecular Spectroscopy, Vol. 56, Issue no. 5, pp 927-930.

Fauconnier, C.J 2005: Investing in African mining conference: Waterberg the future of the South African coal mining, http://www.exxaro.com. Accessed: 16 July 2014.

Fernández-Martínez, G., López-Mahía, P., Muniategui-Lorenzo, S., Prada-Rodríguez, D., Fernández- Fernández, E., (2001), Distribution of volatile compounds during the combustion process in coal-fired power stations, Atmospheric Environment, Vol. 35., pp 5823-5831.

Finkelman, R.B., (1982), Mode of occurrence of trace elements and minerals in coal: An analytical approach, In: Atomic and Nuclear Methods in Fossil Energy Research, R.H Filby, R.H., Carpenter, B.S., Ragaini, R.C., Eds, Plenum, New York, pp 141-149.

Finkelman, R.B., Palmer, C.A., Krasnow, M.R., Aruscavage, P.J., Seller, G.A., Dulong, F.T., (1990), Combustion and leaching behaviour of elements in the Argonne Premium coal samples, Energy Fuels, Vol. 4, No.6, pp 755-766.

Finkelman, R.B., (1994), Modes of occurrence of potentially hazardous elements in coal: levels of confidence, Fuel Processing Technology, Vol. 39, pp 21-34.

Finkelman, R.B., Gross, P.M.K., (1999), The types of data needed for assessing the environmental and human health impacts of coal, International Journal of Coal Geology, Vol. 40, pp 91-101.

Frankie, K.A., Hower, J.C., (1985), Pyrite/marcasite size, form and microlithotype association in western Kentucky prepared coals, Fuel Processing Technology, Vol. 10, pp 269-283.

Frost, R.L., Gobac, Z., Lopez, A., Xi, Y., Scholz, R., Lana, C., Malena, R., Lima, F., (2014), Characterization of the sulphate mineral coquimbite, a secondary iron sulphate from Javier Ortega mine, Lucanas Province, Peru – using infrared, Raman spectroscopy and thermogravimetry, Journal of Molecular Structure, Vol 1063, pp 251-258.

Gaigher, J.L., (1980), The mineral matter in some South African coals, Fuel Research Institute of South Africa, Pretoria, Report 45.

Garcia, A.B., Martinez-Tarazona, M.R., (1993), Removal of trace elements from Spanish coals by flotation, Fuel, Vol. 72, pp 329-335.

Garcia-Vallès, M., Pradell, T., Martinez, S., Vendrell, M., (1993), Mineralogical characterization of the Garumnian subbituminous lignite from the central Pyrenees by SEM-EDX, X-ray diffraction and Mössbauer spectroscopy, Fuel, Vol. 72, no. 7, pp 971- 975.

Gehring, A.U., Hofmeister, A.M., (1994), The transformation of lepidocrocite during heating a magnetic and spectroscopic study, Clays and Clay Minerals, Vol. 42, No. 4, pp 409-415.

Geldenhuis, S., Bell, F.G., (1998), Acid mine drainage at a coal mine in the eastern Transvaal, South Africa, Environmental Geology, Vol. 34, Issue 3/4, pp234-242.

Gentzis, T., Goodarzi, F., Koukouzas, C.N., Foscolos, A.E., (1996), Petrology, mineralogy, and geochemistry of lignites from Crete, Greece, International Journal of Coal Geology, Vol. 30, Issue no.1-2, pp 131-150.

Gentzis, T., Goodarzi, F., (1999), Chemical fractionation of trace elements in coal and coal ash, Energy Sources, Vol. 21, Issue no. 3, pp 233-256.

Given, P.H., Yarzab, R.F., (1979), Analysis of the organic substance of coals; Problems posed by the presence of mineral matter, in Karr, C, ed. Analytical Methods for coal and coal products, Vol.2, Academic Press, New York.

Given, R.N., Miller, P.H., (1987), The association of major, minor and trace inorganic elements with lignites. III. Trace elements in four lignites and general discussion of all data from this study, Geochimica et Cosmochimica Acta, Vol. 51, pp 1843-1853.

Glasspool, I.J., (2003), Hypautochthonous-allochthonous coal deposition in the Permian, South African, Witbank Basin No. 2 seam; a combined approach using sedimentology, coal petrology and palaeontology, International Journal of Coal Geology, Vol. 53, pp 81-135.

Gluskoter, H.J., (1965), Electronic low-temperature ashing of bituminous coal, Fuel, Vol. 44, 285-291.

Gluskoter, H.J., (1975), Mineral matter and trace elements in coal, Illinois State Geological Survey, Urbana, Ill, 61801, pp 1-22.

Gluskoter, H.J., Ruch, R.R., Miller, W.G., Cahill, R.A., Dreher, G.B., Kuhn, J.K., (1977), Trace elements in coal: occurrence and distribution, Illinois State Geological Survey Circular, Vol. 499, pp 154.

Gottlieb, P., Agron-Olshina, N.A., and Sutherland, D., (1991), The automatic measurement of minerals in coal and fly ash: In Proceedings of the Engineering Foundation Conference on Inorganic Transformations and Ash Deposition during Combustion, Palm, Coast, FL.

Gould, K.W, Smith, J.W., (1979), The genesis and isotopic composition of carbonates associated with some Permian Australian coals, Chemical Geology, Vol. 24, pp 137-150.

Gray, D., (1978), Inherent mineral matter in coal and its effect upon hydrogenation, Fuel, Vol. 57, Issue 4, pp 213-216.

Gray, R.J., (1991), Some petrographic applications to coal, coke and carbons, Organic Geochemistry, Vol. 17, No. 4, pp 535-555.

Green, P.D., Johnson, C.A., Thomas, K.M., (1983), Application of laser Raman microprobe spectroscopy to the characterisation of coals and coke, Fuel, Vol. 62, Issue no. 9, pp 1013-1023.

Griffin, G.M., (1971), Interpretation of X-ray diffraction data, in Carver, R.E., ed., Procedures in Sedimentary Petrology: New York, Wiley, pp 541-569.

Grigore, M., Sakurovs, R., French, D., Sahajwalla, V., (2008), Mineral matter in coals and their reactions during coking, International Journal of Coal Geology, Vol. 76, pp 301-308.

Groves, S.J., Williamson, S.J., Sanyal, A., (1987), Decomposition of pyrite during pulverized coal combustion, Fuel, Vol. 66, Issue 4., pp 461-466.

Guedes, A., Valentim, B., Prieto, A.C., Rodrigues, S., Noronha, F., (2010), Micro-Raman spectroscopy of collotelinite, fusinite and macrinite, International Journal of Coal Geology, Vol. 83, pp 415-422.

Guo, Y., Renton, J.J., Penn, J.H., (1996), FTIR micro spectroscopy of particular liptinite-(lopinite) rich, Late Permian coals from Southern China, International Journal of Coal Geology, Vol. 29, pp 187-197.

Gupta, R.P., Wall, T.F., Kajigaya, I., Miyamae, S., Tsumita, Y., (1998)., Computer-controlled scanning electron microscopy of minerals in coal-implications for ash deposition, Progress in Energy and Combustion Science, Vol. 24, Issue, 6., pp 523-543.

Gupta, R, Wall, T.F., Baxter, L.A., (Eds.), (1999) The Impact of Mineral Impurities in Solid Fuel Combustion, Plenum Publishers, New York, pp 768.

Gupta, S., Al-Omari, Y., Sahajwalla, V., and Fench, D., (2006), Influence of carbon structure and mineral association of coals on their combustion characteristic for pulverised coal injection (PCI) application, Metallurgical and Materials Transactions B, Vol 37B, pp 457-473.

Gupta, R. (2007), Advanced coal characterization: A review, Energy and Fuels, Vol. 21, pp 451-460.

Hagelskamp, H.H.B., Snyman, C.P., (1988), On the origin of low-reflecting inertinites in coals from the Highveld Coalfield, South Africa, Fuel, Vol. 67, pp 307-313.

Hai-tao, W., Ling-xue, K., Jin, B., Zong-qing, B., Dong-mei, L., Wen, L., (2015), Transformation of minerals in direct coal liquefaction residue under gasification atmosphere at high temperatures, Journal of Fuel Chemistry and Technology, Vol. 43, Issue no. 3, pp 257-265.

Hanapi, N., Dai, S.A.M (2012), A study on the airborne particulates matter in selected museums of Peninsular Malaysia, Procedia-Social and Behavioral Science, Vol. 50, pp 602-613.

Hancox, P.J., Götz, A.E., (2014), South Africa's coalfields - A 2014 perspective, International Journal of Coal Geology, Vol. 132, pp 170-254.

Hanesch, M., (2009), Raman spectroscopy of iron oxides and (oxy)hydroxides at low laser power and possible applications in environmental magnetic studies, Geophysical Journal International, Vol. 177, pp 941-948.

Harding, N.S., O'Connor, D.C., (2007), Ash deposition impacts in the power industry, Fuel Processing Technology, Vol. 88, pp 1082-1093.

Hartnady, C., (2010), South Africa's diminishing coal reserves, South African Journal of Science, Vol. 106, Issue 9/10, pp 1-5.

Hatt, R.M., (1990), Fireside deposits in coal-fired utility boilers, Progress Energy Combustion Science, Vol. 16, pp 235-241.

Hattingh, B.B., Everson, R.C., Neomagus, H.W.J.P., Bunt, J.R., (2011), Assessing the catalytic effect of coal ash constituents on the CO_2 gasification rate of high ash South African coal, Fuel Processing Technology, Vol. 92, pp 2048-2054.

Hill, R.D., Bates, E.R., (1979), Acid mine drainage and subsidence: Effects of increased coal utilization, Environmental Health Perspectives, Vol. 33, pp 117-190.

Hindmarsh, C.J., Wang, W., Thomas, K.M., Crelling, J.C., (1994), The release of nitrogen during the combustion of macerals, microlithotypes and their chars, Fuel, Vol. 73, Issue 7, pp 1229-1234.

Hippo, E., Walker, P.L., (1975), Reactivity of heat treated coals in carbon dioxide, at 900°C, Fuel, Vol. 54, pp 245-248.

Hirano, K., Kouzu, M., Okada, T., Kobayashi, M., Ikenaga, N., Suzuki, T., (1999), Catalytic activity of iron compounds for coal liquefaction, Fuel, Vol. 78, pp 1867-1873.

Holland, M.J., Cadle, A.B., Pinheiro, R., Falcon, R.M.S., (1989), Depositional environments and coal petrography of the Permian Karoo Sequence: Witbank Coalfield, South Africa, International Journal of Coal Geology, Vol. 11, Issue 2, pp 143-169.

Hower, J.C., Graese, A.M., Klapheke, J.G., (1987), Influence of microlithotype composition of Hardgrove grindability index for selected Kentucky coals, International Journal of Coal Geology, Vol. 7, pp 227-244.

Huang, Y., Jin, B., Zhong, Z., Xiao, R., Tang, Z., Ren, H., (2004), Trace elements (Mn, Cr, Pb, Se, Zn, Cd and Hg) in emissions from a pulverized coal boiler, Fuel Processing Technology, Vol. 86, pp 23– 32.

Huffman, G.P., Huggins, F.E., Dunmyre, G.R., (1981), Investigation of the high-temperature behaviour of coal ash in reducing and oxidizing atmospheres, Fuel, Vol. 60, 585-597.

Huffman, G.P., Huggins, F.E., Shah, N., Shah, H., (1990), Behaviour of basic elements during coal combustion, Progress in Energy Combustion Science, Vol. 16, pp 243-251.

Huggins, F.E., Shah, N., Huffman, G.P., Kolker, A., Crowley, S., Palmer, C.A., Finkelman, R.B., (2000), Mode of occurrence of chromium in four US coals, Fuel Processing Technology, Vol 63, Issues 2-3, pp 79-92.

Huggins, F.E., (2002), Overview of analytical methods for inorganic constituents in coal, International Journal of Coal Geology, Vol. 50, pp 169-214.

Hutton, A., Mandile, A.J., (1996), Quantitative XRD measurement of mineral matter in Gondwana coals using the Rietveld method, Journal of African Earth Sciences, Vol. 23, Issue 1, pp 61-72.

Illiev, M.N., Hadjiev, V.G., Litvinchuk, A.P., (2013), Raman and infrared spectra of brookite (TiO_2): Experiment and theory, Vibrational Spectroscopy, Vol 64, pp 148-152.

International Committee for Coal and Organic Petrology (ICCP), (1998), The new vitrinite classification (ICCP System 1994), Fuel, Vol. 77, Issue no. 5, pp.349.

International Committee for Coal and Organic Petrology (ICCP), (2001), The new inertinite classification (ICCP System 1994), Fuel, Vol. 80, pp.459.

ISO 7404 – 2 (International Standards Organization), (1985), Methods for the petrographic analysis of bituminous coal and anthracite, Part 2: Method of preparing coal samples. Standards South Africa.

ISO 7404 – 4 (International Standards Organization), (1985), Methods for the petrographic analysis of bituminous coal and anthracite. Part 4: Method of determining microlithotype, carbominerite and minerite composition. Standards South Africa.

Izquierdo, M., Moreno, N., Font, O., Querol, X., Alvarez, E., Antenucci, D., Nugteren, H., Luna, Y., Fernández-Pereira, C., (2008), Influence of the co-firing on the leaching of trace pollutants from coal fly ash, Fuel, Vol. 87, pp 1958-1966.

Jambers, W., Smekens, A., Van Grieken, R., Shevchenko, V., Gordeev, V., (1997), Characterisation of particulate matter from Kara Sea using electron probe X-ray micro analysis, Colloids and Surfaces, A, Vol. 120, pp 61-75.

Jeffrey, L.S., (2005), Characterization of coal resources of South Africa, The Journal of the South African Institute of Mining and Metallurgy, pp 95-102.

Jehlička, J., Beny, C., (1992), Application of Raman microspectrometry in the study of structural changes in Precambrian kerogens during regional metamorphism, Organic Geochemistry, Vol. 18, no.2, pp 211-213.

Jenkins, R.G., Nandi, S., Walker, P.L., (1973), Reactivity of heat-treated coals in air at 500°C, Fuel, Vol. 52, pp 288-293.

Jenkins, R.G., Walker, P.L. Jr., (1978), Analysis of mineral matter in coals, Analytical methods for coal and coal products, pp 265-292.

Jenkins, B.M., Bakker, R.R., Wei, J.B., (1996), On the properties of washed straw, Biomass and Bioenergy Vol. 10, Issue no. 4, pp 177-200.

Jenkins, B.M., Baxter, L.L., Miles Jr, T.R., Miles, T.R., (1998), Combustion properties of biomass, Fuel Processing Technology, Vol 54, pp 17-46.

Jin, B., Wen, L., Chun-zhu, L., Zong-qing, B., Bao-qing, L., (2009), Influence of mineral matter on high temperature gasification of coal char, Journal of Fuel Chemistry and Technology, Vol. 32, Issue 2, pp 134-138.

Johannes, A.H., Hamrin, C.E., (1986), Characterization and catalytic activity of coal mineral matter, Fuel Processing Technology, Vol. 13, pp 17-39.

Johnson, C.A., Patrick, J.W., Thomas, K.M., (1986), Characterization of coal chars by Raman spectroscopy, X-ray diffraction and reflectance measurements, Fuel, Vol. 65, pp 1284-1290.

Jorjani, E., Hower, J.C., Chelgani, S.C., Shirazi, M.A., Mesroghli, S., (2008), Studies of relationship between petrography and elemental analysis with grindability for Kentucky coals, Fuel, Vol. 87, pp 707-713.

Jorjani, E., H.G., Chapi, M.T., Khorami, (2011), Ultra clean coal production by microwave irradiation pre-treatment and sequential leaching with HF followed by HNO_3, Fuel Processing Technology, Vol. 92, pp 1898-1904.

Jubb, A.M., Allen, H.C., (2010), Vibrational spectroscopic characterization of hematite, maghemite, and magnetite thin films produced by vapour deposition, ACS Applied Materials and Interface, Vol. 2, No. 10, pp 2804-2812.

Jung, H., Eom, H., Kang, H., Moreau, M., Sobanska, S., Ro, C., (2014), Combined use of quantitative ED-EPMA, Raman micro spectrometry, and ATR-FTIR imaging techniques for the analysis of individual particles, Analyst, Vol. 139, pp 3949-3960.

Kandler, K., Benker, N., Bundke, U., Cuevas, E., Ebert, M., Knippertz, P., Rodríguez, S., Schütz, L., Weinbruch, S., (2007), Chemical composition and complex refractive index of Saharan mineral dust at Izaña, Tenerife (Spain) derived by electron microscopy, Atmospheric Environment, Vol. 41, pp 8058-8074.

Kemezys, M., Taylor, G., (1964), Occurrence and distribution of minerals in Australian coals, Journal of the Institute of Fuel, Vol. 37, pp 389-397.

Khare, P., Barauah, B.P., Rao, P.G., (2011), Application of chemometrics to study the kinetics of coal pyrolysis: A novel approach, Fuel, Vol. 90, pp 3299-3305.

Kimura, T., (1998), Relationships between inorganic elements and minerals in coals from the Ashibetsu district, Ishikari coal field, Japan, Fuel Processing Technology, Vol. 56, pp 1-19.

Kingma, K.J., Hemley, R.J. (1994), Raman spectroscopic study of microcrystalline silica, American Mineralogist, Vol. 79, pp 269-273.

Kiros, A., Gholap, A.V., Gigante, G.E., (2013), Fourier Transform Infrared spectroscopic characterization of clay minerals from rocks of Lablibela churches, Ethopia, International Journal of Physical Sciences, Vol. 83, Issue 3, pp 109-119.

Kiss, L.T., King, T.N., (1977), The expression of results of coal analysis: the case for brown coals, Fuel, Vol. 56, pp 340-341.

Kiss, L.T., King, T.N., (1979), Reporting of low-rank coal analysis-the distinction between minerals and inorganics, Fuel, Vol. 58, pp 547-549.

Korwin-Kossakowski, L.E., Brandt, M.P., Barnardt, J.M., Smith, W.H., (1990), Petrographic characterisation if coal by use of the IBAS image analyser, Journal of South African Institute of Mining and Metallurgy, Vol. 90, No.6, pp125-131.

Kostakis, G., (2011), Mineralogical composition of boiler fouling and slagging deposits and their relation to fly ashes: The case of Kardia power plant, Journal of Hazardous Materials, Vol.185, p 1012-1018.

Krishnamoorthy, V., Pisupati, S.V., (2015), A critical review of mineral matter related issues during gasification of coal in fixed, fluidized, and entrained flow gasifiers, Energies, Vol 8, pp 10430-10463.

Kumar, R.S., Rajkumar, P., (2014), Characterization of minerals in air dust particles in the state of Tamilnadu, India through FTIR, XRD and SEM analyses, Infrared Physics and Technology, Vol. 67, pp 30-41.

Kühn, L., Plogmann, H., (1983), Reaction of catalysts with mineral matter during coal gasification, Fuel, Vol. 62, pp 205-208.

Laban, K.L., Atkin, B.P., (2000), The direct determination of the forms of sulphur in coal using microwave digestion and icp-aes analysis, Fuel, Vol. 79, pp 173-180.

Lapuerta, M., Oliva, F., Agudelo, J.R., Stitt, J.P., (2011), Optimization of Raman Spectroscopy parameters for characterising soot from different diesel fuels, Combustion Science and Technology, Vol. 183, pp 1203-1220.

Laumb, J.D., Folkedahl, B.C., Zygarlicke, C.J., (2008), Characteristics and behavior of inorganic constituents, Combustion Engineering Issues for Solid Fuel System, Chapter 4, pp 133-170.

Lawrence, A., Kumar, R., Nandakumar, K., Narayanan, K., (2008), A Novel tool for assessing slagging propensity of coals in PF boilers, Fuel, Vol. 87, pp 946–950.

Le Blanc Smith, G., (1980), Genetic Stratigraphy of the Witbank Coalfield, Transactions of the Geological Society of South Africa, Vol. 83, No. 3, pp 313–326.

Legodi, M.A., de Waal, D., (2007), Raman spectroscopic studies of ancient South African domestic clay pottery, Spectrochimica Acta Part A: Molecular and Biomolecular Spectroscopy, Vol. 66, Issue no. 1, pp 135-142.

Li, Z., Ward, C.R., Gurba, L.W., (2007), Occurrence of non-mineral inorganic elements in low-rank coal macerals as shown by electron microprobe element mapping techniques, International Journal of Coal Geology, Vol. 70, pp 137-149.

Li, H., Qiu, X., Tang, Y., (2008), Ash melting behaviour by Fourier transform infrared spectroscopy, Journal of China University of Mining and Technology, Vol. 18, pp 245-249.

Li, K., Khanna, R., Zhang, J., Liu, Z., Sahajwalla, V., Yang, T., Kong, D., (2014), The evolution of structural order, microstructure and mineral matter of metallurgical coke in a blast furnace: A review, Fuel, Vol. 133, pp 194-215.

Liem, N.Q., Sagon, G., Quang, V.X., van Tan, H., Colomban, P., (2000), Raman study of the microstructure, composition and processing of ancient Vietnamese (proto) porcelains and celadons (13-16th centuries), Journal of Raman Spectroscopy, Vol. 31, pp 933-942.

Limić, N., Valković, V., (1986), The occurrence of trace elements in coals, Fuel, Vol. 65, pp 1099-1102.

Lin, Q., Guet, J.M., (1990), Characterization of coals and macerals by X-ray diffraction, Fuel, 1990, Vol. 69, pp 821-825.

Linares-Solano, A., Hippo, E.J., Walker Jr.P.L., (1986), Catalytic activity of calcium for lignite char gasification in various atmospheres, Fuel, Vol. 65, Issue no. 6, pp 776-779.

Liu, Y., Gupta, R., Sharma, A, Wall, T., Butcher, A, Miller, G., Gottlieb, P., French, D., (2005), Mineral matter-organic matter association characterisation by QEMSCAN and applications in coal utilisation, Fuel, Vol. 84, pp 1259-1267.

Liu, X., Bi, X.T., (2011), Removal of inorganic constituents from pine barks and switchgrass, Fuel Processing Technology, Vol. 92, Issue no.7, pp 1273-1279.

Liu, B., He, Q., Jiang, Z., Xu, R., Hu, B., (2013), Relationship between coal ash composition and ash fusion temperatures, Fuel, Vol. 105, pp 293-300.

Lu, L., Sahajwalla, V., Kong, C., Harris, D., (2001), Quantitative X-ray diffraction analysis and its application to various coals, Carbon, Vol. 39, Issue 12, pp 1821-1833.

López, I.C., Ward, C.R., (2008), Composition and mode of occurrence of mineral matter in some Colombian coals, International Journal of Coal Geology, Vol. 73, pp 3-18.

Ma, Z., Iman, F., Lu, P., Sears, R., Kong, L., Rokanuzzaman, A.S., McCollor, D.P., Benson, S.A., (2007), A comprehensive slagging and fouling prediction tool for coal-fired boilers and its validation/application, Fuel Processing Technology, Vol. 88, pp 1035-1043.

Mackowsky, M., T., (1968), Mineral matter in coals, In Coal and Coal bearing Strata, Murchison, D,. Westall, T., Eds, American Elsevier, New York, pp 309-321.

Mahdjoubg, N., Allen, N., Kelly, P., Vishnyakov, V., (2010), SEM and Raman study of thermally treated TiO_2 anatase nanopowders: Influence of calcinations on photocatalytic activity, Journal of Photochemistry and Photobiology A: Chemistry, Vol. 211, pp 59-64.

Mahlaba, J.S., Kearsley, E.P., Kruger, R.A., (2011), Physical, chemical and mineralogical characterisation of hydraulically disposed fine coal ash from SASOL Synfuels, Fuel, Vol. 90, pp 2491-2500.

Maldonado-Hódar, F.J., Rivera-Utrilla, J., Mastral-Lamarca, A.M., Ferro-García, M.A., (1995), Influence and transformation of coal mineral matter during hydrogenation, Fuel, Vol. 74, No. 6, pp 818-822.

Manoj, B., Kunjomana, A.G., (2010), Chemical solubilisation of coal using HF and characterisation of products by FTIR, FT Raman, SEM and elemental analysis, Journal of Minerals and Materials Characterization and Engineering, Vol.9, No. 10, pp 919-928.

Martínez-Tarazona, M.R., Spears, D.A, Palacios, J.M., Martinez-Alonso, A., Tascon, J.M.D., (1992), Mineral matter in coals of different rank from the Asturian Central basin, Fuel, Vol. 71, pp 367-372.

Martínez-Tarazona, M.R., Spears, D.A, (1996), The fate of trace elements and bulk minerals in pulverized coal combustion in a power station, Fuel Processing Technology, Vol. 47, pp 79-92.

Mastalerz, M. Bustin, R.M. (1993), Electron microprobe and micro-FTIR analyses applied to maceral chemistry, International Journal of Coal Geology, Vol. 24, pp 333-345.

Matjie, R.H., French, D., Ward, C.R., Pistorius, P.C., Li, Z., (2011), Behaviour of coal mineral matter in sintering and slagging of ash during the gasification process, Fuel Processing Technology, Vol. 92, Issue 8, pp 1426-1433.

Matjie, R.H., Ward, C.R., Li, Z., (2012), Mineralogical transformation of coal feedstocks during carbon conversion based on packed-bed combustor test, Coal combustion and gasification products, Vol. 4, pp 45-54.

Matjie, R.H., Li, Z., Ward, C.R., Bunt, J.R., Strydom, C.A., (2016), Determination of mineral matter and elemental composition of individual macerals in coals from Highveld mines, The Journal of the South African Institute of Mining and Metallurgy, Vol. 116, pp 169-180.

Matsuoka, K., Rosyadi, E., Tomota, A., (2002), Mode of occurrence of calcium in various coals, Fuel, Vol. 81, pp 1433-1438.

McCabe, P.J., (1984), Depositional environments of coal and coal bearing strata, in R.A, Rahmani, R.M, Flores (Eds), Sedimentology of coal and coal bearing strata, Vol. 7, pp 13-42.

McCathy and Pretorious (2009), Coal mining on the Highveld and its implication for future water quality in the Vaal river system https://www.imwa.info/docs/imwa_2009/IMWA2009_McCarthy.pdf

McCarthy, T.S., (2011), The impact of acid mine drainage in South Africa, South African Journal of Science, Vol 107, Issue 5-6, pp 1-7.

McCarthy, T. S., Humphries, M. S. (2013), Contamination of the water supply to the town of Carolina, Mpumalanga, January 2012, South African Journal Of Science, Vol. 109, Issue (9/10), pp 1-10.

Memon, N.K., Anjum, D.H., Chug, S.H., (2013), Multiple diffusion flame synthesis of pure anatase and carbon coated titanium dioxide nanoparticles, Combustion and Flame, Vol 160, pp 1848-1856.

Mennella, V, Monaco, G., Colangeli, L., Bussoletti, E., (1995), Raman spectra of carbon-based materials excited at 1064 nm, Carbon, Vol. 33, Issue 2, pp 115-121.

Mernagh, T.P.,Trudu, A.G., (1993), A laser Raman microprobe study of some geologically important sulphide minerals, Chemical Geology, Vol. 103, pp 113-127.

Méndez, L.B., Borrego, A.G., Martinez-Tarazona, M.R., Menéndez, R., (2003), Influence of petrographic and mineral matter composition of coal particles on their combustion reactivity, Fuel, Vol. 82, Issue 15-17, pp 1875-1882.

Michaelian, K.H., (1986), The Raman spectrum of kaolinite #9 at 21°C, Canadian Journal of Chemistry, Vol. 64, pp 285-289.

Michel, D., Colomban, Ph., Abolhassani, S., Voyron, F., Kahn-Harari, H., (1996), Germanium Mullite: Structure and vibrational spectra of gel, glasses and ceramics, Journal of the European Ceramic Society, Vol. 16, pp 161-168.

Miller, R.N., Yarzab, R.F., Given, P.H., (1979), Determination of the mineral matter contents by low temperature ashing, Fuel, Vol. 58, pp 4-10.

Moyo, S., Mujuru, M., McCrindle, R.I., Mokgalaka-Matlala, N., (2011), Environmental implications of material leached from coal, Journal of Environmental Monitoring, Vol. 13, pp 1488-1494.

Mukherjee, D.K., Chowdhury, P.B., (1976), Catalytic effect of mineral matter constituents in a North Assam coal on hydrogenation, Fuel, Vol. 55, Issue 4, pp 4-8.

Mukherjee, S., Borthakur, P.C., (2001), Chemical demineralization/desulphurization of high sulphur coal using sodium hydroxide and acid solutions, Fuel, Vol.80, pp 2037-2040.

Murad, E., (1997), Identification of minor amounts of anatase in kaolins by Raman spectroscopy, American Mineralogist, Vol. 82, pp 203-206.

Murowchick, J.B., Barnes, H.L., (1986), Marcasite precipitation from hydrothermal solutions, Geochemica et Cosmochimica Acta, Vol. 50, pp 2615-2629.

Nabeel, A., Khan, T.A., Sharma, D.K., (2009), Studies on the production of ultra clean coal by alkali-acid leaching of low grade coals, Energy Sources, Part A: Recovery, Utilization, and Environmental Effects, Vol.31, Issue 7, pp 594-601.

Nakazimo, M., Kammereck, R., Walker, P.L., (1974), Laser Raman studies on carbons, Carbon, Vol. 12, pp 259-267.

Nayak, P.S, Singh, B.K., (2007), Instrumental characterization of clay by XRF, XRD and FTIR, Bulletin of Materials Science, Vol. 30, No. 3, pp 235-238.

Nayak., B., (2013), Mineral matter and the nature of pyrite in some high sulphur tertiary coals of Meghalaya, Northeast India, Journal Geological Society of India, Vol. 81, pp 203-214.

Ninomiya, Y., Sato, A., (1997), Ash melting behaviour under coal gasification conditions, Energy Conversation Management, Vol. 38, pp 1405-1412.

Ninomiya, Y., Zhang, L., Sato, A., Dong, Z., (2004), Influence of coal particle size on particulate matter emission and its chemical species produced during coal combustion, Fuel Processing Technology, Vol. 85, Issue 8-10, pp 1065-1088.

Nutalapi, D., Gupta, R., Moghtaderi, B., Wall, T.F., (2007), Assessing slagging anf fouling during biomass combustion. A thermodynamic approach allowing for alkali/ash reactions, Fuel Processing Technology, Vol. 88, pp 1044-1052.

O'Gorman, J.V., Walker. Jr, P.L., (1971), Mineral matter characteristics of some American coals, Fuel, Vol. 50, Issue 2, pp 135-151.

O'Gorman, J.V., Walker, P.L., (1973), Thermal behaviour of mineral fractions separated from selected American coals, Fuel, Vol. 52, pp 71-79.

Ohsaka, T., Yamaoka, S., Shimomura, O., (1979), Effect of hydrostatic pressure on the Raman spectrum of anatase (TiO_2), Solid State Communications, Vol. 30, pp 345-347.

Oliviera, M.L.S., Waanders, F., Silva, L.F.O., Jasper, A., Sampaio, C.H., McHabe, D., Hatch, R.S., Hower, J.C., (2011), A multiple-analytical approach to understand the chemistry of Fe-minerals in fee coals and ashes, Coal Combustion and Gasification Products, Vol. 3, pp 51-62.

Orheim, A., Bieg, G., Brekke, T., Horseide, V., Stenvold, J., (2007), Petrography and geochemical affinities of Spitsbergen Paleocene coals, Norway, International Journal of Coal Geology, Vol. 70, pp 116-136.

Özbayoğlu, G., Özbayoğlu, M.E., (2006), A new approach for the prediction of ash fusion tempearures: A case study using Turkish lignites, Fuel, Vol. 85, pp 545-552.

Öztaş, N.A., Yürüm, Y., (2000), Pyrolysis of Turkish Zonguldak bituminous col. Part 1. Effect of mineral matter, Fuel, Vol. 79, Issue 10, pp 1221-1227.

Paulson, L.E., Beckering, W., Fowkes, W.W., (1972), Separation and identification of minerals from Northern Great Plains Province lignite, Fuel, Vol. 51, pp 224-227.

Painter, P.C., Coleman, M.M., Jenkins, R.G., Whang, P.W., Walker. Jr., P.L., (1978), Fourier Transform Infrared study of mineral matter in coal. A novel method for quantitative mineralogical analysis, Fuel, Vol. 57, pp 337-344.

Palmer, C.A., Krasnow, H.R., Finkelman, R.B., d'Angelo, W.M., (1993), An evaluation of leaching to determine modes of occurrence of selected toxic elements, Journal of Coal Quality, Vol. 12, Issue 4, pp 135-141.

Patrick, J.W., Shaw, F.H., (1972), Influence of sodium carbonate on coke reactivity, Fuel, Vol. 51, pp 69-75.

Patterson, J.H., Corcoran, J.F., Kinealy, K.M., (1994), Ash and slag qualities of Australian bituminous coals for use in slagging gasifiers, Fuel, Vol. 73, no.11, pp 1735-1745.

Patterson, J.H., Hurst, H.J., (2000), Ash and slag qualities of Australian bituminous coals for use in slagging gasifiers, Fuel, Vol. 79, pp 1671-1678.

Pearson, D.E., Kwong, J., (1979), Mineral matter as a measure of oxidation of a coking coal, Fuel, Vol. 58, pp 63-66.

Penel, G., Leroy, G., Rey, C., Sombret, B., Huvenne, J.P., Bres, E., (1997), Infrared and Raman microspectrometry study of fluor-fluor-hydroxy and hydroxyl-apatite powders, Journal of Materials Science: Materials in medicine, Vol. 8, pp 271-276.

Perdikatsis, V., (2013), Quantitative determination of mineral matter in lignite by X-ray spectrometry, using the Compton effect, Proceedings of the 13th International Congress, Chania, Greece,September, 2013.

Pinetown, K.L., Ward, C.R., van der Westhuizen, W.A., (2007), Quantitative evaluation of minerals in coal deposits in the Witbank and Highveld coalfields, and the potential impact on acid mine drainage, International Journal of Coal Geology, Vol. 70, pp 166-183.

Pollack, S.S., (1979), Estimating mineral matter in coal from its major inorganic elements, Fuel, Vol. 58, pp 76-78.

Porto, S.P.S., Fleury, P.A., Damen, T.C., (1967), Raman spectra of TiO_2, MgF_2, ZnF_2, FeF_2 and MnF_2, Physical Review, Vol. 154, pp 522-526.

Potgieter, P.H., (2010). Water and energy in South Africa-managing scarcity, Munich Personal RePEc Archive, MPRA Paper No. 23360, https://mpra.ub.uni-muenchen.de/23360 cited: 15 November 2015.

Potgieter-Vermaak, S, S., Potgieter, J.H., Grieken, R., (2006), The application of Raman spectroscopy and to investigate and characterize cement, Part 1: A review, Cement and Concrete Research, Vol. 36, Issue 4, pp 656-662.

Potgieter-Vermaak, S, S., Maledi, N., Wagner, N, van Heerden, J.H.P., van Grieken, R, Potgieter, J.H., (2011), Raman spectroscopy for the analysis of coal, Journal of Raman Spectroscopy, Vol. 42, pp 123-129.

Querol, X., Chinchon, S., Lopez-Soler, A., (1989), Iron sulphide precipitation sequence in Albian coals from the Maestrazgo Basin, Southeastern Iberian range, northeastern Spain, International Journal of Coal Geology, Vol. 11, pp 171-189.

Querol, X., Klika, Z, Weiss, Z., Finkelman, R.B., Alastuey, A., Juan, R., López-Soler, A., Plana, F., Kolker, A, Chenery S.R.N., (2001), Determination of element affinities by density fractionation of bulk coal samples, Fuel, Vol. 80, pp 83-96.

Quirico, E., Rouzaud, J.N., Bonal, L., Motagnac, G., (2005), Maturation grade of coals as revealed by Raman spectroscopy: Progress and problems, Spectrochimica, Acta A, Part A, Vol. 61, pp 2368-2377.

Raask, E., (1985), The mode of occurrence and concentration of trace elements in coal, Progress Energy Combustion Science, Vol. 11, pp 97-118.

Ragland, K.W., Baker, A.J., (1987), Mineral matter in coal and wood-replication for solid fuelled gas turbines, Combustion fundamentals and applications, Spring Technical Meeting of Central States Section of the Combustion Institute, pp 117-122.

Ramasamy, V., Suresh, G., (2009), Mineral characterization and crystalline nature of quartz in Ponnaiyar River sediments, Tamilnadu, India, American-Eurasian Journal of Scientific Research, Issue 4, Vol. 2, pp 103-107.

Rao, C.P., Gluskoter, H.J., (1973), Occurrence and distribution of minerals in Illinois coals, Illinois State Geological Survey, Circular 476, pp 1-56.

Reddy, B.J., Frost, R.L., (2005), Spectroscopic characterization of chromite from the Moa-Baracoa Ophiolitic Massif, Cuba, Spectrochimica Acta Part A, Vol. 61, pp 1721-1728.

Reid, W.T., (1984), The relation of mineral composition to slagging, fouling and erosion during and after combustion, Progress in Energy and Combustion Science, Vol. 10, Issue 2, pp 159-169.

Renton, J.J., (1982), Mineral matter in coal, In: Coal structure (ed. R.A. Meyers) Academic Press, New York, pp 283-326.

Reyes, F., Pérez Alcázar, G.A., Barraza, J.M., Bohórquez, A., Tabares, J.A., Speziali, N.L., (2003), Mössbauer and XRD characterization of the mineral matter of coal from the Guachinite mine in Colombia, Hyperfine Interactions, Vol. 148/149, pp 39-46.

Richard, J.J., Vick, R.D., Junk, G.A., (1977), Determination of elemental sulphur by gas chromatography, Environmental Science and Technology, Vol. 11, pp 1084-1086.

Richaud, R., Lachas, H, Healey, A.E., Reed, G.P., Haines, J., Jarvis, K.E., Herod, A.A., Dugwell, D.R., Kanditoyi, R., (2000), Trace element analysis of gasification plant sample by ICP-MS, validation by comparison of results from two laboratories, Fuel, Vol. 79, Issue 9, pp 1077-1087.

Riley, K.W., French, D.H., Farrell, O.P., Wood, R.A., Huggins, F.E., (2012), Modes of occurrence of trace and minor elements in some Australian coals, International Journal of Coal Geology, Vol. 94, pp 214-224.

Ritz, M., Klika, Z., (2010), Determination of minerals in coal by methods based on recalculation of the bulk chemical analyses, Acta Geodynamica et Geomaterialia, Vol. 7, no 4, Issue 160, pp 453-460.

Ríos, C.A., Williams, C.D., Roberts, C.L., (2008), Removal of heavy metals from acid mine drainage (AMD) using coal fly ash, natural clinker and synthetic zeolites, Journal of Hazardous Materials, Vol. 156, pp 23-35.

Roberts, D.L., (1988), The relationship between macerals and sulphur content of some South African Permian coals, International Journal of Coal Geology, Vol. 10, pp 399-410.

Roberts, D.L., (1991), The inherent moisture content of South African Permian coals, International Journal of Coal Geology, Vol. 17, pp 297-311.

Roberts, M.J., Everson, R.C., Neomagus, H.W., Van Niekerk, D., Mathews, J.P., Branken, D.J., (2015), Influence of maceral composition on the structure, properties and behaviour of chars derived from South African coals, Fuel, Vol. 142, pp 9-20.

Rochdi, A., Landais, P., (1991), Transmission micro-infra-red spectroscopy, Fuel, Vol. 70, pp 367-371.

Roets, L., Strydom, C.A., Bunt, J.R., Neomagus, H.W.J.P., Van Niekerk, D., (2015), The effect of acid washing on the pyrolysis products derived from a vitrinite-rich bituminous coal, Journal of Analytical and Applied Pyrolysis, Vol. 116, pp 142–151.

Ruan, C., Ward, C.R., (2002), Quantitative X-ray powder diffraction analysis of clay minerals in Australian coals using Rietveld methods, Applied Clay Science, Vol. 21, Issue 5-6, pp 227-240.

Rubiera, F., Arenillas, A., Pevida, C., García, R., Pis, J.J., Steel, K.M, Patrick, J.W., (2002). Coal structure and reactivity changes induced by chemical demineralization. Fuel Processing Technology, Vol. 79, Issue 3, pp 273-279.

Russell, J.D., (1987), Infrared methods-A handbook of determinative methods in mineralogy, in: Wilson, M.J.,(Ed.), Blackie and Son Ltd., New York, pp 133.

Sager, M., (2013), Environmental aspects of trace elements in coal combustion, Toxicological and Environmental Chemistry, Vol. 71, pp 159-183.

Saika, B.K., Boruah, R.K., Gogoi, P.K., (2007), FT-IR and XRD analysis of coal from Makum coalfield of Assam, Journal of Earth Systems Science, Vol. 116, No 6, pp 575-579.

Saikia, B.J., Parthasarathy, G., (2010), Fourier Transform Infrared Spectroscopic characterisation of kaolinite from Assam and Meghalaya, Northeastern India, Journal of Molecular Physics, Vol. 1, pp 206-210.

Saikia, B.K., Ninomiya, Y., (2011), An investigation on the heterogeneous nature of mineral matters in Assam (India) coal by CCSEM technique, Fuel Processing Technology, Vol. 92, pp 1068-1077.

Samaras, P., Diamadopoulos, E., Sakellaropoulos, (1994), Acid treatment of lignite and its effect on activation, Carbon, Vol. 32, No.5, pp 771-776.

Santos, F.G., Riella, H.G., Martins, M.P.M., Vieira.R., (2014), Effect of pyrite in direct coal liquefaction process, Current Catalysis, Vol. 3, pp 255-259.

Scarlat, N., Dallemand, J.F., Monforti-Ferrario, F., Banja, M., Motola, V., (2015), Renewable energy policy framework and bioenergy contribution in the European Union-An overview from National renewable energy action plan and progress reports, Renewable and Sustainable Energy Reviews, Vol. 51, pp 969-985.

Schoening, F.R.L., (1982), X-ray structural parameter for coal, Fuel, Vol. 61, pp 695-699.

Schwartz, J., Dockery, D.W., and Neas, L.M., (1996), Is daily mortality associated specifically with fine particles? Journal of Air and Waste Management Association, Vol. 46, pp 927-939.

Scott, J.F., Porto, S.P.S., (1967), Longitudinal and transverse optical lattice vibrations in quartz, Physical Review, Vol. 161, No. 3, pp 903-910.

Scott, A.C., (2002), Coal petrology and the origin of coal macerals: a way ahead? International Journal of Coal Geology, Vol 50, pp 119-134.

Sharma, D.K., Mirza, Z.B., (1983), Role of mineral matter in chemical reactivity of coal, Fuel, Vol. 62, Issue 8, pp 916-917.

Sharma, A., Saika, A., Khare, P., Buruah, B.P., (2014), Genesis of some tertiary Indian coals from the chemical composition of ash-a statistical approach: Part 1, Journal of Earth System Science, Vol. 123, Issue no.7, pp 1705-1715.

Shepherd, R.A., Kiefer, W.S., Graham, W.R.M., (1986), Characterization of circle cliff tar sands. Application of the FT-i.r. technique to mineral matter, Fuel, Vol. 65, pp 1261-1264.

Shibaoka, M., (1972), Silica/alumina ratio of the ashes from some Australian coals, Fuel, Vol. 51, pp 278-283.

Shirazi, A.R., Eklund, L., Lindqvist, O., (1994), Direct quantitative analysis of mineral matter and different forms of pyritic sulfur in coal by electron probe microanalysis (EPMA) and automated image analysis (AIA), Fuel, Vol. 73, no. 2, pp 193-198.

Shirazi, A.R., Bortin, O., Eklund, L., Lindqvist, O., (1995), The impact of mineral matter in coals on its combustion, and a new approach to the determination of the calorific value of coal, Fuel, Vol. 74, no. 2, pp 247-251.

Silva, L.F.O., Sampaio, C.H., Guedes, A., de Vallejuelo S.F., Madariaga, J.M., (2012), Multianalytical approaches to the characterisation of minerals associated with coals and the diagnosis of their potential risk by using combined instrumental microspectroscopic techniques and thermodynamic speciation, Fuel, Vol. 94, pp 52-63.

Silva, L.F.O., Fdez-Ortiz de Vallejuelo, S., Martinez-Arkarazo, I., Castro, K., Oliviera, M.L.S., Sampaio, C.H., de Brum, I.A.S., de Leăo, F.B., Taffarel, S.R., Madariaga, J.M., (2013), Study of environmental pollution and mineralogical characterization of sediment rivers from Brazilian coal mining acid drainage, Science of the Total Environment, Vol. 447, pp 169-178.

Skodras, G., Sakellaropoulos, G.P., (2002), Mineral matter effects in lignite gasification, Fuel Processing Technology, Vol. 77-78, pp 151-158.

Smith, R.M.H., Eriksson, P.G., Botha, W.J., (1993), A review of the stratigraphy and sedimentary environments of the Karoo-aged basins of Southern Africa, Journal of African Earth Sciences, Vol. 16, No. 132, pp 143-169.

Smith, W.E., Dent, G., (2005), Application, Modern Raman spectroscopy-A practical approach, Chapter 6, John Wileys and Sons Ltd, pp 135-179.

Smith, J.R., Smith, J.W., (2007), A relationship between carbon and hydrogen contnt of coals and their vitrinite reflectance, International Journal of Coal Geology, Vol. 70, pp 79-86.

Snyman, C.P., Botha, W.P., (1993), Coal in South Africa, Journal of African Earth Sciences, Vol. 16, no. ½, pp 171-180.

Snyman, C.P., (1998), Coal, In: The mineral resources of South Africa, Handbook, Council of Geoscience, Vol. 16, pp 136-205.

Sofianos, A.C., Butler, A.C., Lowrens, H.B., (1989), Catalytic liquefaction of South African coals using the carbon monoxide/water system. Part 1: Pyrite catalysis, Fuel Processing Technology, Vol 22, pp 175-188.

Soundarrajan, N., Krishnamurthy, N., Pisupati, S.V., (2012), Physical and chemical characterization of coal particles used as entrained flow gasifiers feedstock: Heterogeneity in mineral matter distribution, Energy Procedia, Vol. 14, pp 1735-1740.

Spears, D.A., (1987), Mineral matter in coals, with special reference to the Pennine coalfields, Coal and Coal bearing strata, Geological Society Special Publication, No. 32, pp 171-185.

Spears, D.A., Duff, P., Caine, P.M., (1988), West Waterberg tostein, South Africa, International Journal of Coal Geology, Vol. 9, pp 221-233.

Spears, D.A., Martinez-Tarazona, M.R., (1993), Geochemical and mineralogical characteristics of a power station feed-coal, Eggborough, England, International Journal of Coal Geology, Vol. 22, pp 1-20.

Spears, D.A., Manzanares-Papayanopoulos, L.I., Booth, C.A., (1999), The distribution and origin of trace elements in UK coal; the importance of pyrite, Fuel, Vol. 78, pp 1671-1677.

Spears, D.A., (2000), Role of clay minerals in UK coal combustion, Applied Clay Science, Vol. 16, pp 87-95.

Speight, J.G., (2013), Handbook of Coal Analysis, Wiley, New York, NY, USA.

Stach, E., Mackowsky, M., Teichmüller, M., Taylor, G.H., Chandra, D., Teichmüller, R., (1982), Stach's Textbook of Coal Petrology, Gebrüder Borntraeger, Berlin, Germany.

Steel, K.M., Patrick, J.W. (2001), The production of ultra-clean coal by chemical demineralisation, Fuel, Vol. 80, pp 2019-2023.

Stefaniak, E.A., Buczynska, A., Novakovic, V., Kiduk, R., Van Grieken, (2009), Determination of chemical composition of individual airborne particles by SEM/EDX and micro-Raman spectrometry, Journal of Physics, Conference Series, Vol. 162, pp 1-16.

Steyn, M., Minnitt, R.C.A., (2010), Thermal coal products in South Africa, The Journal of Southern African Institute of Mining and Metallurgy, Vo. 110, pp 593-599.

Stock, L.M., Wolny, R., (1990), Elemental sulphur in bituminous coals, In: Orr, W.L., White, C.M., (Eds), Geochemistry of Sulphur in Fossil Fuels, ACS Symposium Series 429, pp 241-248.

Stopes, M.C., (1935), On the petrology of banded bituminous coal, Fuel, Vol. 14**,** pp 4.

Straszheim, W.E., Yousling, J.G, Younkin, K.A., Markuszewski, R., (1988), Mineralogical characterization of lower rank colas by SEM-based automated image analysis and energy-dispersive X-ray spectrometry, Fuel, Vol. 67, Issue 8, pp 1042-1047.

Strydom, C.A., Sehume, T.Z., Bunt, J.R., van Dyk, J.C., (2015), The influence of selected biomass additions on the co-pyrolyis with an inertinite-rich medium rank C grade South African coal, The Journal of the Southern African Institute of Mining and Metallurgy, Vol. 115, pp 707-716.

Su, S., Pohl, J.H., Holcombe, D., (2003), Fouling propensities of blended coals in pulverized coal-fired power station boilers, Fuel, Vol. 82, pp 1653-1667.

Suarez-Fernandez, G.P., Vega, J.M.G., Fuertes, A.B., Garcia, A.B., Martínez-Tarazona, M.R., (2001), Analysis of major, minor, and trace elements in coal by radioisotope X-ray Fluorescence spectrometry, Fuel 80, pp 255-261.

Suárez-Ruiz, I., Ward, C.R., (2008), Basic factors controlling coal quality and technological behaviour of coal, Applied Coal Petrology, pp19-59.

Sun, Q., Li, W., Chen, H., Li, B., (2003), The variation of structural characteristics of macerals during pyrolysis, Fuel, Vol. 82, pp 669-676.

Swaine D.J., (1990), Trace elements in coal, Butterworths, London, pp 278.

Swaine, D.J., (1992), The organic association of elements in coals, Organic Geochemistry, Vol. 18, No. 3, pp 259-261.

Swaine, D.J., (2000), Why trace elements are important?, Fuel Processing Technology, Vol. 65-66, 21-33.

Taylor, J.C., (1991), Computer programs for standardless quantitative analysis of minerals using the full powder diffraction profile, Powder Diffraction, Vol. 6, pp 2-9.

Tchapda, A.H., Pisupati, S.V., (2014), A review of thermal co-conversion of coal and biomass/waste, Energies, Vol. 7, pp 1098-1148.

Thiessen, G., Ball, C.G., Grotts, P.E., (1936), Coal ash and coal mineral matter, Industrial and Engineering Chemistry, Vol. 28, no.3, pp 355-361.

Thitakamol, B., Veawab, A., Aroonwilas, A., (2007), Environmetal impacts of absorption-based CO_2 capture unit for post-combustion treatment of flue gas from coal-fired power plant, International Journal of greenhouse gas control, Vol. 1, pp 318-342.

Tian, F., Zhang, Y., Zhang, J., Pan, C., (2012), Raman Spectroscopy: A new approach to measure the percentage of anatase exposed (001)facets, The Journal of Physical Chemistry C, Vol. 116, Issue 13, pp 7515-7519.

Tickner, J., Roach, G., (2004), Characterisation of coal and minerals using Compton profile analysis, Nuclear Instruments and Methods in Physics Research B., Vol. 213, pp 507-510.

Tomeczek, J., Palugniok, H., (2002), Kinetics of mineral matter transformation during coal combustion, Fuel, Vol. 81, Issue 10, pp 1251-1258.

Tomita, A., Mahajan, O.P., Walker Jr., P.L., (1977), Reactivity of heat-treated coals in hydrogen, Fuel, Vol.56, pp 137-144.

Tompsett, G.A., Bowmaker, G.A., Cooney, R.P., Metson, J.B., Rodgers, K.A., Seakins, J.M., (1995), The Raman spectrum of brookite, TiO_2, Journal of Raman Spectroscopy, Vol. 26, pp 57-62.

Trimble, A.S., Hower, J.C., (2003), Studies of the relationship between coal petrology and grinding properties, International Journal of Coal Geology, Vol. 54, pp 253-260.

Tsu, R., Gonzalez, J.H., Luengo, C.A., (1977), Raman scattering and luminescence in coal and graphite, Solid State Communications, Vol. 24, pp 809-812.

Tuinstra, F., Koenig, J.L., (1970), Raman spectrum of graphite, The Journal of Chemical Physics, Vol. 53, pp 1126-1130.

Unsworth, J.F., Barratt, D.J., Park, D., Titchener, K.J., (1988), Ash formation during pulverised coal combustion, Fuel, Vol. 67, pp 632-641.

Ural, S., Akyidiz, M., (2004), Studies of the relationship between mineral matter and grinding properties of low-rank coals, International Journal of Coal Geology, Vol. 60, pp 81-84.

Ural, S., (2007), Quantification of crystalline mineral matter in some Turkish coals using interactive Rietveld-based X-ray diffractometry, International Journal of Coal Geology, Vol. 71, pp 176-184.

Vaculíková, L., Plevová, E., Vallová, S., Koutník, I., (2011), Characterization and differentiation of kaolinites from selected Czech deposits using infrared spectroscopy and differential thermal analysis, Acta Geodynamica et Geomaterialia, Vol. 8, No. 1, pp 59-67.

Van Alphen, C., (2007), Automated mineralogical analysis of coal and ash products-Challenges and requirements, Minerals Engineering, Vol. 20, pp 496-505.

Van der Flier-Keller,E., Fyfe, W.S., (1988), Mineralogy of lower Cretaceous coals from the Moose river basin Ontarion, and Monkman, British Columbia, Canadian Mineralogist, Vol. 26, pp 343-353.

Van der Spuy, D., Willis, J.P., (1991), The occurrence of aragonite in carbonate lenses in coals from the Witbank area, South African Journal of Geology, Vol. 94, pp 178-180.

Van Dyk, J.C., Baxter, L.L., Van Heerden, J.H.P., Coetzer, R.L.J., (2005), Chemical fractionation tests on South African coal source to obtain species-species information on ash fusion temperature (AFT), Fuel, Vol. 84, pp 1768-1777.

Van Dyk, J.C., Melzer, S., Sobiecki, A., (2006), Mineral matter transformation during Sasol-Lurgi fixed bed dry bottom gasification-utilization of HT-XRD and FactSage modeling, Minerals Engineering, Vol. 19, pp 1126-1135.

Van Dyk, J.C., Benson, S.A., Laumb, M.L., Waanders, B., (2009), Coal and coal ash characteristics to understand mineral transformations and slag formation, Fuel, Vol. 88, pp 1057-1063.

Van Niekerk, D., Pugmire, R.J., Solum, M.S., Painter, P.C., Mathews, J.P., (2008), Structural characterization of vitrinite-rich and inertinite-rich Permian-aged South African bituminous coals, International Journal of Coal Geology, Vol. 76, pp 290-300.

Vamvuka, D., Pitharoulis, M., Alevizos, G., Repouskou, E., Pentari, D., (2009), Ash effects during combustion of lignite/biomass blends in fluidized bed, Renewable Energy, Vol. 32, Issue 12, pp 2662-2671.

Vassileva, C.G., Vassilev, S.V., (2005), Bahaviour of inorganic matter during heating of Bulgarian coals, Fuel Processing Technology, Vol. 86, pp 1297-1333.

Vassilev, S.V., Kitano, K., Takeda, S., Tsurure, T., (1995), Influence of mineral and chemical composition of coal ashes on their fusibility, Fuel Processing Technology, 45 (1995), pp. 27–51.

Vassilev, S.V., Kitano, K., Vassileva, G.C., (1996 a), Some relationship between coal rank and chemical mineral composition, Fuel, Vol. 75. No.13, pp1537-1542.

Vassilev, S.V., Vassileva, C.G., (1996 b), Occurrence, abundance, and origin of minerals in coals and coal ashes, Fuel Processing Technology, Vol. 48, pp 85-106.

Vassilev, S.V., Kitano, K., Vassileva, G.C., (1997), Relations between ash yield and chemical and mineral composition of coals, Fuel, Vol. 76, No. 1., pp 3-8.

Vassilev, S.V., Vassileva, C.G., (1997), Geochemistry of coals, coal ashes, and combustion wastes from coal-fired power stations, Fuel Processing Technology, Vol. 51, pp 19-45.

Vassilev, S.V., Tascón, J.M.D., (2003), Methods for characterization of inorganic and mineral matter in coal: A critical overview, Energy and Fuels, Vol. 17, pp 271-281.

Vassilev, S.V., Vassileva, C., (2009), A new approach for the combined chemical and mineral classification of the inorganic coal. 1. Chemical and mineral classification system, Fuel, Vol. 88, pp 235-245.

Vassilev, S.V., Vassileva, C.G., Baxter, D., Andersen, L.K., (2010), Relationships between chemical and mineral composition of coal and their potential applications as genetic indicators. Part 2. Mineral classes, groups and species, Geologica Balcanica, Vol. 39, Issue 3, pp 43-67.

Vejahati, F., Xu, Z., Gupta, R., (2010), Trace elements in coal: Association with coal and minerals and their behaviour during coal utilization-A review, Fuel, Vol. 89, Issue 4, pp 904-911.

Verra, M.J., Bell, A.T., (1978), Effect of alkali metal catalysts on gasification of coal char, Fuel, Vol. 57, pp 194-200.

Voght, H., Chattopadhyay, T., Stolz, H.J., (1983), Complete first-order Raman spectra of the pyrite structure compounds, FeS_2, MnS_2 and SiP_2, Journal of Physics and Chemistry of Solids, Vol. 44, no. 9, pp 869-873.

Vorres, K.S., (1986) Chemistry of mineral matter and ash in coal: an overview, Mineral matter and ash in coal, Chemistry Division, Argonne National Laboratory, Argonne, IL 60439, Chapter 1, pp 1-8.

Vuthalura, H.B., French, D., (2008), Ash chemistry and mineralogy of an Indonesian coal during combustion, Part 1 Drop-tube observations, Fuel Processing Technology, Vol. 89, pp 595-607.

Waanders, F.B., Vinken, E., Mans, A., Mulaba-Bafubiandi, A.F., (2003), Iron minerals in coal, weathered coal and coal ash-SEM and Mossbauer results, Hyperfine Interact, Vol. 148/149, pp 21-29

Wagner, J., Ramsteiner, M., Wild, C., Koidl, P., (1989), Resonant Raman scattering of amorphous carbon and polycrystalline diamond films, Physical Review B, Vol. 40, no. 3, pp 1817-1824.

Wagner, N.J., Tlotleng, M.T., (2012), Distribution of selected trace elements in density fractionated Waterberg coals from South Africa, International Journal of Coal Geology, Vol. 94, pp 225-237.

Wall, T.F., (1992), Mineral matter transformations and ash deposition in pulverized coal combustion, 24th Symposium (international) on Combustion, The Combustion Institute, pp 1119-1126.

Wall, T. F, Creelman, R. A., Gupta, R.P., Gupta, S.K., Coin, C., Lowe, A., (1998), Coal ash fusion temperatures – new characterization techniques and implications for slagging and fouling, Progress Energy Combustion Science, Vol. 24, pp 345–353.

Wang, Y., Alsmeyer, D.C., McCreery, R.L., (1990), Raman spectroscopy of carbon materials: structural basis of observed spectra, Chemistry of Materials, Vol. 2, pp 557-563.

Wang, W., Brown, S.D., Thomas, K.M., Crelling, J.C., (1994), Nitrogen release from a rank series of coals during temperature programmed combustion, Fuel, Vol. 73, Issue 3, pp 341-347.

Wang, A., Kuebler, K.E., Jolliff, B.L., Haskin, L.A., (2004), Raman spectroscopy of Fe-Ti-Cr-oxides, case study: Martian meteorite EETA79001, American Mineralogist, Vol 89, pp 665-680.

Wang, Q., Zhang, L., Sato, A., Ninomiya, Y., Yamashita, T., (2008), Effects of coal blending on the reduction of PM10 during high temperature combustion 1. Mineral transformations, Fuel, Vol. 87, Issues 13-14, pp 2997-3005.

Wang, P., Massoundi, M., (2013), Slag behaviour in gasifiers. Part 1: Influence of coal properties and gasification conditions, Energies, Vol.6, pp 784-806.

Ward, C. R., (1989), Minerals in bituminous coals of the Sydney basin (Australia) and the Illinois basin (U.S.A), International Journal of Coal Geology, Vol. 13, pp 455-479.

Ward, C.R., Christie, P.J., (1994), Clays and other minerals in coal seams of the Moura-Baralala area, Bowen Basin, Australia, International Journal of Coal Geology, Vol. 25, Issue 3-4, pp 287-309.

Ward, R.C., Taylor, J.C., (1996), Quantitative mineralogical analysis of coals from the Callide basin, Queensland, Australia using X-ray diffraction and normative interpretation, International Journal of Coal Geology, Vol. 30, pp 211-229.

Ward, C.R., Corcoran, J.F., Saxby, J.D., Read, H.W., (1996), Occurrence of phosphorus minerals in Australian coal seams, International Journal of Coal Geology, Vol. 30, pp 185-210.

Ward, C.R., Spears, D.A., Booth, C.A., Staton, I., Gurba, L.W., (1999), Mineral matter and trace elements in coals of the Gunnedah Basin, New South Wales, Australia, International Journal of Coal Geology, Vol. 40, pp 281-308.

Ward, C.R., (1999), Mineral in bituminous coals of the Sydney basin (Australia) and the Illinois basin (U.S.A), International Journal of Coal Geology, Vol. 13, pp 455-47.

Ward, C.R., Taylor, J.C., Matulis, C.E., Dale, L.S., (2001), Quantification of mineral matter in the Argonne Premium Coals using interactive Rietveld-based X-ray diffraction, International Journal of Coal Geology, Vol. 46, pp 67-82.

Ward, C.R. (2002), Analysis and significance of mineral matter in coal seams, International Journal of Coal Geology, Vol. 50, pp 135-168.

Ward, C.R., Gurba, L.W., (2008), Occurrence and distribution of organic sulphur in macerals of Australian coals using electron microprobe techniques, Organic Geochemistry, Vol. 22, Issue 11, pp 635-647.

Wee, H.L., Wu, H., Zhang, D., French, D., (2005), The effect of combustion on mineral matter transformation and ash deposition in a utility boiler fired with a sub-bituminous coal, Proceedings of the Combustion Institute, Vol. 30, pp 2981-2989.

Weeber, S.L., Cairncross, B., Falcon, R.M.S., (2000), Mineralogical, petrographic and geological controls on coal ash fusion temperature from New Clydesdale Colliery, Witbank coalfield, South Africa, Journal of South African Institute of Mining and Metallurgy, pp 181-190.

Wells, J.J., Wigley, F., Foster, D.J., Gibb, W.H., Williamson, J., (2004), The relationship between excluded mineral matter and the abrasion index of a coal, Fuel, Vol. 83, pp 359-364.

Wells, J.J., Wigley, F., Foster, D.J., Livingston, W.R., Gibb, W.H., Williamson, J., (2005), The nature of mineral matter in a coal and the effects on erosion and abrasive behaviour, Fuel Processing Technology, Vol. 86, pp 535-550.

White, C.M., Lee, M.L., (1980), Identification and geochemical significance of some aromatic components of coal, Geochimica et Cosmochimica Acta, Vol 44 pp 1825-1832.

White, S.N., (2009), Laser Raman spectroscopy as a technique for identification of seafloor hydrothermal and cold seep minerals, Chemical Geology, Vol. 259, pp 240-252.

Wigley, F., Williamson, J., Gibb, W.H., (1997), The distribution of mineral matter in pulverised coal particles in relation to burnout behaviour, Fuel, Vol. 76, Issue 13, pp 1283-1288.

Wijaya, N., Kwang Choo, T., Zhang, L., (2011), Generation of ultra clean coal from Victorian brown coal-sequential and single leaching at room temperature to elucidate the elution of individual inorganic elements, Fuel Processing Technology, Vol. 92, pp 2127-2137.

Willis, J.P., Hart, R.J., Roberts, R.J., van der Spuy, D., (1991), The Geochemistry of South African coals Conference on South Africa's coal resources, Geol. Soc. South Africa, Witbank, 6-9 November 1991.

Willscher, S., Pohle, C., Sitte, J., Werner, P., (2007), Solubilization of heavy metals from a fluvial AMD generating tailings sediments by heterotrophic microorganisms. Part 1: Influence of pH and solid content, Journal of Geochemical Explorations, Vol. 92, pp 177-185.

Wilson, M.J., (1987), Clay minerals: A Physico-chemical explanation of their occurrence, Applied Clay Science, Vol. 2, Issue 2, pp 185-186.

Winegartner, E.C., (1974), Coal fouling and slagging parameters, ASME Research Committee on corrosion and deposits from combustion gases, ASME publication.

Xu, M., Yan, R., Zheng, C., Qiao, Y., Han, J., Sheng, C., (2003), Status of trace element emission in a coal combustion process: a review, Fuel Processing Technology, Vol. 85, pp 215-237.

Yan, L., Gupta, R.P., Wall, T.F., (2001), The implication of mineral coalescence behaviour on ash formation and ash deposition during pulverised coal combustion, Fuel, Vol. 80, pp 1333-1340.

Yani, S, Zhang, D., (2009), Transformation of organic and inorganic sulphur in a lignite during pyrolysis: influence of inherent and added inorganic matter, Proceedings of the Combustion Institute, Vol. 32, pp 2083-2089.

Yin, Y., Yin, J., Zhang, W., Tian, H., Hu, Z., Ruan, M., Xu, H., Liu, L., Yan, X., Chen, D., (2017), FT-IR and micro-Raman spectroscopic characterization of minerals in high calcium coal ashes, Journal of the Energy Institute, pp 1-8.

Yossifova, M.G., (2007), Mineral and inorganic chemical composition of the Pernik coal, Bulgaria, International Journal of Coal Geology, Vol. 72, pp 268-292.

Yu, D., Xu, M., Yao, H., Liu, X., Zhou, K., (2008), A new method for identifying the modes of particulate matter from pulverised coal combustion, Powder Technology, Vol. 183, pp 105-114.

Zaida, A., Bar-Ziv, E., Radovic, L.R., Lee, Y.J., (2007), Further development of Raman microprobe spectroscopy for characterization of char reactivity, Proceedings of the Combustion Institute, Vol. 31, pp 1881-1887.

Zhang, L., Sato, A., Ninomiya, Y., (2002), CCSEM analysis of ash from combustion of coal added with limestone, Fuel, Vol 81, pp 1499–1508.

Zhang, L., Ninomiya, Y., Yamashita, T., (2006), Formation of submicron particulate matter (PM_1) during coal combustion and influence of reaction temperature, Fuel, Vol. 85, pp1446-1457.

Zhang, Z., Wu, X., Zhou, T., Chen, Y., Hou, N., Piao, G., Kobayashi, N., Itaya, Y., Mori, S., (2011), The effect of iron-bearing mineral melting behaviour on ash deposition during coal combustion, Proceedings of the Combustion Institute, Vol. 33, pp 2853-2861.

Zhao, Y., Hu, H., Jin, L., He, X., Wu, B., (2011), Pyrolysis behaviour of vitrinite and inertinite from Chinese Pingshuo coal by TG-MS and in a fixed bed reactor, Fuel Processing Technology, Vol. 92, pp 780-786.

Appendix A: Ultimate analyses, ash chemistry and forms of sulphur

Table A-1 shows the ultimate, ash analysis, forms of sulphur of four coals samples submitted at the ALS laboratories in Witbank.

WITLAb (Pty) Ltd

Coal and Mineral Analysts

CERTIFICATE OF ANALYSES

Results reported on an Air-Dry Basis

										Ash Fusion Temperature							
		%	%	%	%	Mj/Kg	%	%	%	°C Reducing Atmosphere				%	%	%	%
Lab No.	Sample Identity	H_2O	Ash	Volatile	F/Carbon	Cal Value	T Sulphur	T Moisture	Phos	Def	Soft	Hem	Flow	Carbon	Hydrogen	Nitrogen	Oxygen
415153	Coal sample A	5.6	35.8				1.03							48.32	2.85	1.14	10.86
415150	Coal sample B	7.9	27.3				1.63							53.24	3.36	1.42	13.05
415152	Coal sample C	4.4	69.3				2.52							17.70	1.80	0.46	8.22
415151	Coal sample D	7.4	19.6				0.49							60.33	3.72	1.53	14.33

		Ash Constituent Analyses												**Forms of Sulphur**			
		%	%	%	%	%	%	%	%	%	%	%	%	%	%	%	
Lab No.	Sample Identity	CaO	MgO	K2O	Na2O	Fe2O3	TiO2	Al2O3	SiO2	Cr2O3	MnO	SO3	P2O5	Mineral	Piritic	Organic	
415153	Coal sample A	0.45	0.19	0.32	0.16	2.11	2.90	42.0	49.3	0.01	N/D	0.07	0.40	0.78	0.09	0.16	
415153	Coal sample B	0.80	0.47	0.83	0.24	6.35	1.61	28.7	57.9	0.01	0.01	0.63	0.24	1.40	0.111	0.12	
415152	Coal sample C	7.53	2.35	0.77	0.60	5.61	1.89	23.8	45.1	0.02	0.02	9.85	0.86	2.34	0.09	0.09	
415151	Coal sample D	3.46	1.95	0.26	0.26	3.23	1.90	36.1	45.5	0.01	0.04	3.96	0.98	0.30	0.05	0.14	

1. The results reported in this certificate relate only to those items listed.
2. This certificate may only be reproduced in full, unless prior written consent of Witlab (Pty) Ltd is obtained.
3. This document is issued in accordance with the Principal's instructions and is subject to the Standard Terms and Conditions of Business of Witlab (Pty) Ltd. (A copy is available on request)
4. Liability shall be limited to an amount equal to the fee paid for the service as instructed and claims in respect of this document will only be considered if based on proven gross negligence.
5. This document is not intended to relieve the parties from their contractual obligations or any sales contract.

Appendix B: Slagging and fouling indices calculations

The slagging and fouling indices calculated in the study include the detrital-authigenic index (DAI), silicion ratio, base-acid ratio, fouling index, Fe/Ca ratio, Fe plus Ca, and Fe index.

$$Detrital - Authigenic\ Index\ (DAI) = \frac{SiO_2+Al_2O_3\ +K_2O+\ Na_2O+TiO_2}{Fe_2O_3+\ MgO+CaO+SO_3}$$ Equation B-1

$$Silicon\ ratio = \frac{SiO_2}{SiO_2+Fe_2O_3+CaO+MgO}$$ Equation B-2

$$Base - acid\ ratio = \frac{Fe_2O_3+CaO+MgO+Na_2O+K_2O}{Fe_2O_3+Al_2O_3+TiO_2}$$ Equation B-3

$$Fouling\ index = \frac{Fe_2O_3+CaO+MgO+Na_2O+K_2O}{Fe_2O_3+Al_2O_3+TiO_2} \times Na_2O$$ Equation B-4

$$Iron\ index = Fe_2O_3 \times \left(\frac{B}{A}\right)$$ Equation B-5

Appendix C: Ash fusion temperature

The ash fusion test was conducted following ISO 540

Table C-1: Ash fusion temperature of SA coals

Sample	Mass (g)	Def (°C)	Soft (°C)	Hem (°C)	Flow (C)
Coal A	100	+1500	+1500	+1500	+1500
Coal B	150	1300	1320	1340	1360
Coal C	130	+1500	+1500	+1500	+1500
Coal D	100	+1500	+1500	+1500	+1500

Appendix D: Thermodynamic equilibrium modelling-FactSage 7.0

Table D-1: Thermodynamic modelling data Coal A

T°(C)	g-GAS	g-xid-SLAGA#1	g-xid-SLAGA#2	g-xid-Cord	g-xid-Mull	g-xid-CORU	g-xid-Feld	g-xid-TiO_2	Total
1100	0.07	34.97	1.02	0.31	58.44	2.06	0.85	2.29	100
1160	0.08	34.93	3.74	0.14	57.82	1.65	0.00	1.64	100
1173	0.08	34.89	4.37	0.00	57.67	1.50	0.00	1.48	100
1233	0.11	33.95	9.37	0.00	56.30	0.00	0.00	0.26	100
1254	0.12	33.80	10.30	0.00	55.78	0.00	0.00	0.00	100
1400	0.21	26.43	22.46	0.00	50.90	0.00	0.00	0.00	100

Table D-2: Thermodynamic modelling data Coal B

T°(C)	g-GAS	g-xid-SLAGA#1	g-xid-SLAGA#2	g-xid-Cord	g-xid-Mull	g-xid-CORU	g-xid-Feld	g-xid-TiO_2	Total
1100	0.65	50.69	0.55	2.95	35.00	6.62	2.89	0.66	100
1160	0.66	51.85	1.70	2.93	34.37	6.29	2.20	0.00	100
1173	0.67	49.14	7.83	2.59	34.05	5.72	0.00	0.00	100
1233	0.75	44.10	18.78	0.00	32.58	3.79	0.00	0.00	100
1254	0.94	35.26	35.40	0.00	28.40	0.00	0.00	0.00	100
1400	1.09	60.92	14.49	0.00	23.51	0.00	0.00	0.00	100

Table D-3: Thermodynamic modelling data Coal C

T°(C)	g-GAS	g-xid-SLAGA#1	g-xid-SLAGA#2	g-xid-Cord	g-xid-Mull	g-xid-CORU	g-xid-Feld	g-xid-TiO_2	Total
1100	10.02	21.04	2.13	15.41	4.10	5.58	40.21	1.50	100
1178	10.06	17.53	14.33	14.86	3.21	4.27	35.74	0.00	100
1225	10.15	46.11	0.00	12.02	3.51	2.20	26.01	0.00	100
1264	10.26	62.96	0.00	5.00	5.48	0.00	16.29	0.00	100
1282	10.28	71.99	0.00	0.00	7.06	0.00	10.67	0.00	100
1329	10.34	83.47	0.00	0.00	6.20	0.00	0.00	0.00	100
1400	10.39	87.99	0.00	0.00	1.62	0.00	0.00	0.00	100

Table D-4: Thermodynamic modelling data Coal D

T°(C)	g-GAS	g-xid-SLAGA#1	g-xid-SLAGA#2	g-xid-Cord	g-xid-Mull	g-xid-CORU	g-xid-Feld	g-xid-TiO_2	Total
1100	4.07	24.30	2.53	12.32	36.64	3.00	15.66	1.47	100
1168	4.11	20.19	14.53	11.95	35.67	1.64	11.93	0.00	100
1210	4.18	36.19	9.77	10.33	35.59	0.00	3.95	0.00	100
1225	4.20	46.19	4.81	8.99	35.81	0.00	0.00	0.00	100
1260	4.22	54.57	0.00	5.93	35.28	0.00	0.00	0.00	100
1304	4.25	60.27	0.00	0.00	35.47	0.00	0.00	0.00	100
1400	4.30	64.33	0.00	0.00	31.37	0.00	0.00	0.00	100

Appendix E: Petrographic composition of selected South African coal samples

Table E-1: Maceral group and mineral matter analyses (presented as a percentage of total sample point counts) of four South African coals calculated on a mineral matter free (mmf.) and including mineral matter.

Sample identification:		Coal A (inc. mm)	mmf	Coal B (inc. mm)	mmf	Coal C	mmf	Coal D (inc mm)	mmf
Vitrinite	Collotelinite	1.8	3.2	7.4	9.7	1.4	4.1	6.6	7.3
	Vitrodetrinite	0.4	0.7	7	9.2	0	0	0.4	0.4
	Corpogelinite	0	0	0.6	0.8	0	0	1	1.1
	Gelinite	0.6	1.1	0.2	0.3	0	0	1.6	1.8
	Pseudovitrinite	0	0	0.6	0.8	0	0	0	0
Inertinite	Fusinite	2	3.5	6.1	8.1	1.2	3.5	3.4	3.8
	Reactive semifusinite	3	5.3	4.5	5.9	0	0	2.2	2.4
	Inert semifusinite	16.6	29.4	16	21	9.8	28.5	23.8	26.5
	Micrinite	0	0	0.4	0.5	0	0	0	0
	Macrinite	0.2	0.4	1.6	2.2	0	0	0	0
	Secretinite	2	3.5	0.4	0.5	3.2	9.3	4.2	4.7
	Funginite	0	0	0.2	0.3	0	0	0	0
	Inertodetrinite	27.4	48.6	28.1	36.9	14.8	43	38	42.3
Liptinite	Sporinite	1.2	2.1	2.7	3.5	4	11.6	5.4	6
	Cutinite	0.4	0.7	0.2	0.3	0	0	3	3.3
	Resinite	0.4	0.7	0	0	0	0	0.2	0.2
	Liptodetrinite	0.4	0.7	0	0	0	0	0	0
Mineral matter	Silicate	17.4		5.3		46.6		4.8	
	Sulfide	5.8		2.5		4		0.8	
	Carbonate	3.8		5.5		1.2		1	
	Quartz	16.2		10.5		13.6		3.4	
	Other	0.4		0.2		0.2		0.2	
Maceral group total (vol.%)	Vitrinite	2.8	5	15.8	20.8	1.4	4.1	9.6	10.7
	Inertinite	51.2	90.8	57.4	75.5	29	84.3	71.6	79.7
	Liptinite	2.4	4.3	2.9	3.8	4	11.6	8.6	9.6
	Mineral matter	**43.6**		**24**		**65.6**		**10.2**	

Appendix F: XRD analyses of low temperature and high temperature ashes

Four powdered coal samples were supplied by the University of the Witwatersrand. A representative portion of each coal was subjected to low-temperature oxygen-plasma ashing, using an IPC 4-chamber asher, as outlined in Australian Standard 1038, Part 22. The mass percentage of low-temperature ash (LTA) was determined in each case. The mineralogy of each LTA was analysed by X-ray powder diffraction using a Phillips X'pert diffractometer with copper K-α radiation, and the minerals present identified by reference to the ICDD Powder Diffraction File. Quantitative analyses of mineral phases in the LTA were made using SIROQUANT™, commercial interpretation software written by CSIRO (J.C. Taylor, Powder Diffraction, 6, 2-9, 1991) based on the Rietveld XRD analysis technique.

Table F-1 provides data on the percentages of the individual minerals in the LTA sample from the Siroquant interpretation. The table lists the estimated weight percentage of the crystalline phases recognised, together with the relative error in the estimation (estimated standard deviation or ESD) for each individual mineral determination. The overall level of fit for the SIROQUANT evaluation is given by the relevant global chi^2 value at the foot of the table. The total error for each mineral percentage can be calculated from the product of the ESD associated with that mineral and the square root of the global chi^2 value for the SIROQUANT analysis. In some cases the error is larger than the actual percentage indicated. The mineral abundance in such cases is close to or below the detection limit of the analysis process, but is mentioned in the table to maintain consistency and to ensure that its possible presence is taken into account.

Traces of anatase and/or rutile may be present in some samples, especially LTA-D. However they could not be quantified by Siroquant, and if present are therefore at concentrations below the detection limit of the XRD system.

The clay fraction (less than 2 μm effective diameter) of each sample was isolated by ultrasonic dispersion in sodium hexametaphosphate (Calgon) and subsequent settling. The clay fraction was investigated further by X-ray diffraction of oriented aggregates, using glycol and heat treatment. The relative proportions of the different clay minerals in this fraction for each sample (Table 2) were determined by the method of Griffin (in R.E. Carver, *Procedures in Sedimentary Petrology,* Wiley, 1971). The inferred chemical composition of the ashes expected from each sample, calculated from the mineral abundance and assumed mineral compositions, is given in Table F-5

High temperature ash XRD diffractograph are presented in Figures F-1 to F-8.

Mineralogical analysis data by powder XRD and Siroquant

Table F-1: X-ray diffraction (XRD) analyses of LTA-A (48.7 wt. %)

Phase	Weight %	Error of Fit
Quartz	4.6	0.17
Kaolinite	79.2	0.68
Mixed layer illite/smectite	10.6	0.64
Dolomite	2.7	0.28
Pyrite	2.1	0.18
Goyazite	0.9	0.23

Global Chi^2: 5.78

Table F-2: X-ray diffraction (XRD) analyses of LTA-B (31.6 wt. %)

Phase	Weight %	Error of Fit
Quartz	20.3	0.28
Kaolinite	47.3	0.62
Mica	2.7	0.17
Illite	2.8	0.70
Mixed layer illite/smectite	12.6	0.46
Calcite	1.4	0.21
Dolomite	7.6	0.43
Pyrite	2.1	0.15
Goyazite	1.4	0.18
Bassanite	1.8	0.21

Global Chi^2: 5.42

Sample: LTA sample C 77.9%

Table F-3: X-ray diffraction (XRD) analyses of LTA-C (77.9 wt. %)

Phase	Weight %	Error of Fit
Quartz	15.2	0.31
Kaolinite	63.7	0.94
Illite	1.5	0.98
Mixed layer illite/smectite	17.2	0.81
Dolomite	1.0	0.25

Global Chi^2: 5.59

Table F-4: X-ray diffraction (XRD) analyses of LTA-D (24.1 wt. %)

Phase	Weight %	Error of Fit
Quartz	1.8	0.15
Kaolinite	93.5	0.57
Mixed layer illite/smectite	4.6	0.55

Global Chi^2: 4.96

Table F-5: Mineralogy of <2 µm fraction (wt. %) in low temperature ash samples by oriented-aggregate XRD analysis

Sample Name	Kaolinite %	Illite %	Expandable clays%	Nature of Expandable Clay
LTA A	96	0	4	Irregular illite/smectite
LTA B	90	0	10	Irregular illite/smectite
LTA C	91	6	3	Irregular illite/smectite
LTA D	97	2	2	Irregular illite/smectite

X-ray diffraction (XRD) analyses of high temperature ashes

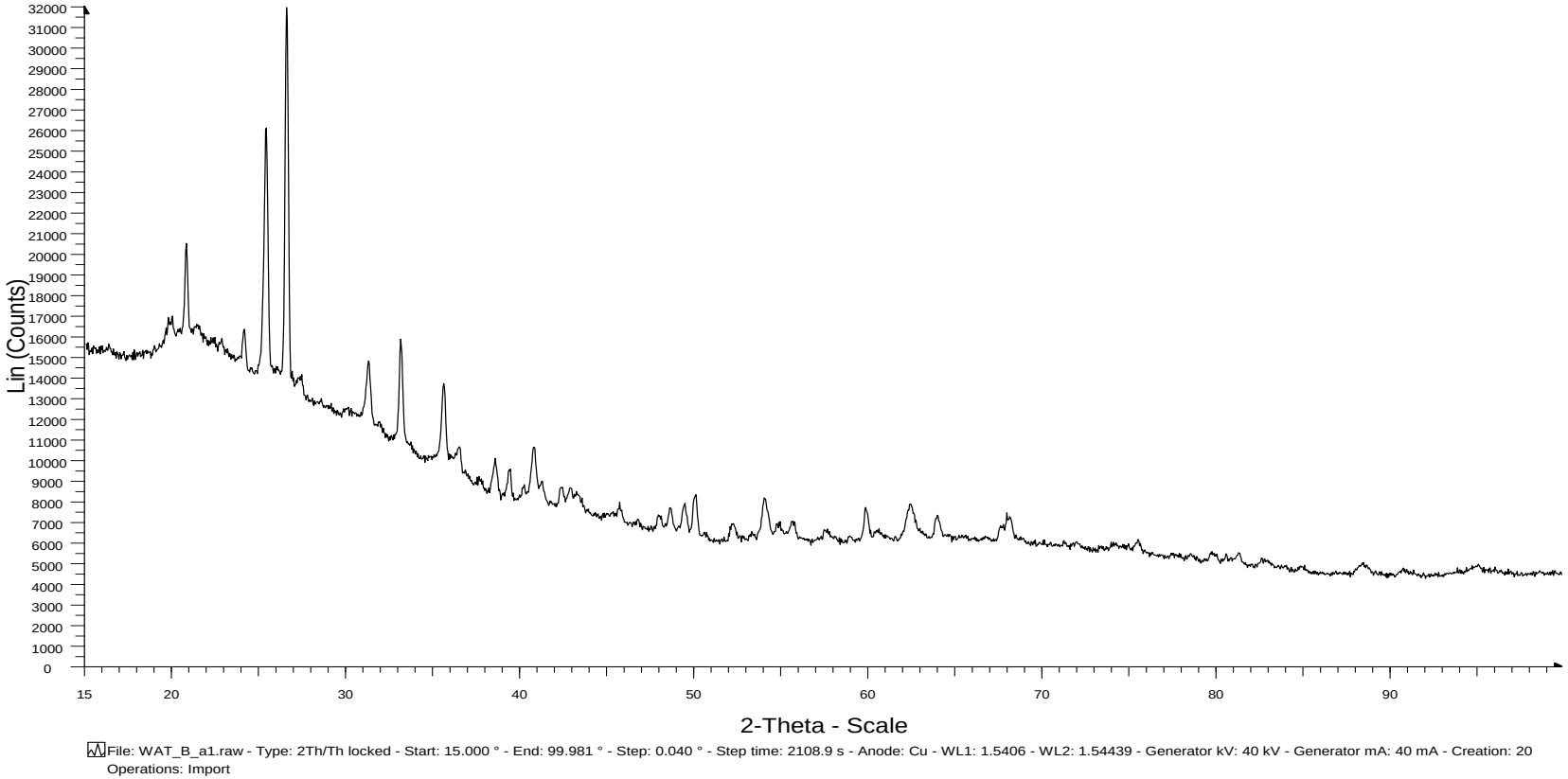

Figure F-1: As measured diffraction pattern of HTA-A.

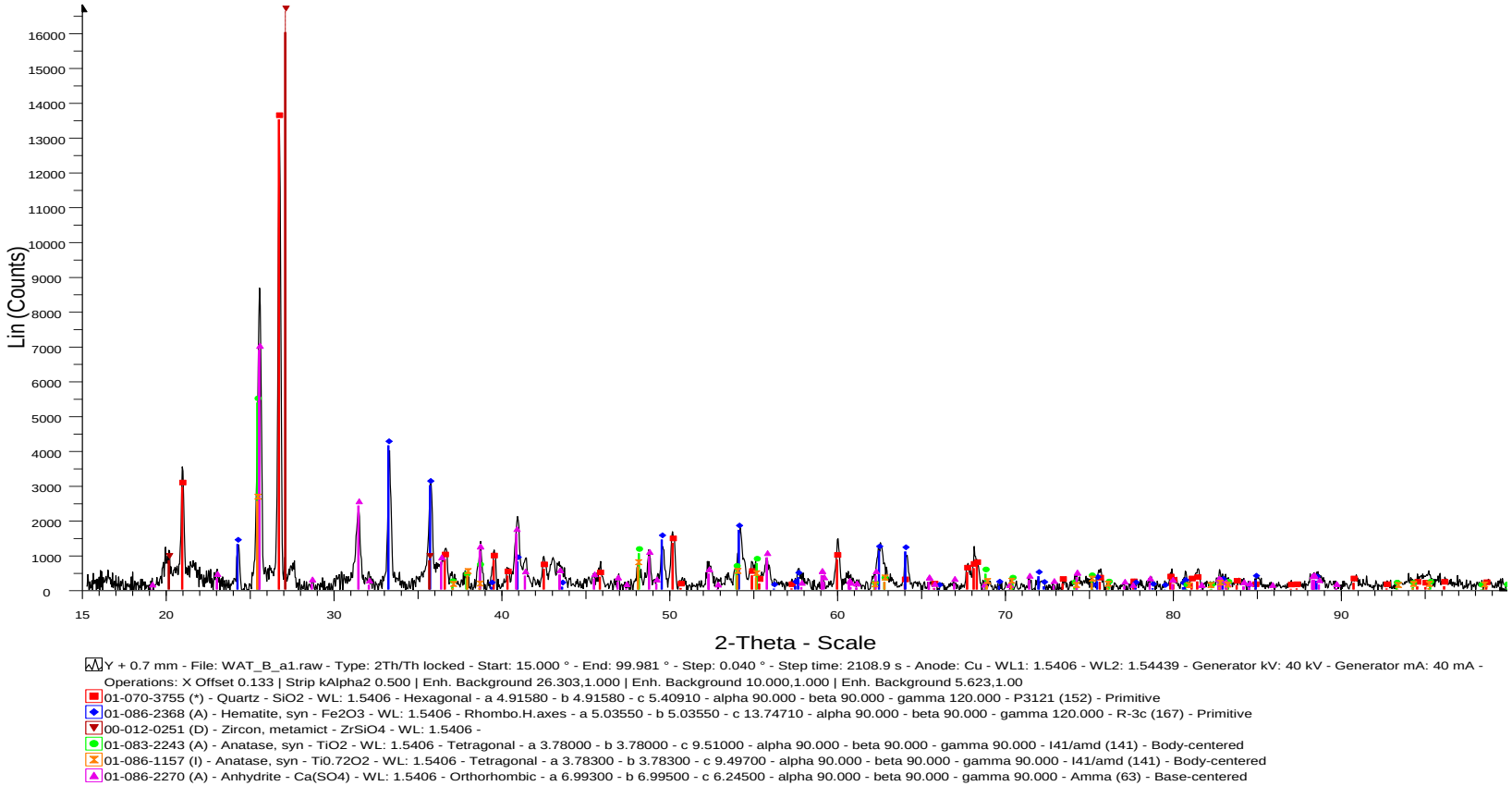

Figure F-2: Background subtracted diffraction pattern of HTA-A overlaid with stick pattern of the proposed phases

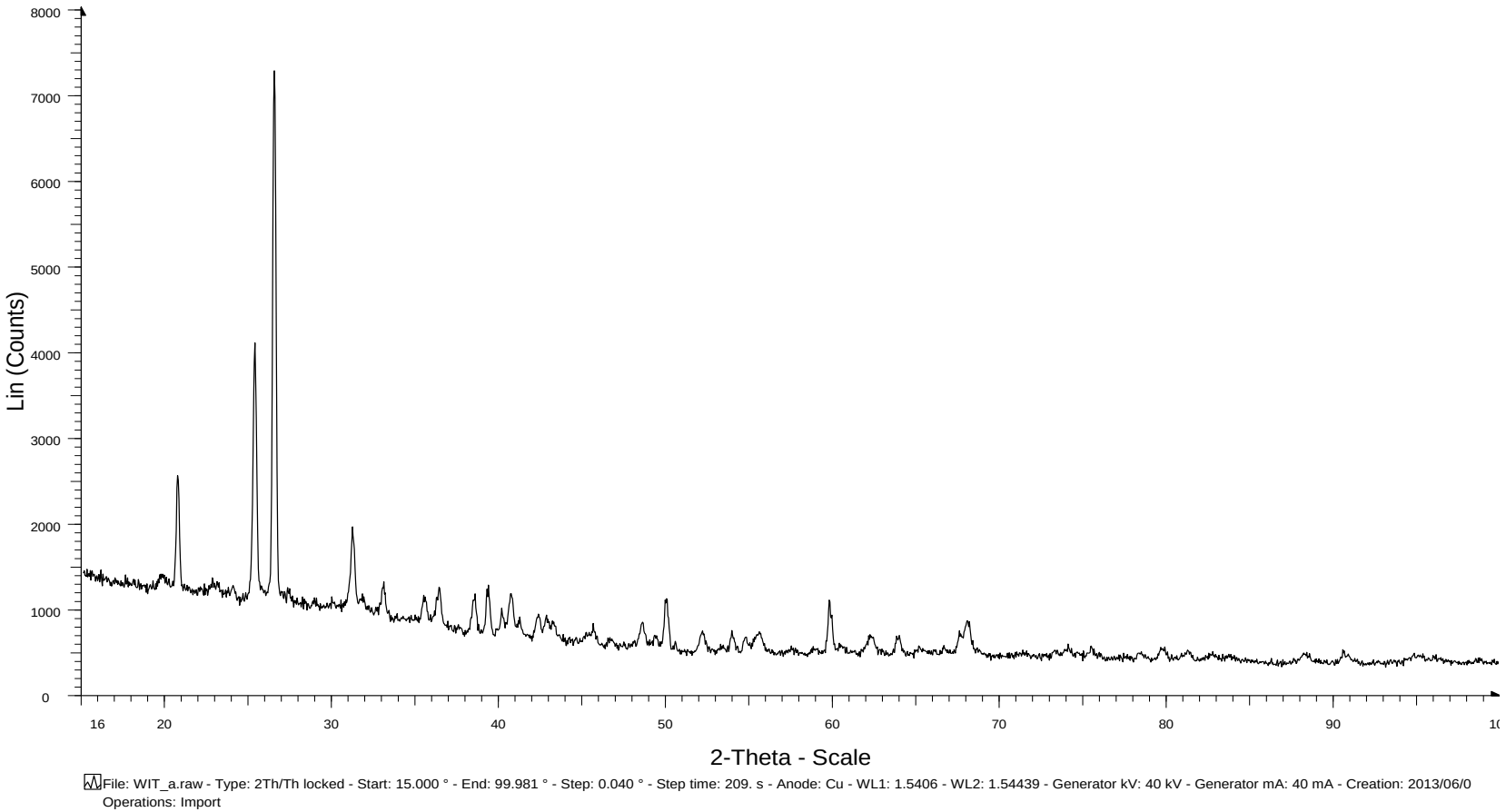

Figure F-3: As measured diffraction pattern of HTA-B

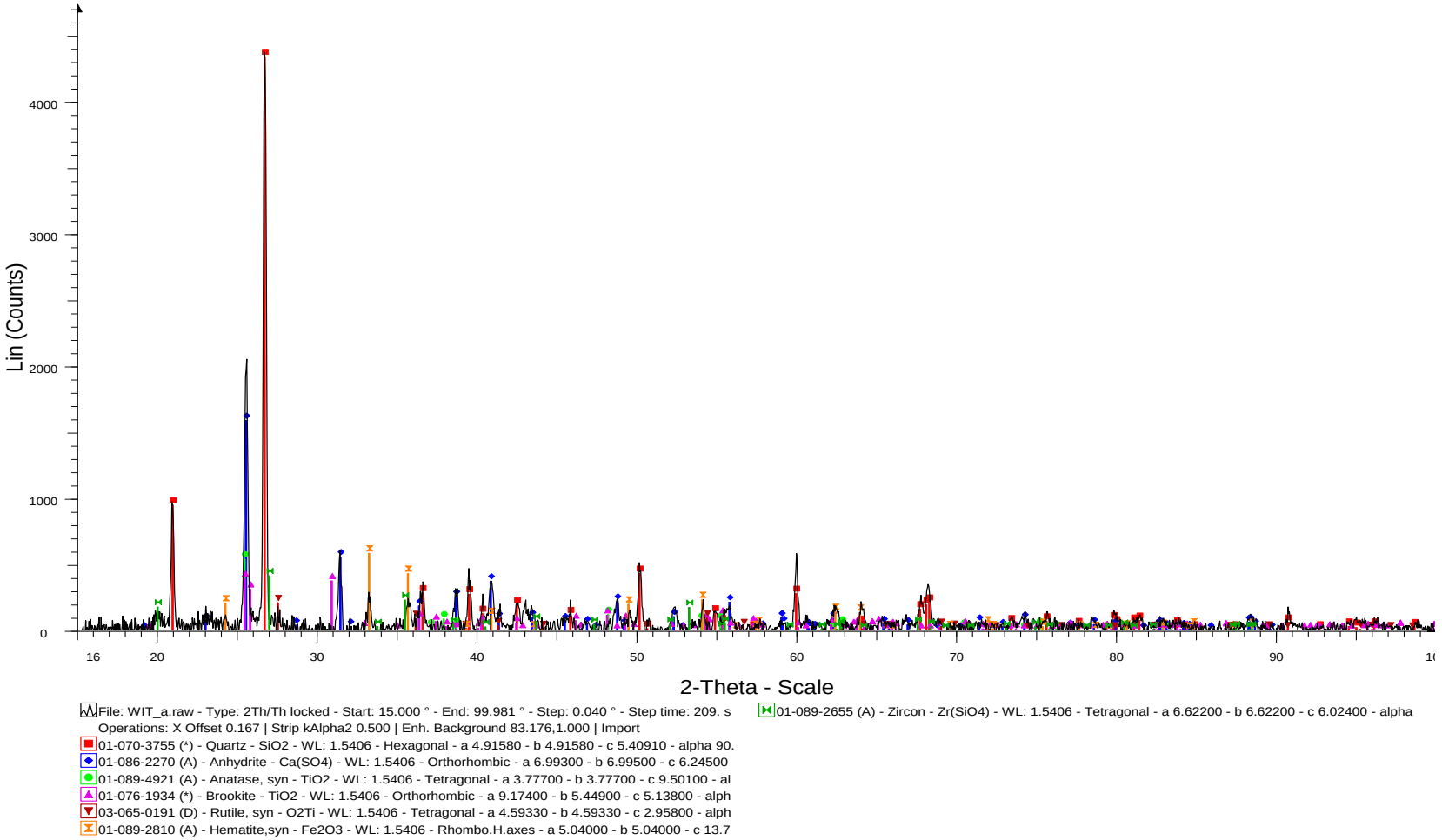

Figure F-4: Background subtracted diffraction pattern of HTA-B overlaid with stick pattern of the proposed phases

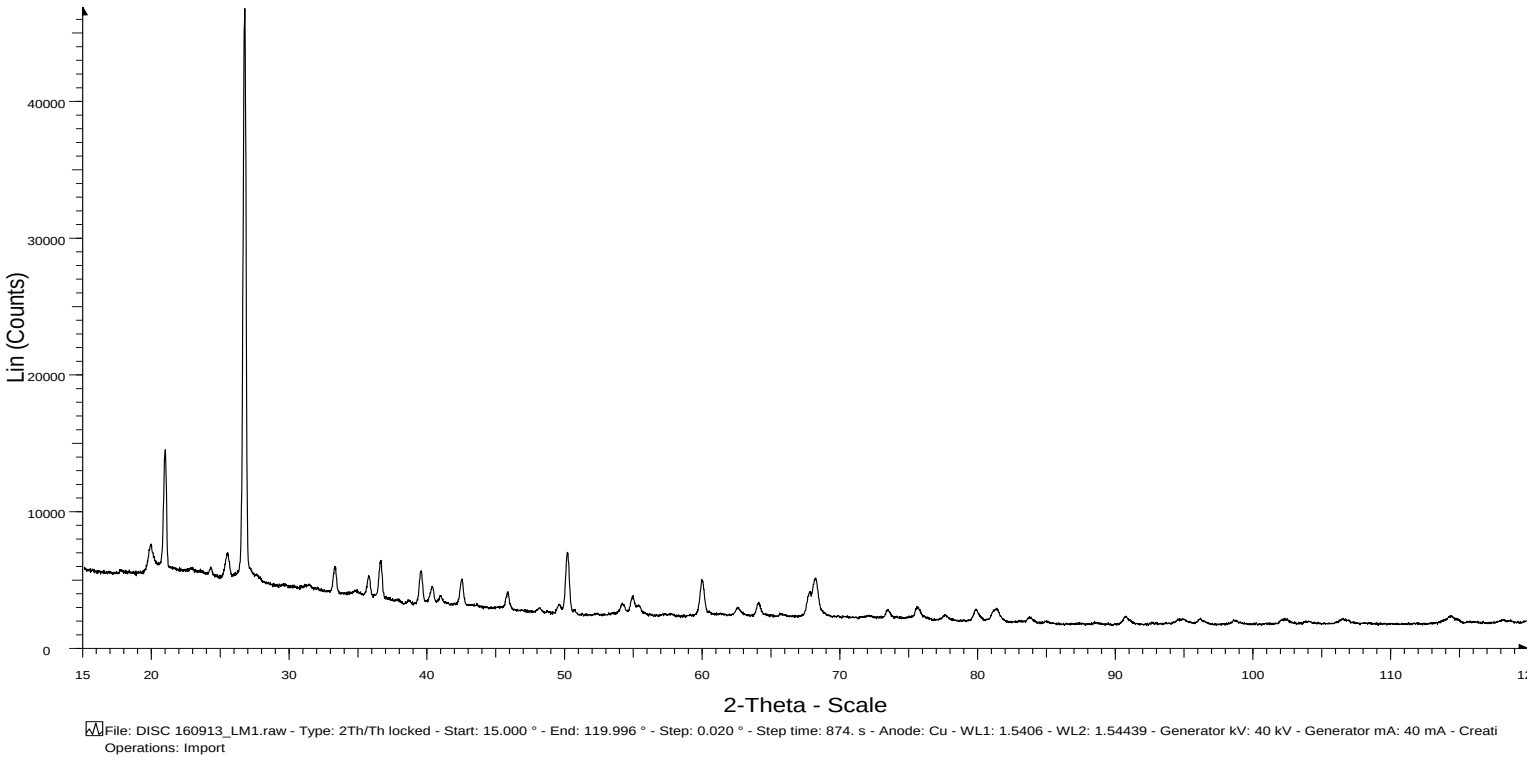

Figure F-5: As measured diffraction pattern of HTA-C

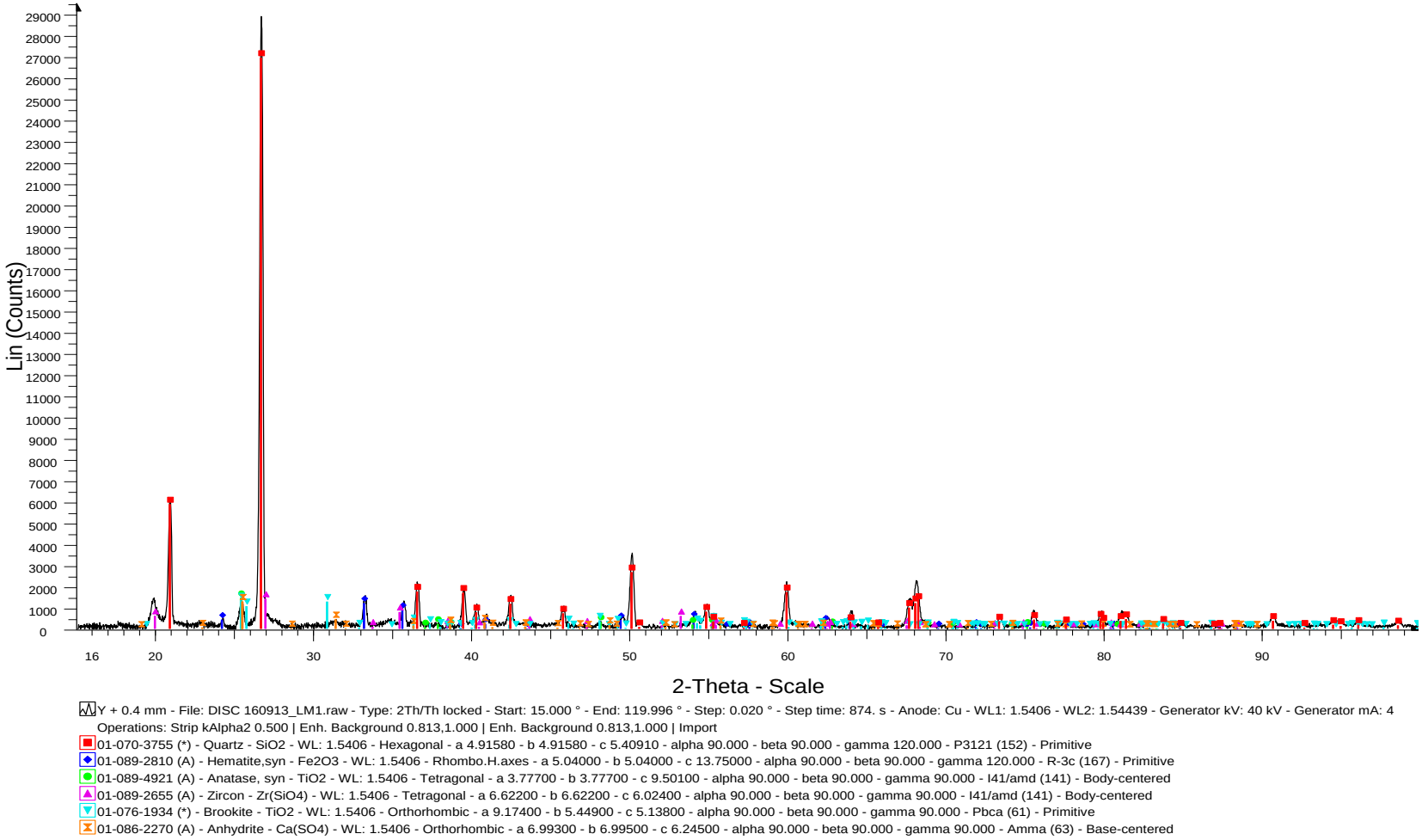

Figure F-6: Background subtracted diffraction pattern of HTA-C overlaid with stick pattern of the proposed phases

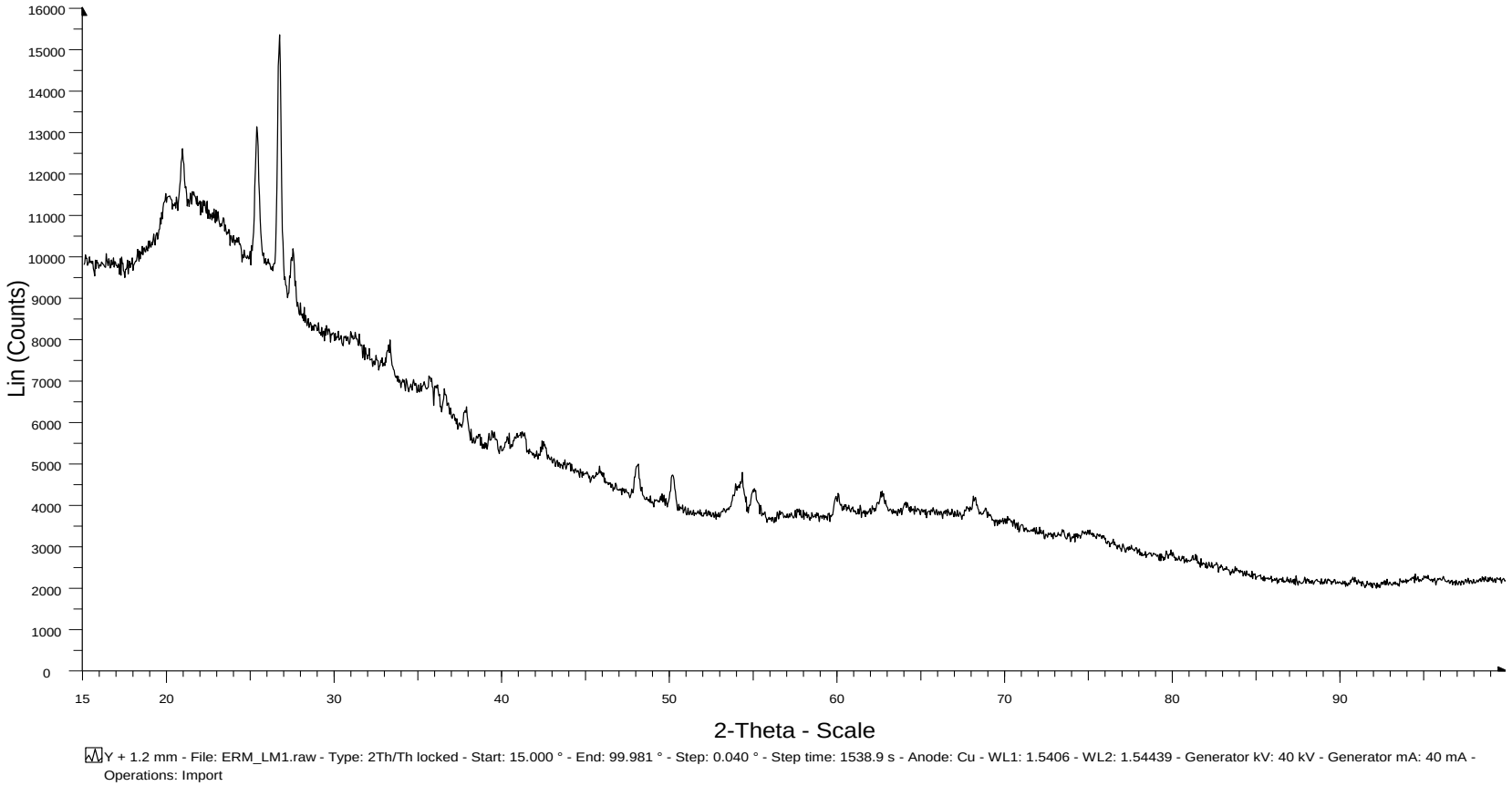

Figure F-7: As measured diffraction pattern of HTA-D

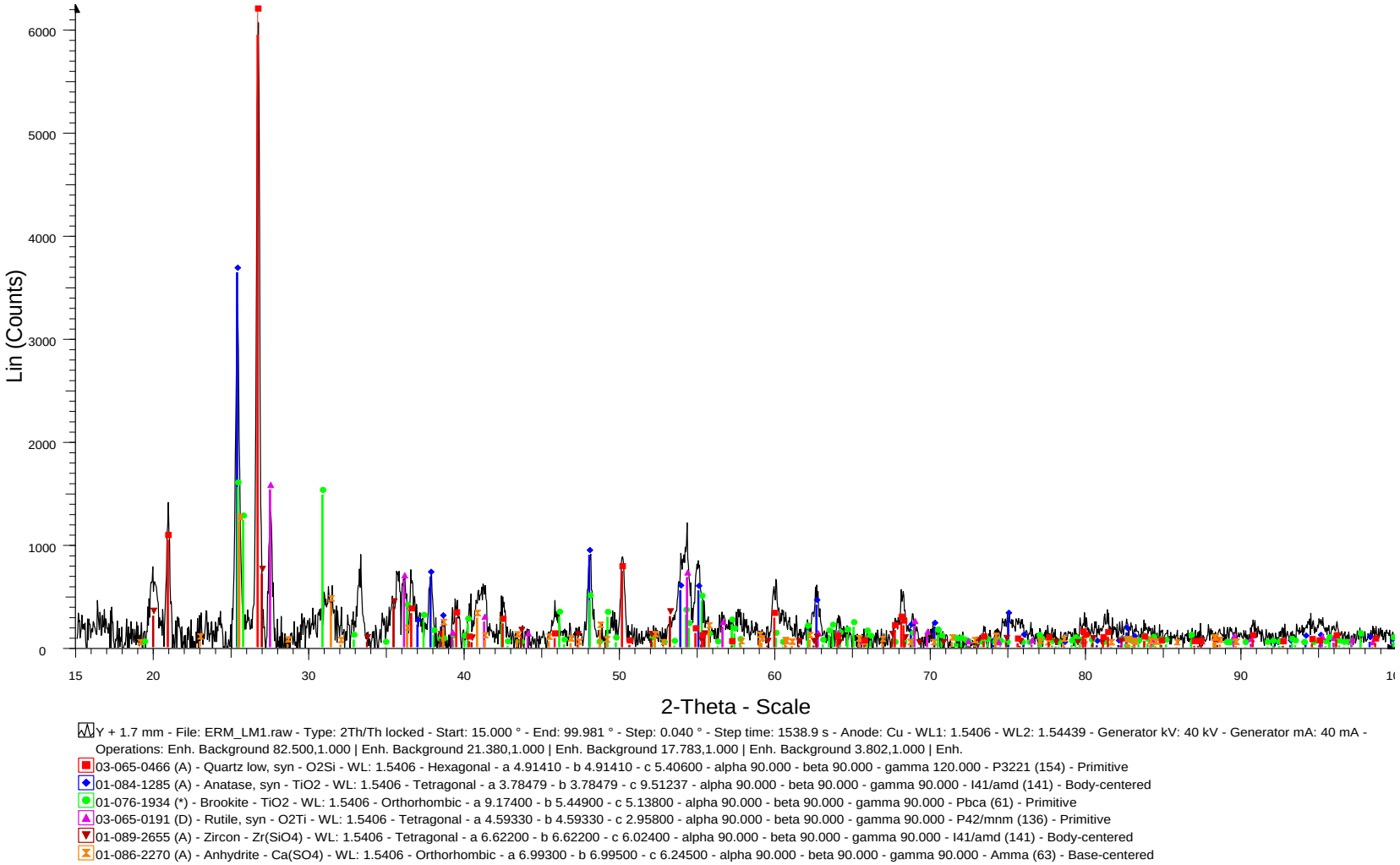

Figure F-8: Background subtracted diffraction pattern of HTA-D overlaid with stick pattern of the proposed phases

Appendix G: Fourier-Transform Infra-Red (FTIR) analyses of raw coals, low temperature and high temperature ashes

Figures G1-G8 represents the actual FTIR spectra obtained from low and high temperature samples. The analyses were recorded over a spectral range of 500 to 4000 cm^{-1}.

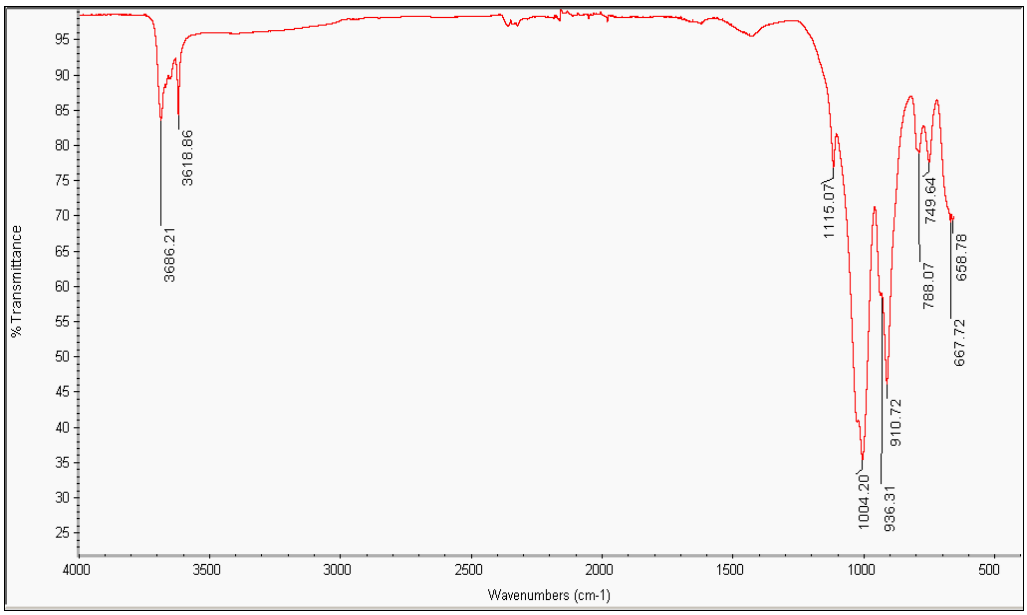

Figure G-1: FTIR spectra of LTA-A

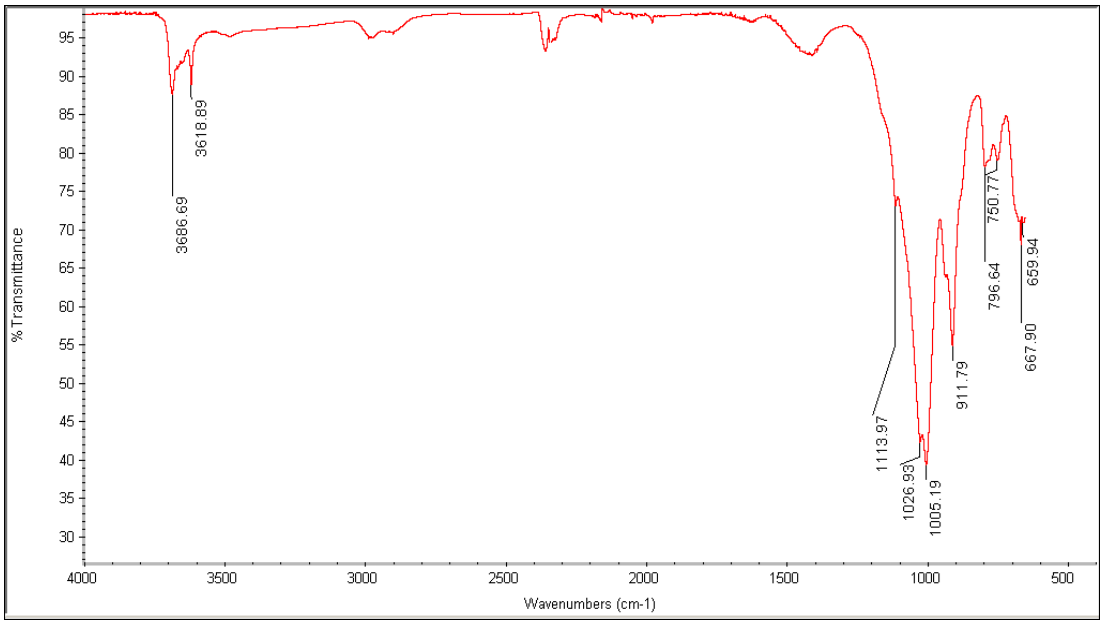

Figure G-2: FTIR spectra of LTA-B

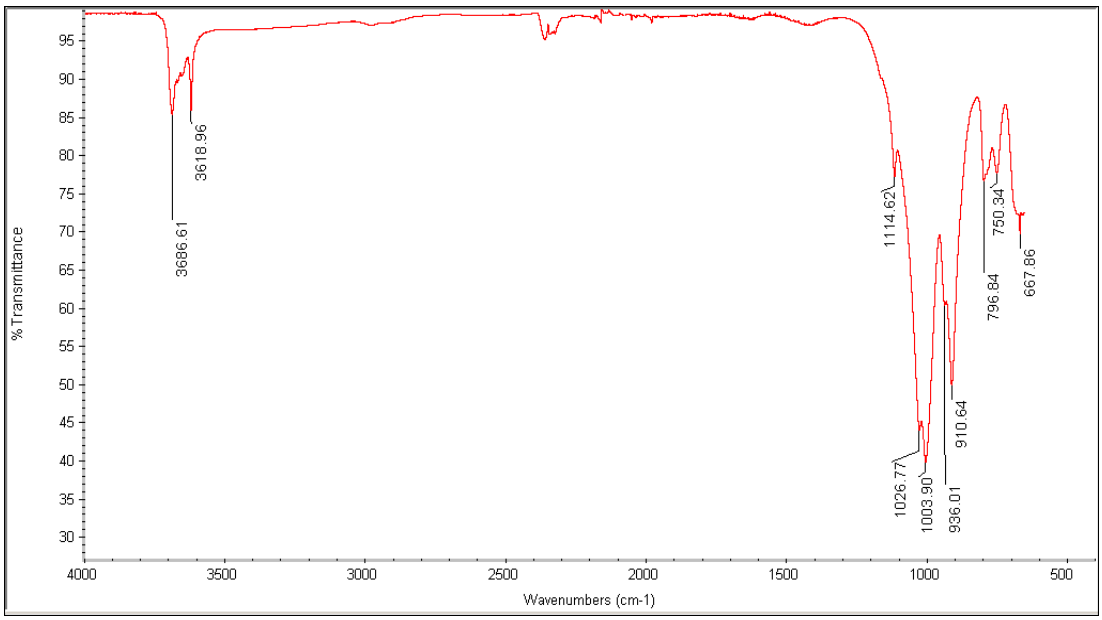

Figure G-3: FTIR spectra of LTA-C

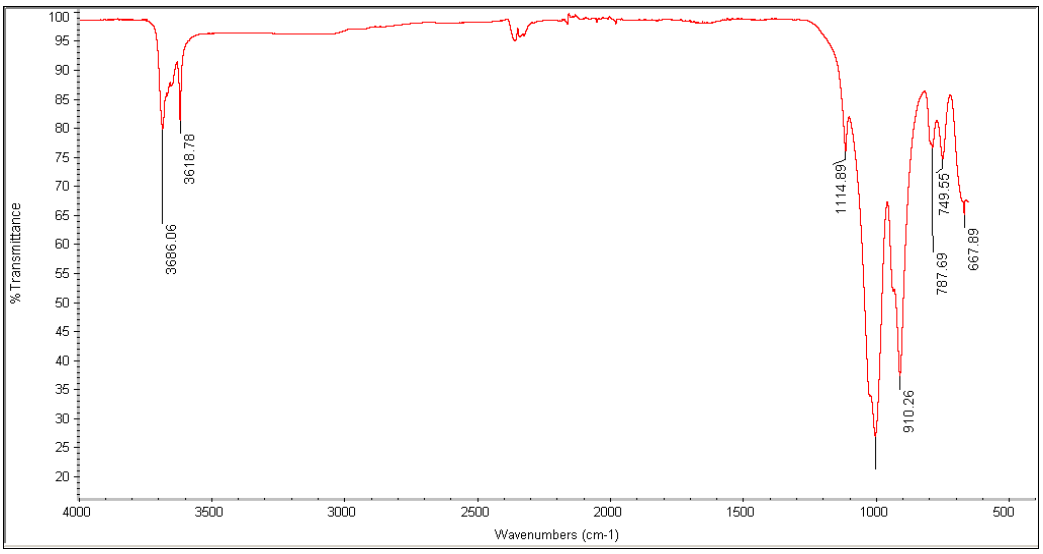

Figure G-4: FTIR spectra of LTA-D

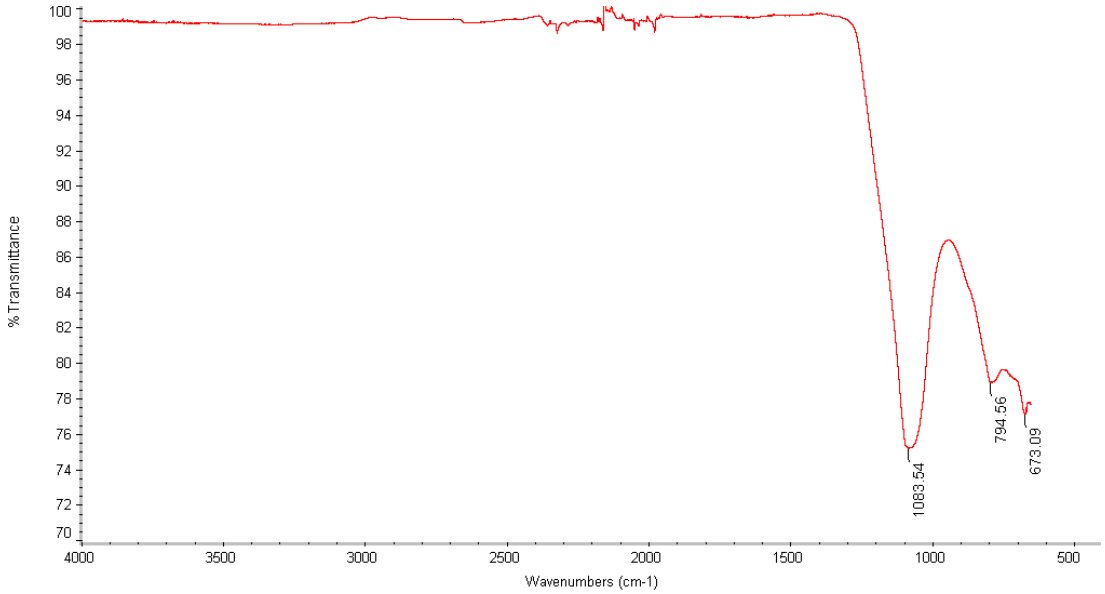

Figure G-5: FTIR spectra of HTA-A

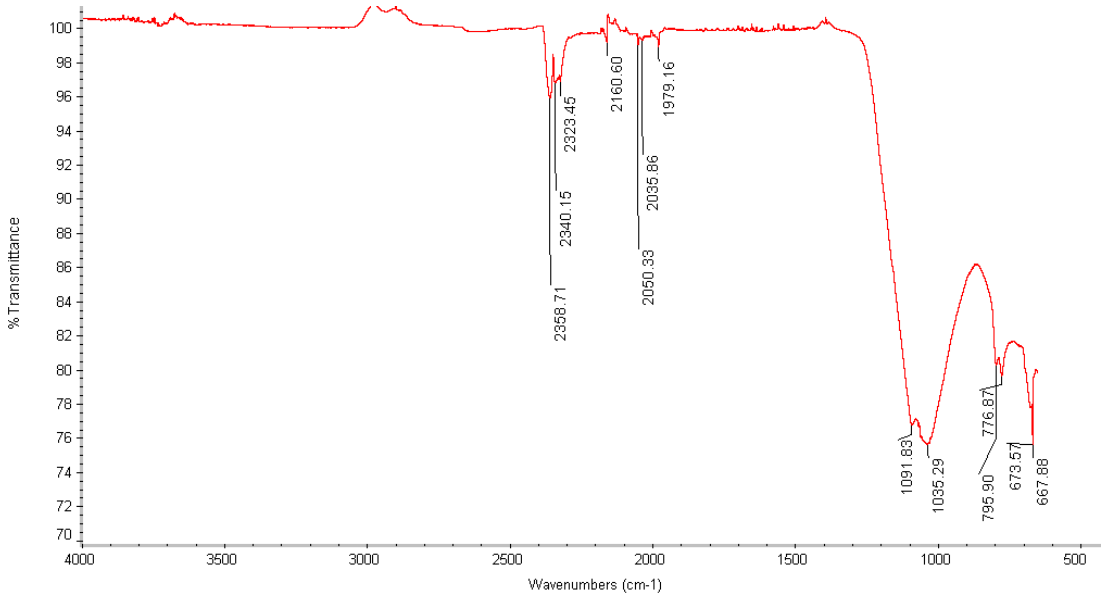

Figure G-6: FTIR spectra of HTA-B

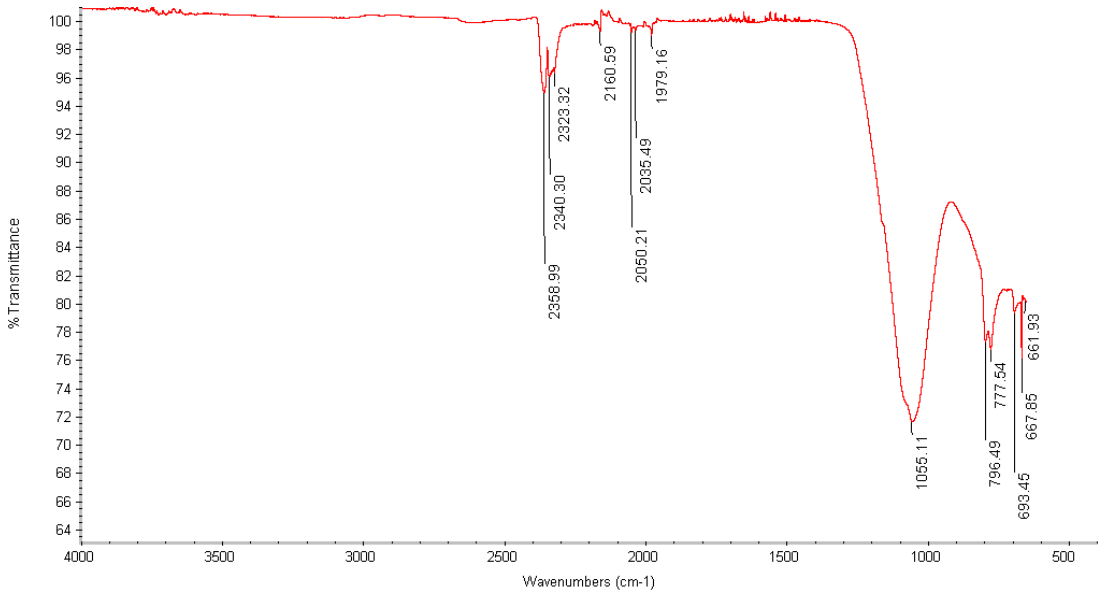

Figure G-7: FTIR spectra of HTA-C

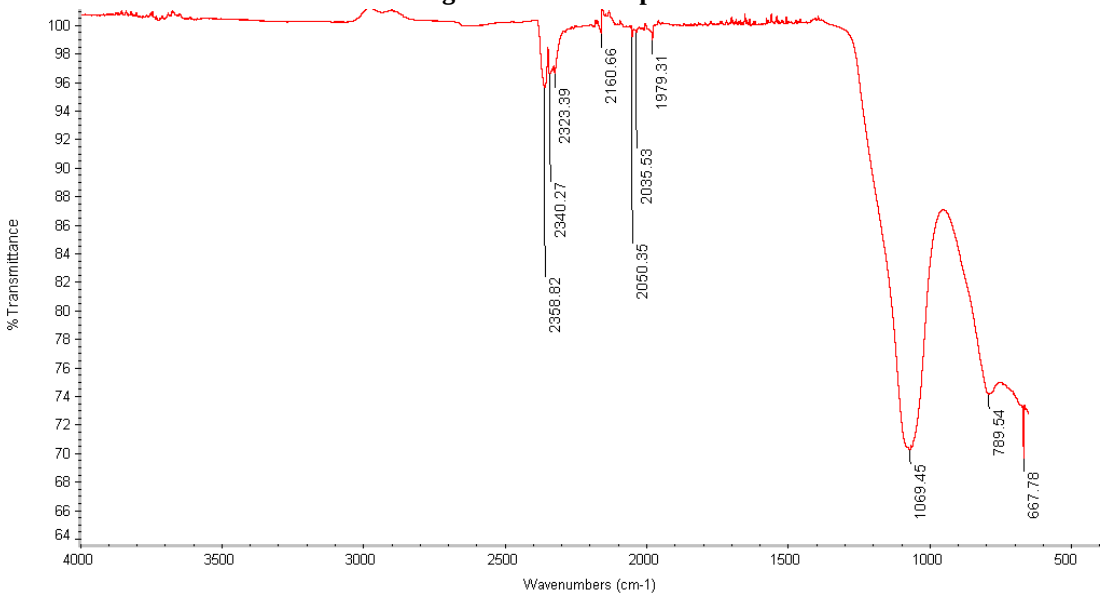

Figure G-8 FTIR spectra of HTA-D

Appendix H: micro-Raman analyses of raw coals, low temperature and high temperature ashes

Figure H-1 to H-5 represent Raman spectra of mineral matter identified in raw coals, low and high ashes. Raman spectra were collected over a spectral range from 50-1500 $cm^{-1.}$

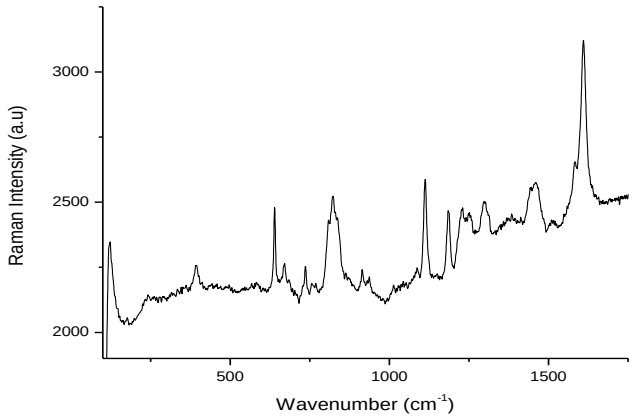

Figure H-1: Raman spectra of jarosite observed in coal B, in the 50-1500 cm^{-1} range (Micro Raman, excitation 532 nm).

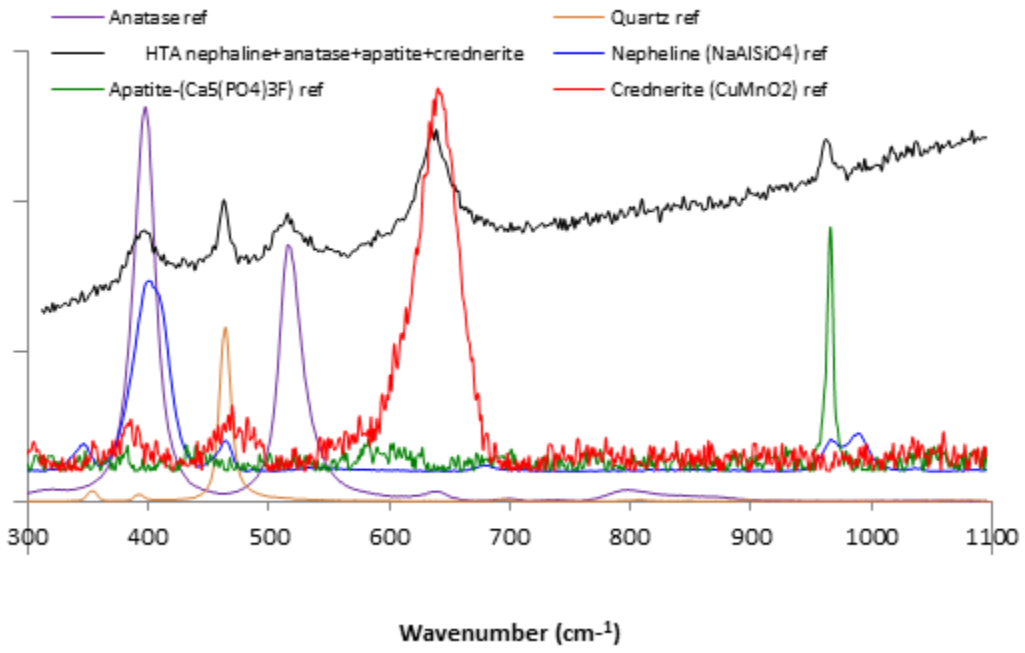

Figure H-2: Raman spectra of a mixture of anatase, quartz, nepheline, apatite, and crednerite in HTA in the 50-1500 cm^{-1} range (Micro Raman, excitation 532 nm).

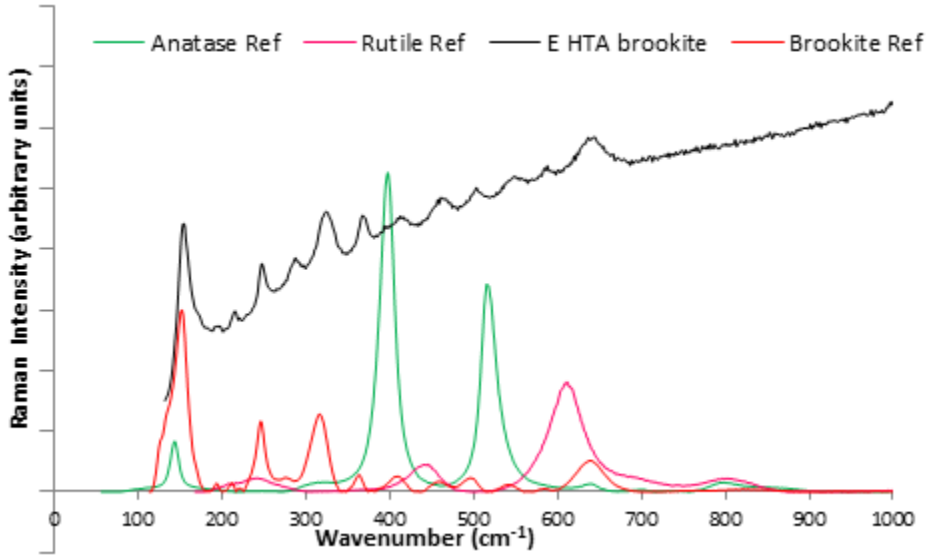

Figure H-3: Raman spectra of a mixture of anatase, rutile and brookite in HTA-D in the 50-1500 cm^{-1} range (Micro Raman, excitation 532 nm).

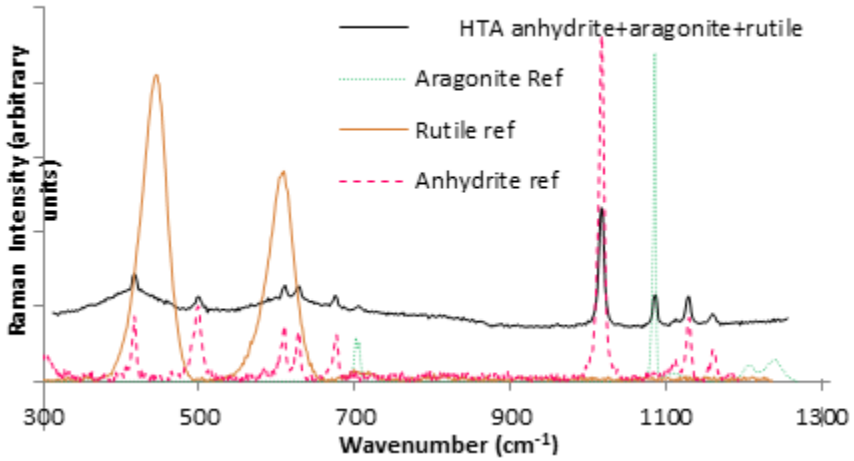

Figure H-4: Raman spectra of a mixture of anatase, rutile, anhydrite in HTA-B in the 50-1500 cm^{-1} range (Micro Raman, excitation 532 nm).

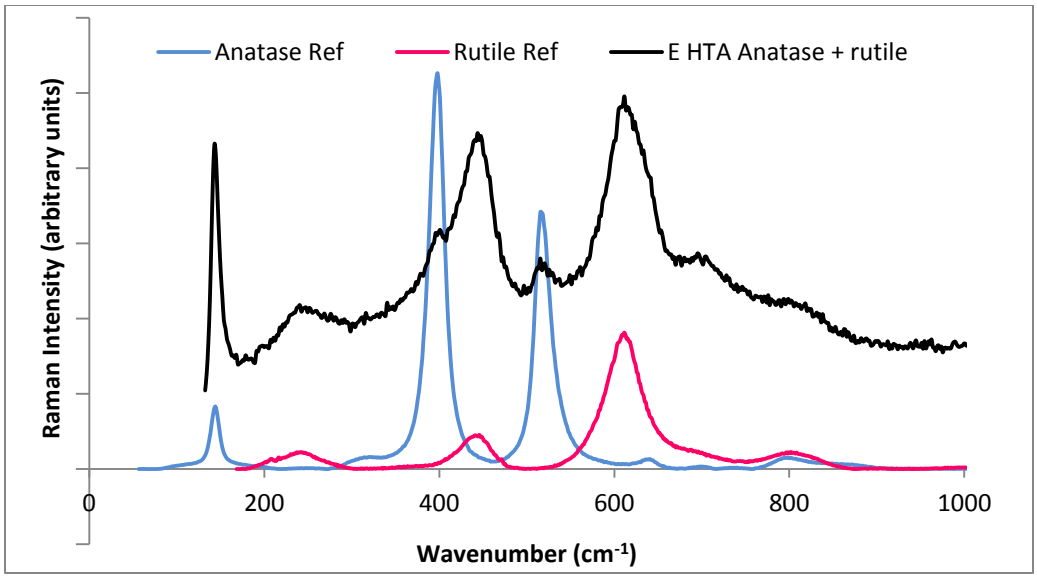

Figure H-5: Raman spectra of a mixture of anatase and rutile in HTA-D in the 50-1500 cm^{-1} range (Micro Raman, excitation 532 nm).

Appendix I: Single particle analysis (SPA)-electron probe X-ray micro analyses (EPXMA) of raw coals

The principal component analysis (PCA) and chemical boundary classification (CBC) data used to determine mineral matter classification. Data was collected on 500 particles.

Table I-1: Single particle analysis (SPA)-elemental abundance in raw coals (mol. %)

Elemental abundance (%)	Coal A	Coal B	Coal C	Coal D
C	24.0	27.1	20.7	22.9
N	24.2	27.0	22.7	22.8
O	3.3	4.1	1.9	6.7
P	0.1	0.1	0.1	0
S	1	0.4	0.4	3.7
Cl	0	0.4	0.5	2.8
Na	0.1	0.1	0	8.4
K	0	0	0	0
Mg	1.1	0.5	0	0.7
Ca	0	0	0	1.5
Al	16.2	11.8	21.1	8.7
Si	15.9	12	22	8.9
Ti	1.3	2.3	1.2	1.4
Cr	2.3	2.8	1.4	2.2
Mn	2.6	3.3	2.2	2.6
Fe	8	8.3	5.6	6.6
Total	**100**	**100**	**100**	**100**

Table I-2: Component matrix extraction loading

	Component					
	1	2	3	4	5	6
Na	.070	.903	-.125	.010	-.230	.028
Mg	.873	.024	.442	-.006	.054	-.010
Al	-.649	.047	.238	.349	.044	-.614
Si	-.709	-.067	.301	-.430	-.053	.427
P	.149	.894	-.112	.032	-.240	.019
S	.493	-.173	-.720	-.066	-.087	-.052
K	-.071	.522	-.078	-.102	.834	.042
Ca	.853	.043	.450	-.002	-.003	-.008
Ti	-.033	-.056	-.029	.889	.064	.446
Mn	.712	-.084	.422	-.006	.060	-.038
Fe	.457	-.199	-.717	-.038	.131	-.036

Extraction Method: Principal Component Analysis.

a. 6 components extracted.

Table I-3: Chemical boundary classification (CBC) mineral composition in raw coals (mol. %)

Mineral	**Coal A**	**Coal B**	**Coal C**	**Coal D**
Fe-rich	98	116	16	112
Quartz	0	7	18	1
Carbonates	2	0	0	5
Silicates	220	256	429	150
Gypsum	4	0	0	0
Ti-rich	6	10	1	4
Sulphate silicate mix	96	91	3	110
Dolomite	21	7	1	45
Sulphates	7	7	3	7
Halite	0	1	0	25
Other Ca-rich	1	0	0	29
Other carbonaceous not assigned	45	5	29	12

Review

Journal of RAMAN SPECTROSCOPY

Received: 14 August 2009 Accepted: 17 January 2010 Published online in Wiley Online Library: 11 March 2010

(wileyonlinelibrary.com) DOI 10.1002/jrs.2636

Raman spectroscopy for the analysis of coal: a review

S. Potgieter-Vermaak,[a,b]* N. Maledi,[c] N. Wagner,[c] J. H. P. Van Heerden,[d] R. Van Grieken[b] and J. H. Potgieter[e]

The advances in the characterization of amorphous carbons by Raman spectroscopy over the last four decades are of interest to many industries, especially those involving the combustion, gasification and pyrolysis of coal. Many researchers report on the Raman character of the natural organic matter in carbon-containing compounds, such as coal, and relate the Raman bands to the structural order of the amorphous carbons. The basis of most of these studies evolved around the assignment of the G (graphitic, ~1580 cm^{-1}) band to crystalline graphite and any other bands, called D bands, (disorder, various from 1100 to 1500 cm^{-1}) to any type of structural disorder in the graphitic structure. Concerning coal analysis, the information gained by Raman investigations has been used to describe char evolution as a function of temperature, the presence of catalysts and different gasification conditions. In addition, researchers looked at maturation, grade, doppleritization and many more aspects of interest. One aspect that has, however, not been addressed by most of the researchers is the natural inorganic matter (NIM) in the carbon-containing compounds. Micro-Raman spectroscopy (MRS) has many advantages over other characterization tools, i.e. *in situ* analysis, nondestructive, no sample preparation, low detection limit, micrometer-scale characterization, versatility and sensitivity to many amorphous compounds. With the distinct advantages it has over that of other molecular characterization tools, such as powder X-ray diffraction (PXRD), Fourier-transform infrared spectrometry (FT-IR) and scanning electron microscopy with X-ray detection (SEM/EDS), it is surprising that it has not yet been fully exploited up to this point for the characterization of the NIM in coal and other amorphous carbons. This paper reviews the work published on the Raman characterization of the natural organic matter (NOM) of coals and reports on preliminary results of the NIM character of various South African coals, whereby various inorganic compounds and minerals in the coal have been characterized.

Keywords: Raman spectroscopy; coal; maceral; mineral matter; carbonaceous matter

Introduction

Raman spectroscopy has had its rightful place in carbon characterization since the discovery of the Raman effect in 1928, and even more so since the renaissance of Raman spectroscopy due to the advancements in laser technology, instrument design and detectors. Even though this review is exclusively concerned with the characterization of coal, mention of graphite-like materials will be made, due to the resemblance between polycrystalline graphite and coal.

Coal is an organic, combustible, sedimentary rock of infinite variations, formed from layered plant remains consolidated under superimposed strata. Depending on the maturation stage reached in the coalification process, coal is mainly composed of carbon, oxygen, nitrogen and sulfur in variable proportions. Graphite, essentially the end point of coalification, only contains carbon. Anthracite represents the highest metamorphic rank in coal (reflectance values >2% RoV). Typically, anthracite contains 5–9% volatile matter (measured as 'dry mass mineral matter free' (dmmf)), carbon content of 92–98% (dmmf), hydrogen 2.9–3.8% (dmmf), low ash and moisture contents. Typically, coals in South Africa are low-rank bituminous (medium rank C/D coals), with only 1% being semi-anthracite/anthracite.

Commercially and analytically, coal is characterized by its chemical properties (particularly volatile matter contents, ash yield and calorific value), its rank (degree of maturity), type (organic composition as determined petrographically), mineral (inorganic) content and the arrangement of the organic and inorganic components. Coal type includes macerals which are typically divided into three maceral groups: namely, vitrinite, inertinite, and liptinite. Macerals are the discrete organic component in coal, originating from differing plant tissue, dependent on plant type/community, climate, ecological conditions, acidity and redox potential of the coal-forming environment. Each maceral category possesses significantly different chemical, physical and performance characteristics, which vary according to coal rank. In the bituminous rank range, and relative to each other, vitrinite

* Correspondence to: S. Potgieter-Vermaak, Department of Chemistry, University of Antwerp, Universiteitsplein 1, B-2610 Antwerp, Belgium.
E-mail: Sanja.potgieter@ua.ac.be

a Molecular Science Institute, School of Chemistry, University of the Witwatersrand, Wits, 2050 South Africa

b Department of Chemistry, University of Antwerp, Universiteitsplein 1, B-2610 Antwerp, Belgium

c School of Chemical and Metallurgical Engineering, University of the Witwatersrand, Wits, 2050 South Africa

d Sasol Technology (PTY) Ltd, Research and Development, Sasolburg, 1947 South Africa

e School of Biology, Chemistry and Health Sciences, Manchester Metropolitan University, Manchester M1 5GD, UK

is oxygen-rich, liptinite is hydrogen-rich and inertinite is carbon-rich. In addition, vitrinite is rich in aromatic structures, liptinite is aliphatic and inertinite is highly aromatic.

The term 'minerals' applies to the natural inorganic constituents of coal. Broadly, these minerals fall into three main groups: silicates (quartz and clays), sulfides, and carbonates. Organic mineral matter may occur in the form of sulfur, calcium, phosphorus, iron, magnesium, potassium and trace elements. Inorganic mineral matter includes clays (illite, kaolinite and rarely montmorillinite), salts, sulfur and silicates (quartz). Generally, the ash yield of a coal is taken as indicative of the inorganic component. Clays in coal are typically illite ($K_2O.3Al_2O_3.6SiO_2.2H_2O$) and kaolinite ($Al_2O_3.2SiO_2.H_2O$), but can also include sericite, smectite, montmorillinite and mixed layers. Carbonate minerals found in coal include siderite ($FeCO_3$), dolomite ($CaMg(CO_3)_2$), ankerite ($(Ca,Mg,Fe)CO_3$), calcite ($CaCO_3$) and magnesite ($MgCO_3$). These carbonates fall into the hexagonal group of carbonates characterized by a dominant rhomboidal cleavage. Sulfides are one of the mineral groups found in coal. They include pyrite, marcasite, mainikovite, sphalerite, galena and chalcopyrite. Sulfate occur as oxidized sulfides, forming gypsum, jarosite and hydrated iron sulfates.

Understanding coal and the ability to predict its behavior in combustion processes is of essence within the coal industry. From the vast amount of literature available in the open domain, it is very clear that the understanding of coal properties in general and as utilized has always been accepted as an important research and operational factor. The complex nature of coal, as in part discussed in this paper, clearly presents among others, analytical experts and researchers with above normal challenges. This is especially true in the field of industrial application of the material where continuous technological improvements require continuous improvements in the accuracy of measurements, additional nonstandard analyses and real-time availability of data. This is furthermore emphasized by the increasing awareness by all stakeholders of health, environment and safety aspects, resulting in increased pressure towards enhanced characterization of coal properties and understanding of the behavior of coal based on relevant coal properties before, during and after utilization.

Real-time accurate measurement of relevant coal properties and the subsequent utilization of the measured data is a real operational requirement in a day and age where competitive edge is in part driven by knowledge.[1] Downtime due to unforeseen changes in coal quality, resulting in production losses leading to loss in turnover and revenue, is definitely not desirable in a production environment. The development of appropriate analytical tools that can be used online to produce real-time analytical data is of great importance to the economic and competitive sustainability of the coal utilization industry.

The complex nature of coal structure makes it difficult to use a single technique to determine its composition.[2] Routine characterization of coal by ultimate and proximate analyses, CV determination, petrology, X-ray fluorescence spectrometry (XRF), powder X-ray diffraction (PXRD) etc. is no longer sufficient.[3] Applications of techniques such as quantitative scanning electron microscopy (QEMSCAN), electron microprobe analysis (EMPA),[4] transmission electron microscopy (TEM) and high-temperature X-ray diffraction (HT-XRD) are becoming more and more essential.[5] A number of authors[6–9] have published review articles on the characterization of inorganic matter in coal, and slowly but certainly these more advanced techniques are being considered as new routine analytical tools complementing the suite of previous routine analyses.[1,2,10–12] The online analytical capability of these highly sophisticated equipment is very limited, and alternatives are required. Raman spectroscopy, already being used as routine online analytical method in the pharmaceutical industry, for example, is one analytical tool that could fill a particular gap in online coal characterization. The application of Raman spectroscopy in the characterization of the inorganic composition of coal is therefore considered by the authors of this paper as a real possibility.

In contrast to others, this paper will report on both the natural organic matter (NOM) as well as the natural inorganic matter (NIM) in coal. The review part of the paper is arranged in eras corresponding to the four decades that passed since the pioneering work of Tuinstra and Koenig[13] and deals mainly with the identification of the structural order of the carbon network in the NOM of coal. Due to the limited number of papers reporting on the NIM, the second part of the paper is devoted to preliminary results on the NIM characterization of South African coals by means of micro-Raman spectroscopy (MRS).

Experimental

For the review part, the data bases used in the search for relevant papers were the following: ISI Web of Knowledge, Sciencedirect, Scirus, Scopus and Wiley. Keywords used in the search were, Raman in conjunction with coal, carbon compounds, coal characterization, carbonaceous material and char. In addition, references were collected in the papers selected from this search, and altogether more than 100 papers were collected and read, of which a number were selected to report on in detail.

For the mineral characterization, different coals used in the study were collected from various South African coal fields throughout the country. The coals studied were from Witbank, Waterberg, Ermelo and Natal coal fields, and also included a discard coal. For this initial investigation, analyses were performed on petrographic blocks to facilitate relocation of a specific area as well as on the 'as-received' powdered coal. A representative sample was crushed using a ring roller mill to ~850 μm passing sieve size and retained on the 450 μm screen. This was done to effectively minimize the amount of fine particles. The blocks were prepared by mounting the samples in cold resin and left for 24 h to set. The blocks were polished in a series of steps on the Struers polisher down to a 1 μm finishing cloth using alumina slurry.

Raman spectra were measured at room temperature on a SENTERRA spectrometer (Bruker). The instrument includes a monochromator, a filter system and a thermo-electrically cooled charge-coupled device (CCD). Continuous wave laser energy at a wavelength of 532 nm was used as the excitation source. The laser power was set at 10 mW to prevent the sample from degrading. The instrument was calibrated using a 520 cm^{-1} silicon wafer. An Olympus 20× objective was used to focus the sample. The integration time varied between 10 and 50 s. The instrument resolution was set at 3–5 cm^{-1} with a spectral range of 50–2750 cm^{-1}. Raman spectra were analyzed using the OPUS 6.5 software. The OPUS software package was used for data analysis, manipulation and spectral identification, utilizing an in-house library.

1970–1979 (The G and D Band Era)

Green and coworkers[14] state as early as 1983 in their paper that the identification of minerals in coals was one of the principal

aims of the study and identified calcite, pyrite and dolomite with the use of a micro-Raman spectrometer. Surprisingly, however, this is one of the very few published articles on inorganic matter characterization of coal by means of Raman spectroscopy, even though mineral characterization by Raman spectroscopy in other matrices is a routine procedure.[15] In contrast, numerous articles have been published since the 1970s exploiting the characteristic Raman scattering of amorphous carbons (of which the macerals in coal is an example) after the classic work by Tuinstra and Koenig[13] on the correlations between the observed Raman bands and the structural parameters of polycrystalline graphite was published. This opened a promising field of investigations into the microstructures of carbonaceous compounds, including coal.

Tuinstra and Koenig[13] and Friedel and Carlson[16] published the first Raman spectra of coal and reported the two broad bands in the regions 1575–1620 and 1355–1380 cm^{-1}, called the G (graphitic) and D (disordered) bands. Tuinstra and Koenig[13] suggested that the 1575 cm^{-1} band could be assigned to the E_{2g} graphite mode with D^4_{6h} crystal symmetry and the band at ~1370 cm^{-1} to the A_{1g} mode, and related the ratio I_D/I_G to the average graphite domain dimension, L_a. Friedel and Carlson[16] debated the origin of the band at 1580 cm^{-1} by investigating IR absorption and Raman scattering of very finely ground graphite (C–C bonds broken), coal and carbon black and suggested that it and the band at 1350 cm^{-1} most likely arose from graphitic structures and not from aromatic[17] or conjugated carbonyls,[18] as has been suggested earlier. Tsu *et al.*[19] speculated that the 1370 cm^{-1} band (disordered induced) could be explained by phonon dispersion of graphite and postulated a typical cluster size for a coal molecule in the order of 65–72 Å. In 1981, Zerda *et al.*[20] gave a short review of the preceding Raman studies of coal, and reported on their investigations on several Polish coals, including samples where the inertinite and vitrinite macerals had been separated. No evident relationship between coal rank and the G and D band positions were reported, but the authors did indicate a broadening of both bands as they moved to the lower ranked coals. In addition, a difference in crystallite size was reported, determined as described by Tuinstra and Koenig.[13] This corresponded to values of 10 nm for higher ranked coals and 6 nm or less for the low-ranked coals, as well as smaller crystallite sizes for vitrinite compared to inertinite. It was concluded by the authors that this method of crystallite estimation can be used successfully only if aromatic structures are predominant.

1980–1989 (Raman and Maturation Grade, Coalification, Graphitization)

In the 1970s, the discussions revolved mainly around the assignment of the observed bands of carbonaceous materials' Raman spectra, and it was generally accepted that the D band at *ca.* 1360 cm^{-1} could be assigned to the A_{1g} mode, forbidden in a hexagonal lattice and activated when symmetry rules are relaxed as a result of boundary discontinuities. One paper, still dealing with the assignment of the observed shifts in the 1980s, that needs mentioning is that of Vidano and Fischbach.[21] This specific paper did not deal with coal at all, but investigated Raman spectra of graphite and disordered glassy and pyrolytic carbons. Vidano and Fischbach[21] mentioned in the paper that, although the Raman active band at 1580 cm^{-1} for the in-plane E_{2g} mode has been assigned (undoubtedly?), the assignment of the observed bands at intermediate wavenumbers (1100–1700 cm^{-1}) remained controversial. In the late 1970s and early 1980s, studies on disordered carbon compounds revealed a number of Raman active bands: G at 1580, D at 1360, G_1' at 2695, G_2' at 2735, D' at 1620 and D'' at 2950 cm^{-1}. The research revolved around a discussion of the matter as well as an interpretation of the progressive downshift in frequency of the D, G' and D'' bands observed with increasing λ of the excitation source. In the 1980s, the research turned more to the application of changes in the Raman spectra to explain characteristics and behaviors of carbon materials, such as coalification, carbonization and graphitization. Marian Wagner[22] studied the differences between xylites, dopplerite xylites, xylitic coal and brown coals. Raman spectroscopy, in addition to various other characterization techniques, was used to derive the conclusion that doppleritization (biochemical gelification of plant material to form dopplerites – compounds formed from the reaction between humic acid and an inorganic basis) and humification of wood in a coal-forming environment give rise to chemically different products. Furthermore, doppleritization leads to the formation of locally organized graphitic domains as evidenced by the appearance of G and D bands. Rouzaud and Oberlin[23] published an article considering nearly pure carbon film deposits which were heat-treated and investigated by means of MRS, TEM and optical microscopy. Results suggested that graphitization takes place in five steps and that the data obtained with the three techniques resulted in the same conclusions. The Raman spectra of the carbon films were deconvoluted into three bands, viz. 1350, 1500 and 1580 cm^{-1}. It was concluded that the 1350 cm^{-1} band is due to the in-plane defects located between adjacent basic structural units (BSUs), which are responsible for the existence of tilt and twist boundaries, and that the 1500 cm^{-1} band can be attributed to interstitial defects, either between the layers or between BSUs. Interstitials were released at about 1400 °C and ended at 1980 °C, as was indicated by the disappearance of the 1500 cm^{-1} band. The removal of the in-plane defects (tilt and twist boundary defects) began above 1980 °C, with a gradual increase in L_a and a drastic decrease in the intensity of the 1350 cm^{-1} band. Lastly, an increase in L_a corresponded to the final removal of all the in-plane defects in the range 2340–2700 °C. The layers were entirely stiff and perfect and the degree of graphitization increased.

Another study was performed in the 1980s[14] to explore the application of Raman spectroscopy to coals and cokes. This comprehensive study investigated the inorganic and maceral character of the coals, the structural changes during the coking of coal as well as the influence of added minerals on the carbonization behavior of the coal. The main aim of the mineral identification by means of the Raman probe was to avoid erroneous results otherwise obtained by either low- or high-temperature ashing by analyzing the raw coal on an as-received basis. As has been mentioned elsewhere in this paper, the minerals that were identified in coal were calcite, pyrite and dolomite. The coals investigated were generally of low rank with typical vitrinite reflectance (RoV%) values less than 1. The paper by Green and coworkers[14] describes five structure-sensitive lines, in contrast to the two and three used in the 1970s. In short, they are the G band at 1580 cm^{-1} due to in-plane vibrations of the layers of BSUs; the D band at 1360 cm^{-1} resulting from structural imperfections in the planes; the D' band at 1620 cm^{-1} observed in disordered carbon and imperfect graphites and often presents together with the G band, shifting it to higher wavenumbers and, finally, the G' doublet at 2700 and 2735 cm^{-1} as overtones of the D band as described in the paper of Vidano and Fischbach.[21] The authors

could not distinguish between different optical textures (therefore different parent coals) and their corresponding Raman spectra at the same temperature, which was similar to the earlier findings of Mochida *et al.*[24] It was, however, clear from the results that there is a correlation between band position and the temperature of carbonization. It was further found that the position of the G (G + D') and the D bands decreased with increase in temperature. Furthermore, the bandwidth of the D band also decreased with increase in carbonization temperature. From the results, it was clear that the ratio I_D/I_G decreased with increasing temperature until it was approximately 0.9 at 2000 °C and this was interpreted as being the result of annealing and a decrease in disorder.

In a continuation of their work, Johnson *et al.*[25] and Johnson and Thomas[26] published two papers on coal and pitch char characterization by means of Raman spectroscopy. The authors found that the D band width for the chars originating from various ranks of coals, decreased with increasing heat-treatment temperature (240 cm^{-1} at 500 °C with $L_a = 2$ nm to 40 cm^{-1} at 1900 °C with $L_a = 7$ nm). In the second paper, this correlation was used to describe the temperature profile of a dugout gasifier. In 1986, however, Kister and Dou[27] published contradictory results and indicated that the G + D' band intensity, D band position, intensity and width differed for the various ranks of coal investigated. This paper gives no information on the experimental conditions and the results are also not interpreted. In this same study, the mineral content of the five different coals investigated were also analyzed by means of FT-IR, whereby nine different minerals were characterized and quantified. Bonny-Bassez and Rouzaud[28] investigated various carbonaceous compounds, viz. thin vapor deposit C-films, synthesized anthracene-cokes, containing only H as heteroatom, synthesized saccharose-cokes, containing both H and O as heteroatoms and natural coal samples with RoV% varying from 0.8 to 5.4. These authors looked at the correlation between the carbonaceous maturation grade and the corresponding Raman spectra. Results by Bonny-Bassez and Rouzaud[28] indicated that the G + D' band width of variable ranked natural coals decreased with increasing rank, but no systematic decrease in the intensity ratio of the D and G bands could be found. The authors postulated that, although the thermal maturation process leads to the progressive elimination of chemical groups, there is no discernable increase in crystallite size, and hence the lack of a measurable change in the intensity ratio.

These findings were substantiated by Roberts *et al.*,[29] where a systematic investigation of a series of chitinozoans varying from low to high ranks displayed the same phenomena. Cottinet and coworkers[30] report on the use of Raman spectroscopy to evaluate the structural rearrangement that takes place during the heat treatment of pitches from the same coal-tar precursor. They found that the isotropic and mesophases had two different spectra (a band at 1600 and two bands at 1580 and 1360 cm^{-1}, respectively) and that Raman indices could be used to follow the evolution of the two phases during heat treatment.

1990–1999 (Continuation of the Work of the 1980s)

Although the debate around the origin of the D band, the correct approach to deconvolution of the obtained Raman spectra and the influence of sample orientation were not continually debated in the 1990s, it is evident from the number of publications that many researchers decided to accept the status quo and used the parameters to interpret various properties and behaviors of coal. A critical approach was followed by Angoni,[31] who postulated a simple qualitative analysis to distinguish between carbon materials with a low, medium and high structural organization after analyzing 15 samples that varied from graphite, coke and coal to anthracite. The classification was based on the number and width of bands present in the first- and second-order spectra. The author also investigated the validity of quantitative analyses and their application to characterize the various carbon-containing materials. It was concluded that Raman bands should be fitted with a Lorentzian profile and that a limit criterion should be established before a decision is made on the presence of another band. An attempt to cover the entire order–disorder spectrum of carbon materials, including natural, synthetic and surface-activated graphite, carbon fibers, pitch, various cokes, glassy carbon, activated carbon, anthracite and sub-bituminous coals resulted in the presentation of Raman spectra and its properties of 29 different carbonaceous materials, analyzed in the powder form.[32] A disorder parameter $(I_D/I_G) + I_G$ was used and it was found that the width of the D band correlated well with the degree of disorder, given as a percentage. Neither the G nor D band positions could be used to indicate the degree of disorder. Sadly, only 2 of the 29 samples were coal and little mention of them is made.

Bustin and coworkers[33] used Raman spectroscopy, among a number of other analytical characterization tools, to determine the importance of deformation upon graphitization and hence understand the mechanism of graphitization in nature. A non-softening, partially graphitizing anthracite coal from Pennsylvania (RoV% 5.27) and a nongraphitizing, softening, highly volatile bituminous coal from Nova Scotia (RoV% 0.68) were selected for this study. Raman investigations were performed on petrographically prepared polished stubs. No obvious systematic decrease in the D band was observed, although greater degrees of graphitization were confirmed by XRD, optical microscopy, and TEM. They speculated that the graphitization process did not remove the defects reflected by the D band, although analyses by XRD and TEM confirmed graphitic crystal growth and suggested that the D band should be affected. Spectra presented in this paper were of poor quality and had considerable amount of noise.

Petrographically prepared stubs of five iron-catalyzed coked samples obtained from different regions in a blast furnace were analyzed by Raman spectroscopy.[34] In addition, a feed coke was graphitized under controlled laboratory conditions with and without the presence of iron. From this work, it is evident that the width of the G band is particularly sensitive and describes the degree of graphitization. It was found that the most noticeable difference between the coke and graphite spectra was the resolution of the second-order G band. It was shown that graphite was formed at temperatures well below normal graphitization temperatures in the presence of iron. By studying the spectral features of the carbon material in, at the edge and away from the iron particles, it could be concluded that the important factors governing the process are temperature, the amount of iron in contact with the coke and the residence time.

Tree *et al.*[35] applied Coherent anti-Stokes Raman Spectroscopy (CARS) to remotely determine gas temperatures in a controlled profile reactor.[35] The developmental work and testing of the CAR spectrometer is, however, not discussed in the paper and is only referred to as part of a PhD thesis by D.K. Pyper in the mid-1990s. Finally, a paper that deserves mention is that of Cuesta and coworkers.[36] This paper addresses the correlation between

I_D/I_G and $1/L_a$ as postulated by Tuinstra and Koenig.[13] Various papers were referenced that applied this method to determine the crystallite size along graphite basal planes and indicated the contradictory results obtained for various carbon materials if compared to XRD measurements, i.e. higher values were obtained for coal[20] and carbon fibers,[17] and lower values for graphites.[18] The authors emphasized that Tuinstra and Koenig's[13] formula can only be used as a first approximation of L_a and the accuracy of such estimation depends heavily on the type of carbon under study. The paper further reports on the rigorous analyses of 45 carbon materials with PXRD and MRS. The main conclusions were as follows: (1) Correlating d_{002} with $(I_D/I_G) + I_G$ showed a general increase in both parameters with an increase in disorder, but with disparity between the two factors in some cases, indicating that the information obtained by the two techniques should be used complementary to each other; (2) This first conclusion led to the confirmation that the first-order Raman spectrum of carbons relates to their in-plane or bidimensional order, while it is well known that tridimensional stacking order is inferred from d_{002}; (3) The contributions to the D band intensity are difficult to separate and are governed by the preferred orientation and the presence of different types of disorders, the former predominating for the well-ordered graphites and the latter for disordered carbons; (4) Tuinstra and Koenig's[13] formula could result in up to 100% errors and will most likely result in an underestimation for disordered carbons.

2000–2009 (Char Structure Era)

Recent research (2000–2009) focused mostly on the application of Raman-sensitive bands, identified in the 1970s, 1980s and 1990s, on various aspects of coal and its use in industry. One of the areas of research frequented the most is that of char structure, and as a result a considerable part of this era's discussions will be dedicated to it. Most of the work has been reported by Chun-Zhu Li, of which an elegant summary is given in Li.[39] He and his coworkers worked on Victorian brown coal and the understanding of its pyrolysis and gasification behavior. Brown coal has many unique features, including a low ash yield, often high alkali content that is usually finely dispersed, low rank, high oxygen content and normally high moisture content. The char structure determines its reactivity and depends on the ease of carbon removal, as well as the catalytic effect of alkalis present in the char. Although SEM and TEM analyses will provide useful information on the morphology and carbon structure, this does not translate into quantitative information on the actual structure of the char.

XRD is extremely useful for the quantitative analysis of crystalline (ordered) compounds if they are present in quantities of 5% or more. Brown coals are not well ordered and some of the minerals could be present in lower quantities, but they still influence the combustion and gasification behavior of the coal. Raman spectroscopy, especially MRS, can on the other hand probe char structures even though they have an amorphous nature. In the first publication,[40] Li *et al.* postulated that brown coals and their corresponding chars are so highly disordered that the broad G and D bands do not allow the application of the correlation postulated by Tuinstra and Koenig[13] and that further deconvolution is essential. These authors used near-infrared (NIR 1064 nm) irradiation as well as FT-Raman, and diluted the material with KBr to reduce beam damage. Contrary to all other publications on carbon materials, Li *et al.*[39] postulated that the density-of-states model used to correlate the Raman spectrum cannot be used in the case of brown coals and its corresponding pyrolysis products. The authors reasoned that the absence of graphitic crystallite structures as determined by XRD for their specific samples before and after pyrolysis at 600–900 °C indicated that the band at 1580–1600 cm^{-1} could not be assigned to the E_{2g} mode of graphite but belonged to the aromatic quadrant ring-breathing mode which is Raman active at the same position. Consequently, the D band cannot be due to disorder in graphite and was assigned to the disorder of fused benzene rings having more than six rings but less than graphite. In their deconvolution, a total of 10 bands were assigned, but reduced to a group of four: two of which are the G and D bands as mentioned in the earlier paragraph, three bands at 1540, 1465, 1380 grouped together, representing 3–5-membered aromatic rings and methylene or methyl aromatic rings with mixed sp^2–sp^3 structures, and lastly the S band representing sp^2–sp^3 carbonaceous structures. Upon studying the D and G band ratios, it was found that it increased and reached a maximum at around 700 °C, after which it underwent a slight decrease. This was ascribed to the initial increase in the 5–6-membered fused benzene ring concentration and the subsequent decrease in defect structure.

In a second publication, Li *et al.*[41] investigated the catalytic gasification of the same coal and related the S band to a measure of cross-linked density and substitutional groups. This led to the conclusion that O-containing functional groups formed preferentially on the sp^2–sp^3 and sp^3 rich sites, and, in the absence of a catalyst it was more likely to be aromatic in nature. In a third study by Li *et al.*,[42] the previously proposed deconvolution was used to investigate the evolution of char during a sodium-catalyzed pyrolysis. By employing FT-IR in conjunction with the Raman studies it was concluded that the smaller aromatic ring systems (presenting the amorphous part of the coal/char) were consumed preferentially during the pyrolysis process, and more so when it was not catalyzed by sodium. The information was therefore used to explain the differences between the reaction pathways of brown coal during catalyzed and noncatalyzed pyrolysis. From the same research group, a recent publication[43] appeared considering the changes in char structure during gasification in the presence of both steam and oxygen. It was determined that the char–oxygen reaction is rate limited by oxygen mass transfer, and concluded that chars derived from steam-only gasification had nearly the same features as those exposed to steam and oxygen combined.

Bar-Ziv *et al.*[44] used petroleum coke and a bituminous South African coal to investigate the evolution of its reactivity during heat treatment under oxidizing conditions. MRS data was correlated with that of thermogravimetric analysis (TGA) by comparing normalized reaction times with intensity ratios, and it was found that a general decrease in reactivity correlated well with an increase in intensity ratios of the D and G bands. From the work, it was reported that no minerals were identified in any of the 100 odd samples investigated. This study was continued[45] by looking at a cellulose char where an initial increase in the ratio of the D to G band was found, with a steady decrease after temperatures around 1000 °C, as reported by many investigators. The approach taken by the authors was also followed in a recent study,[46] where a five-band deconvolution was used to interpret the spectra, which also concluded that reactivity decreased with an increase in intensity ratios. Various ratios of all the D (1–4) bands with the G band were studied in more detail and revealed, in contrast to Bar-Ziv *et al.*[44] and Zaida *et al.*,[46] that there was a general decrease in all of these ratios with an increase in the heat-treatment temperature.

J. Raman Spectrosc. **2011**, 42, 123–129

Raman studies were also used to assist in an investigation of the influence of laminar flow on preorientation of coal-tar pitch.[47] As found by many others, it was also concluded by Urban et al.[47] that the intensity ratio of the D and G bands is not a sensitive indicator of the degree of organization of the amorphous carbon and that the ratio increased from 500 to 1000 °C after which it decreases steadily. This trend was also observed in the width of the D^1 band. The D^3 (1500 cm^{-1}) and D^4 (1220 cm^{-1}) bands did, however, portray a continuous decrease in width and disappeared altogether after 1500 °C. Steam gasification of various coals, mostly sub-bituminous coals from Indonesia, Australia, America and South Africa, were investigated with MRS using a mapping of the sample and correlating it with EDS mapping. The ratio of the width of the D and G bands was used as an indicator of the degree of graphitization. It was concluded that the ratio was mainly affected by the consumption of amorphous carbon and that the apparent increase in order could rather be explained by a preferential gasification of the disordered carbons, resulting in an apparent increase in graphitic content.[48]

A couple of papers dealing with aspects other than char structure were published in the 2000s, which also deserve attention. Quirico et al.[49] gave an overview of the progress and problems of Raman spectroscopy for the determination of the maturation grade of coal. Previous work done by the group of Rouzaud[23] is reported on with an attempt to find a laboratory procedure that could be used on all coals and robust enough to be used in an inter-laboratory manner. The difference between the Raman spectra of low-rank and high-rank coals was firstly indicated, and furthermore it was stated that the classical way of determining the coherent domain length, as suggested by Tuinstra and Koenig,[13] is not possible because of the limited number of coherent domains. This team of researchers infers that Raman spectroscopy is much more sensitive to maturity changes in low-rank coals (RoV % 1–7) and that changes are mainly due to a decrease in O/C and H/C elemental ratios with little structural rearrangements. By performing several analyses on 11 coal samples and keeping the acquisition for each sample constant, they derived a number of spectral parameters that were related to RoV%. In this way, they could establish which parameters were the most sensitive for a specific maturation grade range, in contrast to previous researchers who attempted to use the same parameter for all types of coals. The disadvantage of this study (and as a matter of fact with most of the studies discussed in this review) is that analyses are done manually and to get a statistically representative result would require in the order of 100 analyses per sample. The time constraint that this factor imposes on the research resulted in a reduction of number of samples and hence a statistical variance of unacceptable size.

In contrast to Quirico et al.,[49] Marques and coworkers[50] studied high-rank coals and graphite and found that the full width at half-maximum (FWHM) of the G band could distinguish high rank coals from graphite, but the different ranked coals could not be distinguished from each other. A negative correlation between the FWHMof the G band and RoV% was also reported, namely that the graphitic character increased as the G band became narrower. Nestler et al.[51] investigated 11 coals varying from low to high rank (VoR% from 1.5 to 60). The study was mainly to characterize a fossilized tissue by comparing it with the Raman spectra of various anthracitic and sub-bituminous coals and relate that to the degree of coalification.

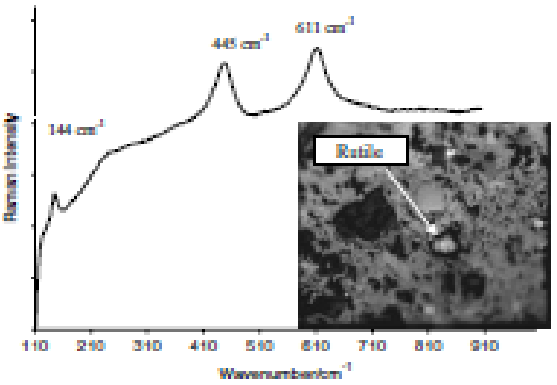

Figure 1. White light image and corresponding Raman spectrum of a rutile particle.

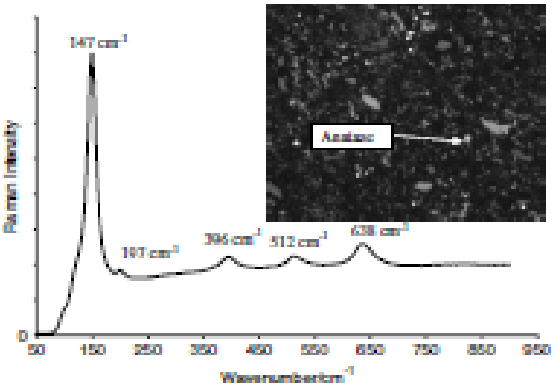

Figure 2. White light image and corresponding Raman spectrum of an anatase particle.

Mineral Characterization

As mentioned elsewhere in the paper, literature on NIM characterization in coal using Raman spectroscopy is very sparse; in fact, the only paper specifically reporting the presence of NIM is by Green et al.,[14] whereby calcite, pyrite and dolomite were identified. During our preliminary investigations, some of the major minerals were identified of which some selected results are presented below. Within the five coal samples, oxides, sulfides and silicates were characterized. The assignment and identification of various minerals were referenced to work presented in the literature. Figures 1 and 2 show that the two polymorphs of titania could be easily identified.

Figure 3 represents two spectra: that of a pure pyrite particle and a pyrite particle intimately mixed with magnetite. Other minerals identified, but not illustrated here, were calcite, pyrrhotite, marcasite and various silicates.

The high fluorescing background experienced when low-rank coals are analyzed makes the identification of minerals a daunting task if one works with a powder instead of a polished block, from which one can identify the minerals more easily and therefore reduce the contribution of the organic matrix by focusing on the mineral only. A much more elegant way would be the combination

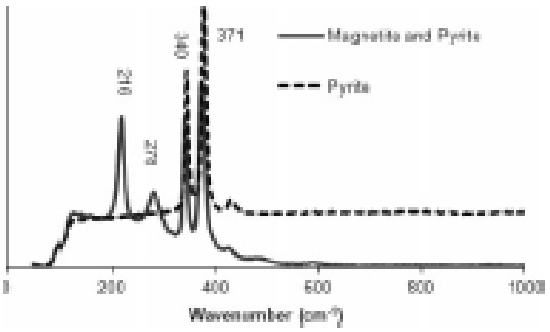

Figure 3. Raman spectra of a pyrite particle and an agglomerate of intimately mixed pyrite and magnetite.

of elemental mappings with a Raman identification performed by an interfaced SEM/EDX–MRS. Investigations of the inorganic content of various South African coals and its association with the macerals are currently in progress.

Conclusions

From the data discussed in this review paper, it is evident that there is still some controversy around the application of changes in the D and G bands to be representative of changes in the order of the amorphous carbons. This is apparently even more so in the case of coal. In general, the papers reviewed indicated that the G band ~1580 cm^{-1} should be assigned to E_{2g} graphite mode with D^4_{6h} crystal symmetry and the D band at ~1370 cm^{-1} to the in-plane defects located between the BSUs. Various postulates were made for the further deconvolution of these bands, of which the one at ~1500 cm^{-1} is probably the most noteworthy and generally assigned to the interstitial defects between the BSUs. An important conclusion that seems to frequent the papers of the last decade is that not all amorphous carbons can be treated the same, and this is eloquently illustrated by the research performed by the group of Li *et al.*[39–47] on Victorian brown coal. Therefore, the correlations between band width and band intensities and graphitization, carbonation, rank/order, char structure and reactivity of coke are not consistent. An obvious area of neglect is the characterization of inorganic matter and minerals in coal with MRS and this evidently deserves more investigation and attention.

References

[1] S. Benson, In *Proceedings of Minnesota Energy Ingenuity Conference*, **2008**, Nov 6–7.
[2] C. van Alphen, *Miner. Eng.* **2007**, *20*, 496.
[3] S. Ural, *Int. J. Coal Geol.* **2007**, *71*, 176.
[4] R. M. Bustin, M. Mastalerz, M. Raudsepp, *Int. J. Coal Geol.* **1996**, *32*, 5.
[5] R. A. Creelman, C. R. Ward, *Int. J. Coal Geol.* **1996**, *30*, 249.
[6] F. E. Huggins, *Int. J. Coal Geol.* **2002**, *50*, 169.
[7] C. R. Ward, *Int. J. Coal Geol.* **2002**, *50*, 135.
[8] R. Gupta, *Energy Fuels* **2007**, *21*, 451.
[9] S. V. Vassilev, C. G. Vassileva, *Fuel Process. Technol.* **1996**, *48*, 85.
[10] J. C. van Dyk, S. Melzer, A. Sobiecki, *Miner. Eng.* **2006**, *19*, 1126.
[11] R. H. Matjie, C. Van Alphen, *Fuel* **2008**, *87*, 1459.
[12] C. van Alphen, R. H. Matjie, P. Rajoo, In *Proceedings of Automated Mineralogy 07*, Brisbane, CD-ROM, **2007**, Sept 1–2.
[13] F. Tuinstra, J. L. Koenig, *J. Chem. Phys.* **1970**, *53*, 1129.
[14] P. D. Green, C. A. Johnson, K. M. Thomas, *Fuel* **1983**, *62*, 1013.
[15] E. Stefaniak, A. Worobiec, S. Potgieter-Vermaak, A. Alsecz, S. Török, R. Van Grieken, *Spectrochim. Acta, Part B* **2006**, *61*, 824.
[16] R. A. Friedel, G. L. Carlson, *Fuel* **1971**, *51*, 194.
[17] C. G. Cannon, B. B. G. Sutherland, *Nature* **1955**, *156*, 240.
[18] J. K. Brown, *J. Chem. Soc.* **1955**, *744*, 752.
[19] R. Tsu, J. González, I. Hernández, C. A. Luengo, *Solid State Commun.* **1977**, *24*, 809.
[20] T. W. Zerda, A. John, K. Chmura, *Fuel* **1981**, *60*, 375.
[21] R. P. Vidano, D. B. Fischbach, *Solid State Commun.* **1981**, *39*, 341.
[22] M. Wagner, *Int. J. Coal Geol.* **1982**, *2*, 181.
[23] J. N. Rouzaud, A. Oberlin, *Thin Solid Films* **1983**, *105*, 75.
[24] I. Mochida, Y. Korai, H. Fujitsu, K. Takeshita, Y. Komatsubara, K. Koba, H. Marsh, *Fuel* **1983**, *63*, 136.
[25] C. A. Johnson, J. W. Patrick, K. M. Thomas, *Fuel* **1986**, *65*, 1284.
[26] C. A. Johnson, K. M. Thomas, *Fuel* **1987**, *66*, 17.
[27] J. Kister, H. Dou, *Fuel Process. Technol.* **1986**, *12*, 19.
[28] C. Benny-Bassez, J. N. Rouzaud, *Scan. Electron. Micros.* **1985**, *1*, 119.
[29] S. Roberts, P. M. Tricker, J. E. A. Marshall, *Org. Geochem.* **1994**, *23*, 223.
[30] D. Cottinet, P. Couderc, J. L. Saint Romain, *Carbon* **1987**, *25*, 339.
[31] K. Angoni, *Carbon* **1992**, *31*, 537.
[32] A. Cuesta, P. Dhamelincourt, J. Laureyns, A. Martínez-Alonso, J. M. D. Tascón, *Carbon* **1994**, *32*, 1523.
[33] R. M. Bustin, J. V. Ross, J. N. Rouzaud, *Int. J. Coal Geol.* **1995**, *28*, 1.
[34] W. Wang, K. M. Thomas, R. M. Poultney, R. R. Willmers, *Carbon* **1995**, *33*, 1525.
[35] D. R. Tree, D. L. Black, J. R. Rigby, M. Q. McQuay, B. W. Webb, *Prog. Energy Sci.* **1998**, *24*, 355.
[36] A. Cuesta, P. Dhamelincourt, J. Laureyns, A. Martínez-Alonso, J. M. D. Tascón, *J. Mater. Chem.* **1998**, *8*, 2875.
[37] E. Fitzer, F. Rozploch, F. Kunkala, In *Carbon '88 Proceedings*, (Eds: B. McEnaney, T. J. Mays), IOPP: Bristol, **1988**, p 248.
[38] J. Nikiel, P. W. Jagodzinski, *Carbon* **1993**, *31*, 1313.
[39] C.-Z. Li, *Fuel* **2007**, *86*, 1664.
[40] X. Li, J. Hayashi, C.-Z. Li, *Fuel* **2006a**, *85*, 1700.
[41] X. Li, J. Hayashi, C.-Z. Li, *Fuel* **2006b**, *85*, 1509.
[42] X. Li, J. Hayashi, C.-Z. Li, *Fuel* **2006c**, *85*, 1518.
[43] X. Guo, H. L. Tay, S. Zhang, C.-Z. Li, *Energy Fuels* **2008**, *22*, 4034.
[44] E. Bar-Ziv, A. Zaida, P. Salatino, O. Sannaca, *Proc. Combust. Inst.* **2000**, *28*, 2369.
[45] A. Zaida, E. Bar-Ziv, L. Radovic, Y.-J. Lee, *Proc. Combust. Inst.* **2007**, *31*, 1881.
[46] C. Sheng, *Fuel* **2007**, *86*, 2316.
[47] O. Urban, J. Jehlička, J. Pokorný, J. N. Rouzaud, *Spectrochim. Acta, Part A* **2003**, *59*, 2331.
[48] Y. Sakino, K. Ishikawa, E. Kikuchi, M. Matsukata, A. Akimoto, *Fuel* **2006**, *85*, 122.
[49] E. Quirico, J.-N. Rouzaud, L. Bonal, G. Montagnac, *Spectrochim. Acta, Part A* **2005**, *61*, 2368.
[50] M. Marques, I. Suárez-Ruiz, D. Flores, A. Guedes, S. Rodrigues, *Int. J. Coal Geol.* **2009**, *77*, 377.
[51] K. Nestler, D. Dietrich, K. Witke, R. Rössler, G. Marx, *J. Mol. Struct.* **2003**, *661–662*, 357.